UNIVERSIDADE FEDERAL FLUMINENSE
INSTITUTO DE GEOCIÊNCIAS
DEPARTAMENTO DE GEOLOGIA E GEOFÍSICA
PROGRAMA DE PÓS-GRADUAÇÃO EM DINÂMICA DOS OCEANOS E DA TERRA

Assessment of spatial and temporal variability of satellite-estimated suspended sediment and chlorophyll over Sofala Bank, Mozambique, and their relation to environmental variables

Hélder Arlíndo Machaieie

NITERÓI
2018

Hélder Arlíndo Machaieie

Assessment of spatial and temporal variability of satellite-estimated suspended sediment and chlorophyll over Sofala Bank, Mozambique, and their relation to environmental variables

Tese apresentada ao .Programa de ..Pós-Graduação em Dinâmica dos. Oceanos e da Terra da Universidade Federal Fluminense, como requisito parcial para obtenção ...do .. Grau de Doutor em Ciências. ... Área.. de ....Concentração: Dinâmica dos Oceanos e da Terra

Orientadores:

Prof. Dr. Cleverson Guizan Silva

Prof. Dr. Eduardo Negri de Oliveira

NITERÓI

2018

Examination Board:

_____

Prof. Dr. Cleverson Guizan Silva (Advisor)
Universidade Federal Fluminense-UFF

_____

Prof. Dr. Eduardo Negri de Oliveira (Co-advisor)
Universidade do Estado do Rio de Janeiro - UERJ

_____

Prof. Dr. Josefa Varela Guerra
Universidade do Estado do Rio de Janeiro – UERJ

_____

Prof. Dr. Milton Kampel
Instituto Nacional de Pesquisas Espaciais-INPE

_____

Prof. Dr. Afonso Moares Paiva
Universidade Federal do Rio de Janeiro-UFRJ

_____

Prof. Dr. Raúl Vicens
Universidade Federal Fluminense-UFF

NITERÓI
2018

Certification

The undersigned certify that they have ready and recommended for acceptance by Universidade Federal Fluminense a Thesis titled: **Assessment of spatial and temporal variability of satellite-estimated suspended sediment and chlorophyll over Sofala Bank, Mozambique, and their relation to environmental variables**, in partial fulfillment of the requirements for the degree of Doctor of Sciences in Dinâmica dos Oceanos e da Terra.

Prof. Dr. Cheverson Guizan Silva

…….

Advisor

Date: ……..

Prof. Dr. Eduardo Negri de Oliveira

……..

Advisor

Date: ……

Declaration and Copyright

I, Hélder Arlíndo Machaieie, declare that this Thesis is my own work and that it has not been presented and will not be presented to any other University for a similar or any other degree award.

Each significant contribution to this dissertation from the work of other people has been cited and referenced.

I hereby give consent for my thesis, if accept, to be made available for photocopying, and for inter-library loan, and the title and summary to be made available to outside organizations.

Signature
(Candidate)

Acknowledgments

I would like to express special thanks to CAPES-PEC-PG for giving me the scholarship.

I am grateful to my advisors Cleverson Guizan Silva and Eduardo Negri de Oliveira for having dedicated some of their time to help me to develop this work.

I would like to thank Professor Davies Bowers for having kindly provided the in situ data used in this work and for good ideas he gave me during the beginning of the project.

I am grateful to Professor Fialho Nehama for the ideas during the conception of the topic of this Thesis. I am also thankful to Dr. Fernanda Soares for all the discussions we had and for introducing me to the Remote Sensing team of PPGG-UFRJ.

My thanks to Professor Antonio Hoguane for the support given during the preparation of my application for doctoral studies.

I would like to express special thanks to my wife, Lidia Chivale and my children, Arlinda and Enzo, for the company and patience they had for my lack of attention.

I am grateful to Marília Nascimento, Miraci Medeiros, José dos Reis Novais, Marta dos Reias Novais, Ana Dalva, José Luiz Cardoso, Fábio and all the members of Igreja evangélica Gonçalense for the friendship and for the special fondness they gave to me and to my family.

Thanks to Domingos Moreira, Gina Sitoe, César Hoguane, Avelino Langa and Flávio Panzho, for the academic support and friendship.

A special thank goes to my parents for the continuous encouragement they have given me in this long journey of study.

I am deeply thankful to God for shining my way and making my dreams come true.

Dedication

This DSc research Thesis is dedicated to all members of Machaieie Xigonati family.

Ficha catalográfica automática - SDC/BIG
Gerada com informações fornecidas pelo autor

M149a Machaieie, Hélder Arlindo
Assessment of spatial and temporal variability of satellite-estimated suspended sediment and chlorophyll over Sofala Bank, Mozambique, and their relation to environmental variables / Hélder Arlindo Machaieie ; Cleverson Guizan Silva, orientador ; Eduardo Negri de Oliveira, coorientador. Niterói, 2018.
149 f. : il.

Tese (doutorado)-Universidade Federal Fluminense, Niterói, 2018.

DOI: http://dx.doi.org/10.22409/PPGDOT .2018.d.06268797795

1. Zambezi River Discharge. 2. Remote Sensing. 3. Wind and Wave Climatology. 4. ENSO. 5. Produção intelectual. I. Silva, Cleverson Guizan, orientador. II. Oliveira, Eduardo Negri de, coorientador. III. Universidade Federal Fluminense. Instituto de Geociências. IV. Título.

CDD -

Bibliotecário responsável: Debora do Nascimento - CRB7/6368

Resumo

As descargas fluviais nos sistemas costeiros têm grande importância nos processos físicos e biogeoquímicos e na produtividade. A descarga do rio Zambezi desempenha um papel importante na variabilidade da qualidade da água, produtividade primária e secundária sobre o Banco Sofala, que é a região de pesca mais importante na plataforma continental de Moçambique. Dada a sua importância, o Banco Sofala tem sido objeto de diversos estudos, porém pouco se sabe sobre a variabilidade espacial e temporal de sedimentos em suspensão e clorofila no Banco Sofala. Assim, esta tese descreve a variabilidade espacial e temporal dos sedimentos em suspensão e das concentrações de clorofila no Banco Sofala e sua relação com as variáveis ambientais. A climatologia de composições normalizadas mensais de água emitindo radiação de 555 nm (nLw555) foi utilizada como *proxy* para os sedimentos em suspensão e a climatologia mensal de sedimentos inorgânicos em suspensão foi estimada a partir da reflectância por sensoriamento remoto, mostrando que a pluma de sedimentos é relativamente estreita, com menor concentração de sedimentos em suspensão de Janeiro a Junho, tornando-se mais ampla, com maior concentração de sedimentos em suspensão de Julho a Dezembro. De Junho a Dezembro, um núcleo da pluma localizado na região sul do Banco Sofala, perto dos rios Pungue e Buzi e outro, localizado na região central, em frente ao Delta do Zambezi se fundem e derivam para o norte. Tanto a dispersão da pluma quanto a concentração de sedimentos em suspensão co-variam com a velocidade do vento e as ondas. As correlações espaciais entre as variáveis ambientais (descarga do rio Zambezi, velocidade do vento e ondas) mostraram que a velocidade do vento e as ondas se correlacionam forte e positivamente com sedimentos em suspensão na maior parte do Banco Sofala. Esses resultados sugerem que a re-suspensão dos sedimentos erodidos pelo vento e pelas ondas é mais importante no controle da variabilidade sazonal dos sedimentos em suspensão do que o rio Zambezi, exceto na região central ligeiramente distante da costa, onde a descarga do rio Zambezi mostra ser o principal controlador. As concentrações de clorofila medidas por satélite no Banco Sofala apresentam dois modos principais: modo alto, variando entre 3,5 e 4 mg m-3 nos núcleos de pluma, estendendo-se de Janeiro a Abril, e modo baixo, com concentrações inferiores a 3 mg m-3 nos núcleos de pluma, estendendo-se de Maio a Dezembro. A covariação das concentrações de descarga e clorofila do rio Zambezi e a forte correlação positiva entre eles sugerem que a descarga do rio Zambezi é o principal controlador da variabilidade anual de clorofila no Banco Sofala, especialmente na região central perto da desembocadura principal do delta de Zambezi. No entanto, a componente do vento ao longo da costa parece desempenhar um papel ao deslocar águas *offshore* com baixa clorofila em direção à costa, diminuindo as concentrações de clorofila em águas costeiras. A descarga do rio aumenta durante eventos frios da Oscilação Sul do El Niño (ENSO) e diminui durante os eventos quentes. Como consequência, na área do Banco Sofala sob a influência da descarga do rio, anomalias positivas de concentração de clorofila ocorrem durante La Niña e anomalias negativas de concentração de clorofila são comuns durante os eventos do El Niño, especialmente na estação chuvosa. Relação inversa significativa de precipitação ENSO observada ao sul de 15°S no baixo Zambezi, sugerem que o sinal ENSO nas águas costeiras, sobre o Banco Sofala é introduzido pelo fluxo do Zambezi.

.

Palavras Chave: Banco de Sofala, Sedimentos em suspensão, clorofila, sensoriamento remoto, descarga do rio Zambezi, ventos, ondas, ENSO.

Abstract

River discharges in the coastal systems have great importance in physical and biogeochemical processes and productivity of continental. The Zambezi River discharge has been pointed to play a major role on the variability of water quality, primary and secondary productivity over Sofala Bank, which is the most important fishing region on the continental shelf of Mozambique. Given its importance, the Sofala Bank has been the subject of several studies, however little is known about the spatial and temporal variability of suspended sediments and chlorophyll in Sofala Bank. Thus, this thesis describes the spatial and temporal variability of suspended sediments and chlorophyll concentrations in the Sofala Bank and their relation to environmental variables. The climatology of monthly-composites of normalized water leaving radiance at 555 nm (nLw555) used as a proxy for the suspended sediments and the monthly climatology of inorganic suspended sediments, estimated from remote sensing reflectance, showed that the sediment plume is relatively narrow, with lower concentration of suspended sediments from January to June and becomes wider, with higher concentration of suspended sediments from July to December. From June to December, the plume core located in the south region of Sofala Bank, near Pungue and Buzi Rivers and the other, located in the central region, in front of the Zambezi Delta merge and drift northwards. Both the plume dispersion and concentration of suspended sediments co-vary with wind speed and waves. The spatial correlations between the environmental variables (Zambezi River discharge, wind speed and waves) showed that the wind speed and waves correlate strong and positively with suspended sediments in most the part of Sofala Bank. These findings suggest that the erosion re-suspension by wind and waves is more important in controlling the seasonal variability of suspended sediment than the Zambezi River, except in the central region slightly away from the coast, where the Zambezi River discharge shows to be the main controller. The satellite measured chlorophyll concentrations in the Sofala Bank present two main modes: high mode, varying between 3.5 and 4 mg m^{-3} in the plume cores, extending from January to April, and low mode, with concentrations less than 3 mg m^{-3} in the plume cores, extending from May to December. The co-variation of Zambezi River discharge and chlorophyll concentrations and the strong positive correlation between them suggest that the Zambezi river discharge is the main controller of annual chlorophyll variability in Sofala Bank, especially in the central region near the main Zambezi delta mouth. However, the alongshore component of wind seems to play a role in pushing low chlorophyll offshore waters to the coast, decreasing chlorophyll concentrations in coastal waters. The river discharge increases during cold events of El Niño Southern Oscillation (ENSO) and decreases during the warm events. As a consequence, in the Sofala Bank area under the influence of the river discharge, positive chlorophyll concentration anomalies occur during La Niña and negative chlorophyll concentration anomalies are common during El Niño events, especially in the wet season. Significant inverse ENSO-precipitation relation observed over south of 15°S in the lower Zambezi, suggest that the ENSO signal in the coastal waters, over Sofala Bank is introduced by the Zambezi flow.

Keywords: Sofa Bank, suspended sediment, chlorophyll, remote sensing, Zambezi River discharge, wind, wave, ENSO.

Contents

List of Figures

List of Tables

Chapter 1

Introduction

1.1 Thesis topic and motivation

River discharges have great importance in physical and biogeochemical processes and productivity of continental shelves because the fresh water and sediments brought into marine environment affect directly in stratification variation, mixture and transparency of the water column, and provide nutrients for primary productivity (Lihan, et al., 2008; Piola et al., 2008). According to Wright and Nittrouer (1995), the process of transport of river-dispersed matter in coastal-marine environment involves several stages: (I) a turbid river-mouth effluent (plume) decelerates and deposits its higher density load immediately seawards of the mouth. (II) Sediment dispersal and dilution follows with gradual sedimentation and accommodation of remaining finer material; (III) waves, currents or slope-failure mechanisms cause re-suspension and transport of recently deposited sediments; (IV) final deposition and long-term net accumulation. In the Sofala Bank, in the central shelf of Mozambique the main river responsible for supplying the freshwater and sediment is the Zambezi River (Figure 1.2), the fourth Largest River in Africa and the largest African river flowing into the Indian Ocean. With the damming of the Zambezi Catchment for the construction of the Cohora Bassa hydropower, in 1984, the natural flow to Zambezi Delta and Sofala Bank started to change. After the construction of the dam, the annual variation of the flow became minimum and the natural seasonal differences between the wet and dry season started to be less pronounced (see Figure 1.3). Many studies have reported the negative effects of the damming in the lower Zambezi and the consequent reduction on freshwater and sediment load over the Zambezi Delta and Sofala Bank (e.g: Gammelsrod, 1996; Davies, et al., 2000; Chenje, 2000; Maueua, et al., 2007; Ronco, et al., 2010). The effects include reduced artisanal fisheries and shrimp industry productivity (Gammelsrod, 1996), saltwater intrusion (Chenje, 2000; Maueua, et al., 2007), reduction in sediment deposition and severe erosion over the Zambezi Delta and adjacent coastal regions (Chenje, 2000; Maueua, et al., 2007; Ronco, et al., 2010). Ronco, et al., (2010), for example, used a morphological model to simulate and predict the present and future effects of the presence of the Kariba and Cahora Bassa dams on the downstream morphology and concluded that the interception of freshwater and sediment loading in the dams have produced erosion of the Zambezi Delta. The rates of erosion along the central coast of Mozambique are worsened by the fact that this region presents the highest tides observed along the coast of Mozambique, which can reach values above 6 m during spring tides (Hoguane, 2007). Gammelsrod, (1996) examined the variation in the catch of shrimp in Sofala Bank outside the mouth of Zambezi River in relation to runoff and concluded that the alteration of seasonal variation in the runoff, due to the construction of Cahora Bassa dam, has caused reduction in fishery productivity. The effect of the Zambezi damming on the suspended sediments in Mozambique shelve have not been analyzed, despite their importance for marine ecology and coastal stability. However, it is presumed that

the quantity of sediments drained to the sea from the Zambezi River might have reduced significantly. In contrast to shrimp catch data, which include periods before and after the damming, the records of the suspended sediments for the period before the damming are scarce or unavailable, causing a limitation to infer the changes in sediment load to Sofala Bank, after the River regulation. The use of satellite images to estimate the suspended sediment concentration and the extent of the plume for periods before and after the damming would be a good alternative, but cloud-free images for the period before the construction of Cahora Bassa dam are also scarce. Even without having preterit data for comparisons, the main hypothesis of the present thesis is that since the actual seasonal variation in the Zambezi River runoff is very small, the Zambezi River discharge is currently not the main driving forcing in the seasonal variability of suspended sediment in Sofala Bank. Nevertheless, the Zambezi River discharge might still be the main source of nutrients and freshwater, constituting the main driving force for the seasonal variability of chlorophyll concentrations and salinity in the plume region. In contrast, the suspended sediments can be supplied by erosion and/or re-suspension, promoted by wind, waves or tides. Although El Niño southern oscillation (ENSO) is centered in the central Pacific Ocean, it influences global atmospheric circulation and Sea Surface Temperature, which in turn affect the precipitation patterns in Africa (Nicholson, 2000). Ward, et al., (2010) observed that ENSO has a significant impact on stream flows around the world, which suggests that ENSO effect can be observed in coastal and shelf waters under influence of River discharge. Saldías, et al., (2016) and Dogliotti, et al., (2016) observed a significant correlation between ENSO and turbidity plumes off central-southern Chile and Río de la Plata, respectively. In this context, in this work, spatial and temporal variability of suspended sediments and chlorophyll concentrations are estimated from Modis-Aqua satellite images and their relation to Zambezi River discharge, wind speed, waves and ENSO is evaluated.

1.2 Oceanographic conditions of the Mozambique Channel and Sofala Bank

Mozambique Channel

The Mozambique Channel (Fig. 1.1) is located between the African Continent and Madagascar island, it is bordered by the South Equatorial Current (SEC) in the north and by the East Madagascar Current (EMC) in the east. The circulation in the Mozambique Channel (MC) is dominated by large (> 300 km) anticyclonic eddies which move to the southerly direction (Ruijter, et al., 2002; Halo, et al., 2014). The flow variability is high in the west side of the channel and low in the east side (Lutjeharms, 2006). The anticyclonic eddies are preferably formed in the north part of the channel, near 12°S, in a frequency of about 4-5 eddies per year (Schoutena, et al., 2003) causing a net volume transport of about 40 Sv to the south (Halo, et al., 2014). The interaction between the anticyclonic eddies and the shelf have resulted in the formation of coastal lee eddy in areas where the orientation of the coast changes, such as Delegoa Bight in the south Mozambique Channel and Angoche in the north of Sofala Bank near

16°S (Lutjeharms, 2006). Ruijter, et al., (2002) suggests that after propagating to the southern Mozambique Channel, the eddies activate the retroflection of the Agulhas current, promoting in this way the exchange of properties between the Indian and Atlantic oceans. In the austral summer, the mean wind direction is uniformly from a southeasterly direction and weak, and during the winter, the northern part up to 15°S is influenced by the extension of the Indian Ocean Monsoon northeasterly winds, while the southern experiences southeasterly winds (Lutjeharms, 2006). The tides in the Mozambique Channel increase from about 2 m in the northern and southern extremes of the channel to about 5m in the central part (Lutjeharms, 2006).

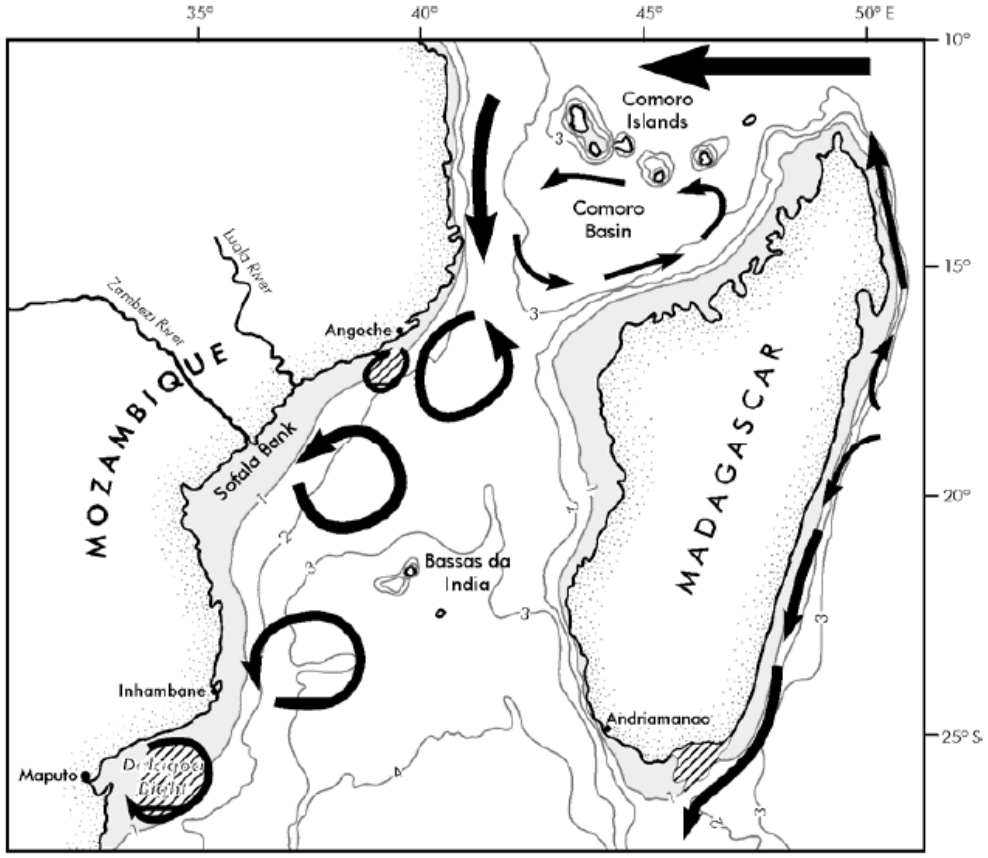

Figure 1.1: Bathymetry of the Mozambique Channel and continental shelf of Madagascar (in km) with the major circulation features. Sheded areas are shallower than 1 km; hatched areas denote upwelling. (souce: Lutjeharms, 2006).

Sofala Bank

Sofala Bank (Fig. 1.2) is a shallow and large shelf located in central Mozambique, extending from Angoche at about 17° S to Nova Mambone near 21° S. It is the largest continental shelf of East African coast with an area of nearly 50.000 Km^2. The productivity of Sofala Bank is highly enriched by the terrigenous input of nutrients from Zambezi River, one of the largest rivers in

Africa, and also by extensive mangroves that provide shelter and nursery ground for important fisheries and crustacean. The regional climate is humid subtropical with two seasons, dry and cold season (May to September) and hot and wet season (October to March). The Sofala Bank hosts the largest tides in the western Indian Ocean (Chevane et al., 2016), reaching about 6.4m of tidal range during spring tides, whereas in the southern and northern Mozambique is about 3 m (Hoguane, 2007). The morphology of the coastal zone of Sofala bank is characterized by flat land with an almost continuous fringe of mangrove swamps (Hoguane, 2007) and the seabed morphology in the central and northern Sofala Bank is flat, whereas the southern part of the bank is characterized by sandwaves due to strong tidal currents (WWF, 2004). Sofala Bank presents an estuarine environment due to the influence of freshwater from Zambezi River, which discharges over 3000 m^3/s on average per year (Gammelsrod 1992; Siddorn et al., 2001) contributing to almost of 85% of total freshwater discharged in Sofala Bank. The Zambezi annual runoff has reduced markedly since the years 1970s, because of regulation of the River by the Cahora Bassa dam, and the difference between flows of wet and dry seasons became less significant. The brackish water may move over oceanic water to about 50 km offshore and may extend to the full depth of water column, presumably because of the shallow nature of the bank and the combined effect of wind and tides (Lutjeharms, 2006; Nehama, 2012). At the southern end of the bank, between 20° and 21°S, there is a large expanse of coastline that is subject to inundation by seawater as result of extreme evaporation and over-transpiration in the mangrove swamps and salt marshes (Brinca et al., 1983; Silva, 1984). The ocean circulation in Sofala Bank is dominated by the passage of south going eddies on the Mozambique Channel (Saetre, 1985; Halo, et al. 2014) offshore the 50 m isobaths (Schulz et al., 2011) and a north going surface nearshore current (Saetre, 1985; Steen and Hoguane, 1990; Machaieie 2012), presumably forced by wind. Fine particles are transported by the longshore current system and deposited in two areas: (1) at the nearshore to northeast covered by muds with up to 50% sand and (2) at the outer shelf below 60 m depth covered by muddy sand with the mud content increasing towards the open waters (Schulz et al., 2011). Sediment transport at shallow depths is also affected by wave action and tidal currents, heavily influenced by monsoonal onshore winds and freshwater input from hinterland (Nehring et al., 1987). Sofala Bank has four water masses, namely: low salinity shelf water at the upper 15m and within 40 km from coastline; warmer oceanic surface waters that occur throughout the bank, at depths not exceeding 70m; deep oceanic waters from the sub-surface layer to the seabed; high salinity shelf water that occurs offshore more than 40 km from the coastline, at depths greater than 15 m (Nehama et al., 2015).

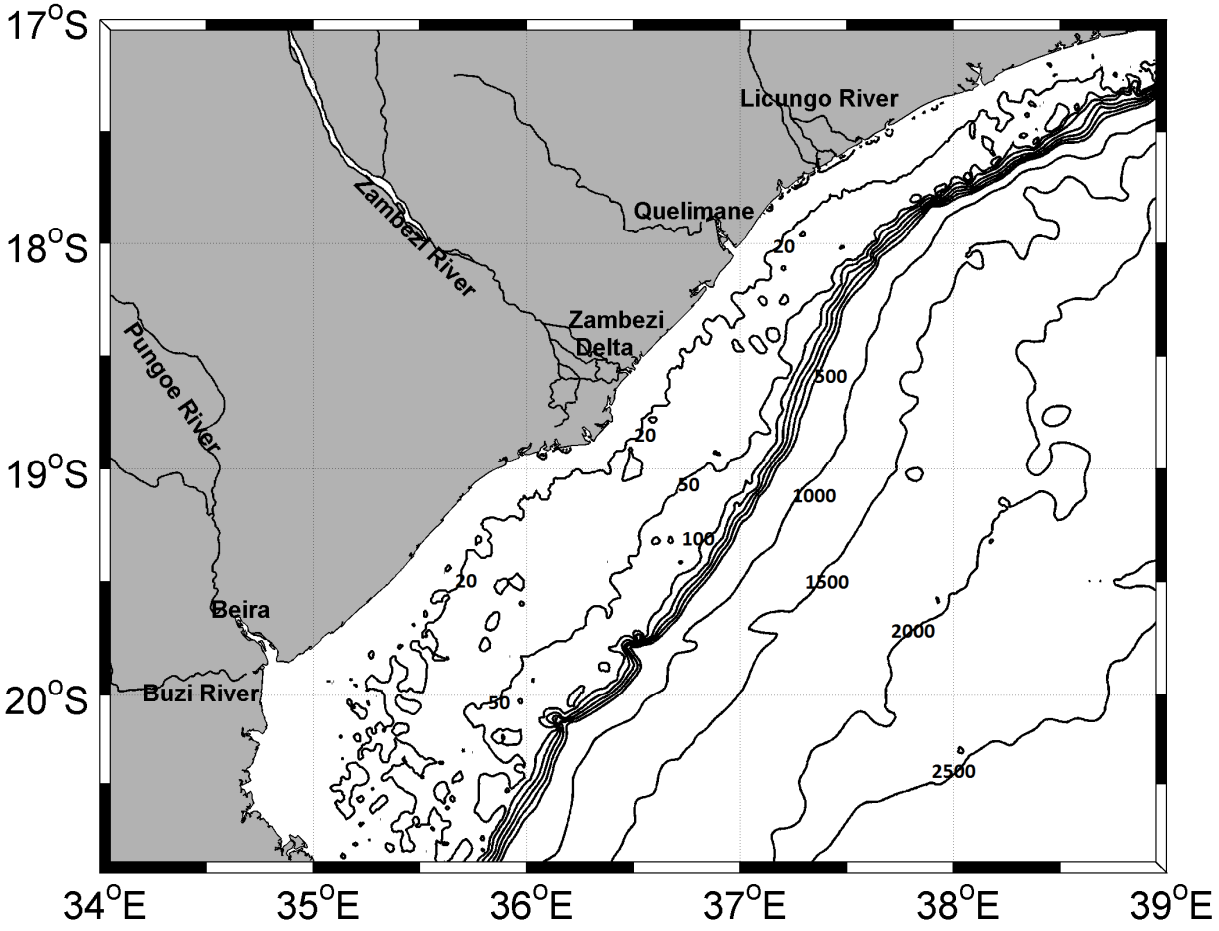

Figure 1.2: Map showing the Sofala Bank. The black lines indicate the [20 50 100 200 300 400 500 1000 1500 2000 2500] isobath which highlight the shelf break descending from about 50 m in the northern tip to about 100 m in the southern tip of the Bank.

1.3 Rationale of the hypotheses

The Zambezi River discharge has decreased significantly after the construction of Cahora Bassa dam, which entered into commercial operation in the year 1977. Figure 1.3 presents the monthly time series (upper left panel), climatology of monthly annual variation for 1955-19976 and 1977-2013 (b), wavelet power spectrum of the monthly time series (c) and its respective global spectrum (c) of Zambezi River discharge, measured at Tete station about 440 km from the main mouth of Zambezi River at Sofala Bank. During the period between years 1955 and end of years 1970, the monthly time series shows a very pronounced seasonal pattern, with river discharge varying between values greater than 10000 and less than 1000 m^3 s^{-1} between wet and dry seasons. From 1980s, period after the commercial operation of the dam, the amplitude between wet and dry seasons became very small, with the difference between high and low flow not

exceeding 1000 m^3 s^{-1} in most of the years and the seasonal pattern started to be less remarkable. Both climatologies of annual variation and wavelet power spectrum are in concordance with the pattern presented in monthly time series. The annual variation shows a very pronounced seasonal variation during 1955-1976 when the difference between the lower discharge observed during September-October and the higher discharge observed during February-March exceeded 4000 m^3 s^{-1}. During 1977-2013, the river discharge showed a decrease of about 2000 m^3 s^{-1} during the wet season and an increase in about 1000 m^3 s^{-1} during the dry season, if compared to the 1955-1976 period, but the seasonal variation became very weak denoting the regulation of the flow. The effect of regulation of the flow is also denoted by the relatively lower standard deviation in the 1977-2013 period. The impact of perturbation of natural flow is also revealed by the vanishing of 12-month periodicity presented in the wavelet power spectrum, which occurs precisely at the beginning of years 1980, just after the damming.

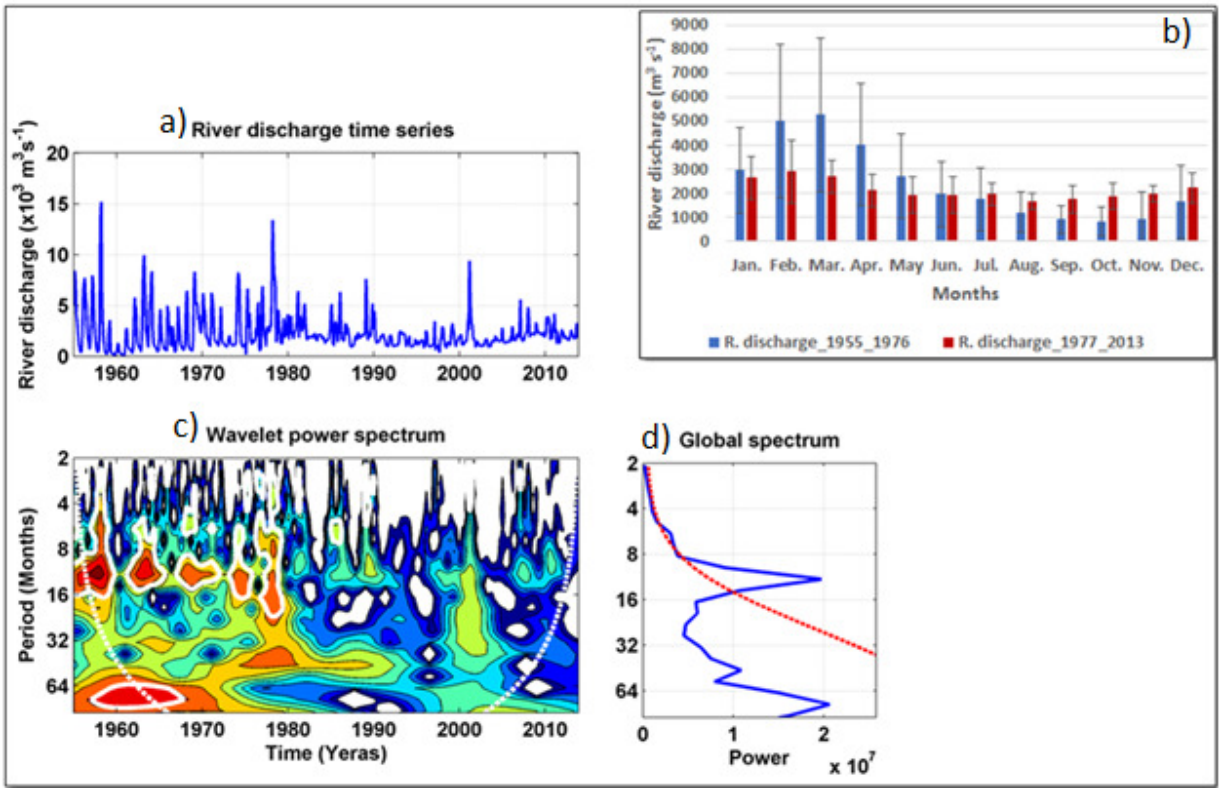

Figure 1.3: Monthly time series (a), climatology of monthly annual variation (b), wavelet power spectrum (c; the white line encloses the area with statistical significance greater than 95%) and its respective global spectrum (d; lower right, the blue thicker blue line enclosing areas with statistical significance greater than 95%) of Zambezi River discharge, measured at Tete station about 440 km from the main mouth of Zambezi River at Sofala Bank

Based on the reduction of the seasonal amplitude of the Zambezi River discharge mentioned above, the following hypotheses were raised to be tested in this thesis:

- ✓ In recent years, the Zambezi River discharge is not the main forcing of the seasonal variability of suspended sediment plume in Sofala Bank.
- ✓ The supply of suspended sediments by wind and waves through erosion and re-suspension on the Sofala Bank might be more important than the supply from Zambezi River discharge.
- ✓ The Zambezi river discharge is still the main forcing making significant changes in salinity and chlorophyll over the plume area.
  Salinity and chlorophyll concentration co-vary with river discharge but other forcings such as the wind and local circulation may play a significant role.
- ✓ El Niño southern oscillation influences the precipitation in the lower Zambezi, and therefore the Zambezi River discharge. Its signal might be observed along the regions under influence of Zambezi River in Sofala Bank.

1.4 Objectives

General objective

The main aim of this thesis is to study the spatial and temporal variability of satellite-estimated suspended sediment and chlorophyll over Sofala Bank, Mozambique, and their relation to environmental variables.

Specific objectives

The specific objectives of the thesis are as follows:

- ✓ To describe the seasonal variability of satellite-estimate suspended sediment concentration
- ✓ To evaluate the influence of Zambezi River discharge, wind speed, waves and ENSO on the variability of suspended sediment concentration
- ✓ To describe the seasonal variability of precipitation in Lower Zambezi basin
- ✓ To evaluate the inter-annual and inter-decadal influence of ENSO on precipitation variability over the Lower Zambezi basin
- ✓ To describe the seasonal variability of satellite-estimated chlorophyll concentration over Sofala Bank

- ✓ To evaluate the influence of Zambezi River discharge, winds and ENSO on the variability of chlorophyll concentration over Sofala Bank.

1.5 General description of the research methodology and outline of the thesis

Dataset

The main dataset used in the research are as follows:

- ✓ Daily and monthly means of Zambezi River discharge measured at the hydrographic station of Tete, located about 440 km from the main mouth of Zambezi River at Sofala Bank, and during the period between 1955 and 2015 were provided by the national directorate for water affairs of Mozambique.

- ✓ In situ remote sensing reflectance, suspended sediments, salinity and Secchi depth and water depth of the sampling stations, collected over the Sofala Bank during an oceanographic cruise held on 1st-5th April 1998 in the Sofala Bank.

- ✓ Daily, 8-days and month-composites images of remote sensing reflectance, chlorophyll concentration and Sea Surface Temperature (SST) from Modis-Aqua satellite sensor, covering the period between 2003 and 2013.

- ✓ Monthly zonal and meridional components of NCEP/NCAR Reanalysis wind speed at 10m above the surface, of 2.5° spatial resolution, covering the period between 2003 and 2013, was downloaded from the website of NOAA Physical Sciences Division of National Oceanic and AmosphericAdmistration (NOAA-PSD).

- ✓ Daily zonal and meridional wind components of gridded and blended sea surface vector winds from multiple satellites components (u and v) at a reference height of 10m above the surface, for the period between 1998 and 2015, with a spatial resolution of 0.25°, obtained at NOAA National Climat Data Center (NOAA-NCDC) website.

- ✓ Monthly installments of 0.5° spatial resolution global wave hindcasts done using the NOAA WAVEWATCH III model, covering the period between 2006 and 2013, download from NASA's website.

- ✓ The monthly Niño 3.4 index data for the period between 1998 and 2017 was obtained from the Physical Sciences Division (PSD).

- ✓ The monthly TRMM 3B43 version 7 NASA's standard precipitation products, of 0.5° spatial resolution, for the period between 1998 and 2017, downloaded from NASA's website.

- ✓ Monthly means of precipitation data derived from the IPCC AR5 Global Circulation Models covering the region of Africa for the period between 1850 and 2100, provided on storage media by the German Climate Computation Center (DKRZ).

Main topics and methods

The main topics covered in the thesis are the variability of suspended sediment plumes and chlorophyll concentrations in the Sofala Bank and the influence of ENSO on spatial and temporal variability of precipitation in the lower Zambezi basin. There is also a short description on chlorophyll and Sea Surface Temperature patterns and influence of mesoscale eddies on the drifting of coastal, chlorophyll enhanced coastal waters, to the mid-Mozambique Channel.

Basically, three different approaches were used for evaluation of the variability of suspended sediment plume, namely, estimation of the area and concentration variability using the green band of normalized water leaving radiance at 555 nm (nLw555), mapping of the variability of the area through applying spectral linear mixing analysis on Landsat satellite images and estimation of the concentrations of total, inorganic and organic suspended sediments from in situ remote sensing reflectance.

The spatial and temporal variability of chlorophyll concentrations were evaluated through monthly climatology of Modis-Aqua satellite-derived chlorophyll.

The spatial and temporal variability of precipitation over the lower Zambezi was performed combining monthly means of TRMM 3B43 version 7 NASA's standard precipitation products and monthly means of precipitation data derived from the IPCC AR5 Global Circulation Models.

The evaluation of the relationship between the variation of suspended sediment plume, chlorophyll concentration and environmental forcings, such as river discharge, wind speed, waves and ENSO was mainly made through correlation and regression analysis. The spatial variability of the correlation coefficient obtained applying regression analysis on the time series of suspended sediment, chlorophyll and precipitation against the forcing parameters was used to evaluate the spatial variation of the influence of each of the forcing parameters analyzed in this work.

The thesis is organized into seven chapters. Chapter 1 provides the introduction, which includes the presentation of the thesis topic and motivation, objectives, rationale of the hypotheses and general description of the research methodology. Chapter 2 presents the application the green band of normalized water leaving radiance at 555 nm (nLw555) to map the variability of suspended sediment plume. Chapter 3 presents the variation of the concentrations of total, inorganic and organic suspended sediments estimated from in situ remote sensing reflectance.

Chapter 4 presents the mapping of suspended sediment plume applying spectral linear mixing analysis on Landsat satellite images. Chapter 5 presents the evaluation of short and long-term ENSO-precipitation relation in lower Zambezi using TRMM Multi-satellite Precipitation Analysis (TMPA) and AR5 Global Climate Models (GCMs). Chapter 6 presents the variability of satellite measured chlorophyll concentrations and its relation to local and remote forcings. Chapter 7 presents a synthesis of the main conclusions, which includes the integration of the results and the main findings.

Chapter 2

Satellite assessment of spatial and temporal variability of satellite estimated suspended sediment plume in Sofala Bank and its relation to environmental variables: Evidence of Zambezi River decreased sediment supply

Abstract: Monthly composites of normalized water leaving radiance at 555 nm (nLw555) from Ocean color imagery from MODIS (Moderate Resolution Imaging Spectroradiometer) onboard the Aqua platform are used to characterize the spatial and temporal variability of suspended sediment plume in Sofala Bank and its correlation to Zambezi River discharge, winds, and waves. Climatology of monthly mean of nLw555 revealed that both suspended sediment plume dispersion and concentration are higher during July-December and low during January-June. High positive correlations of both wind speed and wave significant height to nLw555 monthly time series were obtained, suggesting that the variation of suspended sediment in Sofala Bank is mainly controlled by erosion and re-suspension by wind and wave rather than the Zambezi River discharge. The southern portion of Sofala Bank presents higher nLw555 values and hence higher suspended sediment concentration, if compared to the center region near Zambezi river mouth and northern region, near Licungo river mouth. The high concentrations of suspended sediments in the southern region might be associated to the relatively higher importance of Pungue and Buzi Rivers than dammed Zambezi River in supplying sediments, or to higher re-suspension, due to local tide ranges and shallower bathymetry in the south Sofala Bank. The dominance of wind and waves in controlling the variability of suspended sediments and the eventual relatively greater contribution of Pungue and Buzi River than the Zambezi in supplying sediments show evidence of weakening of Zambezi River supply of sediments, which might have started after damming the Zambezi Catchment.
Keywords: Sofala Bank, suspended sediments, remote sensing, nLw555

2.1 Introduction

Coastal waters are in many cases characterized by high concentrations of organic and inorganic suspended sediments brought by river discharges. River discharges influence physical and biogeochemical processes and primary production of continental shelves because freshwater and sediments brought to marine environment impact directly in stratification and light attenuation of water column, and provides nutrients for primary production (Zavialov et al., 2003; Lihan, et al., 2008; Piola et al., 2008). The plume dynamics is driven by a variety of factors such as river discharge, wind stress, buoyancy currents and tidal currents (Durand, et al., 2002; Warrick, et al., 2007; Liu, et al. 2008). After a long period of special attention to study plumes from large rivers

such as Amazon, Mississipei and La Plata, in recent decades, there has been a significant increase of studies addressed to smaller plumes (e.g. Siddorn et al., 2001; Nezlin et al., 2005; Warrick, 2007) in recognition of their relevance argued by higher ratio of plume area to discharge rate (Warrick and Fong, 2004). The freshwater and its respective suspended matter supplied by Zambezi, Licungo, Buzi and Pungue rivers in Sofala Bank, the western side of Mozambique Channel, is believed to have high influence in secondary coastal production along central shelf of Mozambique (Lutjeharms, 2006; Nehama 2012), and therefore, understanding its variability is of great importance. Despite its importance, as far as we know, the seasonal variability of the Zambezi River suspended sediment plume and its actual main forcing, have not been studied. As well as, the influence of the dams on the Zambezi discharge variability was not yet investigated. The main inconvenience for monitoring plume variability for a long time span in extensive areas, such as Sofala Bank, are the high costs of oceanographic surveys. Many studies have demonstrated the potential of ocean color remote sensing for water quality monitoring in coastal zones (e.g. Nezlin and DiGiacomo, 2005; Warrick et al., 2007; Nezlin et al., 2008; Lahet and Stramski, 2010). Sediment plume, in particular, can easily be distinguished from adjacent oceanic waters due to high backscattering in longer wavelengths of the visible region of the spectrum, caused by higher suspended sediment concentration (Toole and Siegel, 2007). Toole and Siegel, (2001) also found that the maximum correlation between in situ remote sensing and lithogenic silica (which is one of the elements of terrigenous sediments) in moderated turbid waters of Santa Barbara Channel is at 555 nm. The green band is often used to map low to moderate turbid plumes like Sofala Bank (e.g. Nezlin and DiGiacomo, 2005; Thomas and Weatherbee, 2006; Nezlin et al., 2008; Lihan, et al. 2008; Lahet and Stramski, 2010; Saldías et al., 2012) because of its sensibility to variation in suspended sediments and because the light in this band is less absorbed by water. In this study, we use normalized water leaving radiance at 555 nm (nLw555) from ocean color imagery from MODIS (Moderate resolution spectroradiometer) onboard the Aqua platform, to characterize the spatial and temporal variability of suspended sediment plume in Sofala Bank and its relation to Zambezi River discharge, wind speed and waves.

2.3 Study area

Figure 2.1 represents the map of Sofala Bank, located between latitudes 17-21°S and between longitudes 34-49°E.

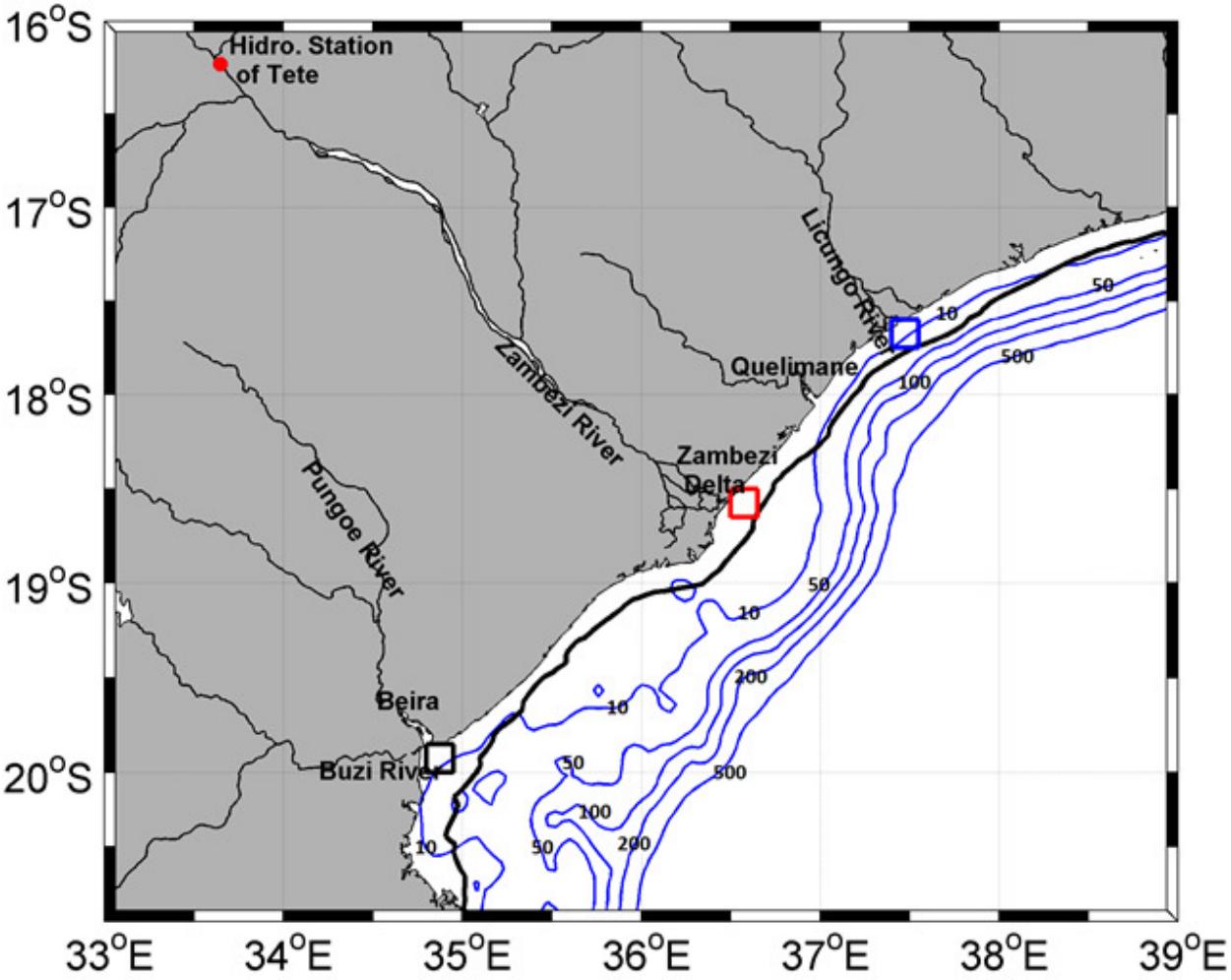

Figure 2.1: Map showing the study area. The black, red and blue boxes are the small domains used to compare the suspended sediment concentrations in southern, central and northern regions of Sofala Bank. The black line represents the isoline of 1.0 mW cm^{-2} μm^{-1} sr^{-1} nLw555 indicating the mean position of sediment plume edge. Note that each box is placed within the mean plume edge and in front of the main river mouths. The blue lines indicate 10, 50, 100, 200 and 500 m isobaths.

2.3 Data and methods

Data

A total of 132 images of monthly composites of normalized water leaving radiation at 555 nm (nLw555) from Ocean color imagery from MODIS (Moderate Resolution Imaging Spectroradiometer) onboard the Aqua platform. The images were analyzed together with wind, waves and river discharge data, to study the multitemporal variability of turbidity plume in

Sofala Bank and its relation to each of these forcings during 2003-2013 period. The images have spatial resolution of 4 km and were downloaded in Giovanni platform (http://giovanni.gsfc.nasa.gov) on 15th August 2015. Monthly mean of Zambezi river discharge, measured at Tete hydrographic station, located at about 440 km upstream the main Zambezi river mouth (Fig. 2.1) was provided by the national directorate for water affairs of Mozambique. Monthly zonal and meridional components of wind from NCEP/NCAR Reanalysis (Kalnay et al., 1996) at 10 m above the surface, with 2.5 km spatial resolution were downloaded in the website of the National Center for Environmental Prediction (NCEP) was downloaded in the website of NOAA Physical Sciences Division (https://www.esrl.noaa.gov/psd/data/gridded/data.ncep.reanalysis.derived.surface.html) on 7th September 2015. The daily wind blended sea surface at 10 m above the surface, with 0.25 ° (Zhang et al., 2006) from NOAA/NCDC was downloaded in https://www.ncei.noaa.gov/thredds/blended-global/oceanWinds.html on 8th March 2017. Monthly installments of 0.5° spatial resolution global wave hindcasts done using the NOAA WAVEWATCH III model and GFS wind analysis (Tolman, 2009) for the 2005-2013 period was downloaded in ftp://polar.ncep.noaa.gov/pub/history/waves/multi_1 on 27 February 2017.

Methods

The first step to evaluate the variability of plume extension and intensity was the delineation of the plume edge. The basic concept is that the variation in the area covered by sediment plume and concentration of suspended sediments is a result of the variation in river discharge and/or wind stress through freshwater input (by the river), sediment plume dispersion and/or sediment re-suspension (by wind stress). To identify the value of nLw555 that best characterize the sediment plume edge, for each image, threshold levels of spatial areas covered by nLw555 were correlated to river discharge and wind, which are assumed to be the main forcings of variation in suspended sediment concentration. The values of nLw555 for threshold levels of sediment plume edge varied from 0.25 to 2.25 with a spacing of 0.25, and the one that presented maximum correlation with one or both of the forcings (river discharge and wind speed) was taken as sediment plume edge in Sofala Bank. This approach was also used in previous studies about river plumes (eg: Nezlin and DiGiacomo, 2005a; Lahet and Stramski, 2010; Saldías, et al. 2016; Fernandez-Nóvoa, et al., 2017). The area was calculated by counting the number of pixels with nLw555 values equal to or above the plume edge value. To infer the reliability of monthly correlation in a daily timescale, a time series of daily nLw555 within the plume edge determined from monthly composites, with daily Zambezi River discharge, and Daily blended sea surface winds. Monthly climatology of spatial variation of nLw555 was analyzed to infer the variability of plume morphology and concentration of suspended sediment in Sofala Bank. Monthly average of nLw555 within the whole plume area and each of the three 22 x 22 km boxes located near Pungue and Buzi mouth (in the south), Zambezi Delta mouths (in the center), and Licungo River (in the north) were determined. These nLw555 monthly time series were used to access the

temporal variability of suspended sediments in Sofala Bak as a whole and compare with much detail the concentrations in south, center and north regions. For each region, one-way Analysis of Variance (ANOVA) was performed to evaluate the significance of differences among the groups following the description in Weiss (2006). The relation between the suspended sediment plume and river, wind speed and waves was accessed using two approaches of linear regression analysis. The first approach was to correlate and plot together with the time series of mean nLw555 within the plume area and the time series of each of these forcings, which gives the general overview of temporal variability. The other approach was to perform a linear regression between the time series of nLw555 maps and time series of each forcing parameter to access their spatial influences in the variability of suspended concentrations. For wind speed, it was considered the monthly time series of areal average over Sofala Bank. For wave Hs, the 0.5° spatial resolution was re-gridded to 4 km to match the resolution of nLw555 so that the regression was performed for time series of each grid. Empirical Orthogonal Function (EOF) was performed on nLw555 image time series in order to infer the dominant modes of spatial and temporal plume extent following the description in Emery and Thomson (2001). The plume extent was taken as the extension between the coast and the plume edge.

2.4 Results and discussion

Figure 2.2.1 shows the statistical results for sediment plume estimation through regression of nLw555 thresholds to river discharge and wind stress. The best correlation of 0.6, found between 1.0 m W cm^{-2} μm^{-1} sr^{-1} threshold and wind speed and thus 1.0 m W cm^{-2} μm^{-1} sr^{-1} is taken as the outer edge suspended sediments plume. The best correlation between river discharge nLw555 was about -0.3.

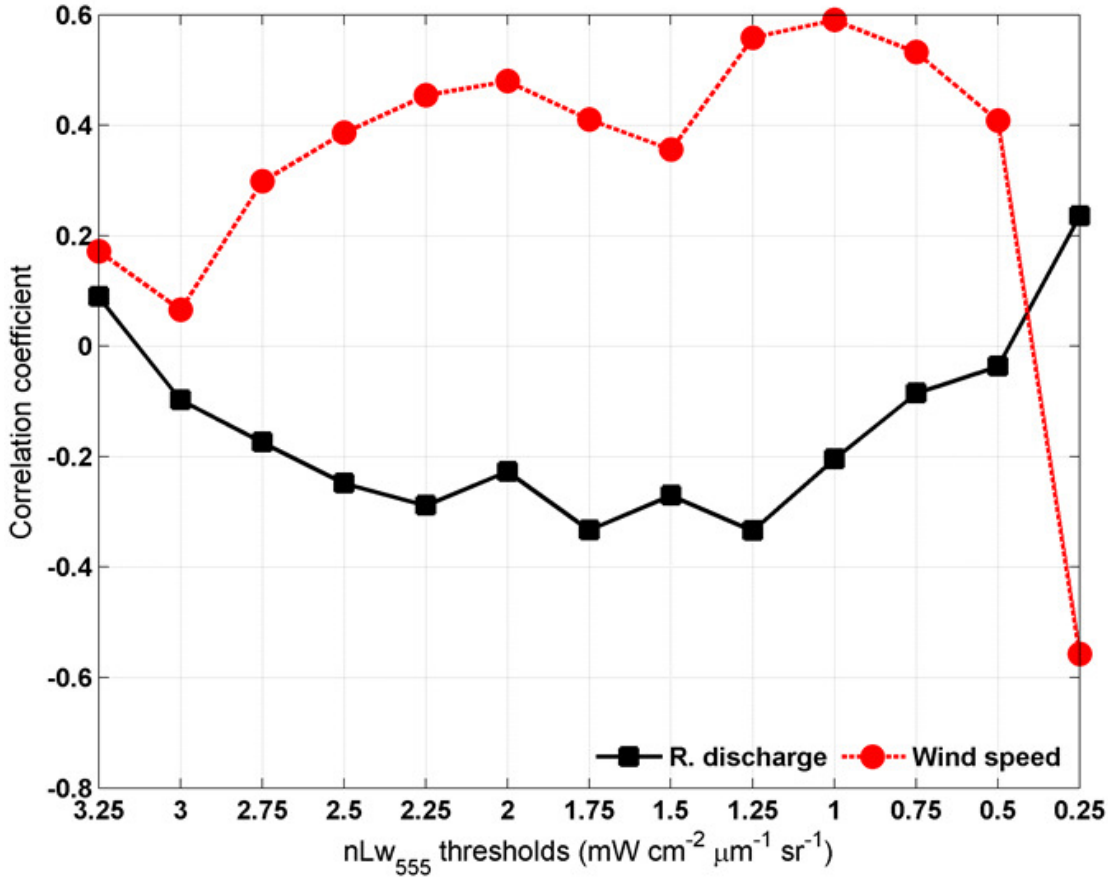

Figure 2.2.1: Correlation coefficient between plume extension for different thresholds levels of nLw555 and monthly river discharge (in black) and wind speed (in red). The threshold values start from higher value to lower to illustrate the nLw555 variation from the coast offshore.

Figure 2.2.2 shows the statistical output of regression between time series of mean nLw555 within the plume area (nLw555 >= 1.0 mW cm^{-2} μm^{-1} sr^{-1}), extracted in 37 level 2 daily Modis-Aqua images for the period between 2009 and 2011 and daily river discharge and wind speed. The statistical outputs for daily analysis also show that the best relationship is found between nLw555 threshold and wind speed, which reinforce the findings of the monthly analysis. The relatively weaker negative correlation between river discharge and the positive relationship between wind speed and nLw555 are both kept in the daily analysis. The higher amplitudes in wind correlation coefficient along the time denotes its dynamics nature in both intensity and direction. It is worth mentioning that negative correlation between river discharge and the thresholds of plume extensions, found in the present study, is uncommon if compared to other studies that correlated thresholds of Normalized water Leaving Radiation and accumulated amount of water or river discharge (e.g. Nezlin and DiGiacomo, 2005; Lahet and Stramski, 2010; Fernandez-Nóvoa, et al. 2017). Nezlin and DiGiacomo, (2005) and (Lahet and Stramski, (2010) found strong positive correlation between nLw555 threshold and accumulated amount of

precipitation in along the São Pedro shelf (Southern California) while Fernandez-Nóvoa, et al., (2017) found strong positive correlation between nLw645 thresholds and the discharge of Tagus River (Spain).

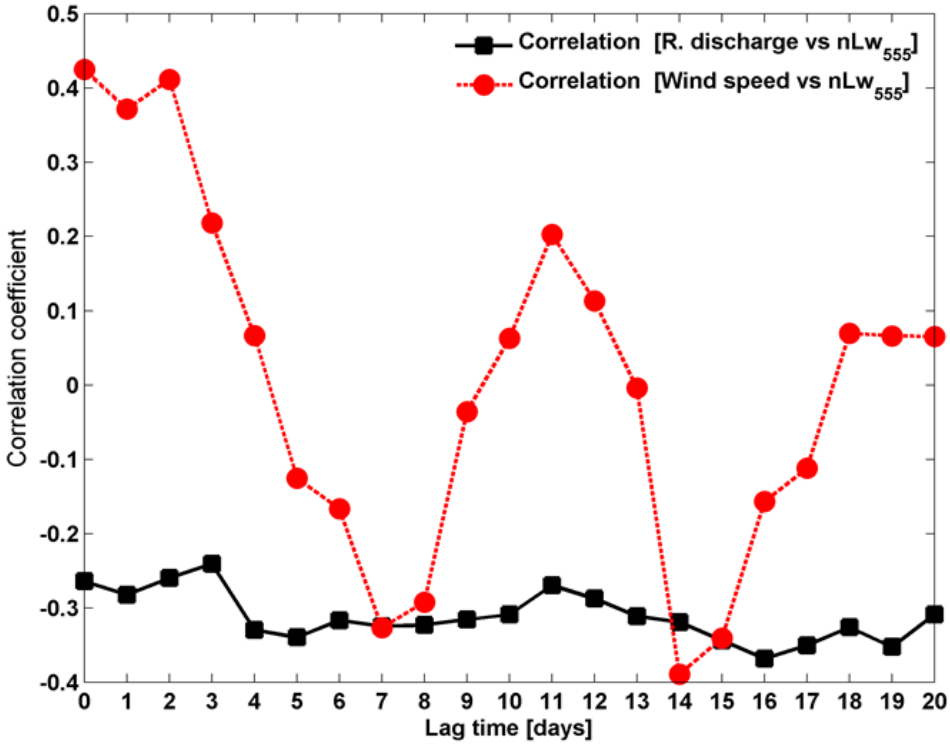

Figure 2.2.2: Correlation coefficient between daily mean nLw555 values inside the plume and daily river discharge and wind speed. Note that the correlation was performed for different lag times.

Figure 2.3 presents the climatology of seasonal variation of plume extension and concentration of suspended sediment, traced by nLw555. Looking at the annual variability of the 1.0 m W cm^{-2} μm^{-1} sr^{-1} isoline (black line) in relation to the coast, one can see that it does not vary much over the year, such that it does not exceed the 50 m isobaths in all twelve months. On the other hand, the variation of suspended sediments traced by variation of nLw555 shows much significant spatial and temporal variations. It is possible to distinguish two main regimes of suspended sediment plume throughout the year. During the period between January and June, the plume extension is relatively narrow, especially at about ~19.5 °S, 35.5°E, between Zambezi Delta in the center and Pungue and Buzi Rivers in the south Sofala Bank. During this period the concentration of suspended sediments is also lower, with nLw555 values less than 2.0 m W cm^{-2} μm^{-1} sr^{-1} in central and north regions and less than 2.5 m W cm^{-2} μm^{-1} sr^{-1} in the south coast of Sofala Bank. During July-December, the plume extension is relatively wider and the

concentration is relatively higher, with nLw555 values greater than 2.5 m W cm^{-2} μm^{-1} sr^{-1} near Pungue and Buzi Rivers in the south and near Licungo River in the north and about 2.0 m W cm^{-2} μm^{-1} sr^{-1} in the central Sofala Bank. During July-December is seems that the south and central plume cores merge and drift to the north Sofala Bank in conformity with findings of Siddorn, et al., (2001).

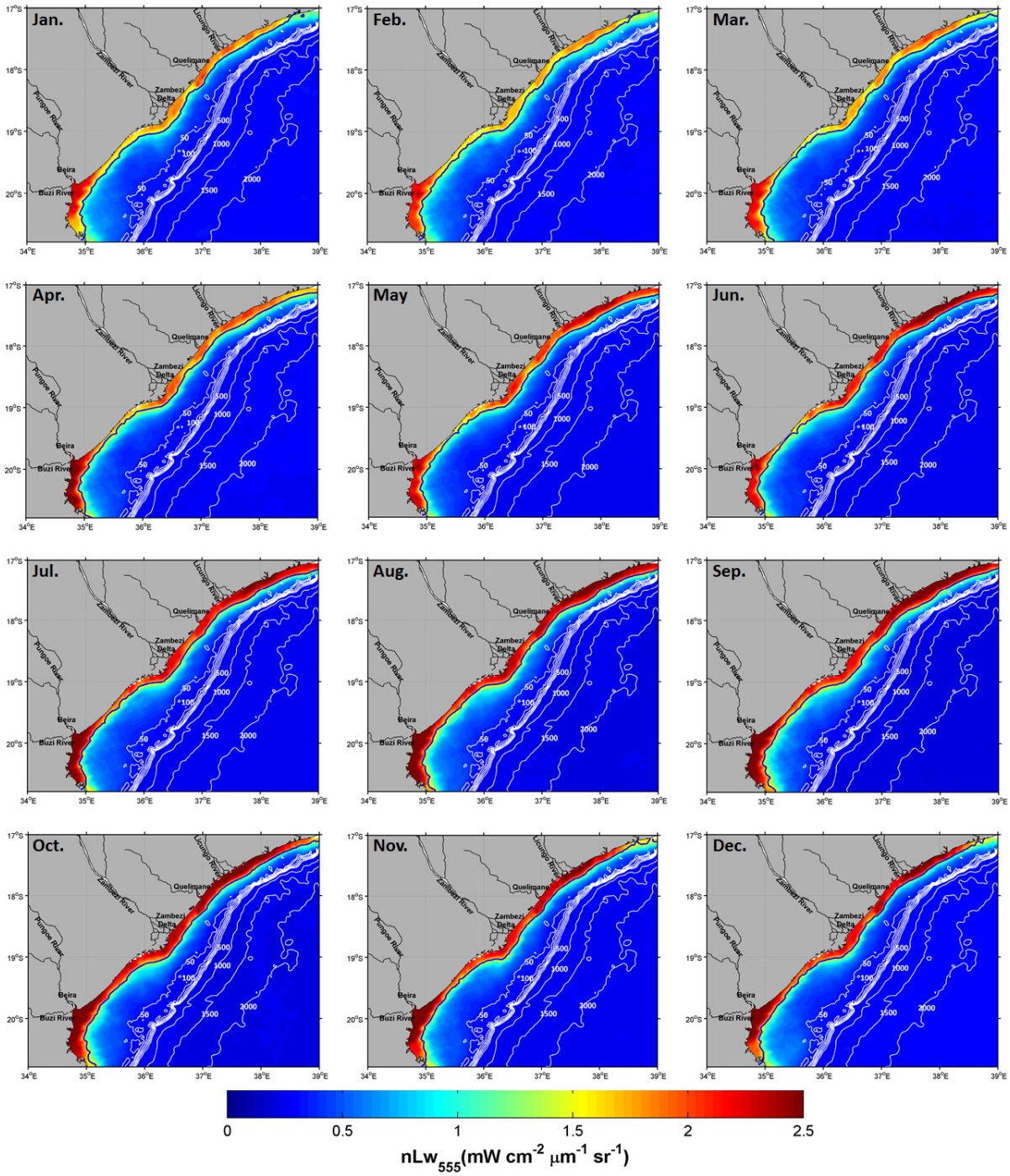

Figure 2.3: Climatology of seasonal variation of nLw555 over Sofala Bank for the period of 2003-2013. The black line represents the sediment plume edge (1.0 mW cm^{-2} μm^{-1} sr^{-1}), estimated from statistical regression

Comparing climatology of the annual variation of suspended sediment plume with annual variations of Zambezi River discharge and wind speed and direction presented in Figures 2.4a and 2.4b, it is possible to note that the variability of suspended sediment plume shows to be more related to wind speed rather than river discharge. Figure 2.4a shows an overlap of the monthly climatology of mean Zambezi River discharge and monthly climatology of mean nLw555 within the plume area during the 2003-2013 period. Although it does not present larger variations between the minimum and maximum flows since the damming of the Zambezi Catchment, the Zambezi river discharge still have two regimes. The high regime extends between October and April with a maximum mean discharge of about 2600 m^3 s^{-1} in February and the low regime extends between May and September with a minimum value of about 1800 m^3 s^{-1} in August. The nLw555 can also be divided into two main regimes, whose temporal sequence is almost an inversion of that of Zambezi River discharge. The high regime of nLw555, whose values are above 1.8 mW cm^{-2} μm^{-1} sr^{-1}, are observed between July and December with an annual peak of about 2.2 mW cm^{-2} μm^{-1} sr^{-1} in September. The minimum annual mean nLw555 is about 1.55 mW cm^{-2} μm^{-1} sr^{-1} and is observed precisely in the month of maximum river flow. The wind speed, in its turn, shows similar variation to nLw555, with a sharp increase from 2 m s^{-1} in February to its peak in October, followed by a steeper decreasing to about 2.8 m s^{-} in December. In our view, the quasi-inverse relation between the annual variation of Zambezi River discharge and suspended sediments proxied by nLw555 is not related to the river discharge and delivery of suspended sediments, otherwise, it is believed that the wind speed, is the main controller of suspended sediments availability (at least when compared to river discharge). The Zambezi river discharge still supplies sediments to Sofala Bank, however, it is no longer driving the seasonal variations due to regulation of the flow in Zambezi Catchment. The difference between the minimum and maximum mean river discharges during 2003-2013 is 800 m^3 s^{-1}, which is only 2% of the 4000 m^3 s^{-1} discharge rates observed from 1955-1976, before the construction of Cahora Bassa dam.

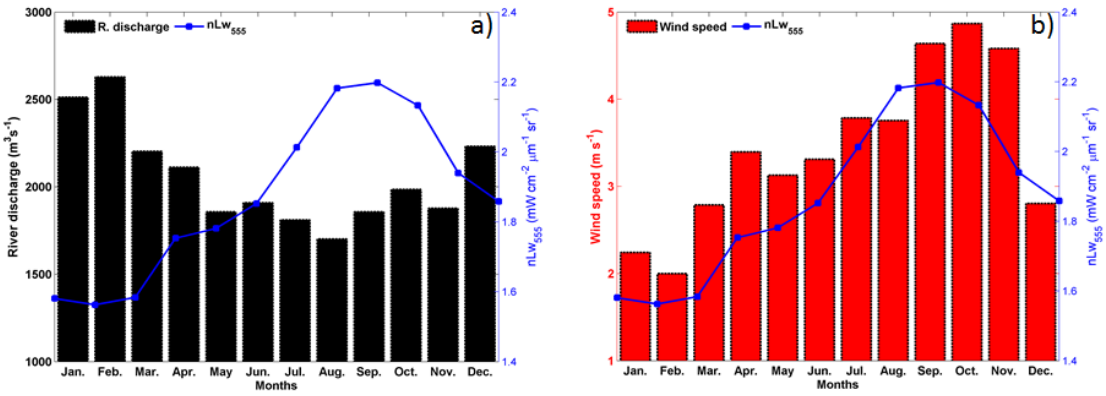

Figure 2.4: Overlap of the climatology of seasonal variation of Zambezi River discharge with nLw555 (a) and wind speed with nLw555 (b) for the 2003-2013 period. The monthly mean nLw555 used to compute the seasonal climatology was extracted from the mean plume area estimated through linear regression.

Figures 2.5 show spatial variations and temporal amplitudes first four modes of zonal variation of plume extent in relation to the coastline, determined from EOF analysis, representing 65.6, 9.4, 5.7 and 2.2 % of the variance, respectively. In general, the four spatial modes present similar patterns, with a wider extension of suspended sediments plume offshore in the south region, ~20.0 °S close to Pungue and Buzi River mouths, and narrowest extension between ~19.5 °S between Zambezi Delta and Pungue and Buzi River mouths. The similarities of the four spatial EOF modes reinforce the findings from annual climatology, which showed that the suspended sediment plume varies more in intensity (sediment concentration) rather than in dispersion offshore.

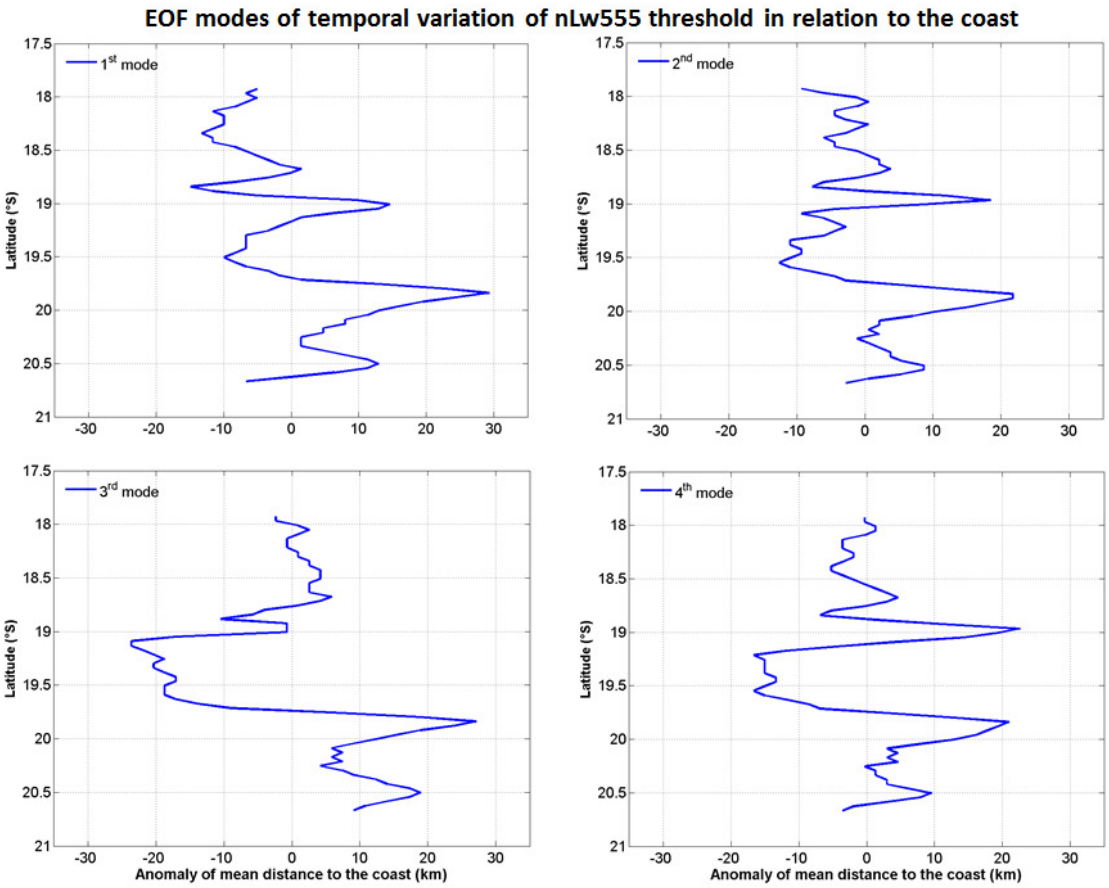

Figure 2.5: EOF modes of zonal variation of suspended sediment plume extent in Sofala Bank. The extent was taken as the distance from the coastline to the line of nLw555 equal to 1.0 mW cm^{-2} μm^{-1} sr^{-1}.

Table 2.1 presents monthly mean time series of nLw555 for north, center and south regions of Sofala Bank, F statistic, F critical and P-value found in one-way ANOVA to evaluate the significance of differences in nLw555. Both F statistic (> F critical) and P value (= 0.00) suggest that the nLw555 in north, center and south Sofala Bank are statistically different. The south region presents the highest nLw555 mean of about 2.45 mW cm^{-2} μm^{-1} sr^{-1}, followed by the north region, which has a mean of about 2.1 mW cm^{-2} μm^{-1} sr^{-1} while the center region presents the lowest nLw555 mean value of about 1.97 mW cm^{-2} μm^{-1} sr^{-1}. These findings imply that despite receiving a higher volume of river discharge, the center region, near Zambezi River Delta, presents lower suspended sediment concentrations than the south region, near Pungue and River mouth, and the north region, near Licungo River.

Table 2.1: Monthly mean values of nLw555 for each region of Sofala Bank and resulting variance analysis for a critical value of 0.001.

Parameter	North	Center	South	F calculated	F critical	P
nLw555(mW cm^{-2} μm^{-1} sr^{-1})	2.1003	1.9764	2.4518	59.4720	3.0186	0.00

Table 2.2 presents statistical outputs of regression of MODIS nLw555 against river discharge, wind speed, and wave Hs. The river discharge correlates weak and negatively to nLw555 (R=-0.36, p-value=0.00). The wind speed and wave Hs correlate strong and positively to nLw555 with correlations coefficients equal to 0.8 and 0.61, respectively and p-values equal to zero. Analogously to findings from climatology of annual variation, wind speed and waves show to be the main forcing of the variability of suspended sediment plume. The fact that wind speed and wave Hs are the main forcings of suspended sediment variability suggests that the main source of suspended sediments in Sofala Bank is local and through erosion and re-suspension. Accounting that most eroded and re-suspended sediments are transported and deposited in deep waters and that the volume of freshwater and sediments have presumably diminished in recent years as presented in Figure 1.3, the actual relationship between suspended sediments concentration (traced by nLw555) indicate a possible unbalance between lost and replacement of sediments along Sofala Bank.

Table 2.2: statistical outputs of the regression of MODIS nLw555 against river discharge, wind speed and, wave Hs.

MODIS nLw_{555}	R. discharge	Wind speed	Wave Hs
R	-0.36	0.80	0.61
R^2	0.13	0.64	0.37
RMSE	0.22	0.14	0.19
p-value	0.00	0.00	0.00

Figure 2.6 shows scatterplots of calibration and validation data set for the estimation model of MODIS nLw555 from river discharge, wind speed and wave Hs (a) and from wind speed and wave Hs (b). The coefficient of determination (R^2) decreases from 0.81 when the nLw555 is estimated from river discharge, wind speed and wave Hs to 0.71 when the river discharge is removed from the estimation model. For validation, in turn, the R^2 increases from 0.68 when all the three variables are used, to 0.72 when the river discharge is removed from the model. The RMSE increases by an order of 0.01 for the calibration and remains the same for the validation when the river discharge is removed. The improvement of R^2 when the nLw555 is estimated from wind speed and wave, without considering the river discharge reinforce the relative importance of these two forcings on the variability of the concentration of suspended sediments. The equations 2.1 and 2.2 present the empirical model to retrieve nLw555 from river discharge, wind speed and wave Hs (2.1) and from wind speed and wave Hs (2.2).

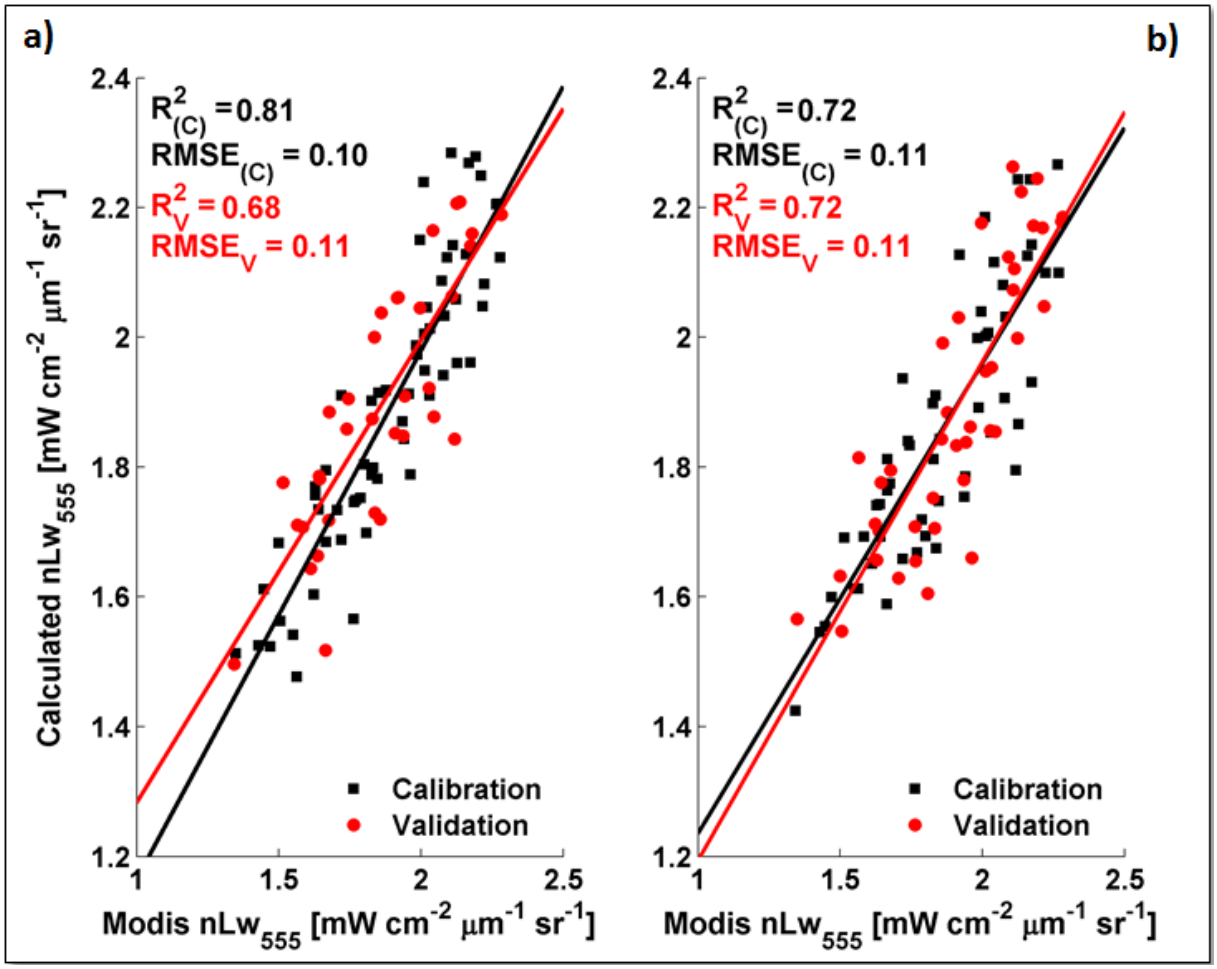

Figure 2.6: Scatterplots of measured MODIS nLw555 against estimated MODIS nLw555 for calibration and validation data set. In Figure 2.6a, the nLw555 is estimated from river discharge, wind speed and, wave and in Figure 2.6b, it is estimated from wind speed and wave Hs (b).

MODIS nLw555 = 0.807 – 1.1 x 10^{-4} (R. discharge) + 0.185 (wind speed) + 0.806 (wave Hs). (eq. 2.1)

MODIS nLw555 = 0.541 + 0.235(wind speed) + 0.806 (wave Hs). (eq. 2.2)

Figure 2.7 shows the overlap of time series of Zambezi River discharge and mean nLw555 within the plume area (a), wind speed and mean nLw555 (b) and wave Hs and mean nLw555 (c). At first sight, it is possible to note that the variation in nLw555 does not accompany the variation in river discharge. While the river discharge starts with a decreasing to its minimum value of about 1000 m^3 s^{-1} in middle 2003, the nLw555 increases to its maximum value of about 2.0 mW cm^{-2} μm^{-1} sr^{-1} in middle 2003. The river discharge presents three distinct long scale variations

within the period of observation: two periods of relatively low discharge occur during the beginning of 2003 to middle 2006 and between beginning of 2011 and end of 2013 with peaks not exceeding 25000 m^3 s^{-1}, separated by a period of relatively high discharges with peaks exceeding 3000 m^3 s^{-1}. The nLw555, in its turn, does not show any noticeable inter-annual variation, and hence, does not respond to inter-annual changes in river discharge. In the overlapping of wind speed and nLw555, there is a clear co-variation of these two parameters, with peaks during August-October and troughs during January-March, reinforcing the statistical outputs, which show a strong positive correlation between the two parameters. The wave Hs (Fig. 2.7c) shows a certain co-variation with some delays during 2003 and ending of 2010, before breaking the co-variation in the rest of the observation. The overlapping of nLw555 time series with each forcings makes it possible to state that among the three forcings the wind speed together with waves, which have a certain linkage, are the main controllers of suspended sediment plume variability in Sofala Bank. The control might be through the re-suspension and erosion of sediments, since the south and southeasterly winds which dominate the region of Sofala Bank do not favor the dispersion of sediment offshore.

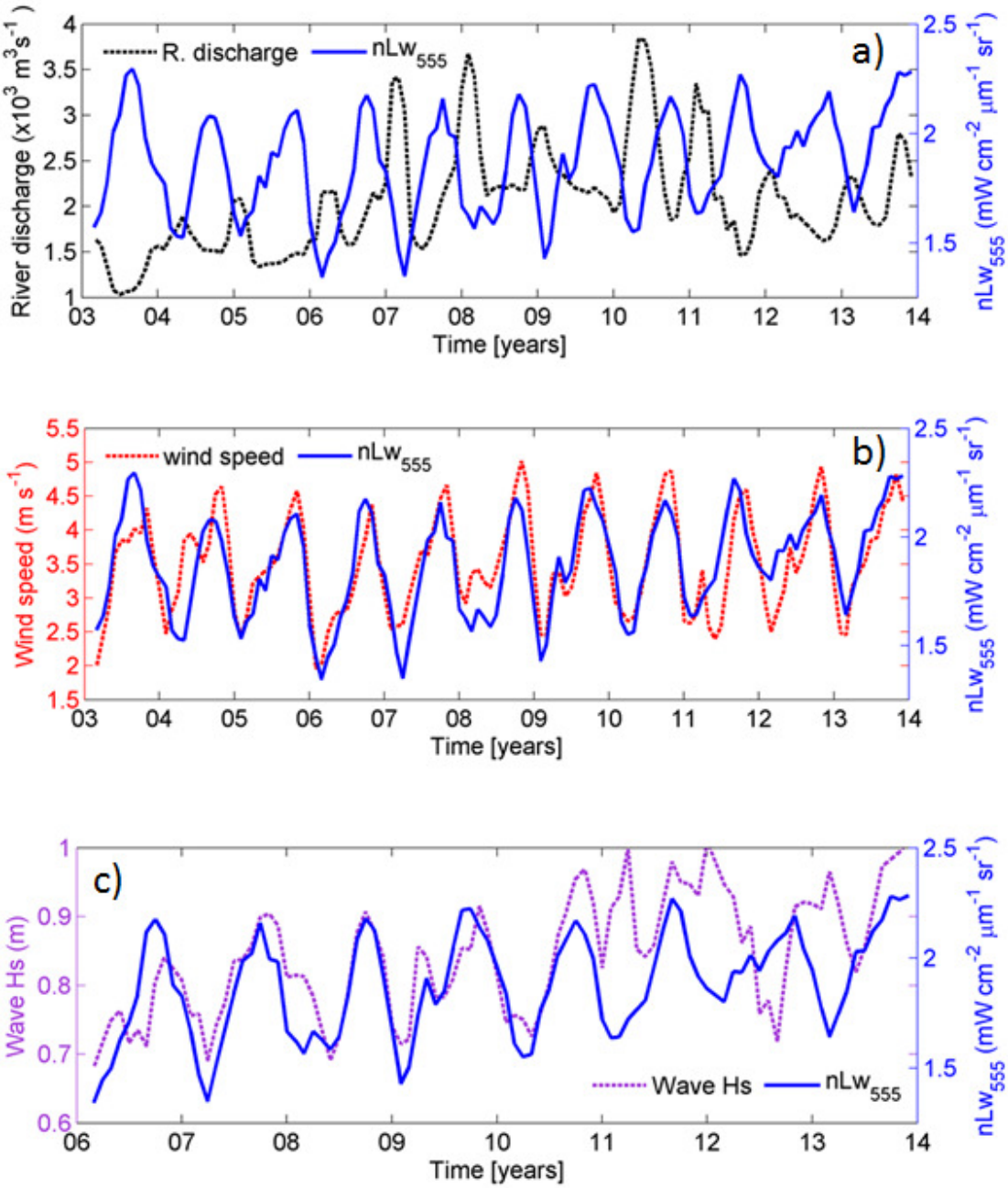

Figure 2.7: Overlap of monthly time series of river discharge with nLw555 (a), wind speed with nLw555 (b), and wave Hs with nLw555. Note that the time span is 2006-2013 for wave Hs against nLw555 plot, and is for 2003-2013 for river discharge against nLw555 and for wind speed against nLw555.

Spatial variation of correlation between Zambezi River discharge and nLw555 is presented in Figure 2.8.1. Analogously to the regression outputs presented in Table 2 for mean nLw555 within the plume area, the spatial correlation also shows negative correlation within the plume

area with the strongest value of about -0.5 occurring in the southern region near the Pungue and Buzi Rivers. Outside the plume area in front of Zambezi Delta, there is a spot of positive correlation denoting the dominance of Zambezi River in draining suspended to deeper waters where the wind and waves are less efficient.

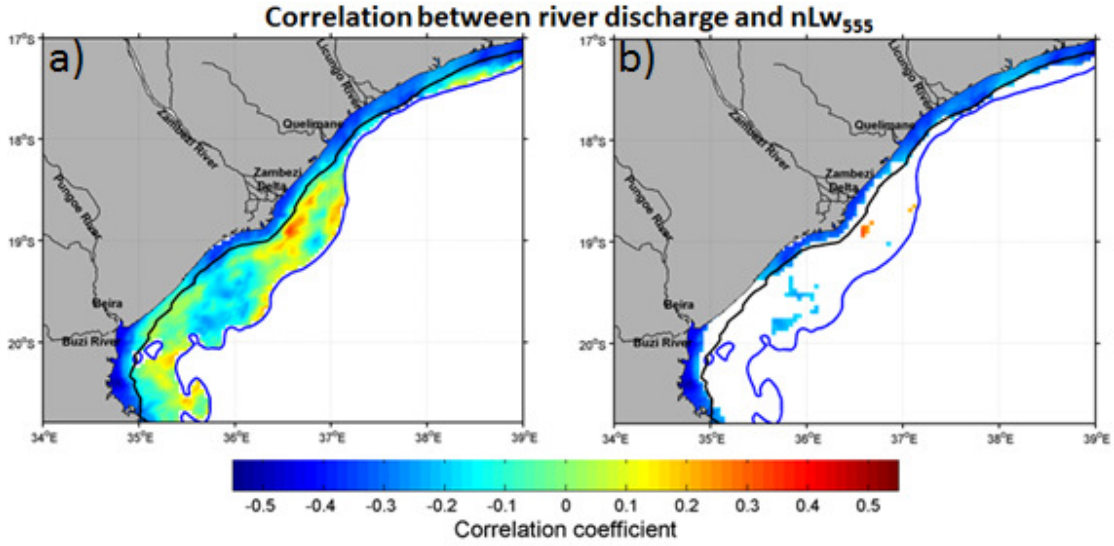

Figure 2.8.1: Spatial correlation between river discharge and nLw555 for the period of 2003-2013 for the whole shelf up 50 m isobaths (a) and with the exclusion of areas of statistical confidence less than 95% (b). The black line indicates the mean plume edge and the blue indicates the 50 m isobaths.

The correlation between wind speed and nLw555 is strong and positive with about 0.77 along the coast and decreases offshore denoting the weakening of wind action as the depth increases (Fig. 2.8.2). In the center region, the map of variation correlation coefficient with values of low statistical confidence excluded (Fig. 2.8.2a) presents a recess precisely in the local of positive correlation of river discharge, which reinforces the statement that the Zambezi River discharge overcomes the wind speed in the outer shelf of the center region.

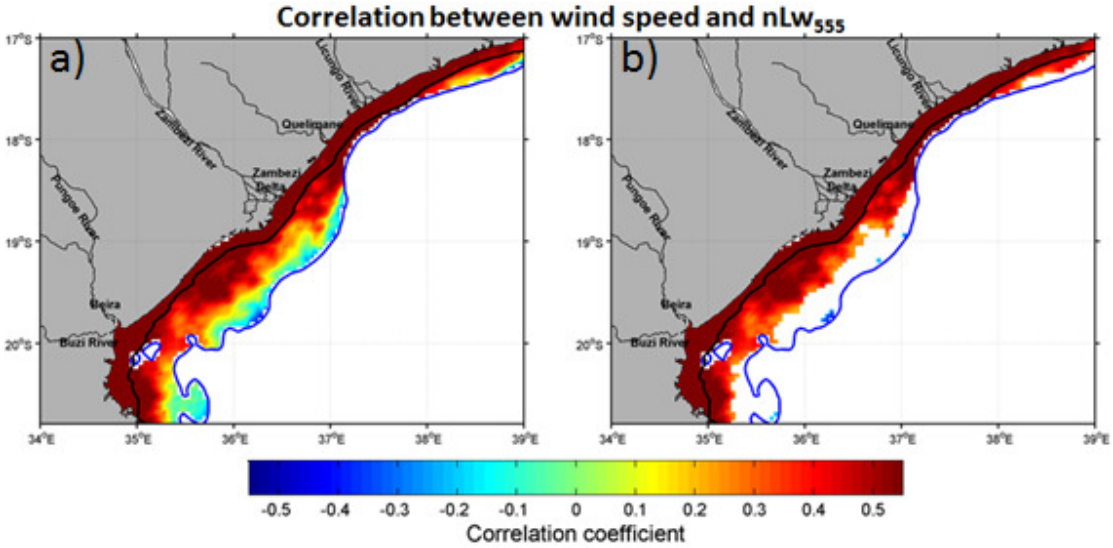

Figure 2.8.2: Spatial correlation between wind speed and nLw555 for the period of 2003-2013 for the whole shelf up 50 m isobaths (a) and with the exclusion of areas of statistical confidence less than 95% (b). The black line indicates the mean plume edge and the blue indicates the 50 m isobaths.

The variation of the correlation coefficient between wave Hs and nLw555 (Fig. 2.8.3) presents a similar pattern to wind discharge but with bathymetry dependence more evident. The strongest positive correlation coefficients denoting the influence of wave in eroding and re-suspending sediments are of about 0.76 occurring along the coast, relatively far from river mouths. In front of the river mouths positive strong correlation are observed but they are not as strong as in places far from the mouths. The recess mentioned in the description of the variation of correlation between wind speed and nLw555 is more evident in the map of correlation between wave Hs and nLw555 (Fig. 2.8.3b).

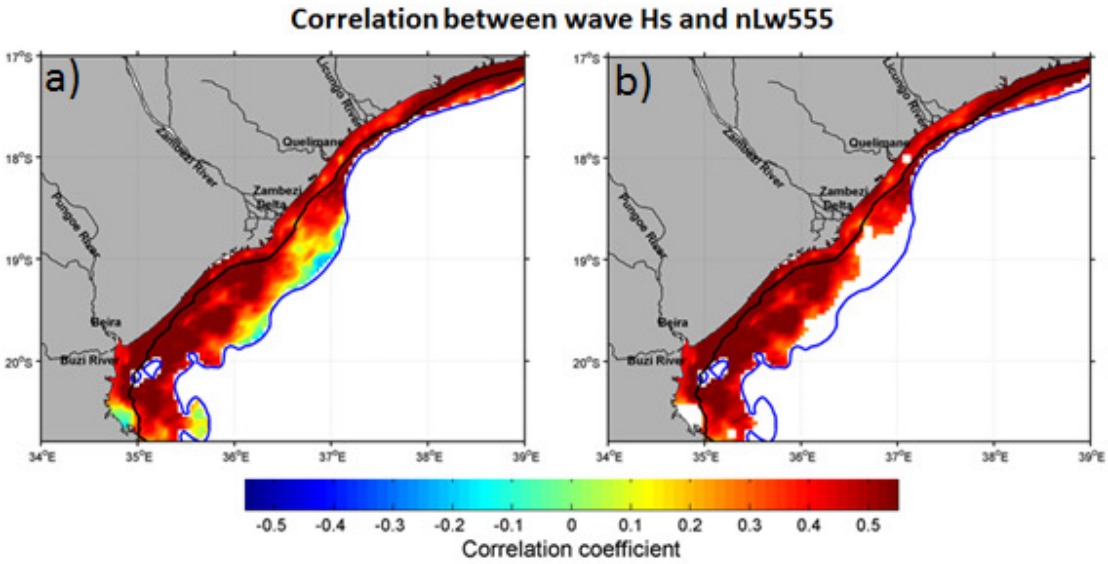

Figure 2.8.3: Spatial correlation between wave Hs and nLw555 for the period of 2003-2013 for the whole shelf up 50 m isobaths (a) and with the exclusion of areas of statistical confidence less than 95% (b). The black line indicates the mean plume edge and the blue indicates the 50 m isobaths.

An overlap of monthly mean time series of nLw555 in north, center and south Sofala Bank for 2003 to 2013 is presented in Figure 2.9. The south region presents the highest values of nLw555, followed by the center region, in accordance with table 2.1. The nLw555 mean presents seasonal variation for all three regions with the south region not in phase with center and north regions especially between 2003 and 2005. In 2003, for example, while the nLw555 starts with a decreasing to reach its annual minimum in May, before showing a continuous increasing to its annual peak of about 2.9 mW cm^{-2} μm^{-1} sr^{-1} in June-July, the center and north region start with a continuous increase and reach their annual maxima of about 2.4 and 2.45 mW cm^{-2} μm^{-1} sr^{-1}, respectively, during September to October. In general, all three regions present annual periodicity with troughs between January-March and peaks during July-October, and do not show a significant inter-annual variability. A curious fact in these three time series is the higher nLw555 range in the north region during 2003-2007 and 2012-2014 when although having a higher peak if compared to the center region, its trough is very low. In 2007, for example, while the center and south regions present minimum of about 2.1, maximum 2.8 mW cm^{-2} μm^{-1} sr^{-1}, which gives an amplitude of about 0.7, minimum about 1.4 and maximum of 2.2, which gives an amplitude of 0.8 mW cm^{-2} μm^{-1} sr^{-1}, respectively the north region presents minimum of 1.1 and maximum of 2.5, which gives an amplitude of about 1.4 mW cm^{-2} μm^{-1} sr^{-1}. This feature might be associated with the relative influence of rivers near these regions, such that during periods of low wind speed and waves, which implies low erosion and re-suspension, the Zambezi River supply in the center, Pungue and Buzi Rivers in the south, supply more sediment than Licungo

River in the North. The confirmation of the statement above requires a specific study and it is beyond the objectives of the present study. On the other hand, the highest values of nLw555 in the south region suggest that it has higher suspended sediment concentrations than in the center region, under Zambezi River influence. The high concentrations of suspended sediments in south region might be associated to relatively higher importance of Pungue and Buzi Rivers than the dammed Zambezi River in supplying sediments, or to higher re-suspension due to local tide ranges and shallower bathymetry in the south Sofala Bank. However, with data and methods used in this research, no definitive conclusion can be drown.

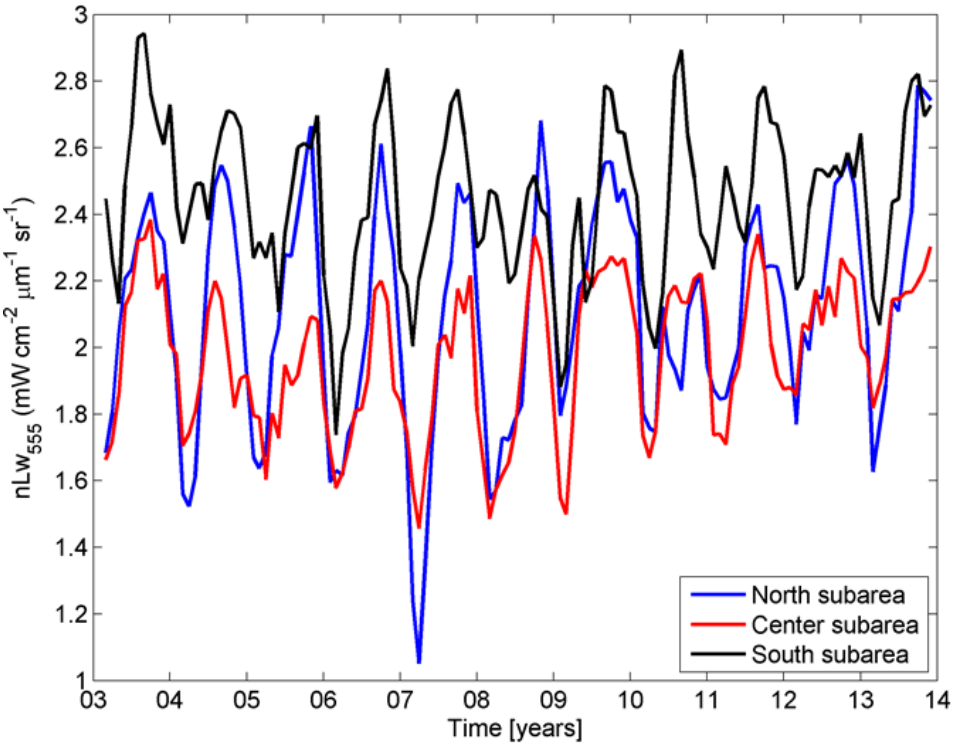

Figure 2.9: Three-month time series of nLw555 in north, center and south regions of Sofala Bank. For each region, the mean nLw555 was calculated for a 22 x22 km box located inside the mean plume edge. The boxes are presented in Figure 2.1.

2.5 Conclusions

Seasonal and inter-annual variability of suspended sediment plume in Sofala Bank was evaluated in related to Zambezi River discharge, wind speed and wave significant height.

The suspended sediment plume is relatively narrow, with lower suspended sediment concentrations, during January-June and wider, with higher suspended sediment concentrations, during July-December. During June-December, the south plume core located near Pungue and Buzi River and the center plume core in front of Zambezi Delta merge and drift north.

Positive strong correlations were obtained between monthly time series of wind and wave Hs with nLw555 suggesting that the erosion re-suspension by wind and waves are the main controller of seasonal variability of suspended sediments if compared to Zambezi River discharge.

The Zambezi River discharge correlates negatively with nLw555 along the whole coast of Sofala Bank and correlates positively in a relatively small area located in outer central shelf off Zambezi Delta where the Zambezi River discharge is more important than wind speed and wave.

The south region, near the mouths of Pungue and Bizi Rivers presents higher nLw555 values and hence higher suspended sediment concentrations if compared to the center region near Zambezi Delta and to the north region near Licungo River.

The dominance of wind and waves in controlling the variability of suspended sediments and the eventual relatively greater contribution of Pungue and Buzi River than the Zambezi River in supplying sediments show evidence of a decreasing Zambezi River supply of sediments, which might have started after damming the Zambezi Catchment.

Analogously to wind speed, the nLw555 within the plume region does not show significant inter-annual variations, which suggests that there is no significant inter-annual variation of suspended sediment plume in Sofala Bank.

Chapter 3

Estimating suspended sediment concentrations from ocean color measurements in Sofala Bank, Mozambique

Abstract: This study investigates the use of single band and color ratio of visible wavelengths to retrieve suspended material in Sofala Bank and applies the most robust relationships on Modis-Aqua images to access spatial-temporal variability of suspended material over Sofala Bank. The influence of Zambezi River discharge, winds, waves and ENSO on the suspended material is inferred through special regression between each of these forcings and the concentrations of suspended material. Color ratio presented the most robust relationship for retrieving all the three types of suspended material with red:green ratio for total suspended material and inorganic suspended material and red:blue ratio for organic suspended material. When regression analysis of color ratio against suspended material is limited to waters located along the coast, relatively dominated by inorganic suspended material, the coefficient of determination (R^2) improves in 58 % for red: green ratio and total suspended material, 16 % for red:green ratio and inorganic suspended material and in 112 % for red:blue ratio and organic suspended material. The concentrations of suspended material in Sofala Bank presents two main regimes: one of low concentrations extending between November and February and other of high concentrations extending

from March to October. Wind spend and wind waves are the main governors of the variability of suspended material in most regions of Sofala Bank coastal waters except in the central region, in front of main mouths of Zambezi Delta mouths, where the Zambezi River is the main controller. Negative strong correlations between 3.4 Niño index and suspended material exactly in areas where the Zambezi river discharge is the main controller of variation in suspended material revealed that ENSO influences Sofala Bank through affecting the rainfall in Zambezi Basin.

Keywords: ocean color, suspended material, Zambezi River, winds, waves, ENSO, Sofala Bank

3.1 Introduction

Freshwater and sediment plumes dispersed from river mouth are very important for coastal and marine ecosystems. According to (Wright and Nittrouer, 1995), the process of transport of river-dispersed matter in coastal-marine environment involves several stages: (I) a turbid river-mouth effluent (plume) spreads decelerates, and initially deposits its higher density load immediately seawards of the mouth. (II) Disperse, dilution, gradual sedimentation and accommodation of remaining finer material; (III) waves, currents or slope-failure mechanisms cause re-suspension and transport of recently deposited sediments; (IV) final deposition and long-term net accumulation. The nature and relative intensities of processes involved in each of these stages of sediment dispersal are dependent of such factors as the water and sediment discharged by the rivers, physical-oceanographic regimes of coastal seas into which sediments a debouched, and geomorphology of the shelves into which sediments a deposited (Wright and Nittrouer, 1995). Coriolis force can also play a major role in the dynamics of suspended sediments plumes in coastal and shelf waters (O'Donnell, 1990; Yankovisky and Chapman, 1997; Fernandez-Nóvoa, et al. 2017). The nutrients from rivers promote productivity in estuaries and coastal waters (Ittekkot et al., 2000) and the sediments supplied by rivers stabilize deltas and coastal zones replacing sediments lost by marine erosion (Ittekkot et al., 2000; Syvitski, et al. 2005). However, river supplied suspended sediments can also be sources of negative environmental impacts on coastal and marine water bodies through the transport of pollutants (Ryan, 1991; Smith and Davies-Colley 2002; Warrick, 2013) and reduction of penetration of light for photosynthesis (Smith and Davies-Colley, 2002; Bowers, et al., 2002). Since the first launch of remote sensing satellites in years 1970's, many studies have been conducted to estimate suspended sediment concentrations from remote sensing reflectance (Curran and Novo, 1988; Dorji and Fearns 2016) for both highly turbid waters (e.g.: Ritchie et al., 1976; Doxaran et al., 2002) and moderately turbid waters (e.g.: Binding et al., 2005). The increase of interest in monitoring water quality from remote sensing is associated to the advantage of spatial coverage, revisiting time and accessibility of satellite images if compared to traditional in situ water sampling methods (Thomas and Weatherbee, 2006). Freshwater and sediments drained by the Zambezi River mouth in Sofala bank (Fig. 3.1), central Mozambique have a major role in local water quality and physical and biological processes (Lutjeharms, 2006; Nehama, 2012). The surface waters close to the Zambezi River mouth may drop as low as 20 pus (Seatre and Silva, 1979) with Secchi depth less than 2 m (Silva, 1984). Although there are some studies on Zambezi river plume in Sofala Bank (Siddorn et al., 2001; Nehama, 2012), as far as we know, none of them were

addressed to the seasonal variability of suspended sediments or their estimation from remote sensing. In the present study, we estimate the suspended sediment concentrations from in situ measured remote sensing reflectance, apply the best-fit relationship on monthly Modis-Aqua remote sensing images to access, and evaluate the spatial-temporal variability of suspended sediments in Sofala Bank. Furthermore, we evaluate the influence of Zambezi river discharge, wind speed and local waves and ENSO on the variability of suspended sediments. The results of this work may serve as a further subsidy for environmental decision-making bodies and as a basis for further studies involving suspended sediments in the region.

3.2 Study area

The study area and the sampling stations are presented in Figure 3.1. The study area is the Sofala Bank is located in the central shelf of Mozambique, between latitudes 17-21°S and between longitudes 34-49°E.

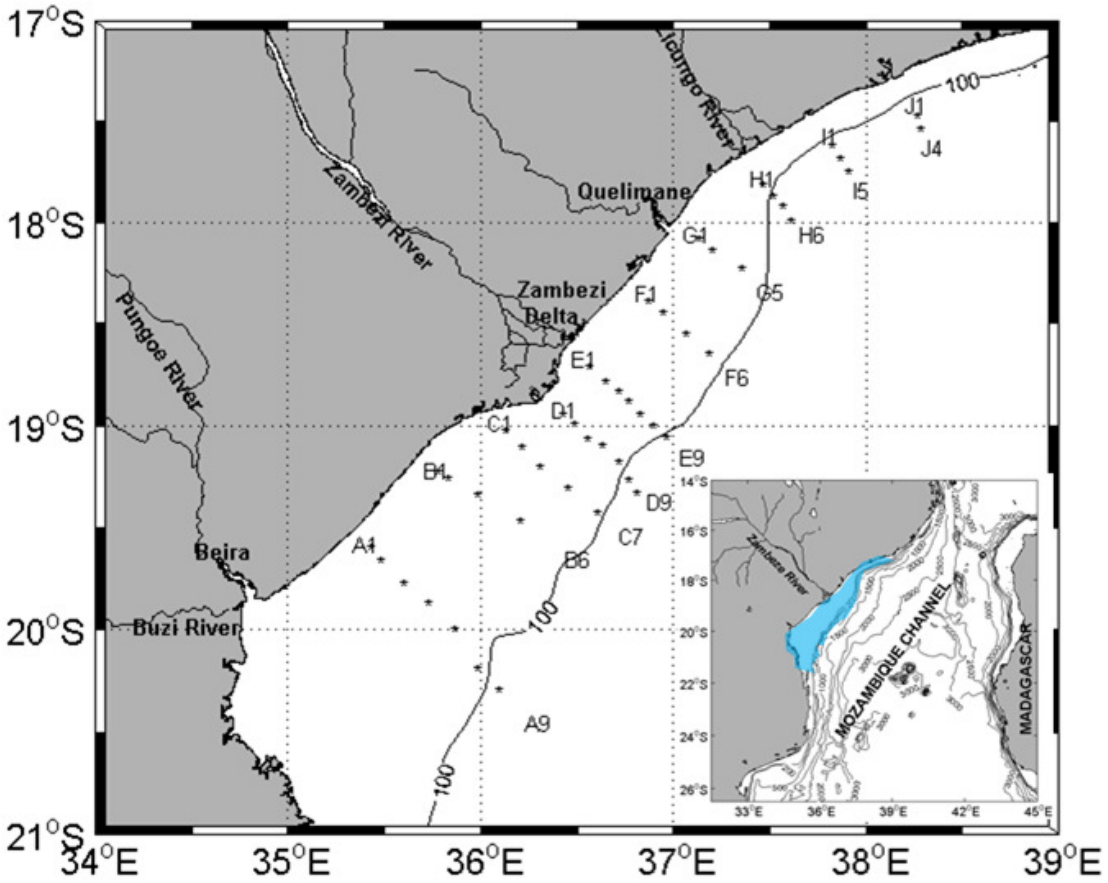

Figure 3.1: Map showing Sofala Bank including the sampling stations. The 100 m isobath is represented for bathymetry reference. The inner image locates regionally the Mozambique coast and the Mozambique Channel. The blue-shaded area in the inner image represents the position of Sofala Bank in the Mozambican shelf.

3.3 Data

In situ remote sensing reflectance and water quality samples

Remote sensing reflectance, salinity, suspended sediments samples, Secchi depth data were collected in 54 stations along Sofala Bank (Fig. 3.1) between 1st April 1998 and 5th April 1998 on board the R/S Fengur led by researchers from the school of ocean sciences of Bangor University. The depth-dependent reflectance values were calculated from the PRR600 radiometer produced by Biospherical Instruments data. This instrument measures downwelling irradiance (Ed) and upwelling Radiance at 412, 443, 490, 510, 555, and 665 nm wavebands. The depth-dependent reflectance values were extrapolated, using a log-linear fit, to the surface to give the near-surface remote sensing reflectance (R_{rs}), defined as the ratio of the upwelling radiance to the downwelling irradiance. Water samples were taken and filtered through Whatman GF/F filters using a hand-powered vacuum pump (Parson et al; 1984). The particulate filters were weighed to give a measure of total suspended material (TSM), and then combusted at 500°C for 3 h and re-weighed to give an inorganic suspended material (ISM). The mass combusted was assumed to be organic suspended material (OSM). Conductivity Temperature Density (CTD) casts were performed using a Valeport 108 MKIII. Salinity was calibrated using a Guideline 8410 portable salinometer. Secchi depths were measured using a standard white Secchi disk. See Siddorn et al., (2001) for more details.

Satellite remote sensing reflectance

Remote sensing reflectance (R_{sr}) images (Level 3 products) for the period between 2002 and 2013 are used. The data have a spatial resolution of 4 km and were downloaded in Giovanni platform (http://giovanni.gsfc.nasa.gov) on 15th August 2015.

Zambezi River discharge

Monthly mean of Zambezi River discharge, collected at Tete station, about 440 km distant to the main Zambezi mouth in Sofala Bank was provided by the national directorate for water affairs of Mozambique.

Wind speed

NCEP/NCAR Reanalysis monthly zonal and meridional components of wind (Kalnay et al., 1996) at 10m above the surface, with 2.5° spatial resolution was downloaded in the website of NOAA Physical Sciences Division (https://www.esrl.noaa.gov/psd/data/gridded/data.ncep.reanalysis.derived.surface.html) on 7th September 2015.

Wave data

Monthly installments of 0.5° spatial resolution global wave hindcasts done using the NOAA WAVEWATCH III model and GFS analysis winds (Tolman, 2009) for the 2005-2013 period was downloaded in ftp://polar.ncep.noaa.gov/pub/history/waves/multi_1, on 27 February 2017.

Niño Index

The monthly Niño 3.4 index data (Rayner et al., 2003) was obtained from the Physical Sciences Division (PSD, https://www.esrl.noaa.gov/psd/gcos_wgsp/Timeseries/Nino34/). The Niño 3.4 region is the most commonly used region for classifying the intensity of El-Niño based on Sea Surface temperature anomalies in the region.

3.4 Methods

Empirical relationship for retrieving suspended sediments for remote sensing reflectance

The empirical relationship for retrieving total suspended material (TSM), inorganic suspended material (ISM) and organic suspended material (OSM) was obtained through regression analyses between remote sensing reflectance and the concentrations of each of classes of suspended sediments collected in 21 stations. The regression analysis was performed for single band and band ratio (Doxaran, et al., 2002; Binding, et al., 2005).

Applying the best-fit empirical relationship to map seasonal variability of suspended sediments concentrations from Modis-Aqua satellite images

The most robust empirical relationships (best coefficient of determination) between remote sensing reflectance and suspended sediments concentrations were applied in corresponding Modis-Aqua bands to retrieve total suspended material (TSM), inorganic suspended material (ISM) and organic suspended material (OSM) concentrations. This procedure may cause errors in the estimation of the concentration because the samples used to establish the empirical relations were collected in a single cruise performed in the dry season, and the empirical relations were not validated. However, we believe that since river discharge does not vary much between the dry and wet seasons, and if the optical properties of water are maintained, it may be reliable, at least for the evaluation of relative variations of suspended sediment concentrations.

Evaluating the spatial influence of river discharge, wind speed, local waves and climate

To evaluate the spatial influence of river discharge, wind speed, local waves, and climate on the variability of suspended material, a linear regression between the time series of maps of spatial variability of the concentration of suspended sediments and time series of Zambezi river

discharge, wind speed, waves and index of Niño3.4 was performed. The wind speed time series was obtained from the areal mean of the study area. The wave data were re-gridded to 4 km to have the same spatial resolution of Modis-Aqua remote sensing reflectance used to map the suspended sediments concentrations.

3.5 Results and discussion

A summary of mean value and ranges of water quality parameters and in situ reflectance sensing reflectance are shown in Table 3.1. From the ranges of total suspended material (TSM) one can see that the water of Sofala Bank is of low turbidity. The high range of salinity in its turn suggests the high spatial variability of salinity in there and that the salinity was measured inside and out of the region of plume influence.

Table 3.1: Summary of mean ranges of water quality parameters and in situ remote sensing reflectance.

	Min	Max	Mean
Depth (m)	9	140	42.44
Secchi (m)	1	33	16.69
Salinity (PUS)	18.49	35.75	33.19
TSM (mg l^{-1})	0.8	5.5	2.4
ISM (mg l^{-1})	0	3.1	0.7
OSM (mg l^{-1})	0.8	3.3	1.8
$R_{sr}412$ (Sr^{-1})	0.0041	0.0783	0.0316
$R_{sr}443$ (sr^{-1})	0.0057	0.0591	0.0281
$R_{sr}490$ (Sr^{-1})	0.0098	0.0481	0.0283
$R_{sr}510$ (Sr-1)	0.0103	0.0456	0.0212
$R_{sr}555$ (Sr^{-1})	0.0075	0.0572	0.157
$R_{sr}665$ (Sr^{-1})	0.0001	0.0328	0.0032

Figure 3.2 presents the spectral variation of remote sensing reflectance in Sofala Bank. There are three main types of spectral shapes, one with the peak in near blue (412 nm), another with a peak in the far blue region of the spectrum (490 nm) and other with the peak in the green region of the spectrum (555 nm). The peak in blue is due to scattering by water molecules while the depressed reflectance in red is due to absorption by water. The peak in green suggests that this group of stations present higher concentrations of sediments if compared to those with the peak in the blue region of the spectrum. It is possible to note that among the group of stations with a peak in green there are stations with reflectance values very close to zero and others with reflectance values closer to 0.1.

These differences might reflect relative differences in the concentration of suspended sediments among the stations of that group so that those with relatively low concentrations are susceptible to absorption by water and therefore there reflectance values close to zero.

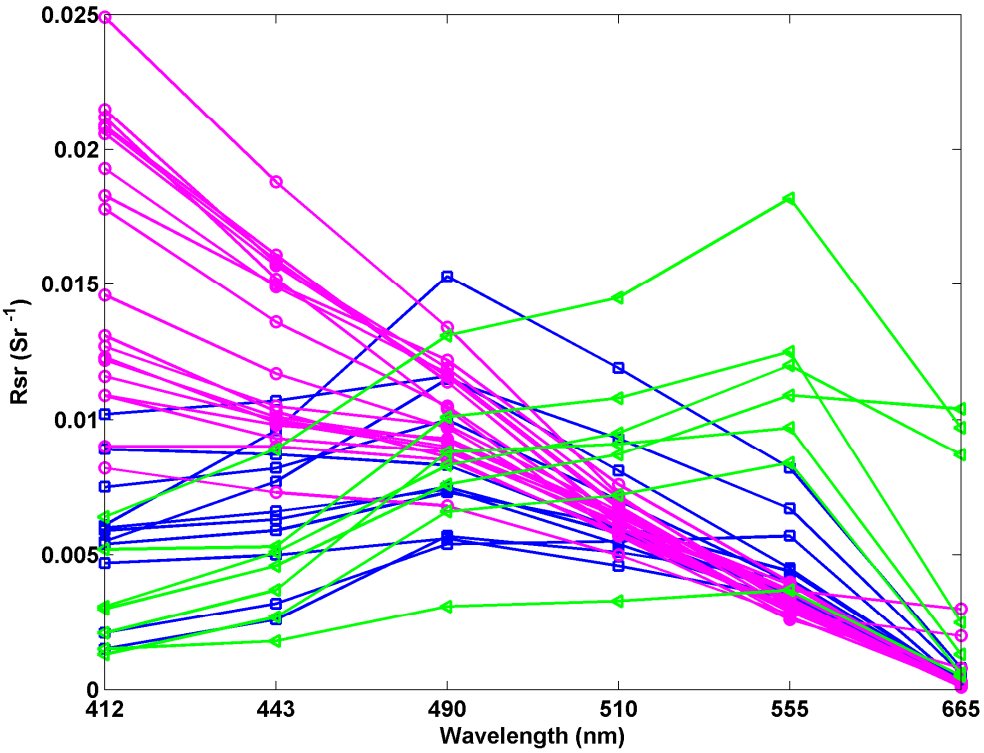

Figure 3.2: Spectral variation of remote sensing reflectance along surface waters of Sofala Bank. The colors were brought to distinguish the spectral shapes of the groups: one with the peak at 412 nm (in purple), another with the peak at 490 nm (in blue) and other with the peak at 555 nm (in green).

The spectral curves of Figure 3.2 are a geographically plotted in Figure 3.3. According to the map, the position of the reflectance peak in the spectrum decreases from the coast offshore suggesting the expected decrease in the concentration of suspended sediments offshore (Jensen, 2011). The reflectance peak in the green region of the spectrum, observed in coastal waters of Sofala Bank is typical of water with low to moderate turbidity. Other examples of moderate turbidity waters are Irish Sea (Bowers et al., 2002; Binding et al., 2005) and Ganges River estuary (Shi and Wang, 2010). Amazon River estuary (Shi and Wang, 2010) and Gironde estuary in Southwest France, where the total suspended material can reach 1000 mg/l are examples of high turbidity waters and their peaks are located between red and near infrared regions of the spectrum.

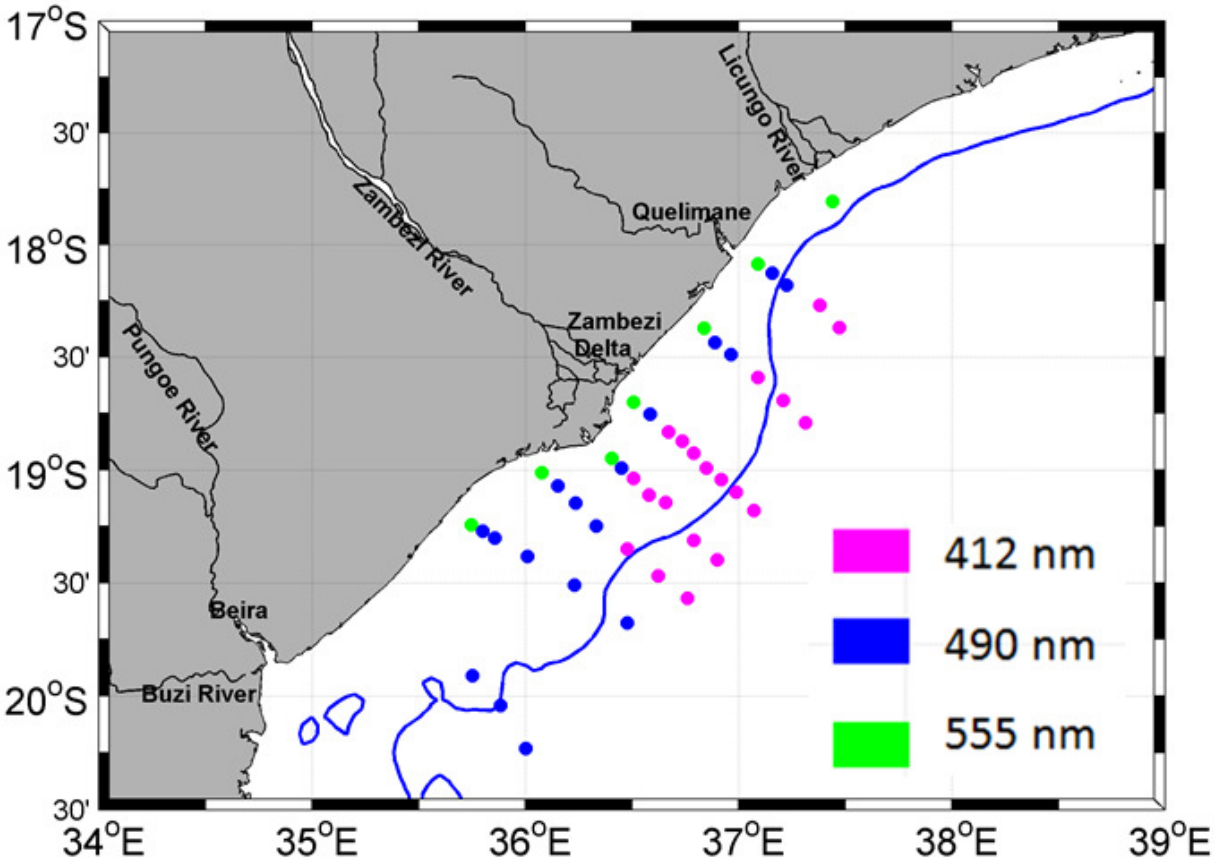

Figure 3.3: Spatial distribution of remote sensing reflectance peak along Sofala Bank during 1st April 1998 to 5th April 1998. The blue line represents the 50 m isobath for bathymetry reference.

Retrieving the concentration of suspended materials from remote sensing reflectance

Single band approach

The regression outputs of the relationship between single bands of remote sensing reflectance and each of the classes (total, inorganic and organic) of suspended material are presented in Figure 3.4. The relationship between the reflectance and the concentrations of suspended improves as the wavelength increases such that the red band (665 nm) showed the strongest relationship for all the three classes, denoting high sensibility of higher wavelengths to the variation of suspended sediments concentration (Jansen, 2011). Among the three classes, the inorganic suspended material showed the strongest with R^2 of about 0.72, followed by total suspended material with R^2 equal to 0.57 while the organic suspended material showed the lowest relationship with R^2 of about 0.31. These results suggesting that the best class of suspended material to be retrieved from remote sensing reflectance is the inorganic suspended material. The lower correlation between organic suspended material and reflectance is justified by its relatively lower backscattering (Bowers and Binding, 2006).

Table 3.2: Regression outputs of the relationship between single bands of remote sensing reflectance and each of the classes of suspended material

Total suspended material						
	R412	R443	R490	R510	R555	R655
R	0.17	0.02	0.12	0.43	0.58	0.76
R^2	0.03	0.03	0.02	0.18	0.34	0.57
SE	1.14	1.16	1.15	1.05	0.95	0.76
P	0.457	0.751	0.594	0.052	0.006	0.000
Inorganic suspended material						
	R412	R443	R490	R510	R555	R655
R	0.21	0.10	0.17	0.54	0.71	0.85
R^2	0.05	0.01	0.03	0.30	0.50	0.72
SE	0.74	0.75	0.75	0.64	0.54	0.40
P	0.353	0.660	0.469	0.011	0.000	0.000
Organic suspended material						
	R412	R443	R490	R510	R555	R655
R	0.21	0.12	0.02	0.25	0.39	0.56
R^2	0.04	0.01	0.00	0.06	0.15	0.31
SE	0.50	0.51	0.51	0.49	0.47	0.42
P	0.361	0.597	0.923	0.280	0.083	0.008

The higher relationship between inorganic suspended material and remote sensing reflectance if compared to other classes of suspended materials is justified by the fact that the backscattering over Sofala Bank is dominated by inorganic sediments (Siddorn, et al., 2001).

Scatter plots of remote sensing reflectance at 555 and 665 nm against each of the three classes of suspended material concentrations are presented in Figure 3.4. The scatter plots involving the two bands are brought because the spreading of their scatter points presents a peculiar behavior, and hence, worthy of special attention. In these two bands the scatter points split into two; this detail is clearer in the red band (665 nm) where the threshold is about 0.005 Sr^{-1}.

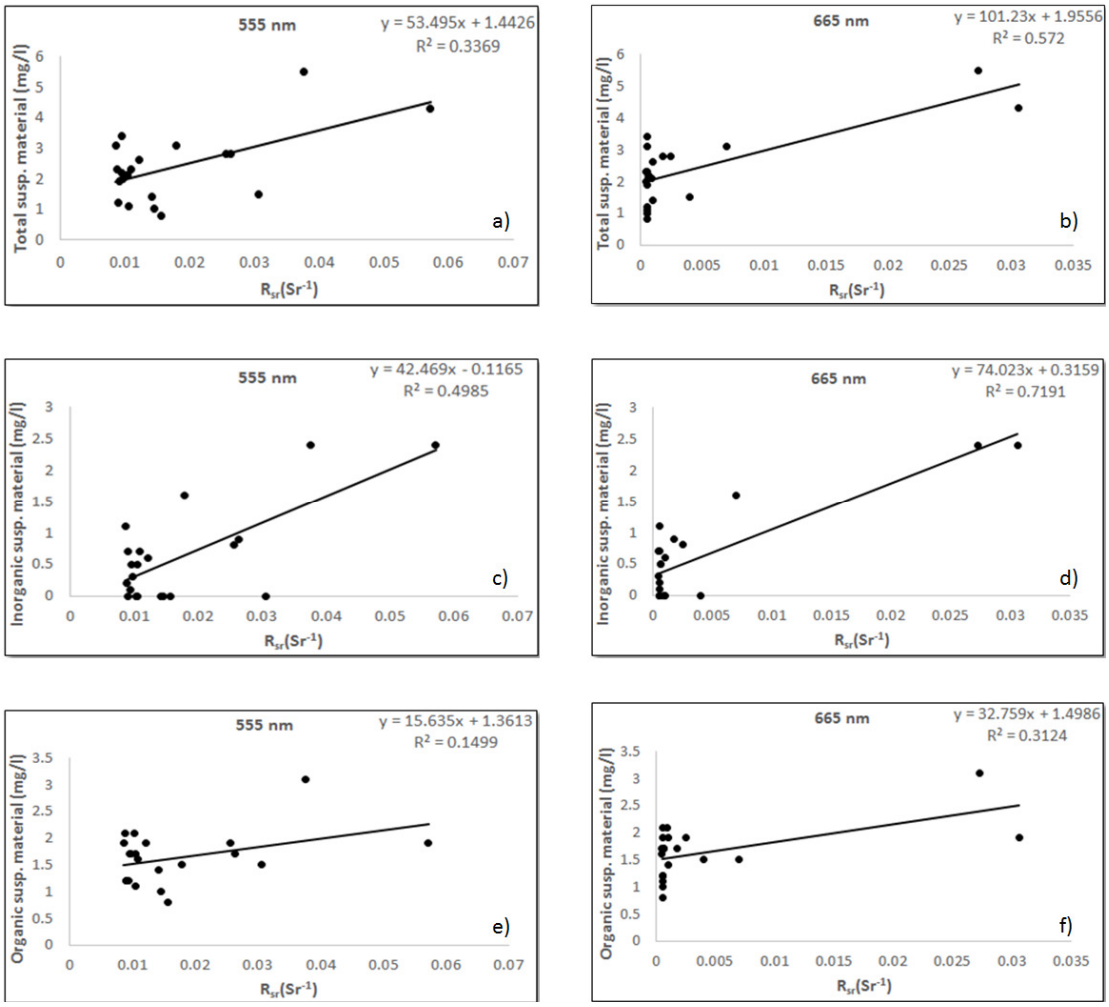

Figure 3.4: Scatter plots of remote sensing reflectance against suspended material concentrations. a) Remote sensing reflectance at band 555 nm against total suspended material. b) Remote sensing reflectance at 665 nm against total suspended material. c) Remote sensing reflectance at 555 nm against inorganic suspended material. d) Remote sensing reflectance at 665 nm against inorganic suspended material. e) Remote sensing reflectance at 555 nm against organic suspended material. f) Remote sensing reflectance at 665 nm against organic suspended material.

Redoing the regression analysis, splitting the scatter points into two groups having the 0.005 Sr^{-1} as the threshold the relationship between the remote sensing reflectance at 665 nm with values greater than 0.005 Sr^{-1} gets improved and the other group gets worse (Fig. 3.5). However, the statistical significance of the improved relationship is decreased by the number lower number of points used in the analysis. A remarkable feature that distinguishes the two groups is that while in the group of $R_{sr} > 0.005$ Sr^{-1} the values of R_{sr} increase linearly with increasing concentrations, in the $R_{sr} < 0.005$ group the R_{sr} seems not responding to changes in concentration.

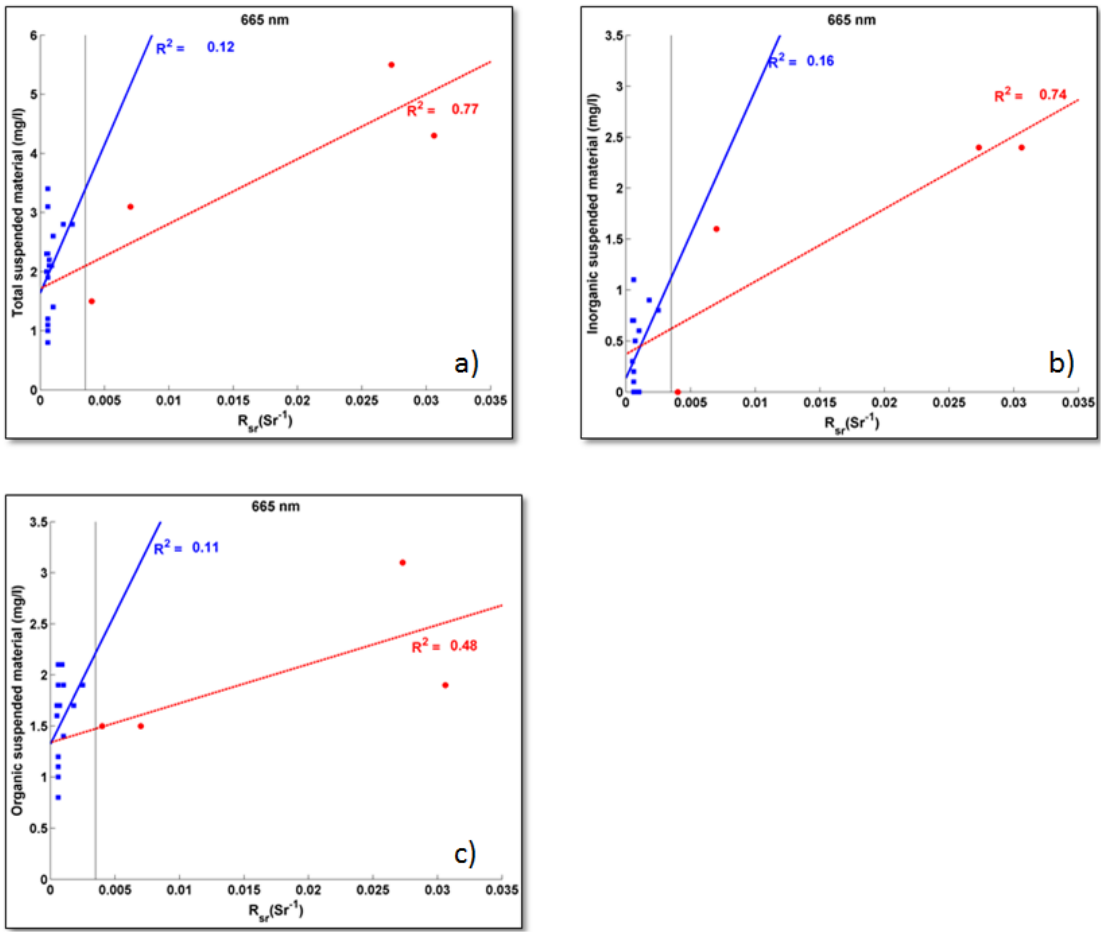

Figure 3.5: Scatter plots of remote sensing reflectance at 665 nm against the concentrations of total suspended material (a), inorganic suspended material (b) and organic suspended material (c). The red points correspond to remote sensing reflectance greater than 0.005 Sr^{-1} and the blue ones correspond to remote sensing values less than 0.005 Sr^{-1}.

Color ratio approach

The analysis of color ratio showed the strongest relationship between each of the concentrations of suspended materials (total, inorganic and organic) and the ratios of the reflectance and the red band to one other band (Table 3.3). While the relationship increases with increasing of the wavelength of denominator getting its best-fit at red:green ratio for total and inorganic suspended materials (R^2=0.63 and 0.76, respectively), it decreases with increasing of the wavelength of the denominator the organic suspended material and its best-fit is red-blue ratio with R^2=0.41. The color ratio approach shows better performance for all the three classes if compared to the single band approach.

Table 3.3: Regression outputs of the relationship between the color ratio of red to other band and each of the classes of suspended material.

Total suspended material					
	R665/R412	R665/R443	R665/R490	R665/R510	R665/R555
R	0.77	0.78	0.79	0.79	0.80
R^2	0.60	0.60	0.62	0.62	0.63
SE	0.74	0.73	0.72	0.71	0.70
P	0.000	0.000	0.000	0.000	0.000
Inorganic suspended material					
	R665/R412	R665/R443	R665/R490	R665/R510	R665/R555
R	0.82	0.84	0.86	0.86	0.87
R^2	0.68	0.71	0.73	0.74	0.76
SE	0.43	0.41	0.39	0.38	0.37
P	0.000	0.000	0.000	0.000	0.000
Organic suspended material					
	R665/R412	R665/R443	R665/R490	R665/R510	R665/R555
R	0.64	0.62	0.62	0.62	0.62
R^2	0.41	0.39	0.39	0.38	0.38
SE	0.39	0.40	0.40	0.40	0.40
P	0.002	0.002	0.003	0.003	0.003

The splitting of scatter plots observed in single band analysis still appears in the color ratio analysis with about 0.1 as the threshold of red:green ration in total and inorganic suspended materials concentrations and 0.25 as the threshold of red:blue ratio in organic suspended material concentrations (Fig. 3.6).

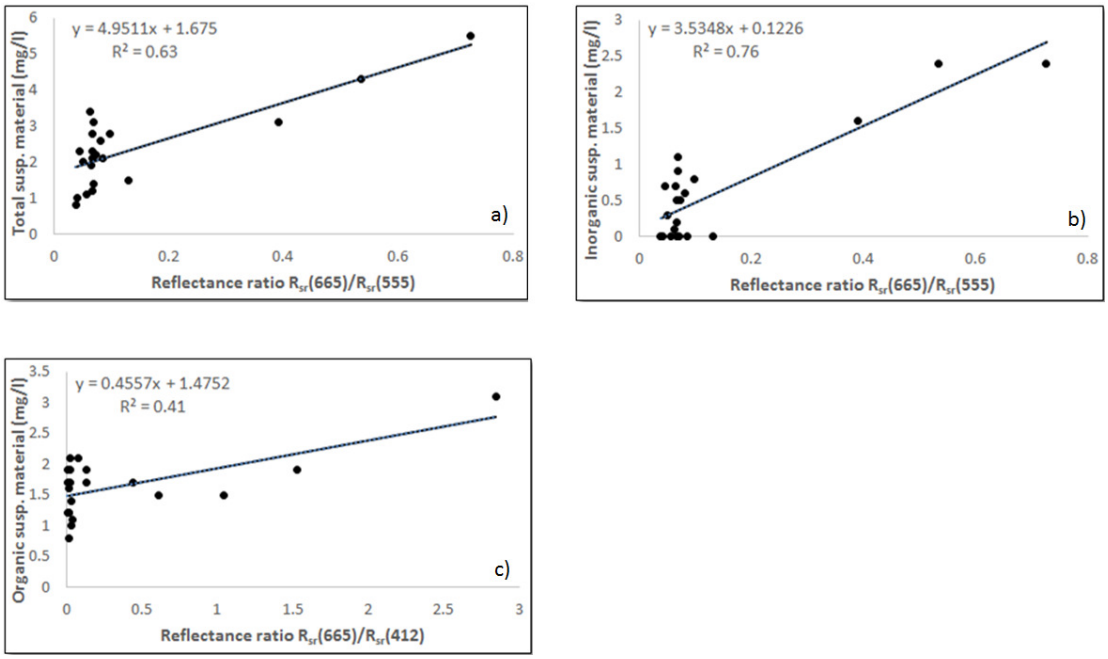

Figure 3.6: Scatter plots of color ratios against the suspended material concentrations. a) red:green ratio against total suspended material. b) Red:green ratio against inorganic suspended material. c) Red:blue ratio against organic suspended material.

Again, in the color ratio approaches, splitting of the scatter points into two groups and improves the relationships for points corresponding to color ration greater than the given threshold (Fig.3.7). The regression analysis of total suspended material and inorganic suspended mater against red:green ratio with 0.12 as the threshold and organic suspended material against red:blue ratio with 0.25 as the threshold, give the following equations:

TSM = 0.5685 + 6.8017 (red:green); R^2 = 1.00; $p < 0.002$; standard error = 0.116; (n=4). [3.1]

ISM = -0.288 + 4.2362 (red:green); R^2 = 0.88; $p < 0.06$; standard error = 0.47561; (n=4). [3.2]

OSM = 1.1048 + 0.646070 (red:blue); R^2= 0.87; $p < 0.02$; standard error = 0.2815; (n=5). [3.3]

As can be seen from the equation the number of points (n) used in the regressions is very low and this situation has implications in the reliability of the relationship such that although the relationship between inorganic suspended material and red:green ratio is strong the p-value is greater than 0.05 and therefore out of 95% of confidence.

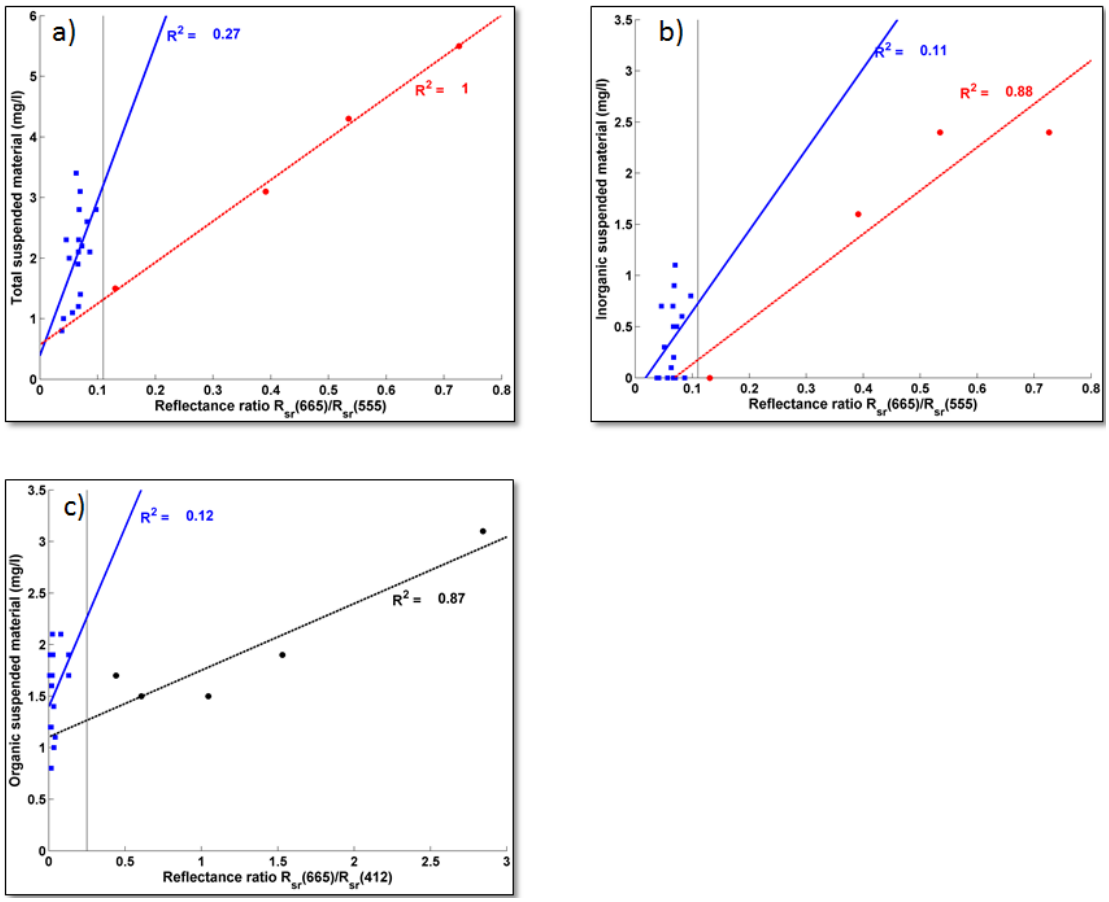

Figure 3.7: Scatter plots of color ratio against the concentrations: red:green ratio against of total suspended material: (a) red:green ratio inorganic suspended material (b) and red:blue ratio against organic suspended material (c). The red points correspond to red:green ratio greater than 0.1 and black ones correspond to red:blue ratio less than 0.25.

Scatter plot of inorganic suspended material:total suspended material (ISM:TSM) ratio against red:green ratio (Fig. 3.8) shows that except the point with ISM:TSM =0, all the other points from red:green > 0.1 are of ISM:TSM > 0.4 while the points from the other group (red:green < 0.1) are of ISM:TSM < 0.4. This feature suggests that the improvement of the relationship between red band or red:green ratio and the concentrations of suspended materials is achieved by considering waters in which the total suspended material is less dominated by the organic suspended material (or relatively dominated by inorganic suspended materials). These results are analog to findings of Binding (2003), Bowers and Binding (2006) and Bowers et al. (2007) in the Irish Sea. Bowers et al. (2007) improved the red:green ratio against the concentration of the inorganic suspended material to about 90% of explained variance by limiting the regression to water with mainly inorganic suspended material (ISM:TSM < 0.7) in the Irish Sea. According to Bowers et al., (2007), the reason for this improvement of the relationship when limiting the regression to

inorganic materials is that they are better at backscattering light than organic particles per unit of concentration, and so they produce a greater reflection for a given reflectance ratio.

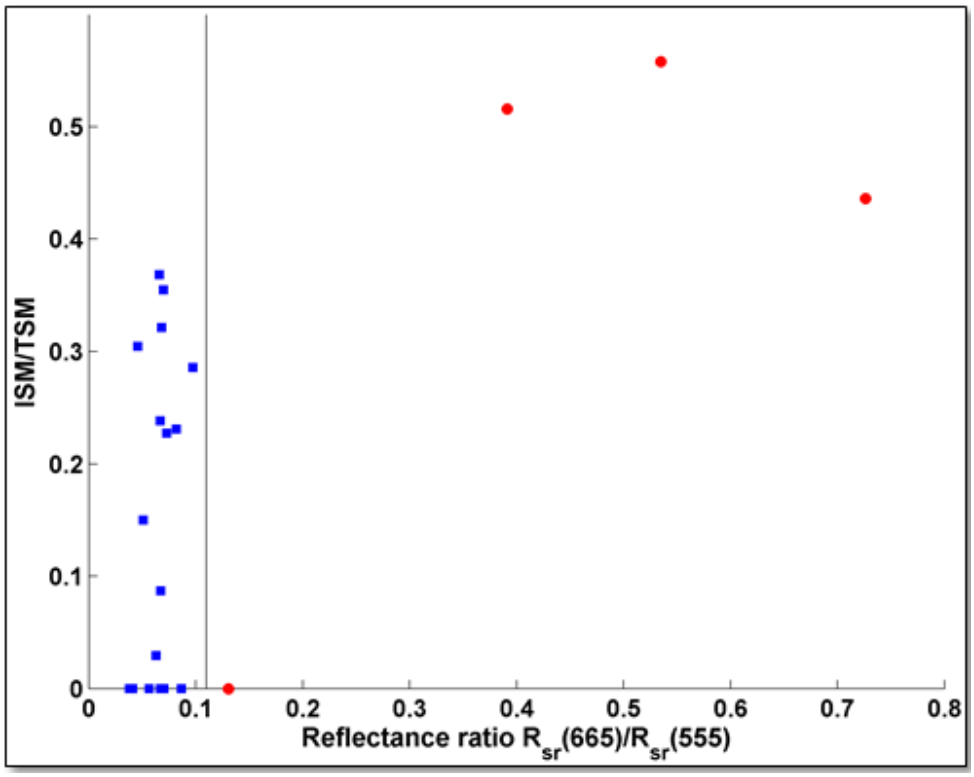

Figure 3.8: Relationship between red:green ratio of remote sensing reflectance and ISM:TSM. The red points represent the group of red:green > 0.1 while the blue ones represent the group of red:green < 0.1.

In Figure 3.9 local depth (a), Secchi depth (b) and salinity (c) are plotted against red:green ration. Despite existing two points of red:green < 0.1 with characteristics of red:green > 0.1, it is also possible to distinguish the two groups from their ranges of water depth, Secchi depth and salinity. The red:green > 0.1 (in red) points are mainly located in water with depths not greater than 20 m, Secchi depth not deeper than 10 m and salinity not higher than 31 PUS. These characteristics suggest that the red:green > 0.1 group is located more inshore and are more influenced by the continental inputs.

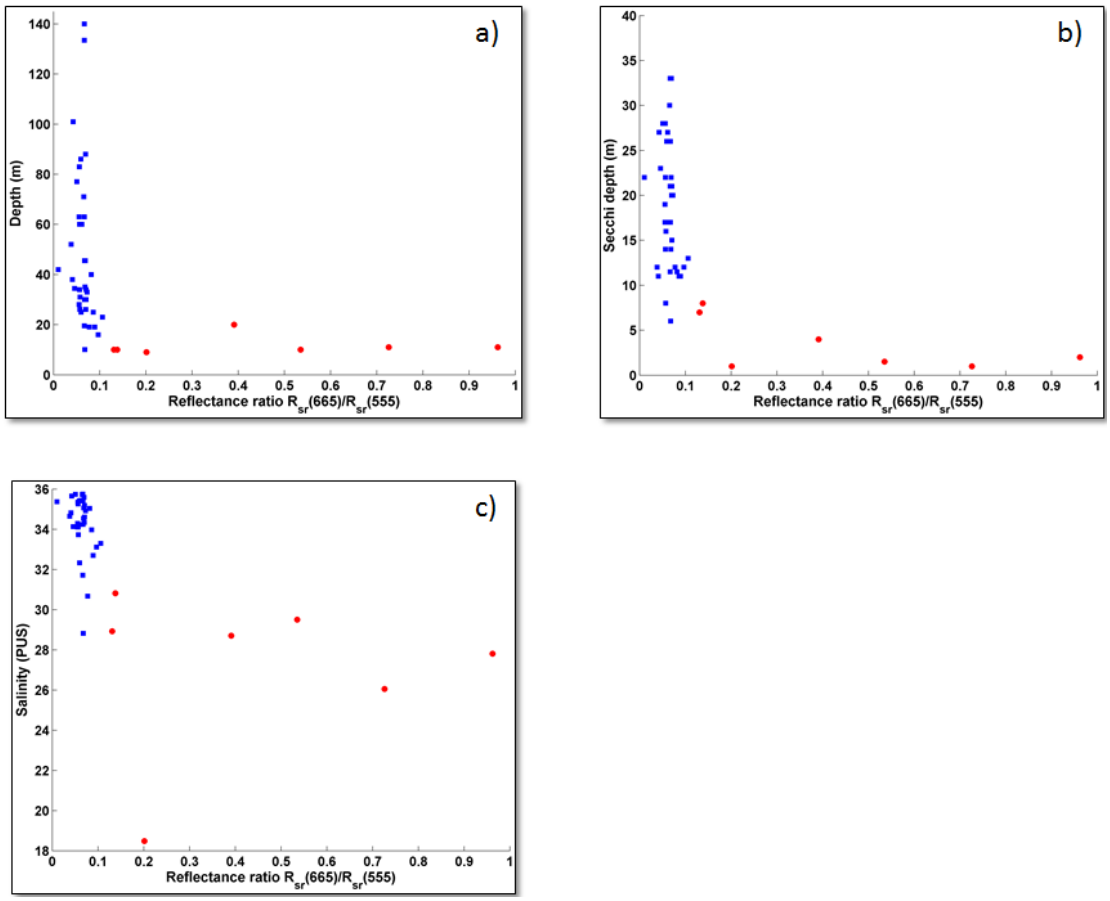

Figure 3.9: Relationship between red:green ratio of remote sensing reflectance and water depth (a), Secchi depth (b) and salinity (c). The red points represent the group of red:green > 0.1 while the blue ones represent the group of red:green < 0.1.

As for using of the red:green to map the suspended material from satellite images, for example, it is necessary to know the geographical region of Sofala Bank where it applies. Figures 3.10a and 3.10b presents the geographical location of waters with red:green > 0.1 and those of red:green < 0.1. The classification was done from in situ remote sensing reflectance. As can be seen from the Figures both red:green ratio used to estimate total and inorganic suspended material and red:blue ratio, used to estimate the organic suspended material have their best performance near the coast. The red:green > 0.1 and red:blue > 0.25 are the same with peak at the green region of the spectrum, dominated by suspended materials, presented in Figure 3.3. The red:green < 0.1 and red:blue < 0.25 corresponds to waters with peak in blue an a depressed reflectance in red due to scattering and absorption by water, respectively. These results together with the observation of Figure 3.9 suggest that at least for the dry season, the red:green ratio is more efficient if applied to retrieve suspended material in coastal waters with depths not greater than 20m.

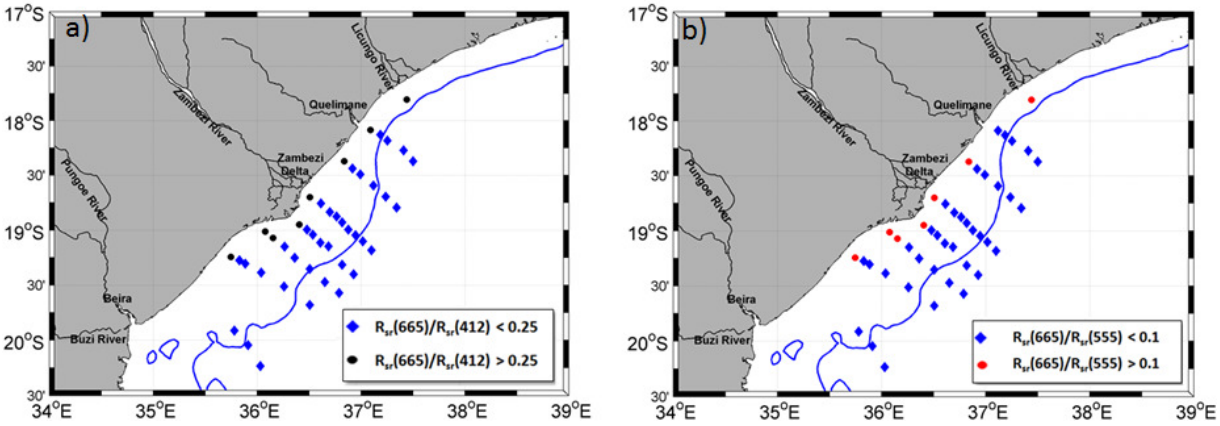

Figure 3.10: Geographical location of water with red:green > 0.1 and red:green < 0.1(a); water with red:blue > 0.25 and red:blue < 0.25 (b). The blue line represents the 50 m isobaths for bathymetry reference.

Seasonal variability of suspended materials in Sofala Band and evaluation of spatial influence of river discharge, winds, waves and ENSO

In this section, the spatial and seasonal variability of suspended material estimated using equations 1, 2 and 3 are evaluated and confronted to the variation of Zambezi river discharge, wind speed, waves and ENSO, with the aim of inferring the spatial-temporal influence of each of these forcings.

River discharge

In Figure 3.11, we presented the seasonal variation of Zambezi river discharge during the period before the damming of Zambezi Catchment (1955-1976) and the period corresponding to the time series of Modis-Aqua data used to compute the monthly climatology (2003-2013). Although we could not access the variability of suspended material before the damming of Zambezi catchment, we deliberately compare the seasonal variation of discharges of that period with the actual discharge to hypothesize how the changes in river flow might have influenced the spatial-seasonal variability of suspended material in Sofala Bank. During the 1955-1976 period, there were high flows in February-April, which varied between 4000, and 5200 m^3 s^{-1} followed by a progressive decrease to minimum flows of about 800-900 m^3 s^{-1} in October-November. The seasonal variation during 1955-1976 reflects the rainfall regime controlled by the Intertropical Convergence Zone (TCZ) between Northeast Monsoon and the Southeast Trades for the Middle and Lower Zambezi, and Congo air boundary between Southwest Monsoon and Southeast Trades for upper Zambezi (Moore et al., 2007). These two climatic boundaries bring more rainfall as they move south. During the winter, they move to the north, resulting in drier conditions in the Zambezi Basin. During the 2003-2013 period, higher flows are observed between October-Marc with respective peak of 2600 m^3 s^{-1} in February and lower flows are

observed between May-September with minimum moth value of about 1700-1800 m^3 s^{-1} in August-September. In contrast to 1955-1976 period when the difference between maximum and minimum flows was about 85 %, in recent years including 2003-2013 period there is no time interval where one can highlight as interval of high flow; the maximum-minimum discharges difference in 2003-2013 period is only 36 % probably because of the damming. Another feature worthy of appreciation is the difference in the magnitude of standard deviations of 1955-1976 and 2003-2013 periods. The 1955-1976 period presented high standard deviations suggesting also high inter-annual variations in river discharge while the 2003-2013 period presents lower standard deviation suggesting lower inter-annual variations due to regulation through damming.

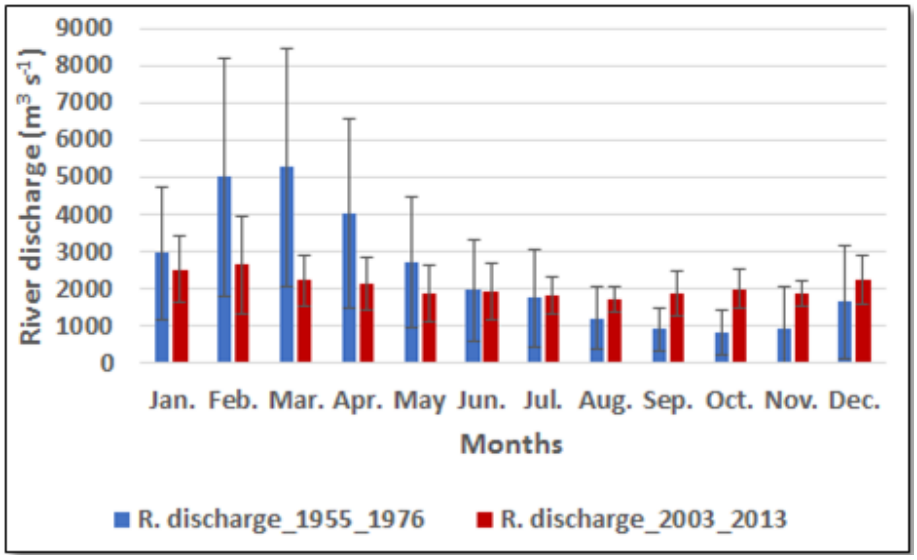

Figure 3.11: Monthly climatology of Zambezi river discharge measured at Tete station, about 440 Km to the main Zambezi mouth in Sofala Bank, for the 1955-1976 period (blue) and 2003-2013 period (red).

Wind speed and direction

Figure 3.12 presents wind roses computed from monthly average wind in Sofala Bank. The prevailing winds in Sofala Bank are southerly during January-May and southeasterly during June-December. The wind speed varies from 0-3 m s^{-1} between December-March and June to about 3-5 m s^{-1} during April-May and July-November. In general, the southerly winds are relatively weaker than southeasterly.

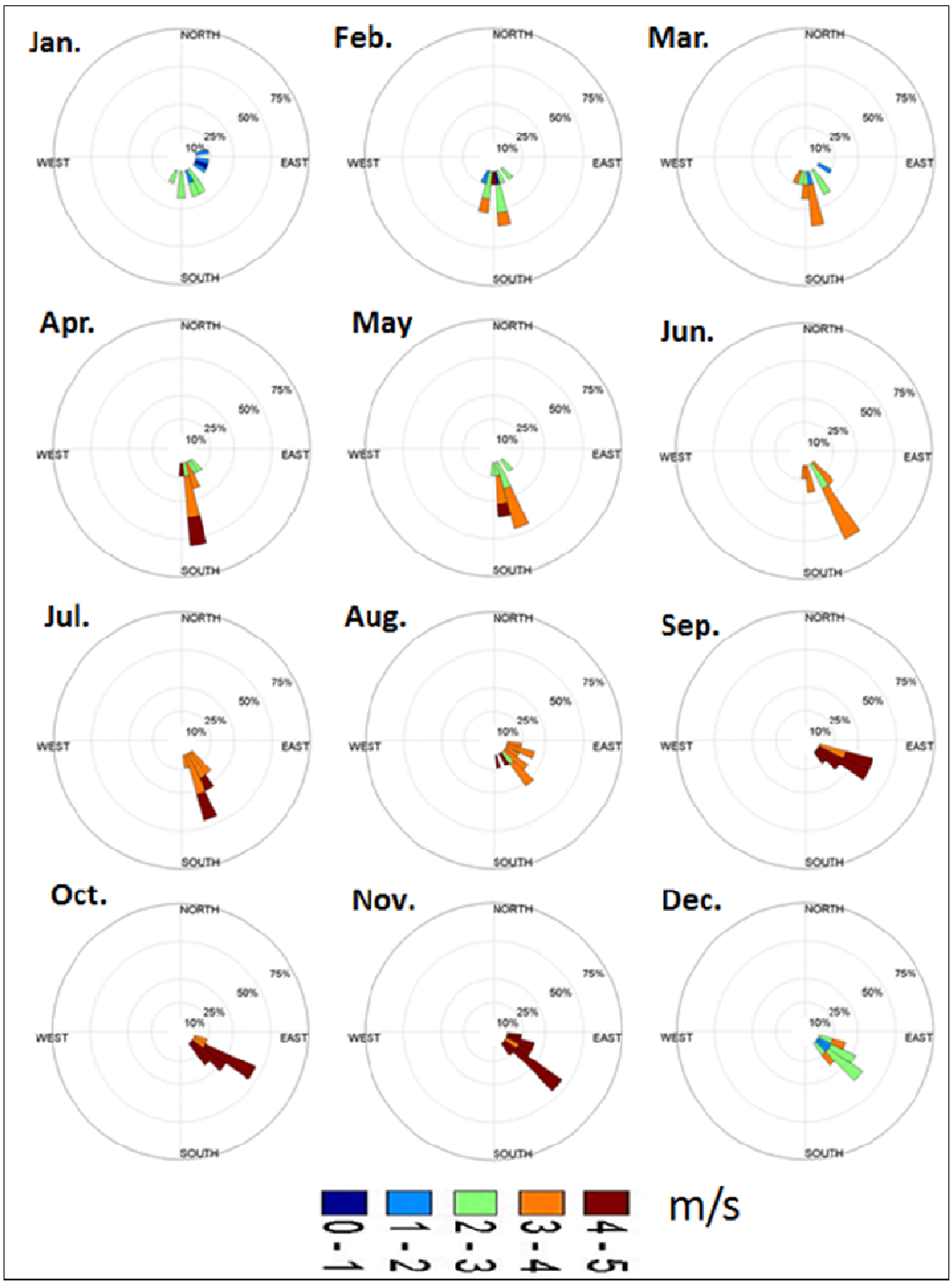

Figure 3.12: Monthly Climatology of wind rose computed from NCEP/NCAR Reanalysis monthly zonal and meridional components of wind over Sofala Bank.

Total suspended material

Monthly climatology of total suspended material (TSM) estimated using the retrieving relationship created from in situ observation is presented in Figure 3.13. In general, the plume of suspended material presents two cores, one in South about 20°S with high influence of Pungue and Buzi rivers and other in the central Sofala Bank about 18°S, near the main mouth of Zambezi delta. Both of cores present two regimes of suspended material concentrations, one with concentrations not reaching 3.0 mg/l during November-February and the other with concentrations exceeding 3.5 mg/l in the plume cores during March-October. The plumes of the total suspended material seem to stagnate near the mouths of Zambezi River and Buzi during November-February when the concentrations are low and moves northwards during high concentration regime presenting a narrower connection of south and center cores in the coast. The annual variation of total suspended material is more similar to wind speed variation that to river discharge. Confronting the annual variation of total suspended material with the annual variation of river discharge during 2003-2013, one can observe that they have almost opposite behaviors. While the river discharge presents its high regime between November-April the total suspended material presents its high regime during March- October. This quasi-opposite relation between river discharge and suspended material concentrations does not necessarily imply that the increase in river discharge may cause a decrease in the concentration of total suspended material but might mean that the influence of river discharge in eroding and re-suspend sediments to water column overcomes the supply of sediments by Zambezi River. In March although the wind speed is relatively weak there is a feature of high concentration near the Zambezi mouth, a clear demonstration that in absence of significant winds the Zambezi flow may control the variability of suspended material in Sofala Bank. Comparing the variation pattern of Zambezi discharge before the Zambezi Catchment and recent years we hypostatize that the weakening of river discharge in influencing the annual variation of total suspended material might have started after the regulation of Zambezi River flow when the differences between high and low flows regime started to be less significant.

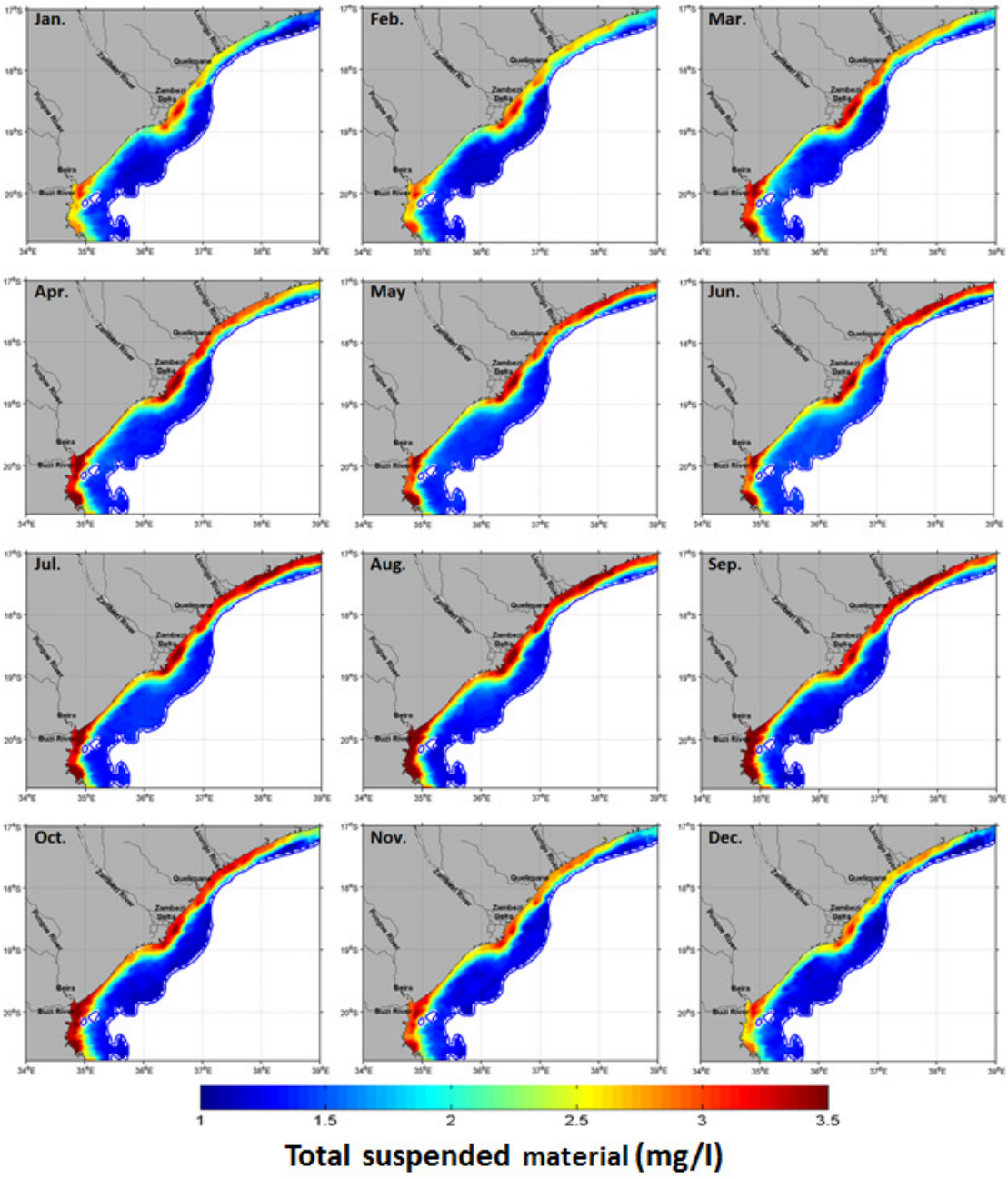

Figure 3.13: Climatology of total suspended material computed from monthly composites of Modis-Aqua images by applying the red-green ratio relationship obtained from regression of in situ remote sensing reflectance and is situ suspended material. The TSM was estimated for depths not greater than 50 m.

Organic suspended material

The seasonal variation of organic suspended material (Fig. 3.14) presents a similar pattern to total suspended material. It also presents two regimes, a low regime with concentrations lower than 1.6 mg/l in the plume cores running from November to February and a high regime with concentrations exceeding 1.7 mg/l in the plume cores and running from March to October. Analogously to total suspended material, the organic suspended material is also more controlled by wind rather than by river discharge. During high regime the plumes of organic suspended materials seam to move north and a high concentration core appears near 17.5°S in front of Licungo River mouth. The appearance of this core during the regime of greater wind speeds suggest that the re-suspension by wind and wind waves may be important over there.

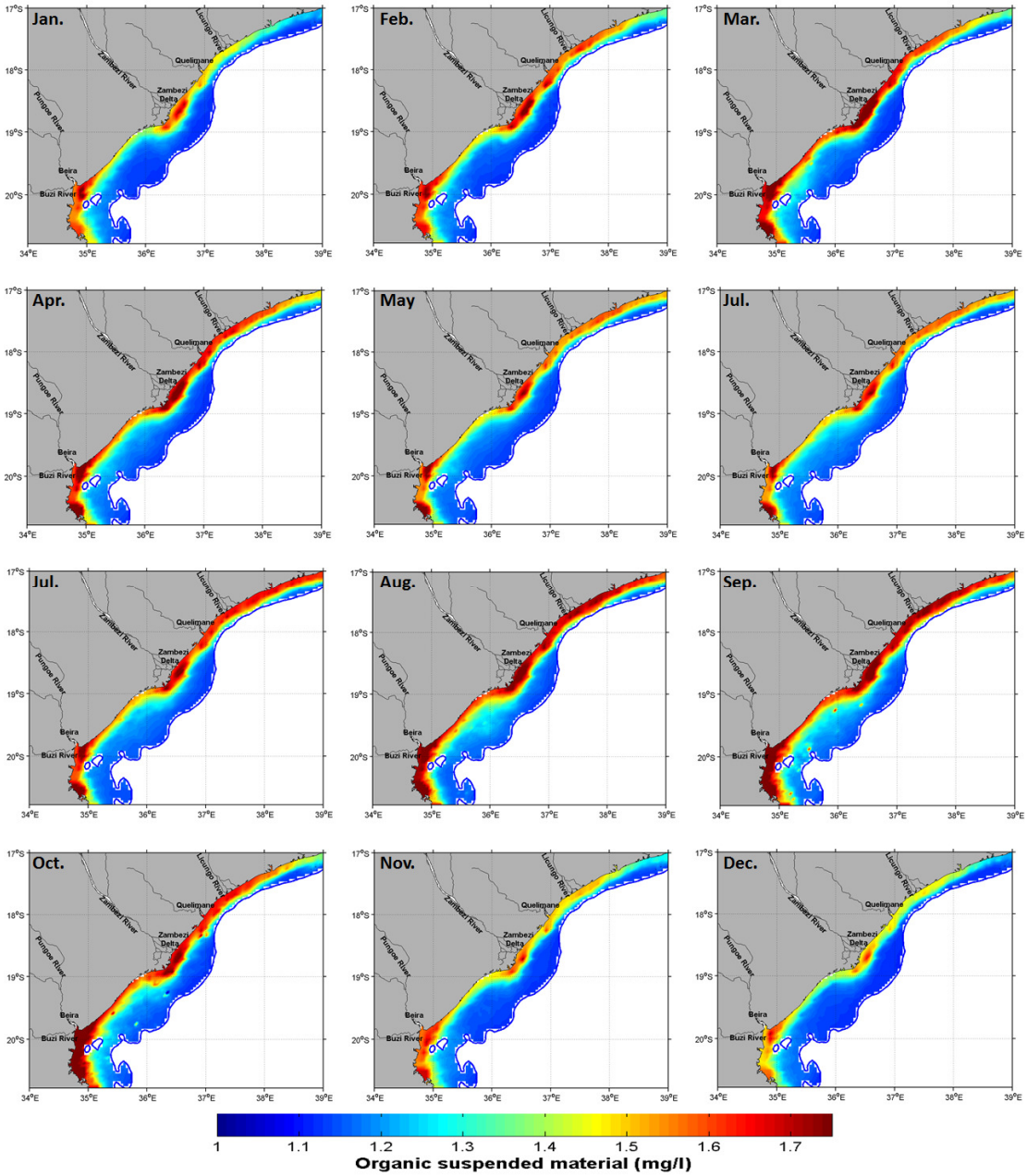

Figure 3.14: Climatology of organic suspended material computed from monthly composites of Modis-Aqua images by applying the red-blue ratio relationship obtained from regression of in situ remote sensing reflectance and is situ suspended material. The OSM was estimated for depths not greater than 50 m.

Influence of Zambezi river discharge on total suspended material

The influence of the Zambezi River in the concentration variation along the Sofala Bank is evaluated through the correlation between the monthly average flow rate of the Zambezi River and the spatiotemporal variation of the concentration of the total suspended material. Strong

positive correlations indicate that river discharge increases the concentrations of total suspended material. Figure 3.15.1 and 3.15.2 present spatial correlation between Zambezi River discharge and total suspended material concentrations for Lag time equal zero (total suspended material correlated to river discharge of same month) to Lag equal three (total suspended material correlated to river discharge of three months before). The strongest correlations are found in front of Zambezi Delta a bit far from the coast, showing the importance of Zambezi discharge in supplying sediments to central Zambezi Delta. The dispersal of suspended sediments away from the coast is presumably promoted by winds and local circulation. Around the south region of Sofala Bank, near the mouths of Pungue and Buzi Rivers, there is an area of strong negative correlation between the Zambezi River discharge and TSM near the coast, followed by a spot of weak positive correlation, located a bit far from the coast. These features suggest that in this region, Pungue and Buzi plumes might push the south-going branch of the Zambezi plume offshore. During second and third months after the Zambezi flow enters Sofala Bank (Lag=2 and Lag=3), the south and center signals of positive high correlations seem to merge and move mainly south Sofala Bank, suggesting that the total suspended material drained by Zambezi river into Sofala Bank drifts mainly southwards, not stuck to the shore. As mentioned before, the negative correlation between the Zambezi River discharge and the total suspended material in other regions of Sofala Bank do not necessarily imply that the Zambezi discharge inhibits the increases in suspended material but may mean that it is not the main governor of the variation of suspended material.

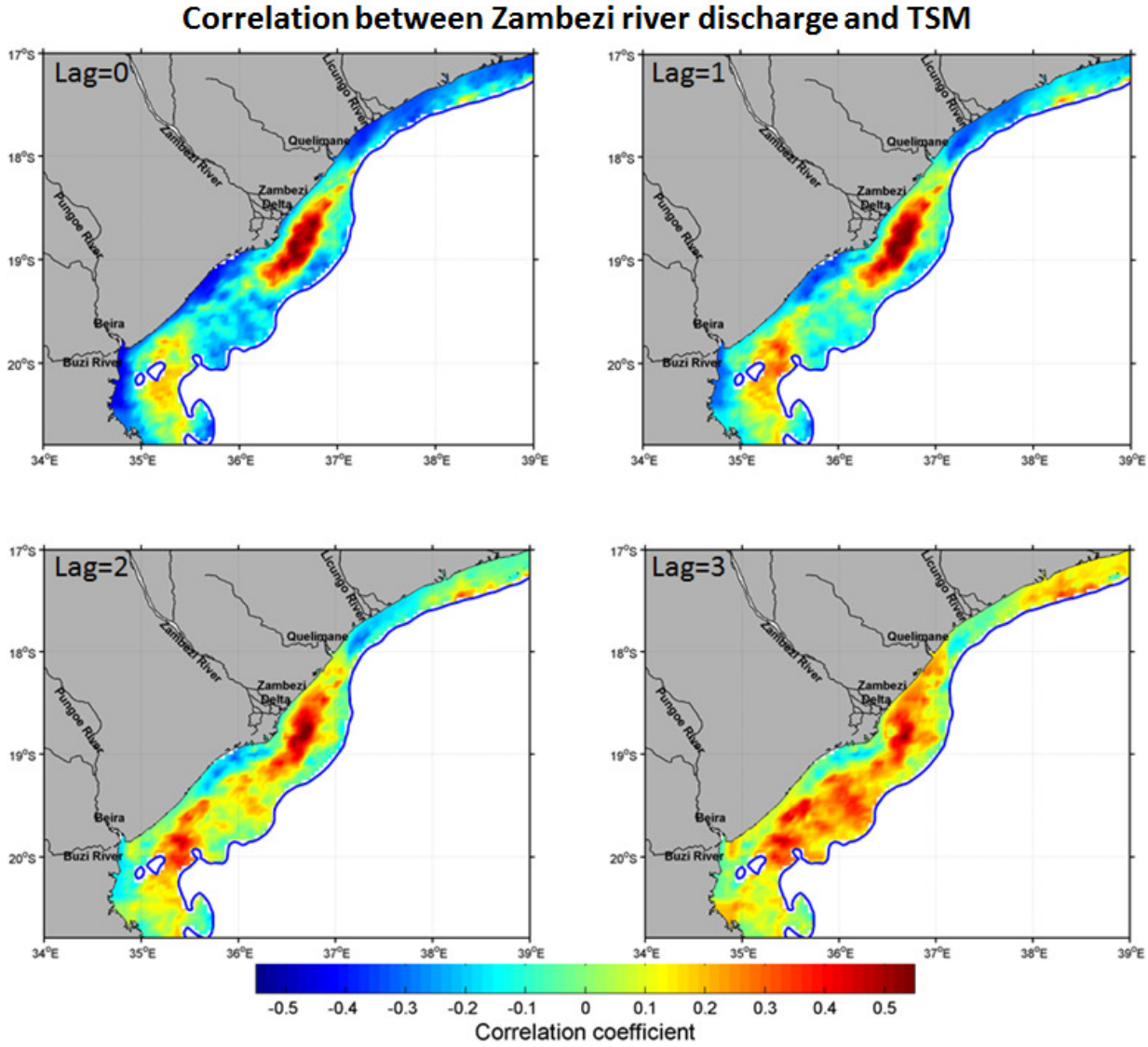

Figure 3.15.1: Spatial correlation between Zambezi River discharge and TSM for the period of 2003-2013.

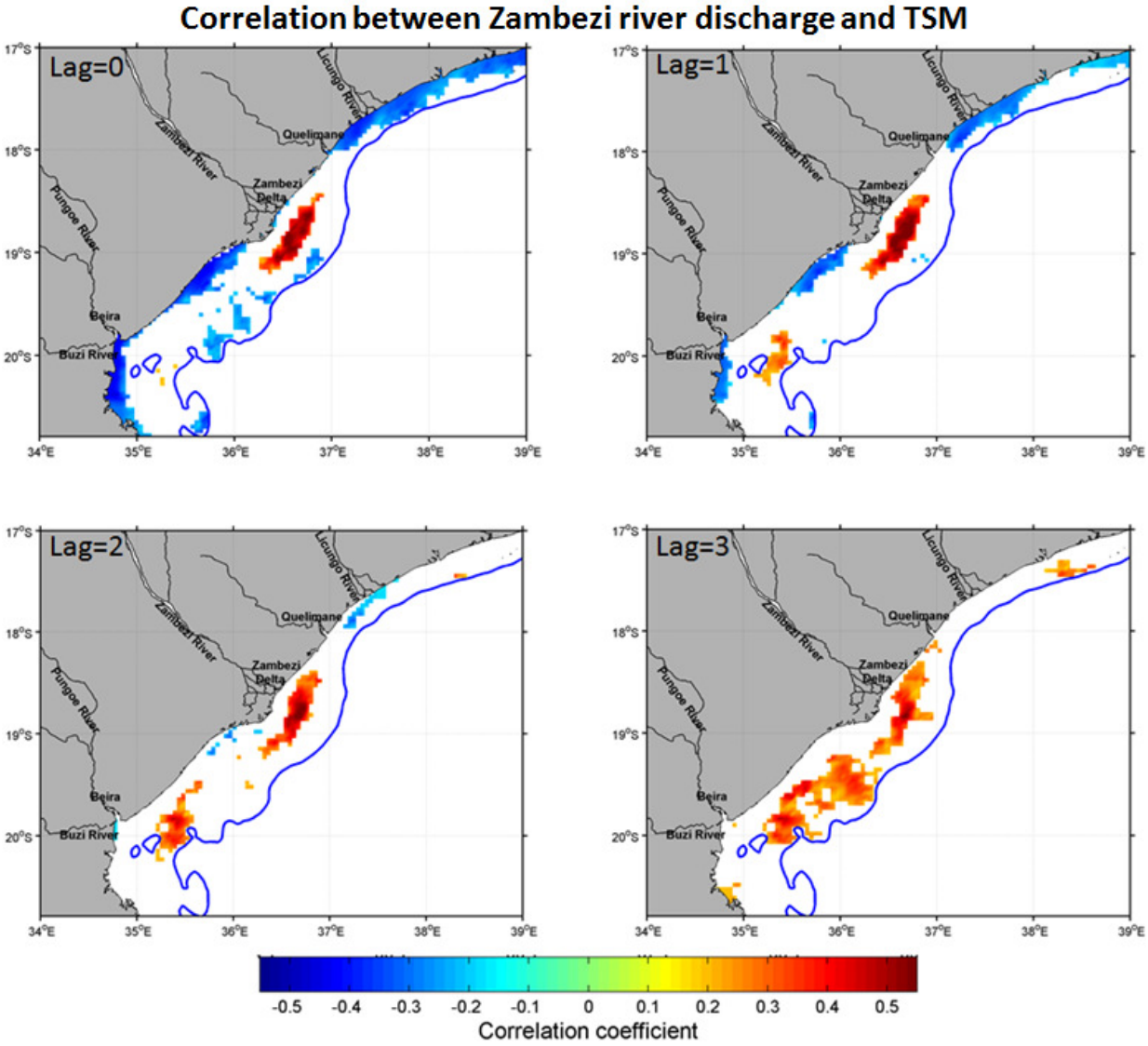

Figure 3.15.2: Same information presented in Figure 3.15.1 with the areas of statistical confidence less than 95% excluded.

Influence of wind speed on the variability of total suspended material

To evaluate the spatial influence of wind on the variation of total suspended material a monthly time series of monthly mean wind speed over Sofala Bank is correlated to the time series monthly mean of total suspended material (Fig. 3.15.3). The correlation coefficient decreases from the coast denoting the weakening of wind and wind wave action in re-suspend sediments as the depth increases. Comparing the spatial variation of correlation of river discharge against TSM and wind speed against TSM, one can note that they are opposites, that is, in regions where the correlation of river discharge is stronger, as is the case of central Sofala Bank near the main mouths of Zambezi Delta, the correlation of wind speed is weaker or negative. The spatial

variation of correlation between wind speed and TSM suggest that wind speed is the main governor of the variations in total suspended material in coastal shallow waters of Sofala Bank except in the central region where the Zambezi River is the main governor.

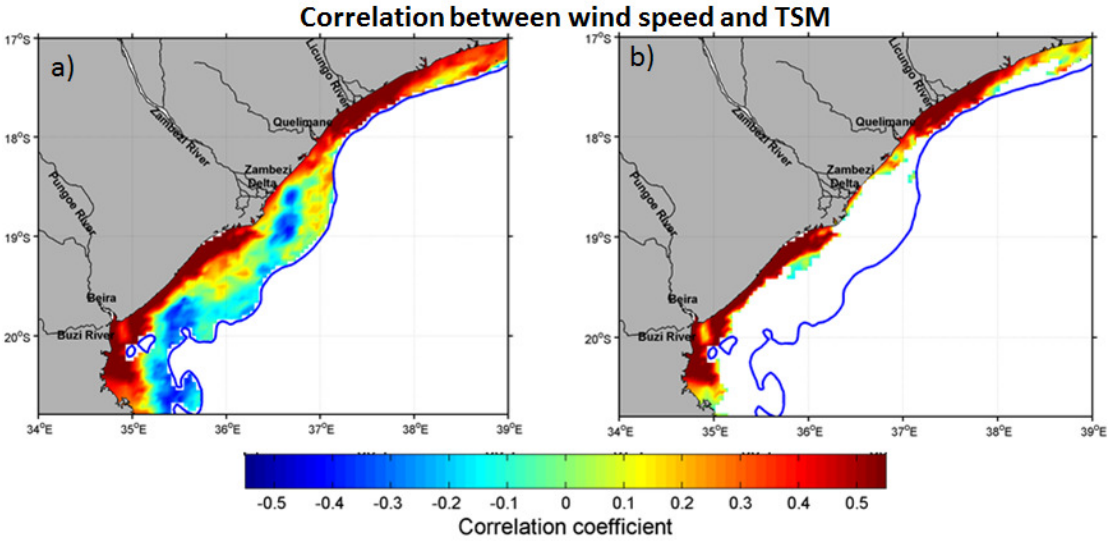

Figure 3.15.3: Spatial correlation between wind speed and TSM for the period of 2003-2013 (a); repetition of Figure 15.3a but with areas whose statistical confidence are less than 95% excluded (b).

Influence of waves on the variability of total suspended material

The spatial distribution of correlation between wave significant height (Hs) and concentrations of total suspended material (TSM) presented in Figure 3.15.4 is similar to that of wind speed and TSM, but with more remarkable low efficiency in channels and deep waters. According to correlation variation, increasing Hs promotes increasing in TSM concentrations except near Zambezi Delta mouths; Buzi mouth and Licungu were the inputs from rivers might overcome the wave action. Weak or negative correlations in front of river mouths and other coastal areas might denote the relative strength of river discharge and limitation of waves on remobilize sediments due deeper waters and channels.

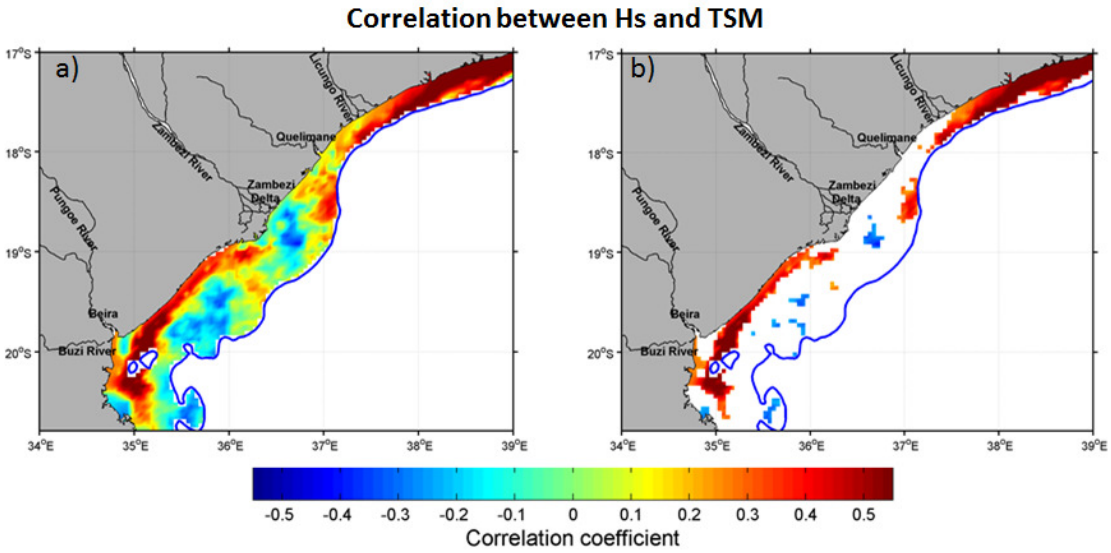

Figure 3.15.4: Spatial correlation between wave height and TSM for the period of 2003-2013 (a); repetition of Figure 15.4a but with areas whose statistical confidence are less than 95% excluded (b).

Influence of ENSO on the variation of total suspended material

The spatial influence of ENSO on the variability of total suspended material (TSM) in Sofala Bank is inferred through correlation between Niño 3.4 index, which is the most ENSO-representative (Barnston, et al., 1997), and monthly time series of spatial variability of TSM over Sofala Bank. The spatial distribution of correlation between Niño 3.4 index and TSM presented in Figure 3.15.5, repeated in Figure 3.15.6, shows two spots of stronger negative correction, one in front of Zambezi Delta ~18°S and other more south ~20°S, a bit offshore in front of Buzi River mouth during Lag equal zero and Lag equal one. Although being somehow confusing to interpret, analogously to the correlation between river discharge and TSM it seems that during two and three months after Niño index was observed (Lag = 2 and Lag =3) the Zambezi Delta spot moves south and merge the one located in the south region and drift south. The analogy of distribution of positive correlation between spatial distribution of correlation coefficient between Zambezi River discharge against TSM and correlation between Niño 3.4 index and TSM suggest that Zambezi River discharge is affected by ENSO through weakening (enhancing) precipitation over the Zambezi basin during El Niño (La Niña) events. As consequence, strong inverse ENSO-TSM relation is found in regions where the Zambezi River is its main governor. The south drifting of Zambezi River and ENSO correlation signals a bit far from the coast of Sofala Bank suggest that in contrast to coastal plume, which drifts north under influence of coastal north going wind current (Siddorn et al., 2001), the TSM drifts south under influence of south going flow outer Sofala Bank shelf.

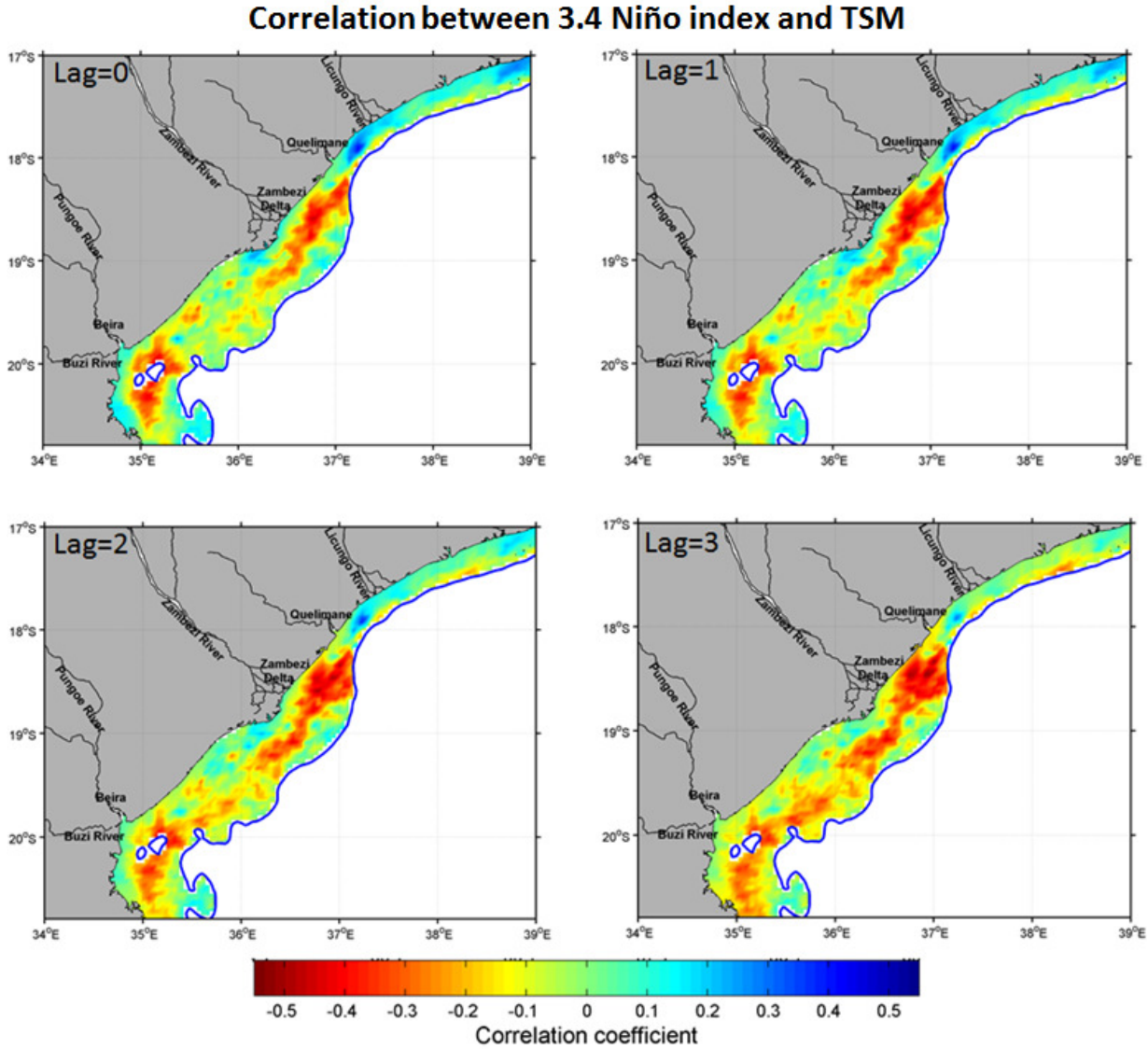

Figure 3.15.5: Spatial correlation between Niño 3.4 index and TSM for the period of 2003-2013. The color map values were deliberately set to increase from red to blue to facilitate the comparisons between these maps and those of correction between the Zambezi River discharge and TSM.

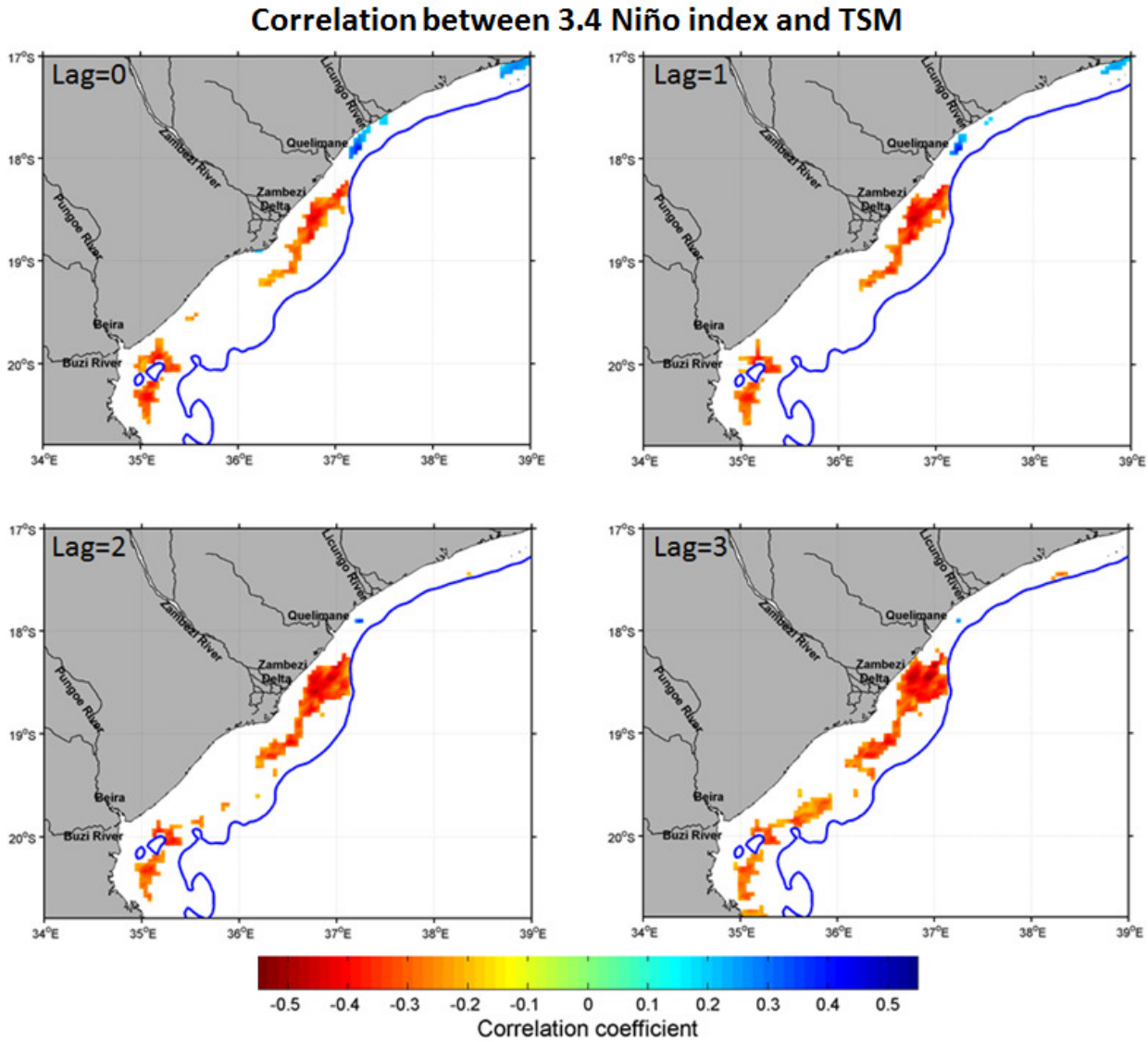

Figure 3.15.6: Repetition of Figure 3.15.5 but with areas whose statistical confidence are less than 95% excluded

Influence of Zambezi River discharge on the variation of organic suspended material

Analogously to TSM, the evaluation of the spatial influence of the Zambezi River discharge on the organic suspended material (OSM) was done through regression analysis between Zambezi River discharge and time series of spatial variability of OSM presented in Figure 3.16.1. Again, for OSM, during Lag equal zero and lag equal one the influence of Zambezi River is denoted by two spots of positive correlation in Sofala Bank, a stronger one located in central region ~18°S in front of main Zambezi Delta mouths and other relatively weak located south ~20°S, a bit far from the mouth of Buzi River. Two and three months after the Zambezi discharge is drained in

Sofala Bank, the spots merge and drift north along the coast suggesting that OSM supplied by Zambezi River in Sofala Bank mainly drifts northwards along the coast of Sofala Bank. This finding is consistent with Siddorn et al., (2001) who observed the north going of Zambezi River plume in Sofala Bank using in situ data.

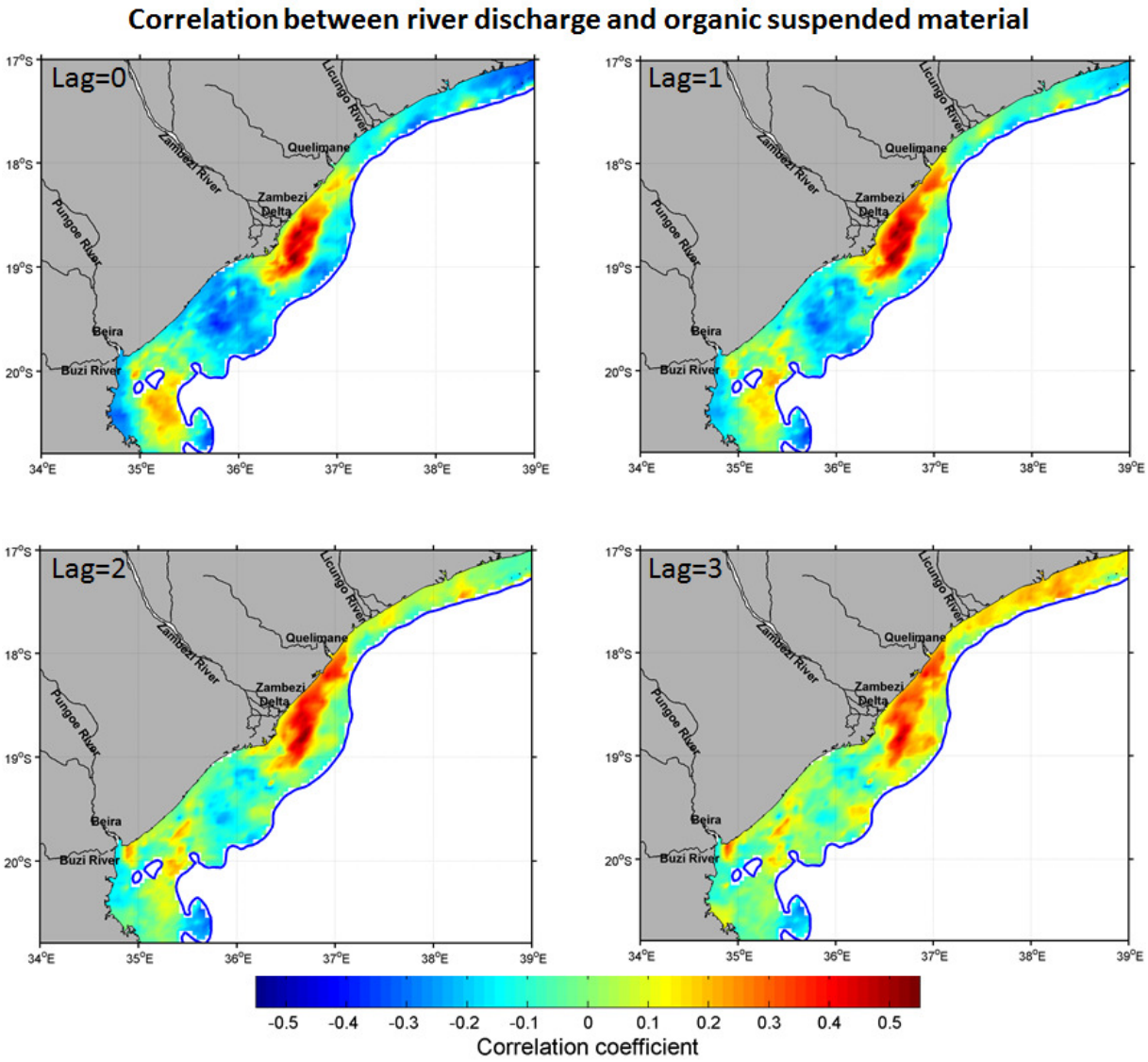

Figure 3.16.1: Spatial correlation between the Zambezi River discharge and OSM for the period of 2003-2013.

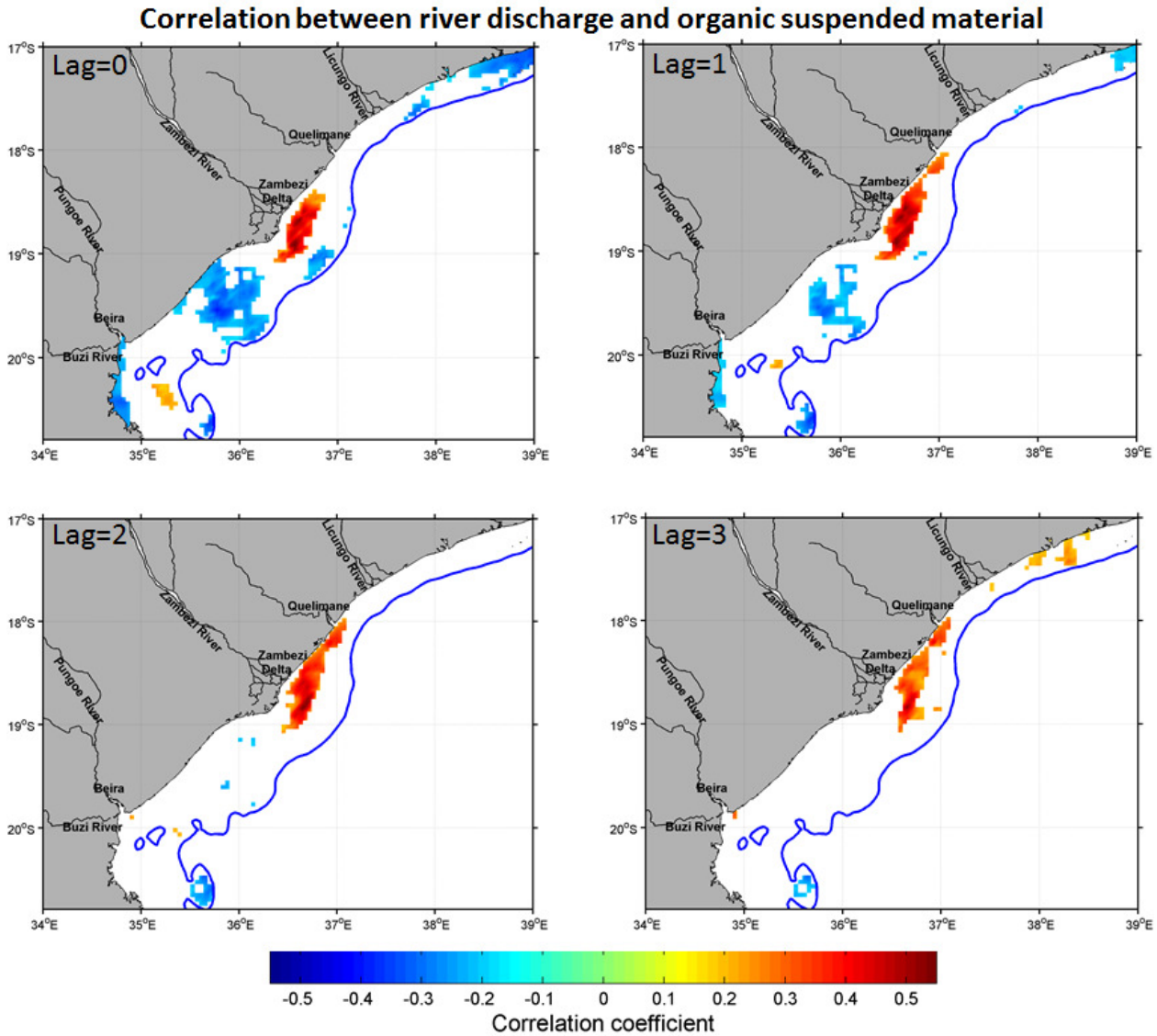

Figure 3.16.2: Same information presented in Figure 3.16.1 with the areas of statistical confidence less than 95% excluded.

Influence of wind speed on the variation of organic suspended material

Figure 3.16.3 presents the evaluation of the spatial influence of wind on organic suspended material (OSM) Sofala Bank performed through regression analysis between the monthly mean wind speed over Sofala Bank and monthly organic suspended material along Sofala Bank. As observed on TSM analysis, the correlation between wind speed and OSM decreases towards offshore denoting the weakening of wave action in remobilize sediments as the depth increases. The correlation distribution suggests that the wind speed dominates the OSM availability in most parts of coastal shallow Sofala Bank except in central region ~18°S and south ~20°S where the

correlation coefficients are weaker and out of 95 % of confidence (Fig. 3.16.3a). The areas where the wind speed has weak and statistically insignificant correlations coincide exactly with places where two spots of positive stronger correlation between Zambezi River discharge and OSM are located, suggesting that the influence of Zambezi River discharge overcomes the wind action in those regions.

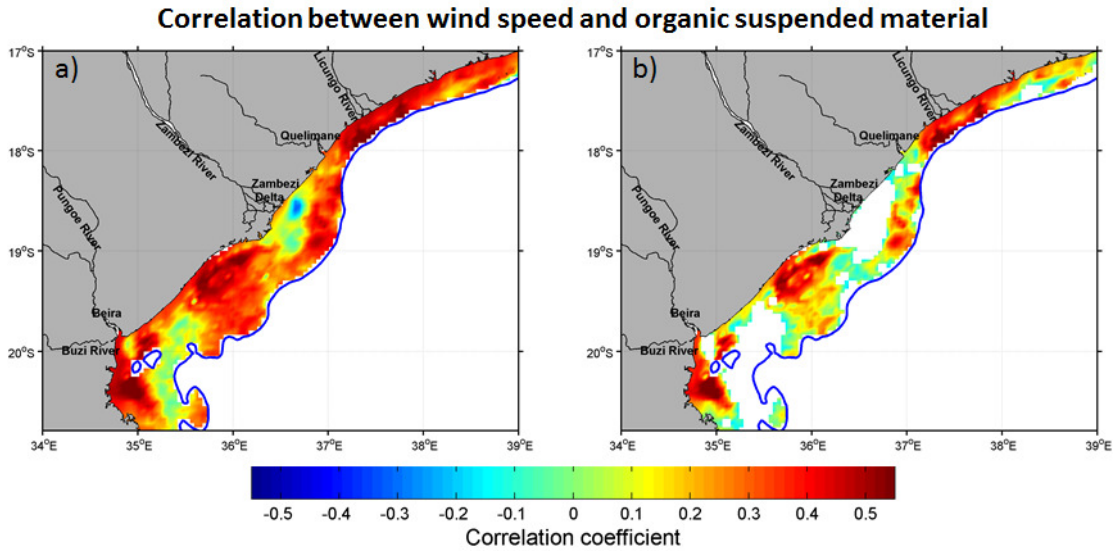

Figure 3.16.3: Spatial correlation between wind speed and OSM for the period of 2003-2013 (a); repetition of Figure 3.16.3a but with areas whose statistical confidence are less than 95% excluded (b).

Influence of waves on the variation of organic suspended material

Figure 3.16.4 presents the spatial correlation between wave significant height (Hs) and concentrations of organic suspended material (OSM). Unlike suspended material (TSM), the influence of waves on OSM seems to be weaker, with statistical confidence lower than 95% in most of Sofala Bank (Fig. 16.4b) except in north and south extremes where the influence of wave is highlighted by high positive correlations. The lower wave influence on OSM in contrast to TSM might reflect the difference in their main sources. While the inorganic suspended material (ISM) is supplied by re-suspension and erosion along the whole coast of Sofala Bank, the main source of the organic material might be the Zambezi River.

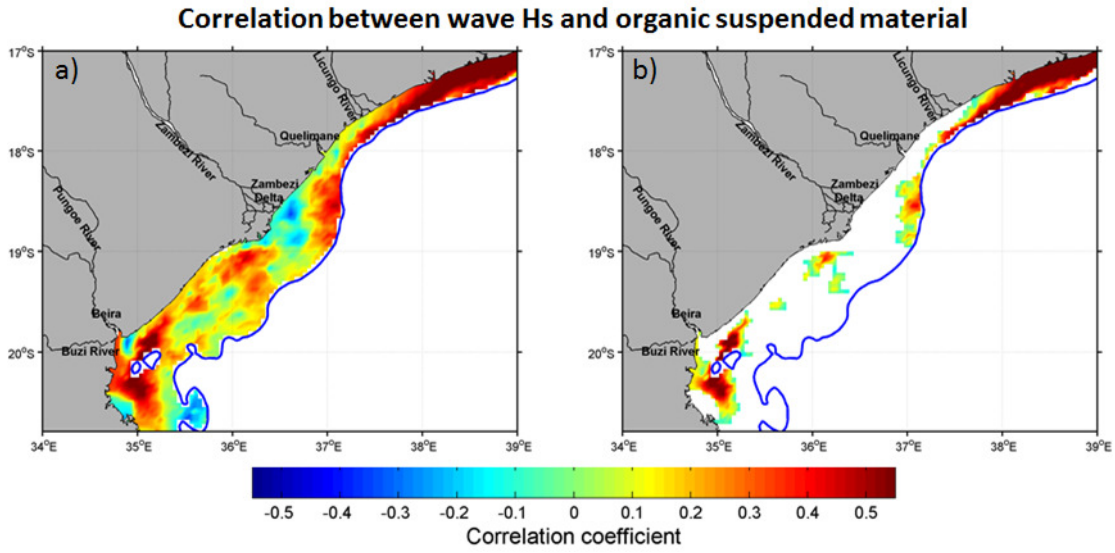

Figure 3.16.4: Spatial correlation between wave height and OSM for the period of 2003-2013 (a); repetition of Figure 16.4a but with areas whose statistical confidence are less than 95% excluded (b).

Influence of ENSO on the variation of organic suspended material

Spatial variability of correlation between 3.4 Niño index and organic suspended material (OSM) over Sofala Bank is presented in Figure 3.16.5. The pattern of the distribution of the correlation coefficients between the 3,4 Niño index and OSM is Similarly to that between Zambezi River discharge and OSM, with two spots of negative correlation located in central Sofala Bank ~18°S in front of Zambezi Delta mouths and in south ~20°S near Buzi River during Lag zero and Lag one. These features show that since the river discharge, which is the main controller of OSM in those regions is affected by ENSO the OSM over those regions is also affected. The apparent merge and north drifting of the spots suggest again that the OSM supplied by Zambezi River in Sofala Bank mainly drifts northwards along the coast.

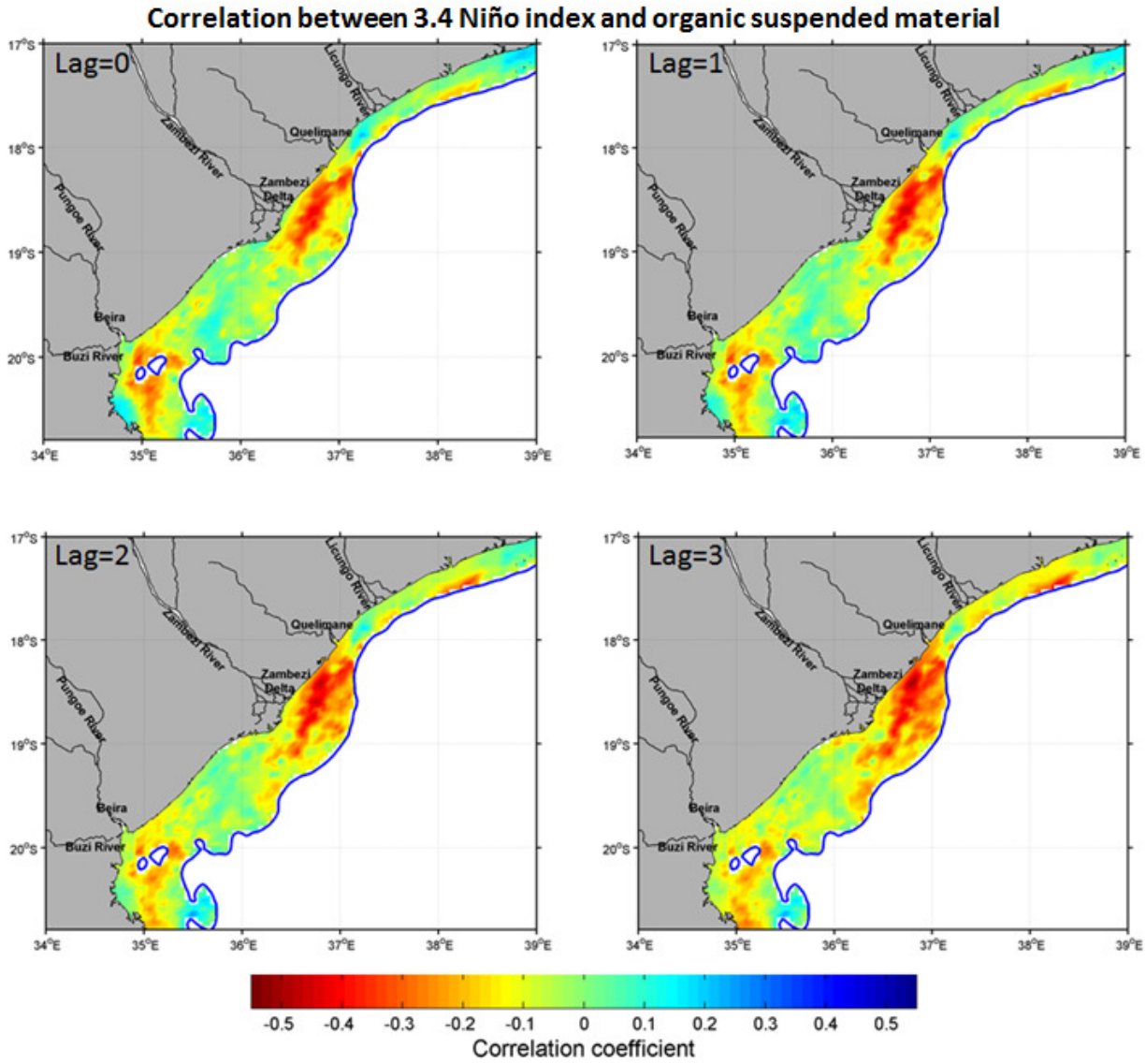

Figure 3.16.5: Spatial correlation between Niño 3.4 index and OSM for the period of 2003-2013. The color map values were deliberately set to increase from red to blue to facilitate the comparisons between these maps and those of correction between Zambezi River discharge and OSM.

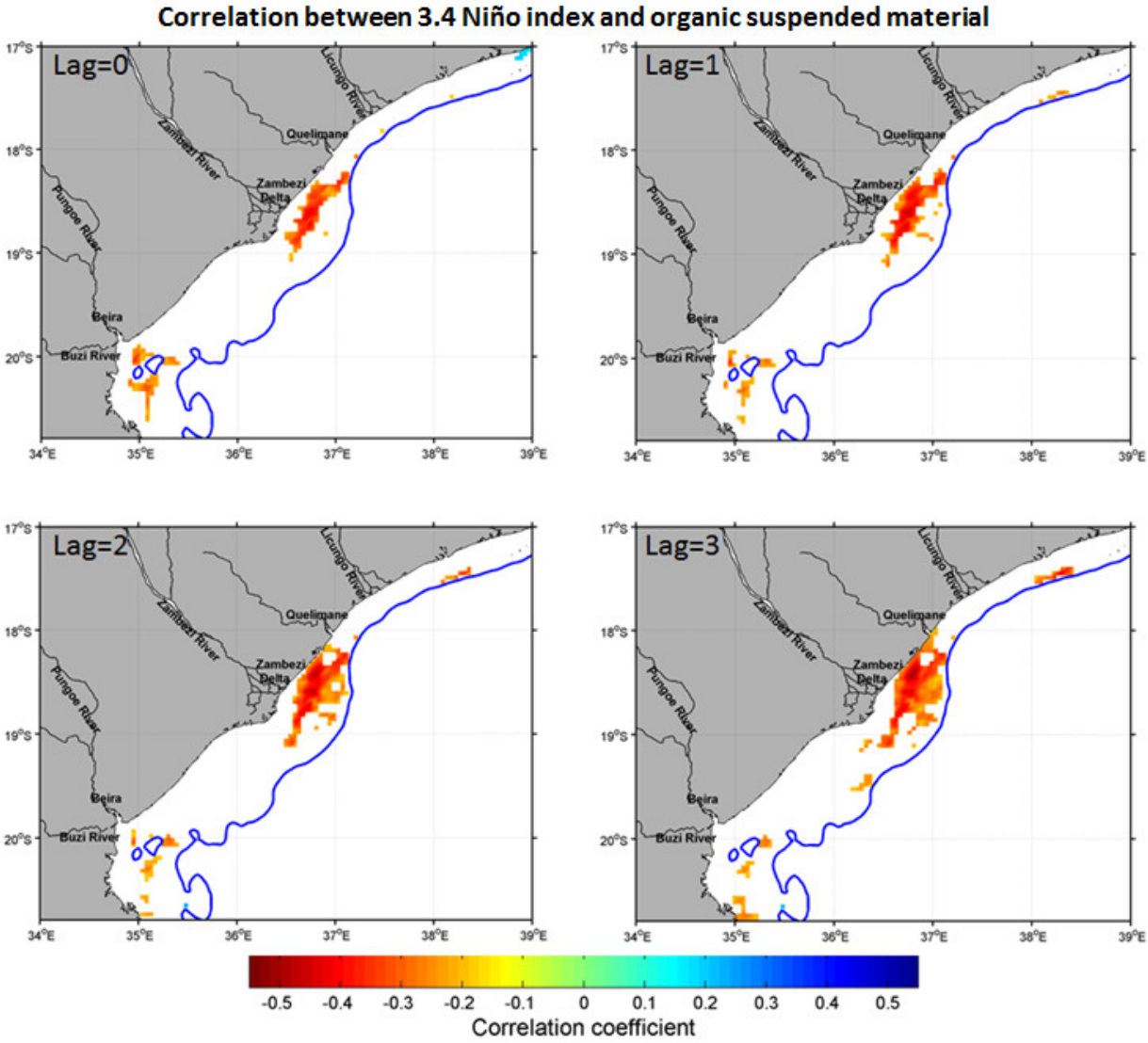

Figure 3.16.6: Repetition of Figure 3.16.5 but with areas whose statistical confidence are less than 95% excluded

3.6 Conclusions

There are two main surface water types in Sofala Bank, one located onshore with peak in the green region denoting presence of sediments drained from the continent, and other located in the outer shelf with the peak of reflectance located in blue region due to scattering by water molecules and depressed reflectance in the red region due absorption by waters. These findings suggest that the plume waters, dominated by continental inorganic sediments can be distinguished from the adjacent waters through their spectral characteristics.

Color ratio relationship showed the most robust for retrieving suspended material and it improves when the regression analysis is limited to more onshore, relatively dominated by

inorganic suspended material, presenting peak in the green region of the spectrum, with red:green ratio greater than 0.1 and red:blue ratio greater than 0.25.

Evaluation of seasonal variability of suspended material retrieved through applying empirical relationship on Modis-Aqua monthly composite revealed that suspended material in Sofala Bank presents two regimes: one of low concentrations extending between November and February and other of high concentrations extending between March and October.

Wind spend and waves are the main governors of the variability of suspended material in most of the Sofala Bank coastal waters except in the central region, in front of main mouths of Zambezi Delta, where the Zambezi River is the main controller.

The variation of Zambezi river discharge and suspended material suggested existence of two pathways of Zambezi suspended materials along Sofala Bank. Organic suspended material drift north along the coast presumably under the action of wind currents, and the inorganic suspended material that reaches the outer shelf drifting to the south, under the action of the Mozambique Channel south going flow, which affects the shelf break.

Regions under influence of Zambezi River present strong negative correlations between 3.4 Niño index and concentrations of suspended materials suggesting that El Niño Southern Oscillation (ENSO) causes decreasing (increasing) in the concentration of suspended material over Sofala Bank through weakening (enhancing) rainfall in Zambezi Basin.

Chapter 4

Mapping suspended sediment plume in Sofala Bank, central Mozambique

Abstract: Sediments and other materials brought by Rivers to the marine environment are of great importance for marine productivity. The aim of this study was to map the spatial-temporal variability of sediment plume and mixed waters in Sofala Bank using Landsat images dataset. We applied spectral linear mixing analysis (SLMA) in eleven Landsat images from TM Landsat-5 and OLI Landsat-8 to map three fractions of water types using their reference spectral curves as input end-member. The water types were following: sediment plume, with high sediment concentration and located near the coast; mixed waters, with intermediate concentration of sediments and located in inner shelf between the coastal waters and offshore waters; offshore clear waters located further offshore. Sediment plume and mixed waters showed high temporal variability and their extension varied inversely suggesting that when the sediment plume extends offshore the mixed waters are pushed further offshore and sink in deep waters. The wind speed presented a strong coefficient of determination to the area of sediment plume, suggesting being the main governing factor of sediment plume dispersion in the Sofala Bank. The mixed waters correlated weakly to both Zambezi river discharge and wind speed, suggesting that there are other factors controlling the variability of their extension.

Keywords: Sofala Bank, image processing, Landsat, spatial-temporal variability, sediment plume

4.1 Introduction

The river discharges have great importance in physical and biogeochemical processes and productivity of continental shelves because the fresh water and sediments brought into marine environment affect directly in stratification variation, mixture, and transparency of the water column, and provide nutrients for primary productivity (Lihan, et al., 2008; Piola et al., 2008). The water supplied by Zambezi River in Sofala Bank, the western side of Mozambique Channel, is believed to have high influence in secondary coastal production along the central shelf of Mozambique (Lutjeharms, 2006; Nehama, 2012). Sediment plume dispersion is of high spatial and temporal variability and can be controlled by a number of factors including storms, river discharges, wind speed and wind direction. These various factors can complicate the monitoring of plume dynamics by traditional approaches such as mooring arrays and shipboard surveys (Thomas and Weatherbee, 2006). In the other hand, field measurements are restricted to a limited number of stations (and/or samples) that are usually inadequate to resolve and characterize plume dynamics in both space and time (Nezlin and DiGiacomo, 2005). The use of remote sensing data becomes a good option for plume study as it offers synoptic and frequent regional view that enable more effective analysis of temporal and spatial variations of parameters that can be measured from space (Nezlin and DiGiacomo, 2005). Satellite ocean color observation of coastal surface water can be used to distinguish the sediment plume from the adjacent water masses especially based on increased sediment concentration in the plumes (Meters and Warrick, 2001; Nezlin and DiGiacomo, 2005). Despite offering a high temporal resolution, and thus, offering possibility of much details for analysis of temporal variability, the sensors that are commonly used for ocean color studies become inadequate for monitoring plumes from low and medium river discharge because of their low spatial resolution. Landsat dataset is a good option to map small and medium plumes like Zambezi river plume in Sofala Bank as they present relatively higher spatial resolution and contain visible and infrared bands of electromagnetic spectrum, which are ideal to map water quality. Image classification, a technique commonly applied for land targets, has been successfully applied to map river plumes (Warrick, et al. 2004, Thomas and Weatherbee, 2006; Lihan et al., 2008; Zoffoli et al., 2011). The challenge of using image classification in optically complex coastal waters, characterized by a mixture of optically active substances (OAS) such as sediments, colored dissolved substances and photosynthetic pigments (D'sa and Miller 2005) is to separate water types from each other. Two methods commonly used to map river plume and coastal waters are maximum likelihood (Warrick, et al. 2004, Thomas and Weatherbee 2006, Lihan, et al. 2008, Zoffoli, et al. 2011) and spectral linear mixing analysis (Novo and Shimabukuro, 1994; Rudorff et al., 2007; Rudorff et al., 2011). Although it has been used successfully in other works of mapping plumes and other coastal waters, the maximum likelihood is a subjective and time-consuming method mainly in studies involving time series analysis. The subjectivity of this method is created by the fact that for each image to be classified it requires a new collection of samples, with the possibility of having samples with different spectral characteristics in the same class. The spectral linear mixing analysis (SLMA) uses end-members with ideal characteristics of each class or OAS and the end-

members can be applied to several images for time series analysis (Rudorff et al., 2007). The critical part of SLMA is to select the pure end-members that represent the elements present in the scene Rudorff et al., (2011) compared mixiumum likelihood (ML) and SLMA methods for mapping Paraíba do Sul River plume (Brazil) and found that SLMA had some relevant advantages including having more information spectral variability and distribution of water constituents. The present work aims to analyse the spatial-temporal variability of Zambezi River plume applying SLMA method on Landsat-5 TM and Landsat-8 OLI images.

4.2 Study area

Figure 4.1 presents the location of the study area considered for the present study, which is located within Sofala Bank, in front of the Zambezi Delta mouths.

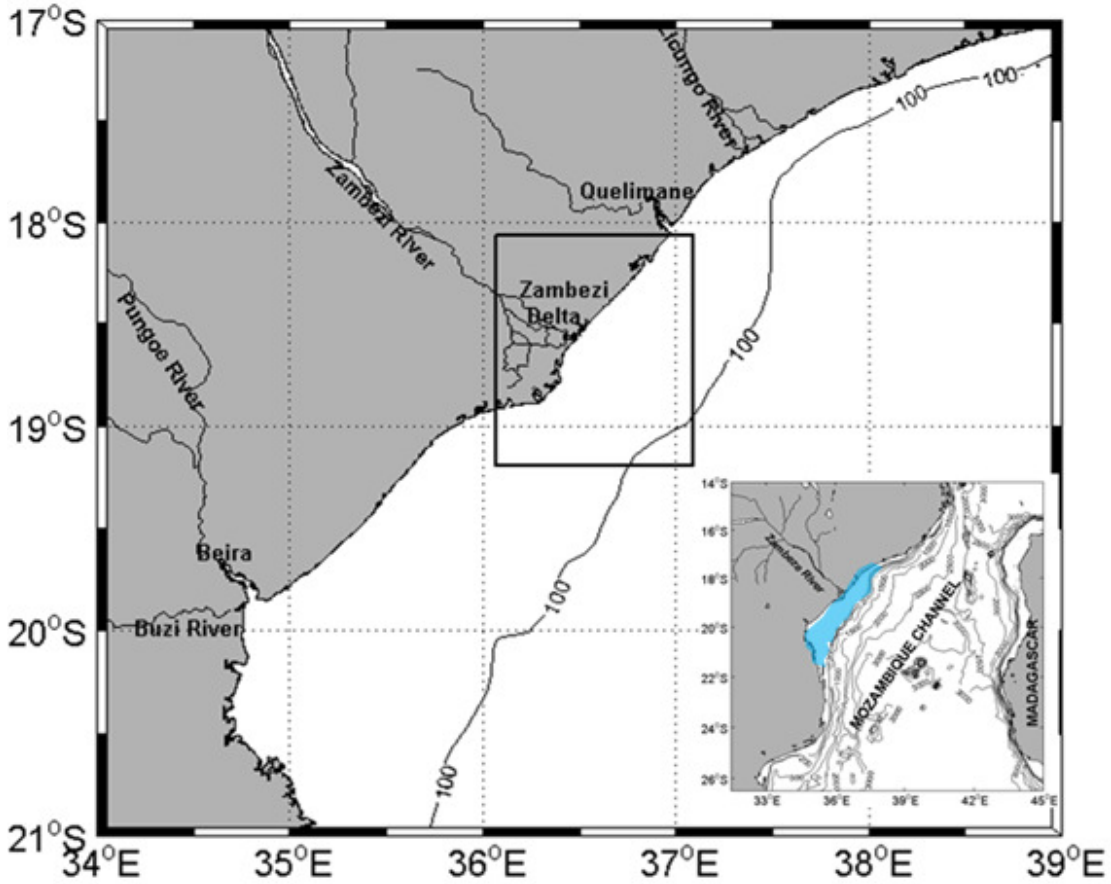

Figure 4.1: Map showing Sofala Bank and the area considered for Landsat dataset analysis (back box). The 100 m isobath is represented for bathymetry reference. The inner image locates regionally the Mozambique coast and the Mozambique Channel. The blue-shaded area in the inner image represents the position of Sofala Bank in the Mozambican shelf.

4.3 Data and methods

Landsat image dataset

A total of eleven Landsat images from TM and OLI corresponding to path 166 and row 73 for the period between 1998 and 2015 were used to access the sediment plume characteristics in Sofala Bank. The images were provided by the United States Geological Survey (USGS) with atmospheric corrections already performed. Only bands corresponding to the visible region of the electromagnetic spectrum (435-2345 nm) were used for the study. The area considered for in the present study is between 36°/37° E longitude and 18°/19° S latitude (Fig. 4.1). It was considered to be more representative for the sediment plume characterization because it includes the widest Zambezi river mouth in Sofala Bank, which is located around 18.7°S. The date and time of acquisition, the hydrological season and the local tide phase are presented in Table 4.1.

Table 4.1: Date and time of Landsat image acquisition, local tide phase, and hydrological season

Aquisition Date	Orbital sensor	Scene Center time (GMT)	Local tide phase	Local Season
03/07/1998	TM Landsat 5	07:13:43	Neep tide	Dry
07/10/1998	TM Landsat 5	07:14:26	Spring tide	Wet
10/09/2000	TM Landsat 5	07:13:47	Neep tide	Dry
08/05/2001	TM Landsat 5	07:15:48	Spring tide	Dry
30/09/2007	TM Landsat 5	07:28:34	Spring tide	Dry
31/08/2008	TM Landsat 5	07:21:06	Spring tide	Dry
02/10/2008	TM Landsat 5	07:20:07	Spring tide	Wet
26/06/2013	OLI Landsat 8	07:33:33	Spring tide	Dry
13/08/2013	OLI Landsat 8	07:37:37	Neep tide	Dry
18/07/2015	OLI Landsat 8	07:35:10	Spring tide	Dry
19/08/2015	OLI Landsat 8	07:35:21	Spring tide	Dry

LSMA

Spectral linear mixing analysis (SLMA) assumes that the reflectance value in each pixel is a linear combination of responses of each distinct component in the mixed target (Holben and Shimabukuro 1993; Rudorff et al., 2007). Each component is a fraction of the pixel value and the

SLMA aims to decompose each pixel and estimate the abundance of each pure component or endmember. The basic mixture model may be formulated as:

$$r_i = \sum a_{ij}.x_j + e_i$$

r_i is spectral reflectance for a pixel in a band i; a_{ij} is spectral response of mixture component, j, for spectral band i; $x_j$is proportion of mixture component, j, for a pixel; e_i is the error term for spectral band i is the sum of the fractions at each pixel must range between 0 and 1 or at least close to. For this study, there was defined three end-members: (i) sediment plume, (II) mixed waters and (III) offshore waters. The spectral curve of each end-member was selected using visual interpretation of the scenes. There was considered the end-members extracted from 8th May 2001 image as input for TM Landsat 5 images and end-members of 18th July 2015 image as input for OLI Landsat 8 images. The end-members from these two images were selected because they look more representative to those of other images, therefore it is presumed that the use of end-member of one single image as the reference did not influence the results since they all looked very similar.

Classification of SLMA fractions

To achieve the aim of evaluate the spatial-temporal variability of sediment plume and mixed waters, three fractional bands, resulted from SLMA were converted into classification maps, with classes separated by intervals of fractional abundance, following the criteria adopted by Rudorff et al., (2011). The classes were defined as follows: (i) high abundance: 0.66 to 1.0; (II) medium abundance: 0.33 to 0.66 and (II) low abundance: 0.0 to 0.33. After the classification the area of high and medium abundance were estimate for further analysis.

Evaluating the influence of river discharge, wind speed and tides on sediment plume dispersion

To evaluate the influence of river discharge, and wind speed on sediment plume dispersion, a linear regression of river discharge and wind speed with areas high abundance classes of sediment plume and mixed was performed taking into account the lag time that the plume may take to respond to the river and/or wind action. Daily Zambezi River discharge data, collected at Tete station, about 440 km distant to the main Zambezi mouth in Sofala Bank was provided by the national directorate for water affairs of Mozambique. Daily zonal and meridional wind components of gridded and blended sea surface vector winds from multiple satellites components (u and v) at a reference height of 10m above the surface with a spatial resolution of 0.25° (Zhang et al., 2006) from NOAA/NCDC was downloaded in https://www.ncei.noaa.gov/thredds/blended-global/oceanWinds.html on 8th March 2017.

4.4 Results and discussion

Spectral curves and fractional abundance classification

Figures 4.2.a and 4.2.b represent the spectrum end-members of sediment plume, mixed waters and offshore waters for TM-Landsat 5 image of 8th May 2001 (2a) and OLI Landsat image of 18th July 2015 (2b). In 8th May 2001 plume end-member curve increases from the blue band (locate at 485 nm) to the red band (660 nm) and decreases to reach its minimum values in infrared bands (1650 and 2215 nm). The mixed waters end-member presents an increase from the blue to the green band followed by a steep decrease to the infrared bands. The offshore waters end-member curve presents a sharp decrease from the blue to the red band followed by a small peak in the near-infrared band (830 nm) and a decrease to minimum reflectance values in the far-infrared band. In the OLI Landsat-8 end-member curves of 18th July 2015, the plume end-member shows a similar behavior to 8th May 2001, with an increase from the blue bands to the red band where reaches its peak, and a decrease from red band to infrared bands where it reaches the minimum reflectance values. The mixed waters end-member also shows a similar behavior to its corresponded curve on TM Landsat-5 image of 8th May 2001, increasing from blue bands to reach its peak in green followed by a steep decrease to near-infrared which continues sharply to far-infrared bands. The offshore waters end-member presents a slight increase from the coastal blue (440 nm) to the blue band (480 nm) followed by a steep decrease to the red band and continues decreasing sharply to reach the minimum reflectance values in the far-infrared bands. For the two images, there is a difference in reflectance magnitude and spectral shapes between the three end-members. The plume end-member peaks at red band and has higher reflectance magnitude due to its relatively higher concentrations of suspended sediments if compared to the peak at green band for less turbid mixed waters (Shi and Wang, 2010; Jansen, 2011). The location of reflectance peak in blue region for offshore waters end-member is expected, as the scattering coefficient in more clean water is higher in shorter wavelengths of the spectrum (Kampel and Novo, 2005). There is a slight difference between the shape of offshore end-members for TM Landsat-5 and OLI Landsat-8. The TM curve presents lower reflectance values, compared with the curves of sediment plume and mixed waters in all visible bands, and presents a small peak in the near-infrared band, in response to the presence of dissolved organic matter. The OLI curve of offshore waters end-member shows higher reflectance values than sediment plume and mixed water's curves in the blue and green bands, and does not present the small peak in the near-infrared band. The differences between the curves of offshore waters for TM and OLI might be due to their differences in spectral sensitivity associated to band location, radiometric

characteristics of the sensors. It is worth to mention that higher reflectance values in offshore waters than plume and mixed waters was also observed in situ measurements.

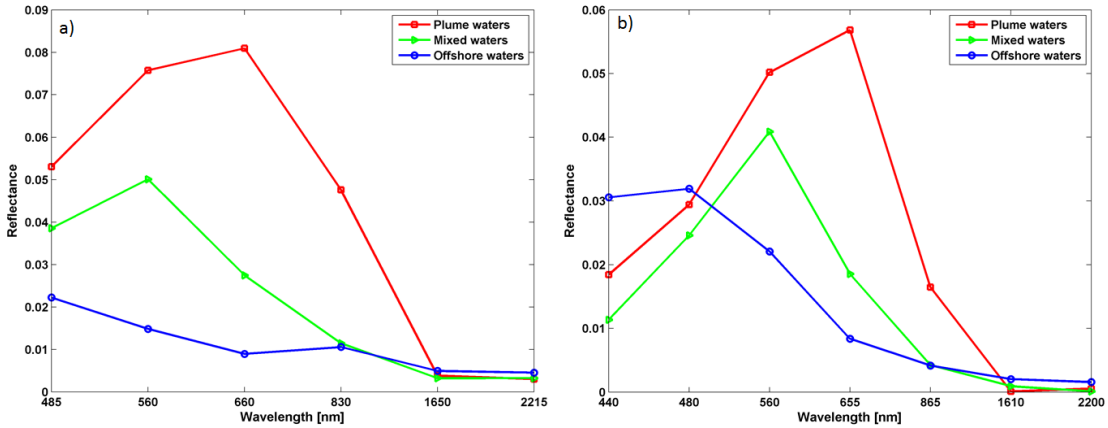

Figure 4.2: Spectral curve of the plume, mixed waters and offshore waters for TM-Landsat 5 images of 8th May 2001 (2a) and OLI Landsat image of 18th July 2015 (2b).

Maps of fractional abundance of each of the end-members are presented in figure 4.3. In general, all fractions presented coherency in terms of location of low and high values. Sediment plume fraction (Fig. 4.3a) presented higher values near Zambezi delta mouths and delineated well the region of plume dominance. The mixed waters fraction (Fig. 4.3b) had higher values in the inner shelf between the plume and the offshore waters. As expected, the offshore fraction (Fig. 4.3c) presented higher values over offshore region, which tended to decrease towards the coast. The RMSE (Fig. 4.4d), which gives the accuracy of model estimated reflectance in relation to the given "reference reflectance" provided as end-member for each fraction. Higher values of RMSE are found in mixed waters and offshore fractions. For mixed waters fraction it is probably associated with the fact that this water type is made up of plume dispersal waters and offshore waters, making it very complex and thus, much difficult to the model. Higher values of RMSE on offshore water fraction are possibly associated with the relatively higher variation of its spectral characteristic due to the influence of offshore dynamic parameters, such as currents and roughness. Figure 4.3e presents a color composite with sediment plume fraction in red, mixed waters fraction in green and offshore fraction in blue. The color composite reproduces clearly, what has been interpreted in fraction abundance maps separately, with plume fraction near the coast and with high values near Zambezi Delta mouths; mixed waters in the inner shelf, between the plume and the offshore regions; and offshore waters in the outer shelf and offshore.

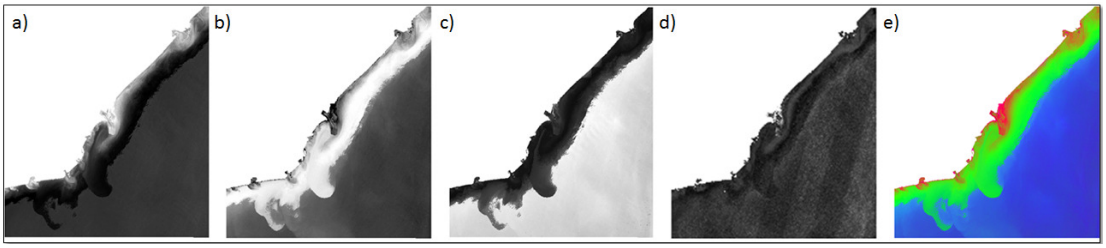

Figure 4.3: Mapped fraction abundance of the end-members by SMLA, on 18th July 2015 image: a) sediment plume; b) mixed waters; c) offshore waters; d) RMSE of the model estimation; e) color composite of plume-Red, mixed waters-Green and offshore waters-Blue. The brightness and darkness correspond to high and lower values respectively, and range close to zero and one.

The outputs fraction abundance classification for plume and mixed waters are presented in figures 4.4.1 and 4.4.2, respectively. For the plume fraction, the high abundance class is close to the coast and wider close to the Zambezi Delta mouth as expected. The medium abundance class is between the high abundance class and low, located offshore. There are some incoherences on 30th September 2007 and 13th August 2013 images, for example, where the medium abundance class is found more offshore where is expected to be the region of low abundance. The incoherence is probably associated with overestimation of phytoplankton-dominated waters induced by the presence of haze (Rudorff et al., 2007; Rudorff et al., 2011). The maximum and minimum extensions of high abundance class of plume fraction were observed on 30th September 2007 and 3rd July 1998. It is worth to mention that all the images are from the dry season (May-September) except the 2nd October one, which is from the beginning of the wet season (October-March). The high abundance class of mixed waters class is located between two medium abundance classes, one in along the border with the plume abundant fraction and other along the border with the mixed waters abundant fraction. From the abundance maps it is also possible to see that the extension of the plume high abundance class has an inverse relation to the extension of mixed waters high abundance class, that is, while the area of plume high abundance class is wider as on 30th September 2007 image, the respective area of mixed waters high abundance class is narrower. The opposite is observed on 3rd July 1998 image. This behavior suggests that when there is higher plume inflow the mixed waters are pushed offshore and sink and disappear where the bathymetry gets steeper.

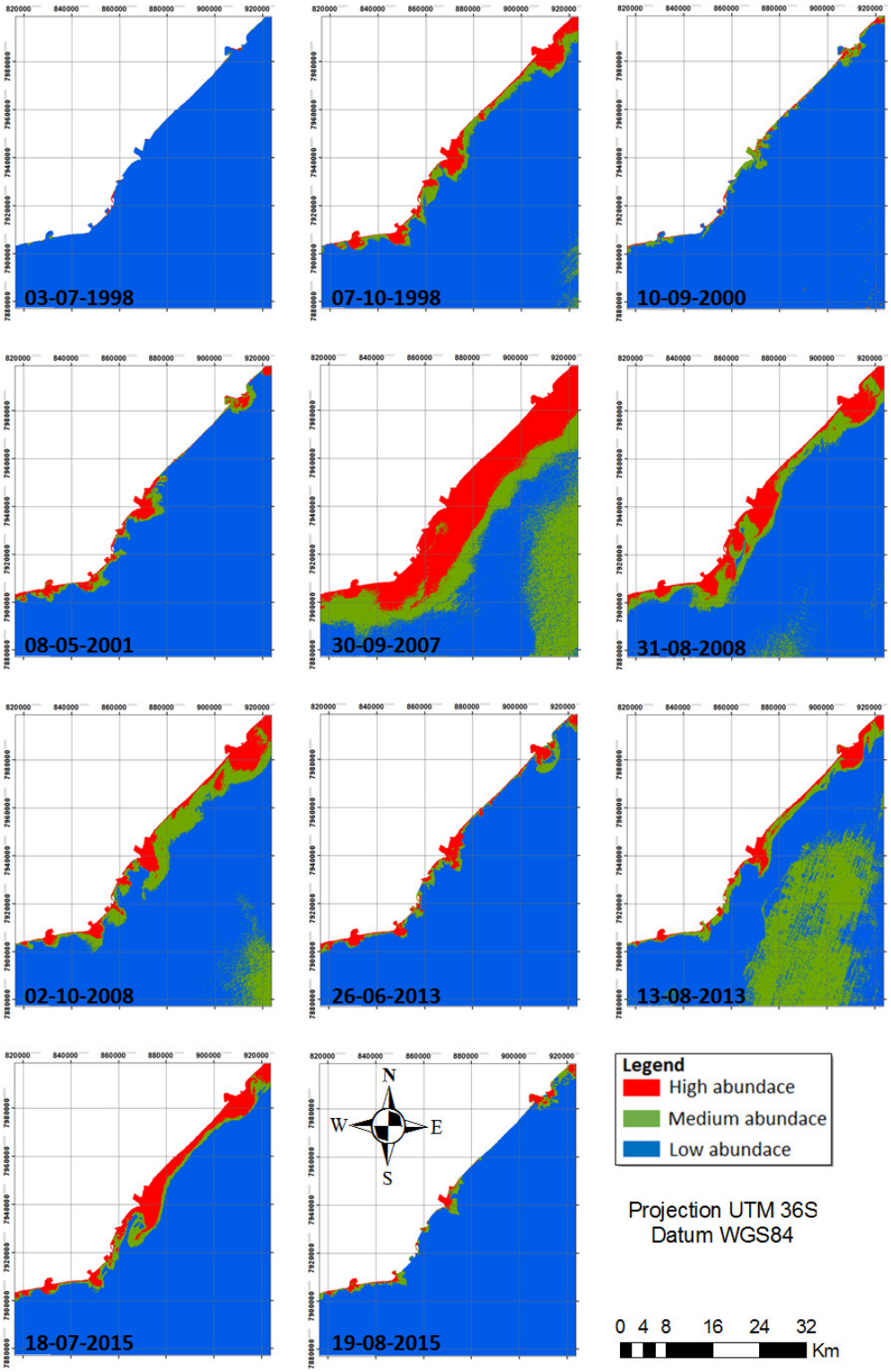

Figure 4.4.1: SLMA classified sediment plume fraction. The fractional abundances of the classes are as follows: 0.66 to 1.0 for high abundance; 0.33 to 0.66 for medium abundance; 0.0 to 0.33 for low abundance.

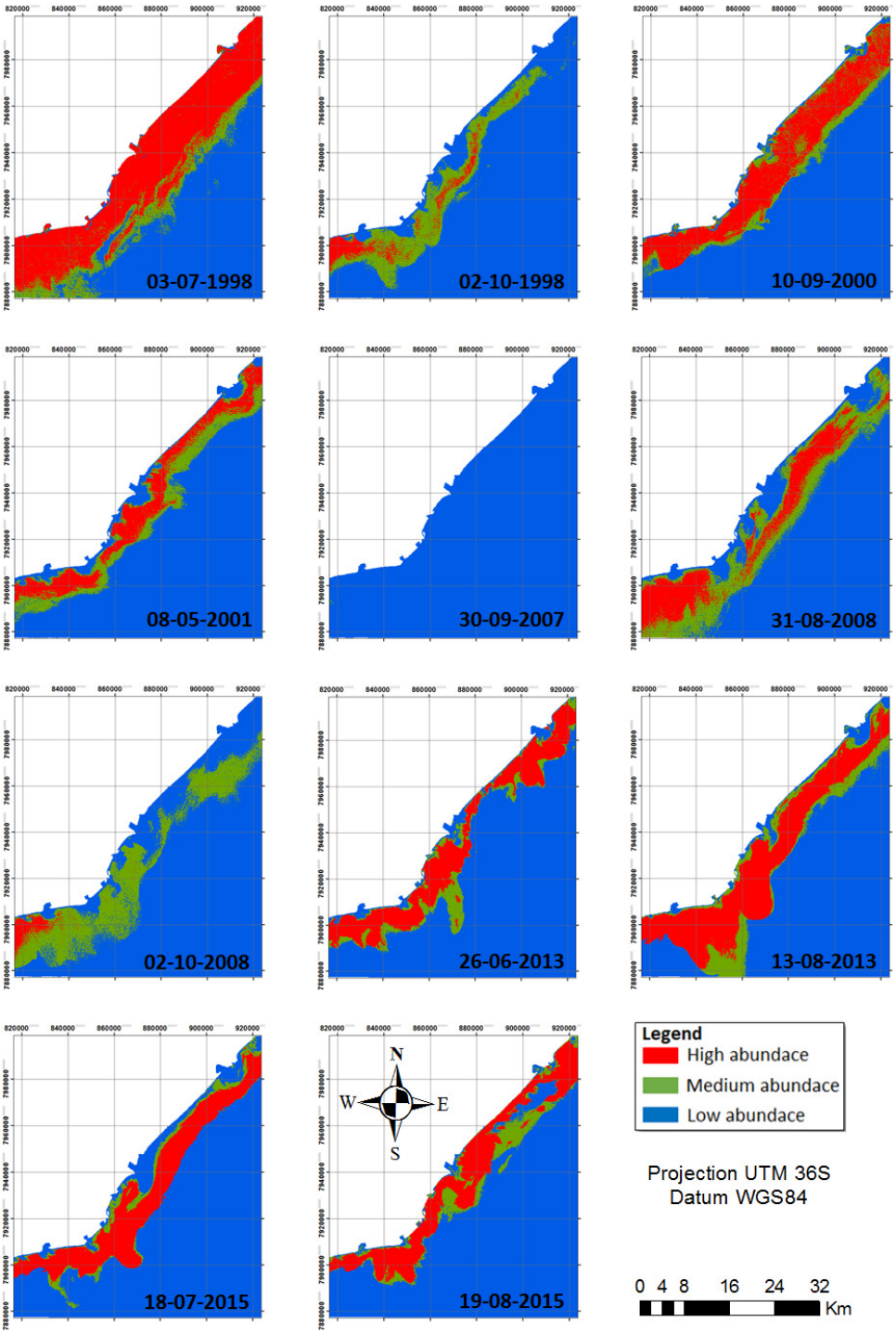

Figure 4.4.2: SLMA classified mixed waters fraction. The fractional abundances of the classes are as follows: 0.66 to 1.0 for high abundance; 0.33 to 0.66 for medium abundance; 0.0 to 0.33 for low abundance.

Temporal variability and influence of river discharge and wind speed

Figures 4.5a, 4.5b, 4.5c and 4.5d show the temporal variability of river discharge and area of high abundance class of sediment plume (a), wind speed and area high abundance class of sediment plume (b), river discharge and high abundance class of mixed waters area (c), wind speed and high abundance of mixed waters area (d). For both river discharge and area of sediment plume, there is no clear tendency over the years. While the river discharge increases from its minimum value (about 1000 m^3 s^{-1}) on 3rd July 1998 to its maximum value (about 3500 m^3 s^{-1}) on 8th May 2001, the area of sediment plume shows an increase from 3rd July 1998 to 7th October 1998 and then decreases slightly on 10th September 2000 before reaching its maximum (about 2000 km^{-2}). From 10th September 2000 on, they show a similar tendency with a gradual decrease to about 2000 m^3 s^{-1} of river discharge and about 300 km^2 of the area of sediment plume followed by an increase to 18th July 2015 to about 2200 m^3 s^{-1} of river discharge and about 600 km^2 of the area of sediment plume. While the river discharge continues increasing to a little more than 1000 m^3 s^{-1}, the area of sediment plume, in contrast, decreases to less than 20 km^2 on 19th August 2015. The wind speed starts with a different tendency to the area of sediment plume in first four images and then shows similar tendency from 8th May 2001 to 19th August 2015. It increases from about 1 m s^{-1} on 8th May 2001 to reach its maximum of about 11 m s^{-1} on 30th September 2007, the same date the area of sediment plume was maximum and then decreases to about 4 m s^{-1} on 26th June 2013. From 26th June 2013, it increases again to about 8 m s^{-1} on 18th July 2015 before decreasing to its minimum of about 1 m s^{-1} when the area of sediment plume is less than 20 km^2. The variability of mixed waters area (Fig. 4.5c and 4.5d) presents several oscillations and does not show any relation to river discharge and wind speed variability except on 8th May 2001 and 31st August 2008 where it seems to have opposite tendency to wind speed.

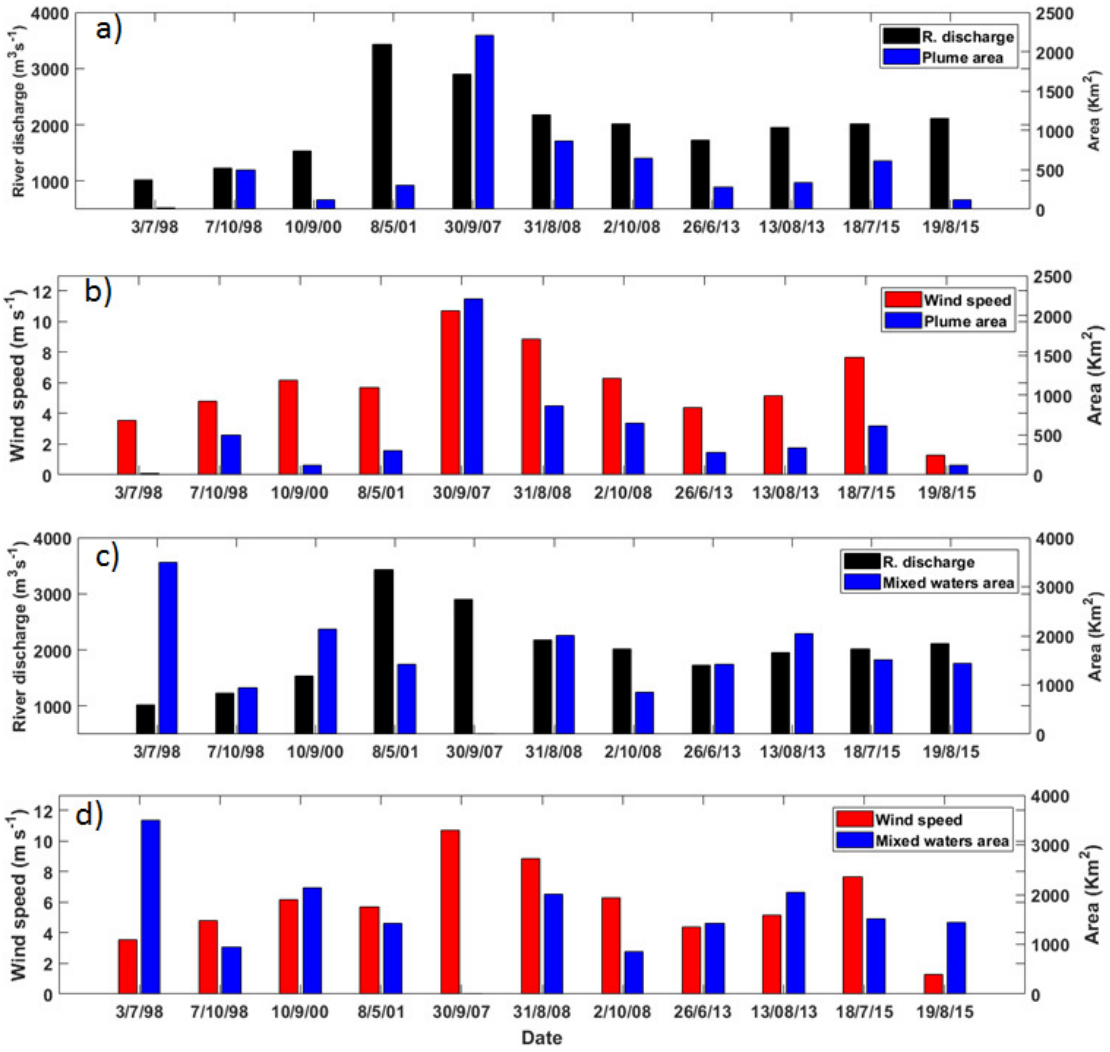

Figure 4.5: River discharge and area of high abundance fraction of SLMA classified sediment plume (a); wind speed and area of high abundance of SLMA classified sediment plume (b); river discharge and area of high abundance of SLMA classified mixed waters (c); wind speed and area of high abundance of SLMA classified mixed waters (d). Note that the time interval between the dates is not the same.

Figures 4.6a, 4.6b, 4.6c and 4.6d present the scatter plots of river discharge and area of high abundance class of sediment plume (a), wind speed and area high abundance class of sediment plume (b), river discharge and high abundance class of mixed waters area (c), wind speed and high abundance of mixed waters area (d) and respective regression outputs. River discharge correlates weakly with both sediment plume and mixed waters having a weak positive correlation to sediment plume with a coefficient of determination (R^2) of about 0.23 ($p<0.13$) and having a weak negative correlation to mixed waters with a coefficient of determination of about 0.27 ($p<0.09$). The wind speed has a strong positive correlation to sediment plume with a

coefficient of determination of about 0.67 ($p < 0.02$) and a weak negative correlation to mixed waters with coefficient of determination of about 0.18 ($p < 0.18$). In agreement with the previous chapters, where the sediment plume was mapped using monthly composites of Modis-Aqua images, the regression outputs and the temporal variability of river discharge and wind speed with the area of sediment plume and mixed waters suggest that the wind is the main governing factor of sediment plume in Sofala Bank. The sediment supply from wind might be trough coastal erosion, sediment re-suspension and surface dispersal of the plume. It is worth mentioning that the southerly winds, which dominate the region of Sofala Bank, do not favor the dispersal of the sediment plume offshore. The week correlation between mixed waters with both river discharge may suggest that there are many other factors controlling its dispersion, as they are located further offshore where other processes such as ocean currents become more important.

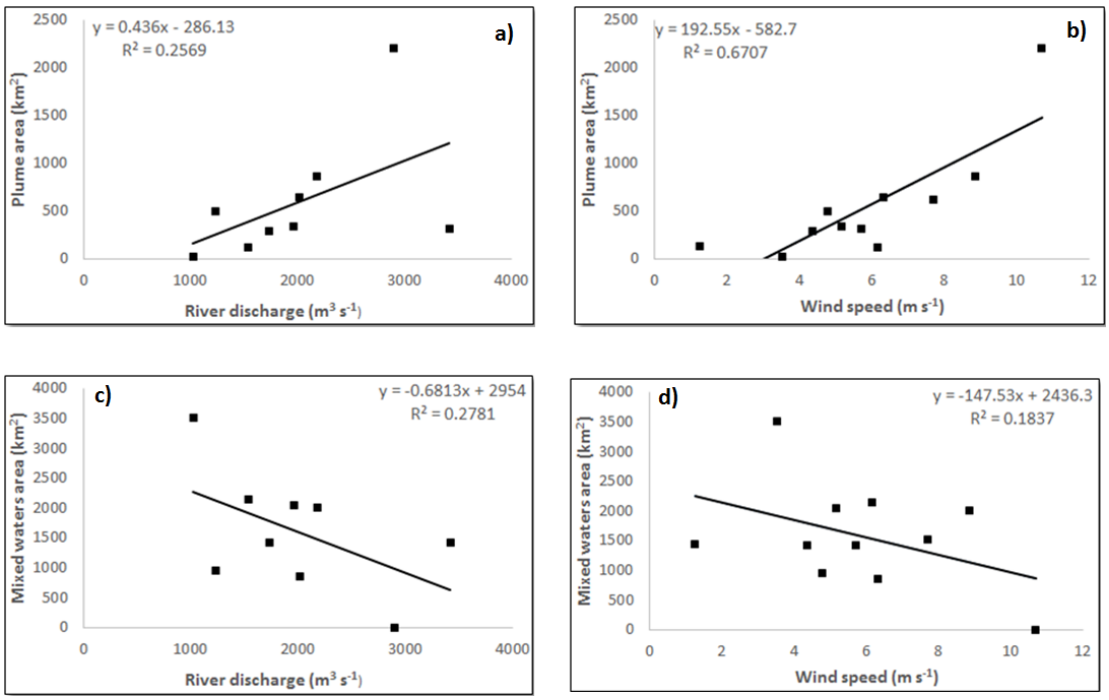

Figure 4.6: Scatter plots of river discharge and area of high abundance class of sediment plume (a), wind speed and area high abundance class of sediment plume (b), river discharge and high abundance class of mixed waters area (c), wind speed and high abundance of mixed waters area (d) and respective regression outputs.

The weak correlation between Zambezi river discharge and sediment plume observed in Sofala Bank, which is an unusual situation when compared to other studies (ex: Nezlin and DiGiacomo, 2005; Thomas and Weatherbee, 2006; Rudorff et al., 2011) where the plume variability is contralled mainly by river discharge reveals the impact of flow regulation after the construction of Cahora Bassa dam. Figure 4.7 shows climatology of seasonal variation of Zambezi river discharge during the period before and after the construction of Cahora Bassa dam, measure at

Tete station, about 440 km upstream the Zambezi mouth. It is possible to note that the difference between the discharges of the wet and dry seasons has reduced significantly after the flow started to be regulated. Although it was not possible to access any cloud-free image showing the dispersion of the sediment plume before the flow regulation it believed that the Zambezi river discharge must have been the main driving factor of plume dispersal before the implementation of Cahora Bassa dam, which entered into commercial operation in the year 1977.

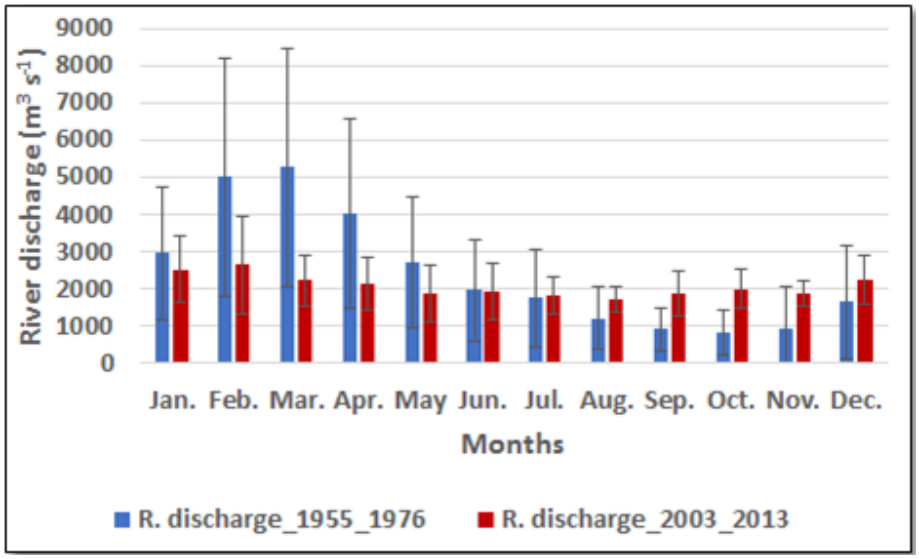

Figure 4.7: Climatology of seasonal variation of the Zambezi river discharge measured in Tete hydrological station, located about 400 km upstream the Zambezi mouth.

4.5 Conclusions

SLMA was applied to map sediment plume, mixed waters and offshore waters in Sofala Bank from TM Landsat 5 and OLI Landsat 8 images. The results showed that sediment plume and mixed waters showed high temporal variability and their extensions vary inversely suggesting that when the sediment plume extends offshore the mixed waters are pushed offshore and sink in deep waters. The wind speed presents a strong coefficient of determination to the area of sediment plume, suggesting that the wind speed is the main governing factor of sediment plume dispersion in the Sofala Bank. The weakening of the Zambezi River discharge on controlling the sediment plume variability must have started after the construction of Cahora Bassa dam when the flow began to be regulated. The mixed waters area correlated weakly to both Zambezi river discharge and wind speed, suggesting that there are other factors controlling the variability of their extension, since they are located further offshore where other processes such as ocean currents become more important.

Chapter 5

Evaluation of short and long term ENSO-precipitation relation in lower Zambezi using TRMM Multisatellite Precipitation Analysis (TMPA) and AR5 Global Climate Models (GCMs)

Abstract: the main aim of the present study was to evaluate the short and long term of the influence of ENSO on precipitation in lower Zambezi basin. In order to meet the objective TRMM 3B43-v7 precipitation data for the 1998-2017 period was used to evaluate the short-term influence of ENSO and the CESM1(CAM5) model outputs for 1850-2005 period was used to evaluate the long-term variability of the influence of ENSO on precipitation. The main methods used in the study were the spatial correlation between 3.4 Niño index with TRMM 3B43-v7 precipitation and evaluation of variability of precipitation anomalies in years of moderate and strong ENSO events for short-term, and evaluation of variability of 20 years sliding correlation between 3.4 Niño index and CESM1(CAM5) precipitation predictions for long term. The results showed that ENSO influences the precipitation of wet season of south 15°S with low precipitation rates during El Niño and high precipitation rates during La Niña. During some years of moderate or strong ENSO, the precipitation did not show any changes that could be interpreted as caused by ENSO effects, suggesting that besides ENSO there might be other factors influencing the precipitation variability in there. For the long term of ENSO-precipitation relation, the results showed that the inverse relation, denoted by the negative correlation between Niño index and precipitation, is the most dominant and alternates with phases of weaker and positive relationship in a periodicity of about 21 years.

Keywords: ENSO, precipitation, TMPA, GCMs, lower Zambezi

5.1 Introduction

Changes in precipitation strongly influence the ecologic, hydrologic and socio-economic components especially in places where the survival of the people depend on agriculture and fishing activities. Southern Africa is reported to be one of the regions in which rainfall is likely to decrease significantly in the future (IPCC, 2013) and the distribution, variation, and frequency of future rainfall are still uncertain (Giannini, et al., 2008). The understanding and prediction of African climates has become a major challenge due theirs spatial and temporal variability, which range from humid equatorial to Mediterranean-type presenting high seasonal, inter-annual and inter-decadal variability, which make it difficult to understand and predict it. (Hulme, et al. 2001). The migration of the intertropical convergence zone (ITCZ), sea surface temperature (SST) in Indian and Atlantic Oceans and ENSO are principal mechanisms driving rainfall pattern in Southern Africa (Mason, 2001). The impact of ENSO in precipitation can vary in space and time; Kumar et al., (1999) examined the linear relationship between monsoonal precipitation and ENSO and found that they were related negatively until the years 1990s when the negative relation broke down; Zhang, et al., (2013) found that the eastern Pacific warming brings more precipitation in spring and winter in the Eastern Basin, south China but less precipitation in summer. The El Niño over southern Africa occurs largely because of a weakening of tropical convection over the subcontinent and usually is associated with below-normal rainfall over much of southern Africa (Mason, 2001). Ward, et al., (2010) evaluated the global impact of ENSO on precipitation by analysing the correlation of annual mean and flood discharge with Southern

Oscillation Index (SOI) and observed that on average ENSO has a greater impact on annual high flow events that on annual mean, and that depending on the region it can intensify or attenuate the precipitation.

The Zambezi River is vital to the economy of many African countries and ensures the survival of many people. It hosts half of the installed hydropower of southern Africa stimulating the economy and jobs for local people, offers fishing, and subsistence agriculture conditions for people who live near it. In the lower side of Zambezi River, the drainage of freshwater and sediments, including nutrients into the shelf waters of central Mozambique have an important role in the local fishing productivity (Lutjeharms, 2006; Nehama, 2012). The variability of chlorophyll (an indicator of ocean productivity), along the coastal waters of Mozambique showed to be governed mainly by Zambezi River discharge and both chlorophyll concentration and Zambezi River discharge in Tete station in Mozabique presented a significative correlation with ENSO. In this context, a deeper undestanding the spatial and temporal influence of ENSO on the precipitation within the Zambezi Basin is important for predictions productivity in agriculture and fishing. Furthermore, the findings about the relationship between ENSO and precipitation in the lower Zambezi basin, which has a direct influence on the shelf water off central Mozambique would confirm the preliminary finds which indicate that the signal of ENSO into the chlorophyll variability is brought by Zambezi discharge. Within many developing countries especially in southern Africa crossed by the lower Zambezi, the hydrological gauges are dispersal and in many cases, their records are not continuous due to economic limitations to create denser gauge stations and guarantee their maintenance (Hughes, 2006) which makes it difficult to use gauge networks to study long-term variability of precipitation in larger areas. Some studies have reported the performance of satellite based precipitation products in reproducing the ground observations over Africa (Su, et al., 2007; Liechti, et al., 2012; Thieming, et al., 2012), which suggest that they are a good alternative for monitoring the spatial-temporal trends of precipitation. Liechti, et al., (2012) and Thieming, et al., (2012) emphasized the performance of the Tropical Rainfall Measuring Mission (TRMM) on capturing the north-south gradient of precipitation over Zambezi basin, especially in monthly time steps. The limitation of most satellite products of precipitation for long-term analysis is their short time span. The TRMM-3B43-7, for example, had a time span of only 17 years, which extended between 1998 and 2015. The Intergovernmental Panel on Climate Change (IPCC) has joined many scientific institutions committed in developing Global Circulation Models (GCMs) for predicting precipitation at various space and time scales, which become an alternative for long-term precipitation trends monitoring. However, these GCMs may fail to simulate the annual and inter-annual precipitation variations (Alves, et al., 2016) and therefore the evaluation of their performance is necessary (Yoo and Cho, 2018). Is this study, the seasonal variability of precipitation over the lower Zambezi basin (Fig. 5.1) and its relation to ENSO are evaluated using TRMM-3B43-7 data set for the 1998-2015 period. The TRMM-3B43-7 is also used as the reference to evaluate the performance of output of IPCC Fifth Assessment Report (AR5) models. The outputs of best-performed model are correlated to the time series of 3.4 niño index to

evaluate the long-term variability of relationship between ENSO and precipitation over lower Zambezi basin.

5.2 Dataset and Methods

The study area is located in the Lower Zambezi Basin, in the Southern Africa, covering Malawi, Zimbabwe and the Zambezi Delta in Mozambique, within latitudes 9°S to 20°S and longitudes 30°E to 37°E (Figure 5.1) which was subdivided into the following subareas: northwest [9-14.5°S, 30-33.5°E], northeast [9-14.5°S, 33.5-37°E], southwest [14.5-20°S, 30-33.5°E] and southeast [14.5-20°S, 33.5-37°E]. The monthly TRMM 3B43 version 7 NASA's standard precipitation products (Huffman, et al., 2007), for the 1998-2017 period was downloaded in Giovanni. (https://giovanni.gsfc.nasa.gov/giovanni/#service=TmAvMp&starttime=&endtime=&dataKeyword=TRMM_3B43) on the 20th October 2017. The 3B43 dataset is the monthly version of the 3-hours average 3B42 dataset, which is produced in four steps (Huffman, et al., 2007): (1) microwave precipitation estimates are calibrated and combined, (2) Infrared estimations are created using calibrated microwave precipitation, (3) microwave and infrared estimates are combined and (4) gauge data from Global Precipitation Climatology Center (GPCC) is incorporated to rescale the data to monthly total. The IPCC AR5 data for the region of Africa was provided on storage media by the German Climate Computation Center (DKRZ). The data is subdivided in historical, which refers to simulations on recent past (1850-2005) and future projections (2006-2100) forced by RCP2.6, RCP4.5 and RCP8.5 for the radioactive forcing of 2.6, 4.5 and 8.5 W m^{-2} in the year 2100, respectively. The name, the owner institution and spatial grids of GCMs are listed in Table 5.1. To evaluate the annual variation of precipitation over lower Zambezi, monthly climatology and respective standard deviations for the 1998-2017 period were created from the TRMM dataset. The influence of ENSO on precipitation was evaluated for short (1998-2017) using the TRMM dataset (1850-2005) and for long-term using GCM outputs, which was found to best represent the TRMM dataset from statistical analysis. For the short-term period there was created maps of spatial variation of Person correlation coefficient between 3.4 Niño index and precipitation over lower Zambezi and anomalies of precipitation during positive Niño index taken as 3.4 Niño index with values above the threshold +0.5, negative Niño index taken as the 3.4 Niño index with values below the threshold -0.5. Anomalies of precipitation during years of moderate and strong El Niño/La Niña events for wet (October-March) and dry (May-September) seasons were also used to evaluate the influence of ENSO on precipitation. The 3.4 Niño index data was obtained from the Climate Prediction Center (CPC, http://www.cpc.noaa.gov/) on 20th October 2017. The precipitation anomaly in each of the following subareas was calculated as a percentage in relation to the mean, following Zhang, et al., (2013, Eq. 5.1).

$$An_{ij}=\left(\frac{P_{ij} \times 100\%}{P_i}\right)-100 \qquad \text{(Equation 5.1)}$$

where:

An_{ij} is precipitation anomaly in specific j;

P_{ij} is Accumulated precipitation registered during a specific ENSO year j;

$\overline{P_i}$ is the mean precipitation in each grid point for short-term analysis of the areal mean in each subarea for long-term analysis, calculated from years of moderate and strong El Niño/La Niña events.

For evaluation of skill of GCMs in assimilating the precipitation in lower Zambezi, historical data from nine GCMs output for the 1998-2017 period were re-sampled to 0.5° grid (to match the TRMM grid spatial resolution) and compared to TRMM data set in terms of correlation coefficient and Root Mean Square Error (RMSE). The model with the best correlation and lower RMSE was taken as the best and was used to evaluate the long-term multi-decadal influence of ENSO on precipitation over lower Zambezi basin. The multi-decadal influence of ENSO on precipitation was inferred through 20 years sliding correlation between 20 years running average of 3.4 Niño index and 20 years running average precipitation of best GCM. To infer the periodicity of oscillation of correlation between 3.4 Niño index and precipitation the wavelet analysis (Torrence and Compo, 1998) was performed.

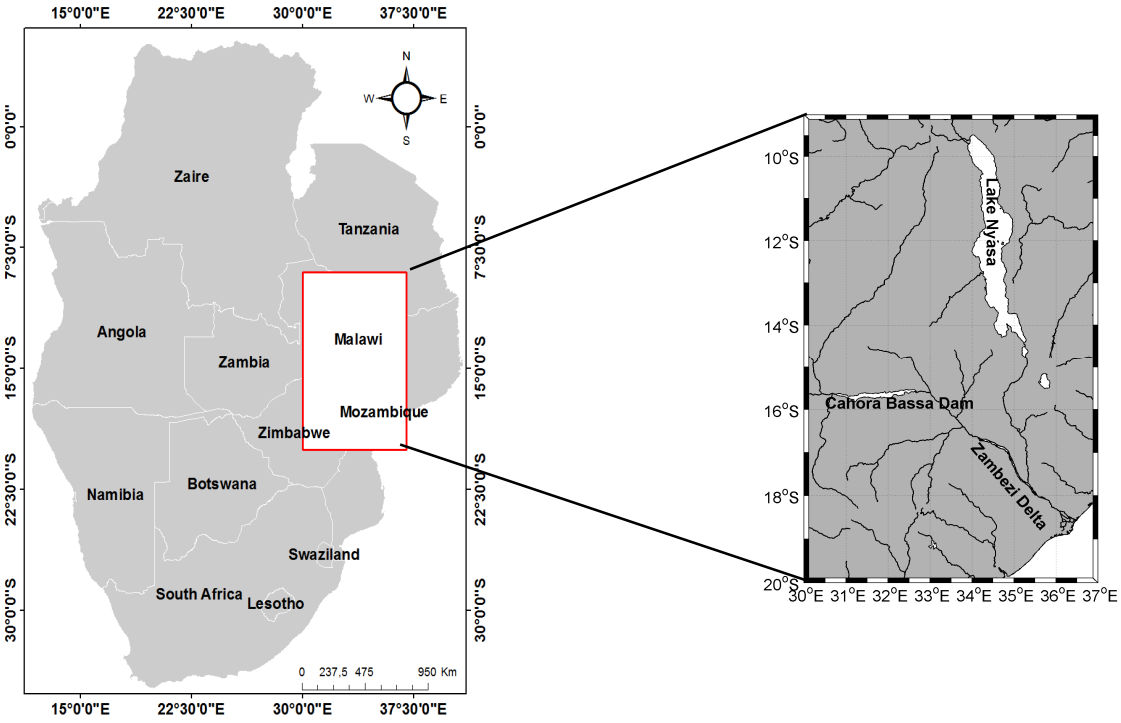

Figura 5.1: Study area. The red box represents the position of the satudy area within Southern Africa

Table 5.1: Models used for elaboration of the Intergovernamental Panel on Climate Change (IPCC) Fifth Assessment Report (AR5)

Institute	Model	Grid points Longitude X Latitude
CSIRO-BOM	ACCESS1.0	57 x 79
BCC	BCC-CSM1.1	96 x88
CCCma	CanESM2	38 x 35
NCAR	CCSM4	86 x 104
NCAR	CESM1(CAM5)	86 x 104
CMCC	CMCC-CMS	57 x 52
NASA-GISS	GISS-E2-R	43 x 49
INM	INM-CM4	54 x 66
IPSL	IPSL-CM5A-MR	43 x 77

CSIRO-BOM, Commonwealth Scientific and Industrial Research Organisation/Bureau of Meteorology, Australia; BCC, Beijing Climate Center, China; CCCma, Canadian Centre for Climate Modelling and Analysis, Canada; NCAR, National Center for Atmospheric Research, USA; CMCC, Centro Euro-Mediterraneo sui Cambiamenti Climatici, Italy; NASA-GISS, NASA Goddard Institute for Space Studies, USA; INM, Russian Academy of Sciences, Institute of Numerical Mathematics, Russia; IPSL, Institut Pierre Simon Laplace, France .

5.3 Results and discussions

The seasonal variability of precipitation over lower Zambezi is presented in Figure 5.2 through monthly climatology of TRMM data for the 1998-2017 period. There are two main seasons of precipitation. One of the seasons is of high precipitation rates extending between November and March with values varying between 150 mm/month in November and about 350 mm/month in January when the more expressive values are observed in northeast and east regions of lower Zambezi. The season of low precipitation rates, with values not exceeding 100 mm/month in whole study area except in the region of Lake Nyasa (~12.5°S, 35°E) where the values exceed 150 mm/month, is more evidenced during May to October. In general, the spatial variation shows a decreasing from the north to the south and is in agreement with observations from Liechti, et al., (2012) and Thieming, et al., (2012) who compared TRMM precipitation products with gauge observation over Zambezi basin. Liechti, et al., (2012) compared ground station data over the Zambezi basin to three satellite-derived precipitation products including TRMM and found that in general, all the products captured the North-South precipitation gradient.

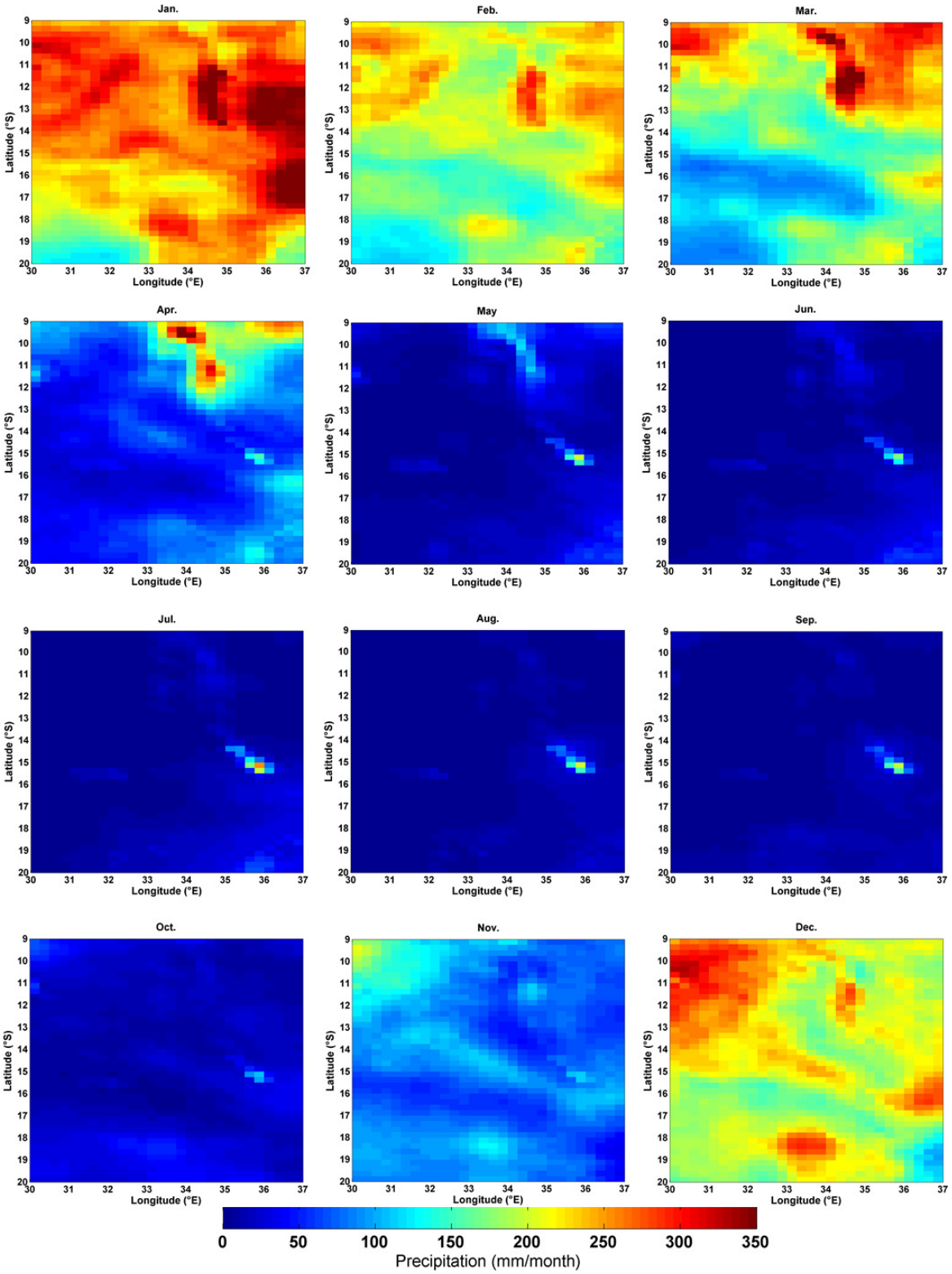
Jan.
Feb.
Mar.
Apr.
May
Jun.
Jul.
Aug.
Sep.
Oct.
Nov.
Dec.
Latitude (°S)
Longitude (°E)
0
50
100
150
200
250
300
350
Precipitation (mm/month)

Figure 5.2: Monthly climatology of TRMM 3B43-v7 precipitation over lower Zambezi basin (covering east Zimbabwe, Malawi and west Mozambique) for the period between 1998 and 2017.

The evaluation of the relationship between ENSO and precipitation during the wet season (October-March) over lower Zambezi basin is presented by means of correlation coefficients for zero, one, two and three months lagging time (Fig. 5.3.1 and Fig. 5.3.2). The absolute values of the positive correlation coefficient are very low, not exceeding 0.1 for all the lagging time (Fig. 5.3.1), with statistical confidence less than 95% (Fig. 5.3.2). The negative values, in turn, are relatively high especially in the south region (~15 to 20°S) with a west-east gradient, decreasing from more than 0.35 in the southwest to about 0.3 in the southeast region during zero and one month legging time. During two and three months lagging time, the correlation coefficient decreases to about zero. The spatial distribution of the correlation coefficient suggests that during the wet season, the precipitation in the lower Zambezi basin presents low rates during high positive 3.4 Niño index (which denotes El Niño events). Opposite situation is observed during La Niña events. The weakening of the negative correlation coefficient in the two and three months lagging time suggests that the effects of ENSO on the precipitation in the lower Zambezi basin are negligible or not observed after one month of its registration.

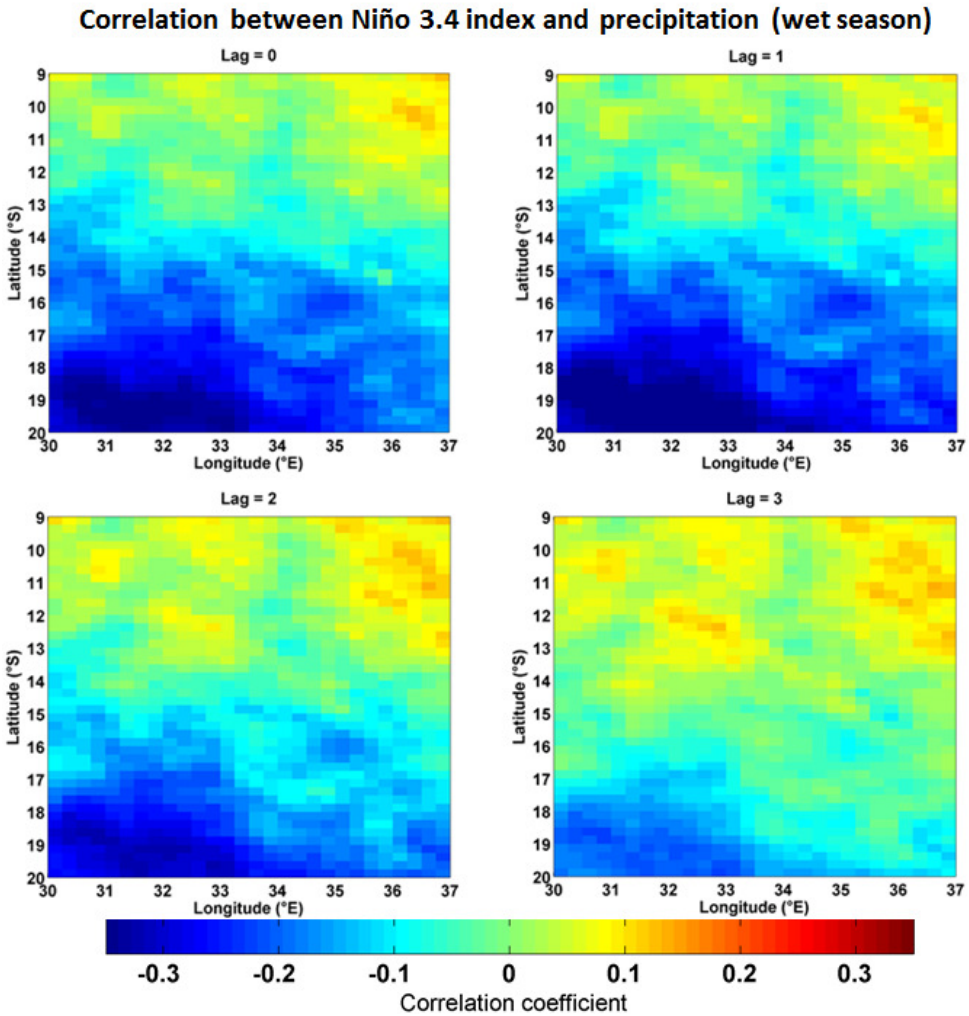

Figure 5.3.1: correlation between monthly 3.4 Niño index and time series of monthly TRMM precipitation products for wet season (October-March) precipitation over lower Zambezi basin during the 1998-2017 period.

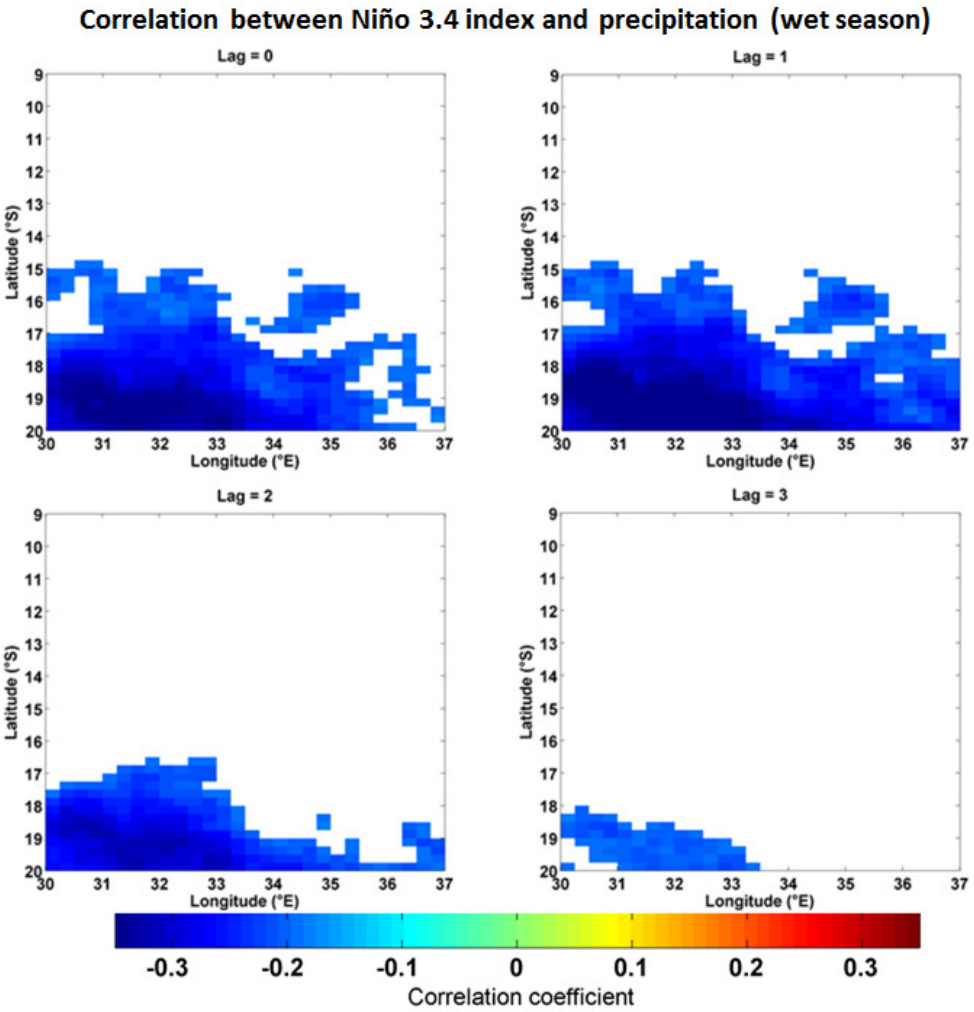

Figure 5.3.2: Repetition of Figure 5.3.1 but with areas whose statistical confidence are less than 95% excluded

The maps of correlation between 3.4 Niño index and precipitation for dry season (May-September) are presented in Figures 5.3.3 and 5.3.4. In the dry season, the values of positive correlation coefficient are lower than 0.1 and are observed in almost the whole study area except in the southeast region where negative values of module greater than 0.35, with statistical confidence higher than 95%, are observed. The patterns of distribution of correlation between 3.4 Niño index and precipitation during the wet and dry seasons suggest that ENSO presents more influence on the whole south 15°S during the wet season and southeast during the dry season, with relatively more intensity in the wet season rather than in dry season. However, the relatively low correlation coefficients suggest that besides ENSO there are other factors influencing the precipitation variability over the lower Zambezi basin. Jury (1997) analyzed 49 southern Africa summer precipitation predictors (including Sea Surface Temperature, surface pressure and winds and cloud albedo) and found that one-third of them correlated to ENSO, other one-third to transition of the Indian monsoon, one-quarter to conditions in South Atlantic.

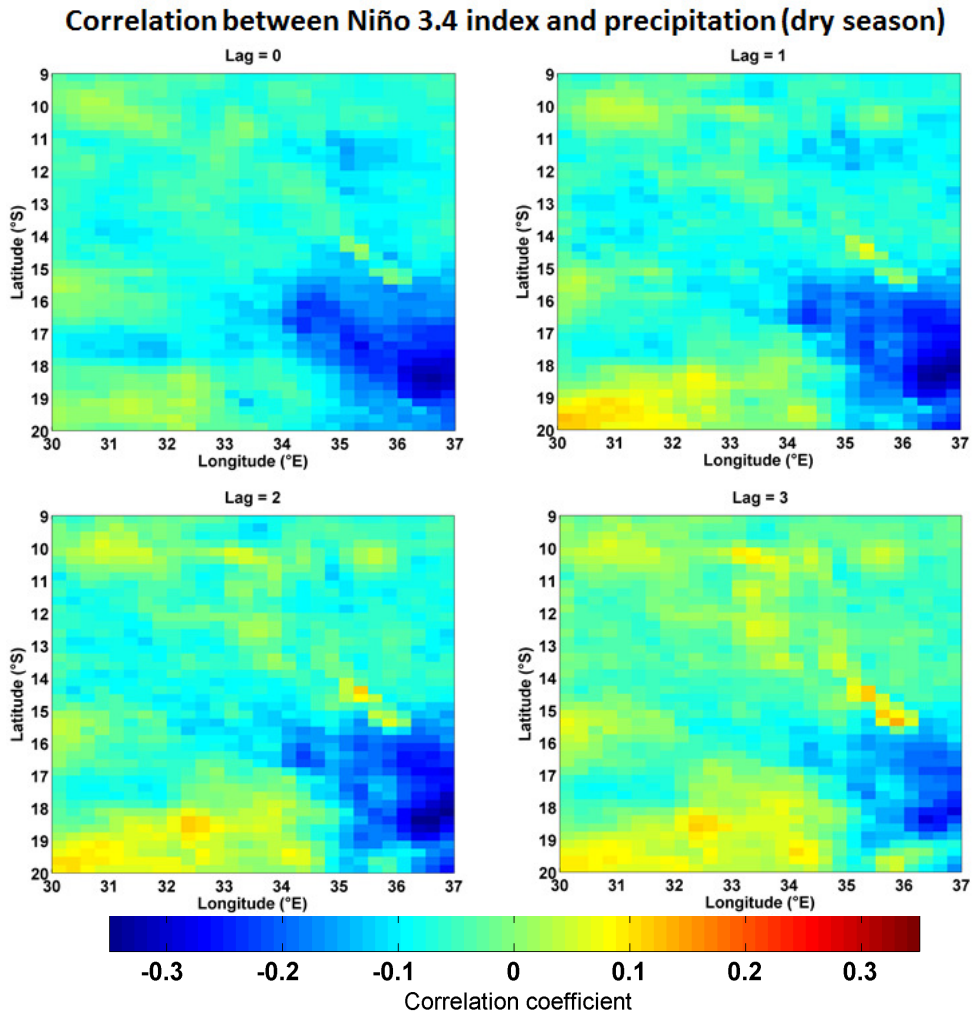

Figure 5.3.3: Correlation between monthly 3.4 Niño index and time series of monthly TRMM precipitation products for dry season (May-September) precipitation over lower Zambezi basin during the 1998-2017 period.

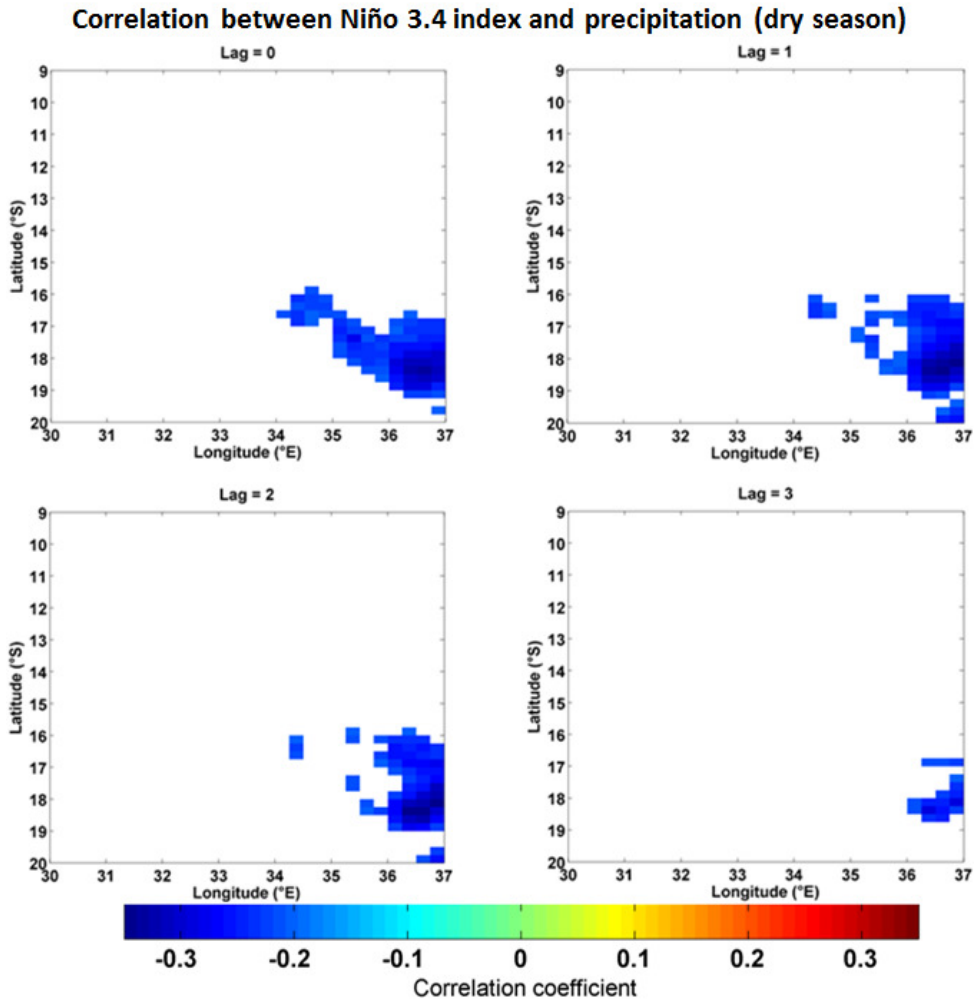

Figure 5.3.4: Repetition of Figure 5.3.3 but with areas whose statistical confidence are less than 95% excluded

The distribution of precipitation anomaly during positive (above +0.5) 3.4 Niño index and negative (below -0.5) 3.4 Niño index calculated in relation to the climatological mean of the wet season precipitation are presented in Figure 5.4.1. During positive 3.4 Niño index, the precipitation anomaly is positive and varies between 5 and 10 above the climatological mean in the northern portion and negative varying between -20 and -5 % below the climatological mean of the wet season. During negative 3.4 Niño index, the precipitation anomaly is positive over the whole study area, with higher values exceeding 25% of the climatological mean of the wet season in the southeast sub region. The negative precipitation anomalies during the positive 3.4 Niño index and positive precipitation anomalies during negative 3.4 Niño index, especially in the south regions of the lower Zambezi basin are in agreement with the significant negative correlations between the 3.4 Niño observed in the wet season. The distribution of correlation coefficients and precipitation anomaly suggest that during wet season there is a decreasing in

precipitation during positive 3.4 Niño index and increase in precipitation during negative 3.4 Niño index.

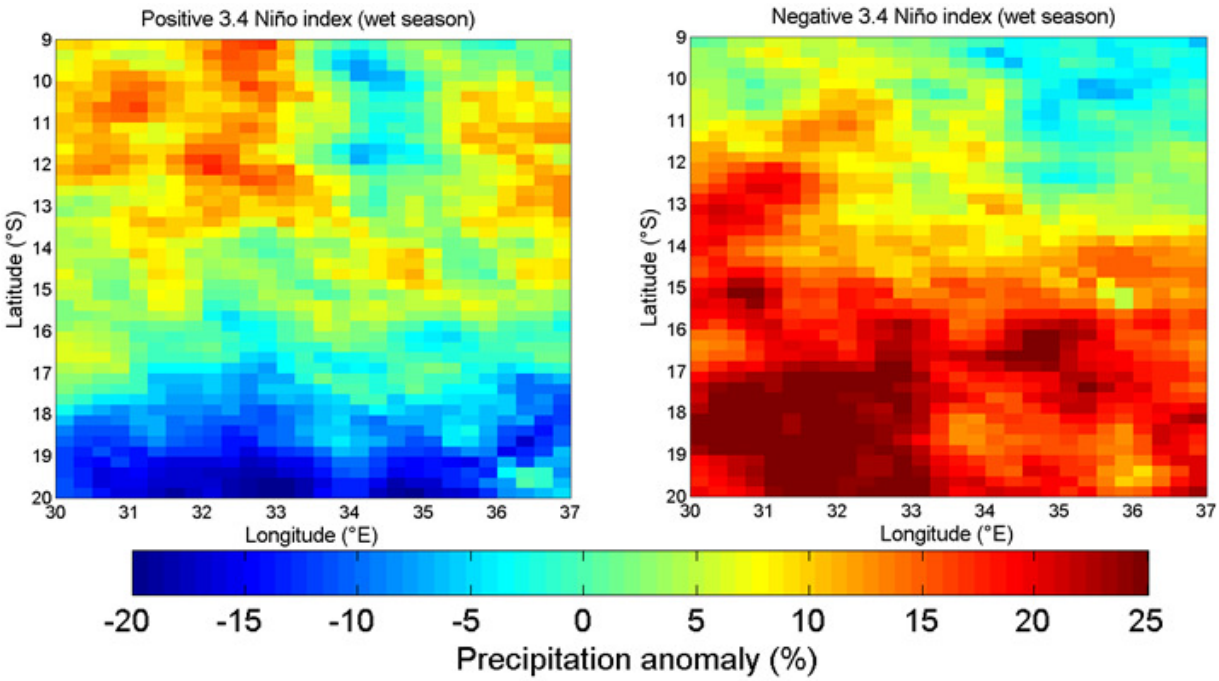

Figure 5.4.1: Distribution of precipitation anomaly (%) over the lower Zambezi basin during positive and negative 3.4 Niño index in the wet season. The 3.4 index was taken as positive when it was above +0.5 and was taken as negative when it was below -0.5. The precipitation anomaly was calculated in relation to the climatological mean of the wet season using the equation 1.

The distribution pattern of precipitation anomaly during positive and negative 3.4 Niño index of the dry season are presented in Figure 5.4.2. During the positive 3.4 Niño index, the precipitation anomalies are negative in most of the study with values varying between 50 and 100 below the climatological mean of the dry season, notwithstanding the existence of some pixels with positive anomalies exceeding 100 % above the climatological mean of the season. During the negative 3.4 Niño index, the precipitation anomalies are positive in most of the study area, especially the southwest region where the anomaly is about 150% above the climatological mean of the dry season. The distribution of precipitation anomaly during the positive and negative 3.4 Niño index denotes a decrease in precipitation during positive 3.4 Niño index and an increase of precipitation during 3.4 Niño index.

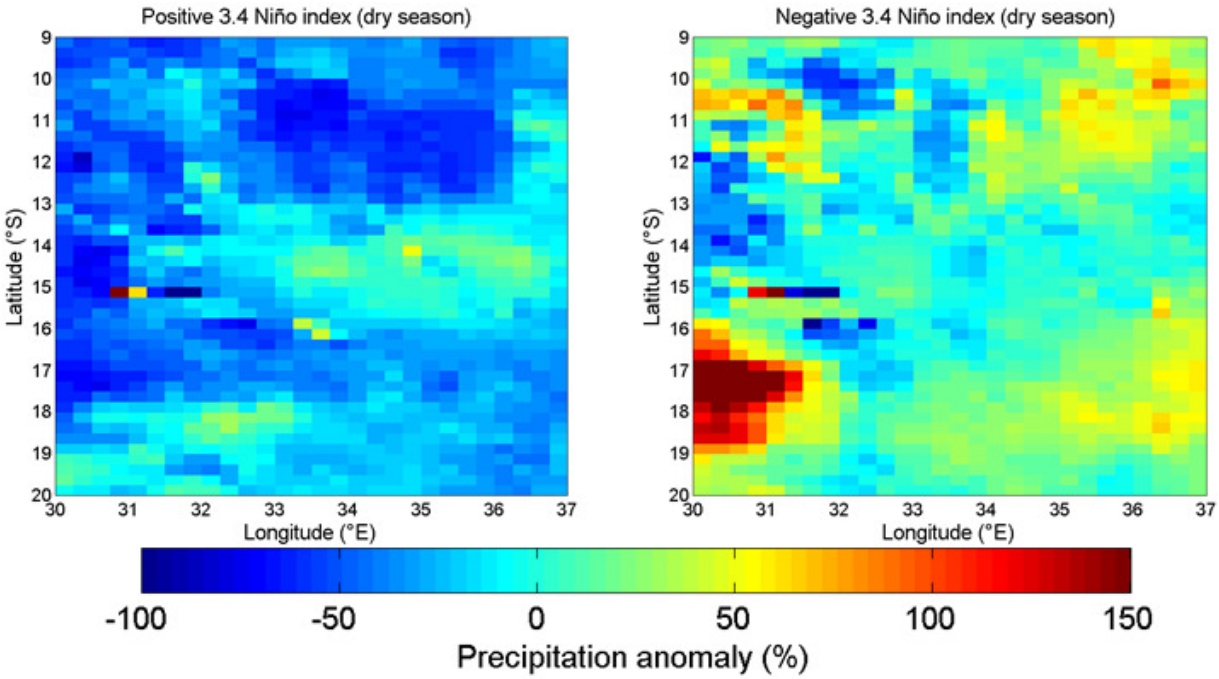

Figure 5.4.2: Distribution of precipitation anomaly (%) over the lower Zambezi basin during positive and negative 3.4 Niño index in the dry season. The 3.4 index was taken as positive when it was above +0.5 and was taken as negative when it was below -0.5. The precipitation anomaly was calculated in relation to the climatological mean of the dry season using the equation 1.

Figure 5.4.3 presents the anomaly of precipitation calculated using Equation1 for wet season of years of moderate and strong El Niño/La Niña according to the classification of NOAA-CPC, available at http://ggweather.com/enso/oni.htm. During 1998/98 and 2007/08, years of strong La Niña, there are positive anomalies of precipitation exceeding 50 mm/month in the south region, which was found to be more influenced by ENSO events. The negative effects of the 2015/16 strong El Niño are also denoted by high negative anomalies exceeding 50 mm/month over south of ~14°S. During 1999/00 and 2010/11 strong La Niña, in contrast to what is observed in other strong La Niña events, the precipitation anomalies presented negative anomalies in the northern region during 1999/00 and during 2010/11 the negative anomalies in the northeast and southeast regions. During moderate El Niño events of the years 2002/03 and 2009/10, the precipitation variability does not show any region of a clear pattern of the negative or positive anomaly to be related to ENSO. The discrepancy between the strength of ENSO and precipitation have also been observed in previous studies (Ward, et al., 1994; Kane 1999). Kane, (1999), analyzed the effects of the very strong 1997-1998 El Niño for several regions and concluded that ENSO effect on precipitation in some regions were not as expected, droughts did not occur in some regions where was expected and occurred in others where was not expected. In India, for example, where droughts were expected, there was observed normal precipitation. The disparity between the strength of ENSO and precipitation observed during some ENSO events might be due to other

parameters that influence precipitation such as local Sea Surface Temperature (Kane, 1999) and land-atmosphere feedback (Nicholson, 2000). In some occasions, the variability of these parameters may not be related to ENSO and their strength on the precipitation can overcome the ENSO effect.

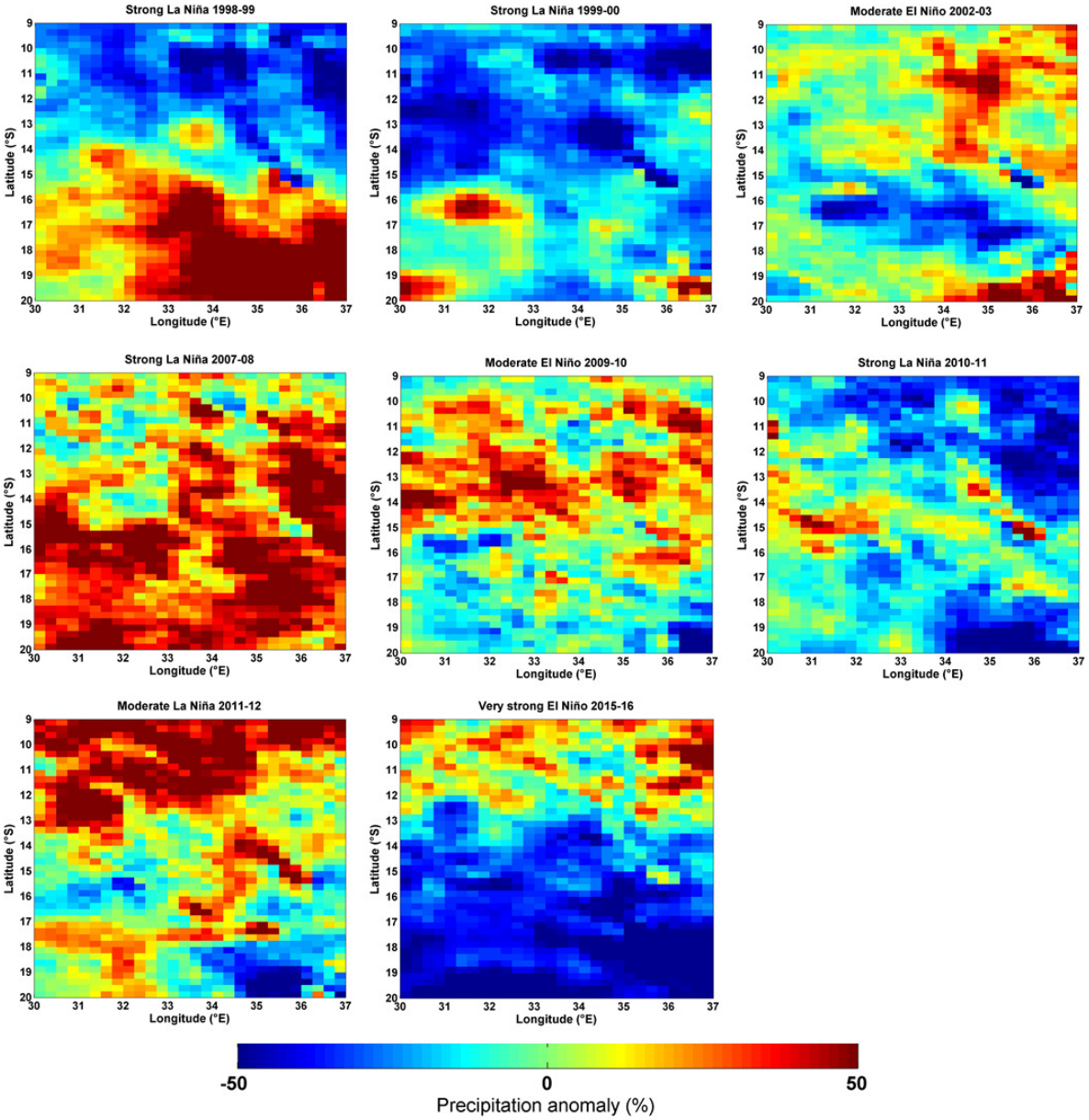

Figure 5.4.3: Anomaly of precipitation (%) over lower Zambezi basin during the wet season of years of moderate and strong ENSO intensities. The mean precipitation value from which the anomalies were calculated was determined using annual means of precipitation of years of moderate and strong ENSO.

During the dry season, the anomaly of precipitation over lower Zambezi basin does not show any clear relation to ENSO events in most of the cases (Fig. 5.4.4). The very strong 1997/98 El Niño and strong 1999/00 La Niña were captured by strong negative anomalies in the south region and strong positive anomalies in the southwest, respectively. During the other ENSO events the distribution of does not show any indication of ENSO influence, suggesting that as shown in the correlation between 3.4 Niño index and precipitation, the dry season is less influenced by ENSO compared to the wet one. These findings corroborate to strong positive/negative anomalies of chlorophyll concentrations along coastal waters under Zambezi flow influence in Sofala Bank, Mozambique during the wet season of moderate and strong El Niño/La Niña years and no clear pattern during the dry season.

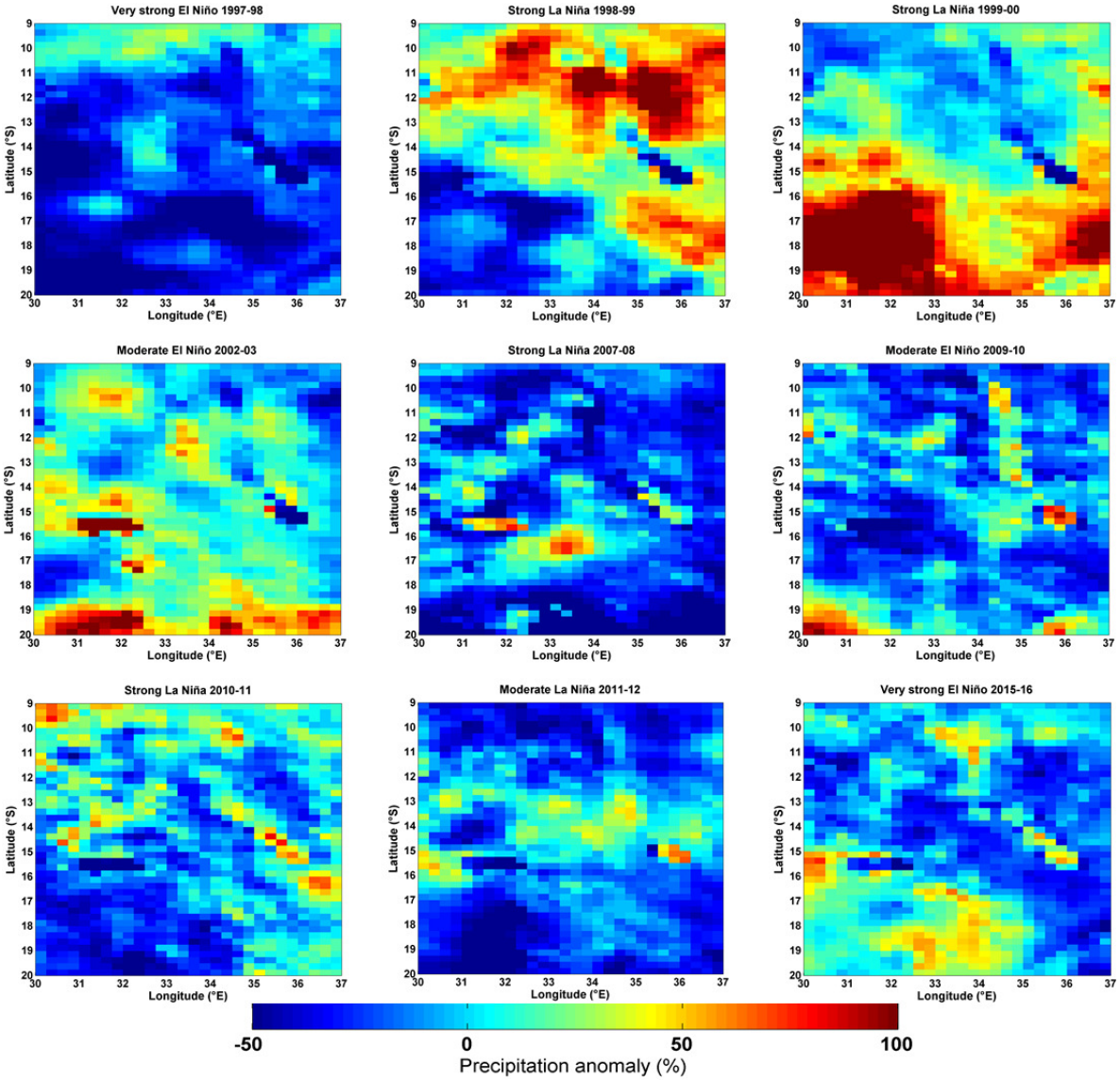

Figure 5.4.4: Anomaly of precipitation (%) over lower Zambezi basin during the dry season of years of moderate and strong ENSO intensities. The mean precipitation value from which the

anomalies were calculated was determined using annual means of precipitation of years of moderate and strong ENSO.

The precipitation anomalies are presented in terms of areal mean over subareas: northwest [9-14.5°S, 30-33.5°E], northeast [9-14.5°S, 33.5-37°E], southwest [14.5-20°S, 30-33.5°E] and southeast [14.5-20°S, 33.5-37°E] subareas in Figures 5.5.1 and 5.5.2. During the wet season (Fig. 5.5.1) both northwest and northeast regions do not show any indication of ENSO influence agreeing with insignificant correlations between 3.4 Niño index and precipitation in the north region presented in Figures 5.3.1 and 5.3.2. The southwest and southeast regions, in turn, show more evident relation to ENSO. During the strong 1998/99 and 1999/00 La Niña years the anomaly of precipitation exceeds 25 % of the mean and during the very strong 2015/16 El Niño event the precipitation in the southwest region was more than 35 % below the mean in the southwest region, which denotes its relatively higher intensity if compared to 2002/03 and 2009/10 moderate El Niño when the precipitation was not below 20 % of the mean. In the southeast region, the high positive anomalies in 1998/99 and 1999/00 strong La Niña events are observed but with 1999/00 anomaly decreased to about 20%. On the other hand, the negative anomaly of precipitation in southeast region during the 2015/16 strong El Niño is less than in southwest region, suggesting that the ENSO effect decreases from southwest to southeast, in agreement with the spatial variation of correlation coefficients between 3.4 Niño index and precipitation presented in Figure 5.3.1.

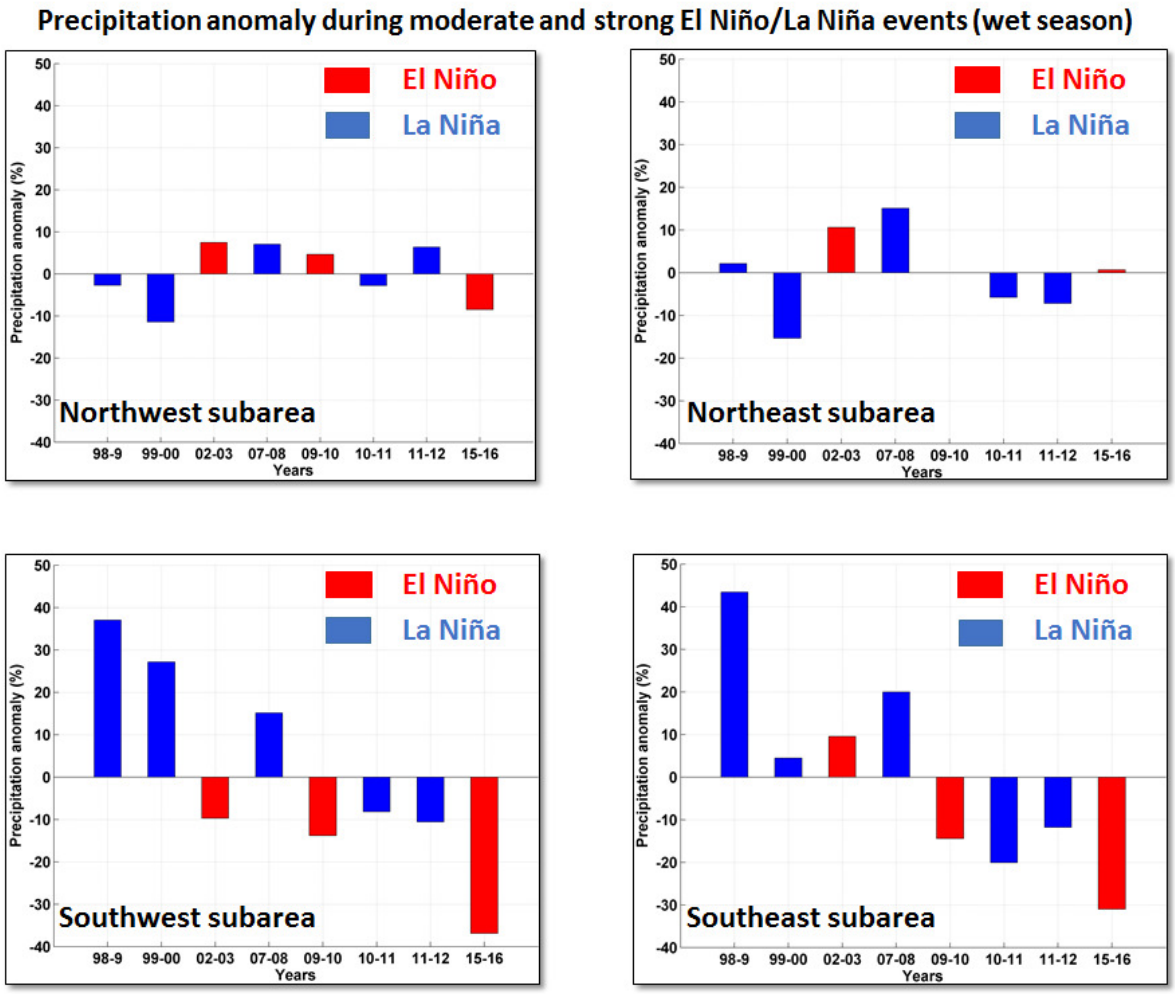

Figure 5.5.1: Areal anomaly of precipitation (%) over northwest [9-14.5°S, 30-33.5°E], northeast [9-14.5°S, 33.5-37°E], southwest [14.5-20°S, 30-33.5°E] and southeast [14.5-20°S, 33.5-37°E] subareas during the wet season of years of moderate and strong ENSO intensities. The mean precipitation value from which the anomalies were calculated was determined using annual means of precipitation of years of moderate and strong ENSO

During the dry season analogously to results presented in Figure 5.4.2, the distribution of precipitation anomaly along the moderate and strong ENSO years is very random to be related to ENSO (Fig. 5.5.2). During moderate 2011/12 La Niña when it is expected to be a year of precipitation above the mean according to the negative correlation between ENSO and precipitation, the observed precipitation rates were below the mean and less than observed during the very strong 2015/16 El Niño event in southwest and southeast regions. The random distribution between precipitation and ENSO events in the dry season, reinforce that the precipitation in the dry season is less or not influenced by ENSO, as previously observed in Figures 5.3.3 and 5.4.2. The Pacific Sea Surface Temperature maximum and Southern Oscillation Index (SOI) minimum, which denote ENSO, coincide with wet season of the low

Zambezi basin in the most of ENSO events analyzed (not shown). The discrepancy between the occurrence of ENSO in Pacific and the dry season of lower Zambezi might be the reason of lower or no influence of ENSO on precipitation during the dry season.

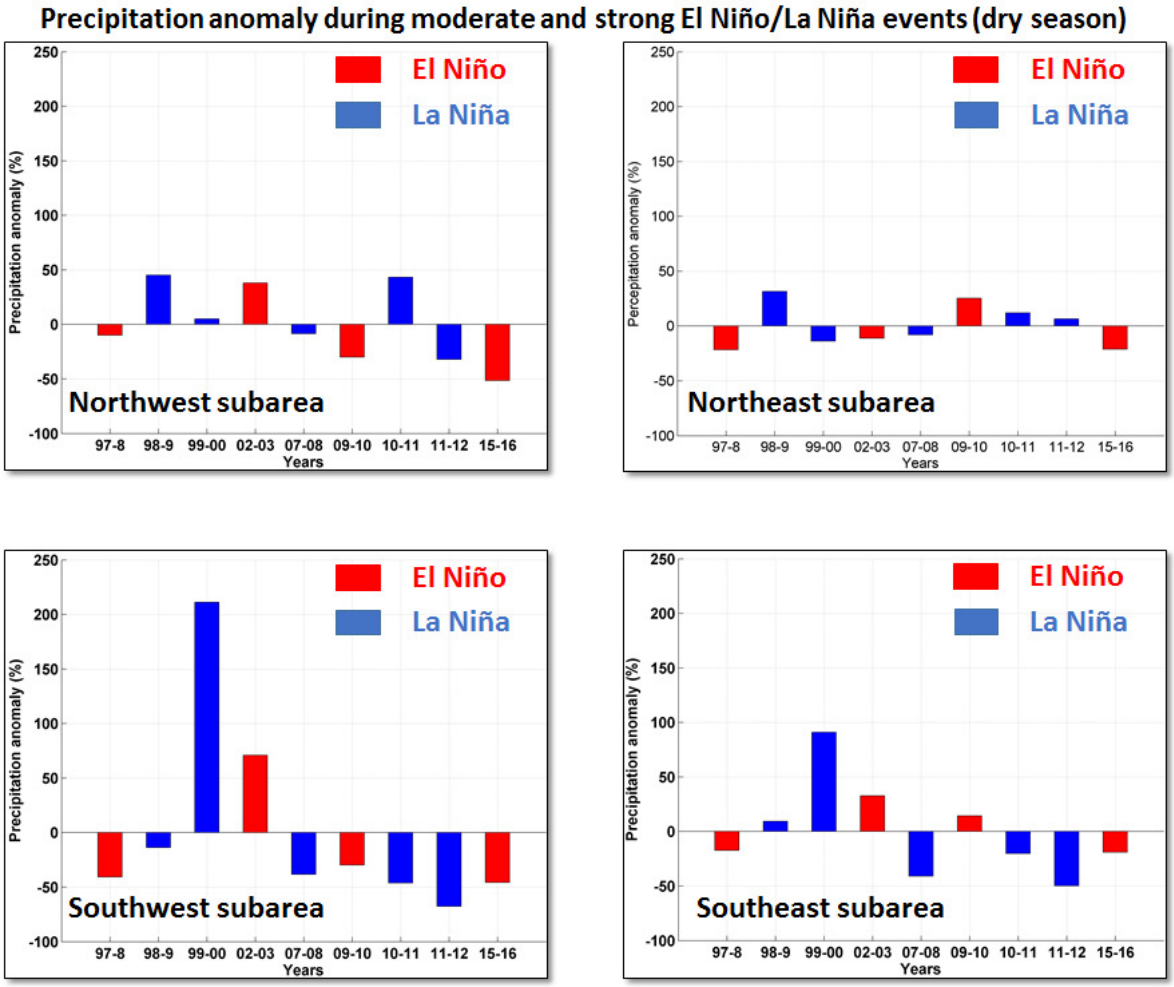

Figure 5.5.2: Areal anomaly of precipitation (%) over northwest [9-14.5°S, 30-33.5°E], northeast [9-14.5°S, 33.5-37°E], southwest [14.5-20°S, 30-33.5°E] and southeast [14.5-20°S, 33.5-37°E] subareas during the dry season of years of moderate and strong ENSO intensities. The mean precipitation value from which the anomalies were calculated was determined using annual means of precipitation of years of moderate and strong ENSO.

The spatial variability of correlation between TRMM 3B43-v7 precipitation and each of the nine GCMs during 1998-2005 is presented in Figure 5.6. In general, the values of correlation coefficients decrease from west to east and from north to south except in GISS-E2-R model where the maximum correlation is found in the northeast region. The values decrease from about 0.9 in the northeast to about 0.4 in the southern regions meaning that although they can differ in magnitude, the GCMs can predict the variability of TRMM 3B43-v7 precipitation in about 90%

in the northeast region and in about 40% in most of the south regions. As for using the GCMs outputs for describing long term variability of precipitation having TRMM 3B43-v7 as reference, ACCESS1.0, CanESM2 and CESM1(CAM5) model are better off than others because they present relatively higher correlation coefficients in most of the southern regions.

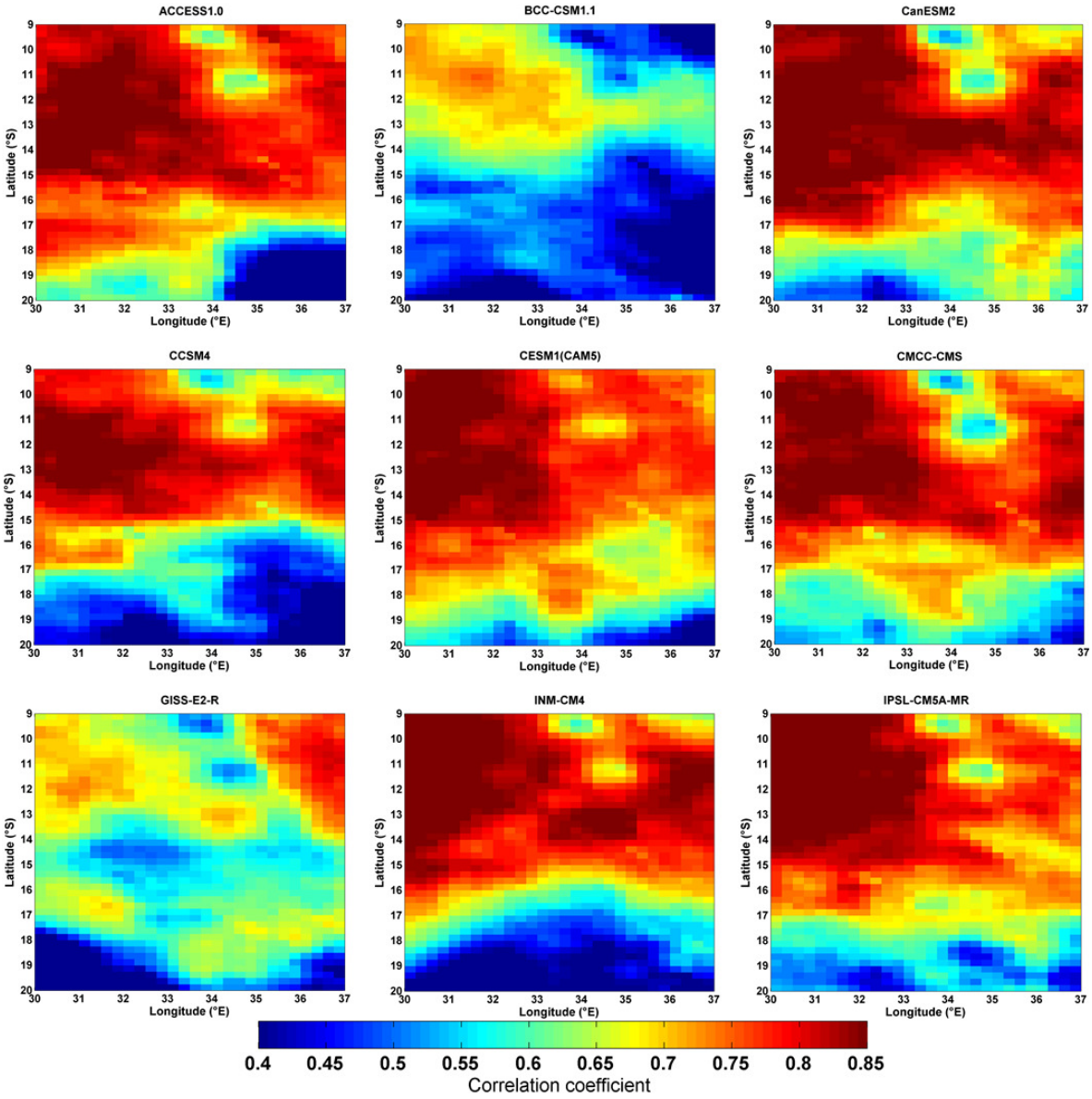

Figure 5.6: Spatial variability of correlation between monthly TRMM 3B43-v7 precipitation and monthly GCMs precipitation for the period 1998-2005.

Attempting to speculate the reason for lower correlation coefficients over the south region of lower Zambezi basin, we compared to the spatial variation of correlation between 3.4 Niño index and TRMM 3B43-v7 precipitation and spatial variation of TRMM 3B43-v7 standard deviation for the period 1998-2017 (Fig. 5.7). The distribution of standard deviation does not show a clear

difference between north and south regions, however, in some months of the wet season (December. January, February, and March) it is higher in the south regions, meaning that the south regions present higher inter-annual variation. On the other hand, the strong relationship between ENSO index and precipitation variability is found in the south region (Fig. 53.1 and 5.3.2). The above findings suggest that the lower correlation between TRMM 3B43-v7 precipitation and GCMs in the south regions might be due to the lack of GCMs in forecasting the contribution of ENSO on the inter-annual variability of precipitation. The failure of GCMs in capturing the effect of ENSO on the inter-annual variability of precipitation was previously pointed out in Asian-Australian Monsoon (Wang, et al., 2004).

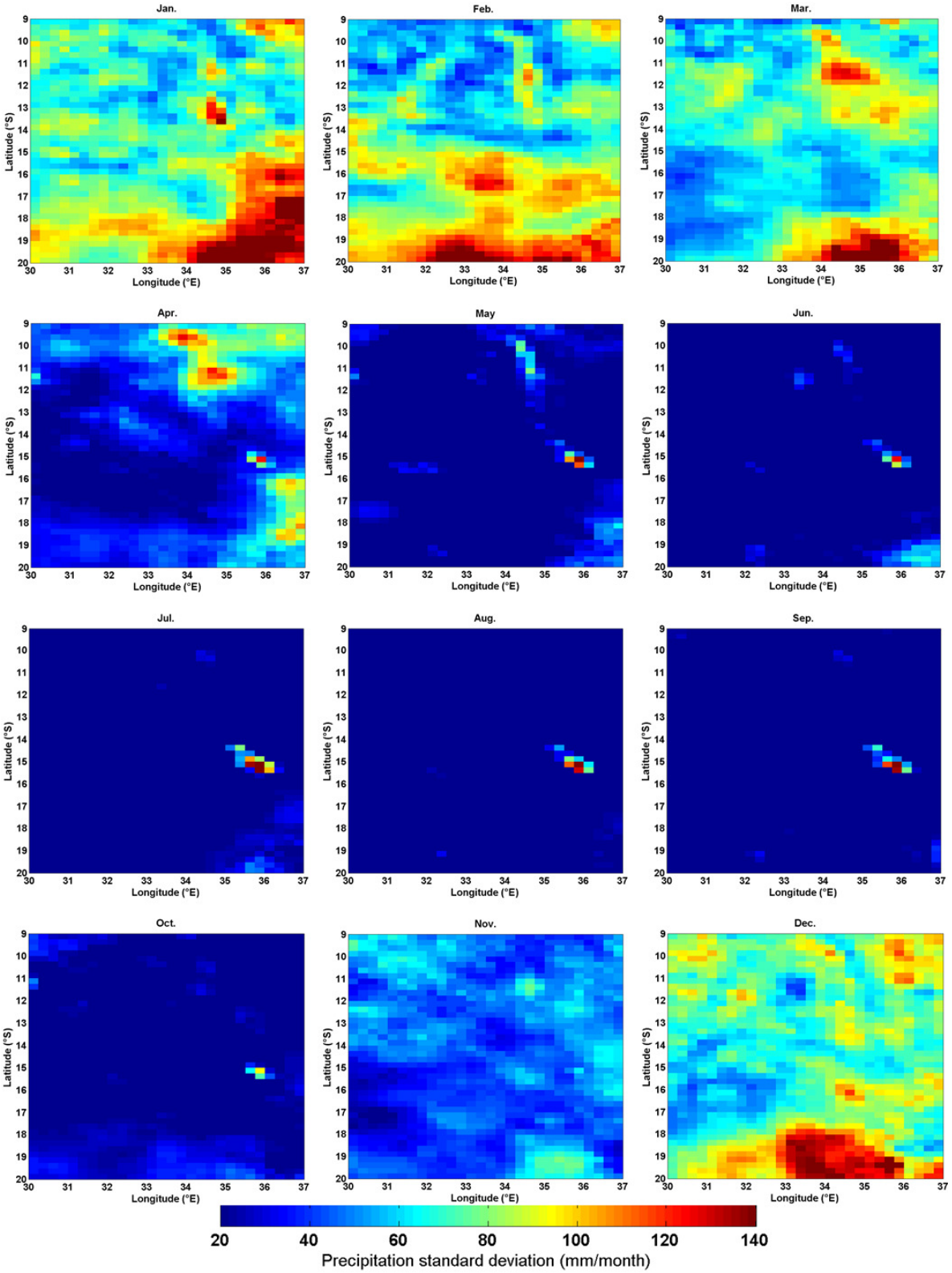

Figure 5.7: Spatial distribution of TRMM 3B43-v7 precipitation standard deviation for the 1998-2017 period.

The spatial variation of Root Mean Square Error (RMSE) of GCMs in relation to TRMM 3B43-v7 precipitation is presented in Figure 5.8. The RMSE values vary between about 10 and about 70 mm and do not show any clear pattern in its distribution. Again, as observed in the correlation coefficient maps the ACCESS1.0, and CESM1(CAM5) models present lower RMSE values but CanESM2 model presents relatively higher values exceeding 70 mm/month in the southeast region, and thus becomes less preferable than other two for being used to describe long-term precipitation variability. The distribution of RMSE for ACCESS1.0, and CESM1(CAM5), which were taken as the best performed in terms of correlation with TRMM 3B43-v7 precipitation, are very similar and thus, their performance in RMSE would not be the best criteria for choosing which of them is best.

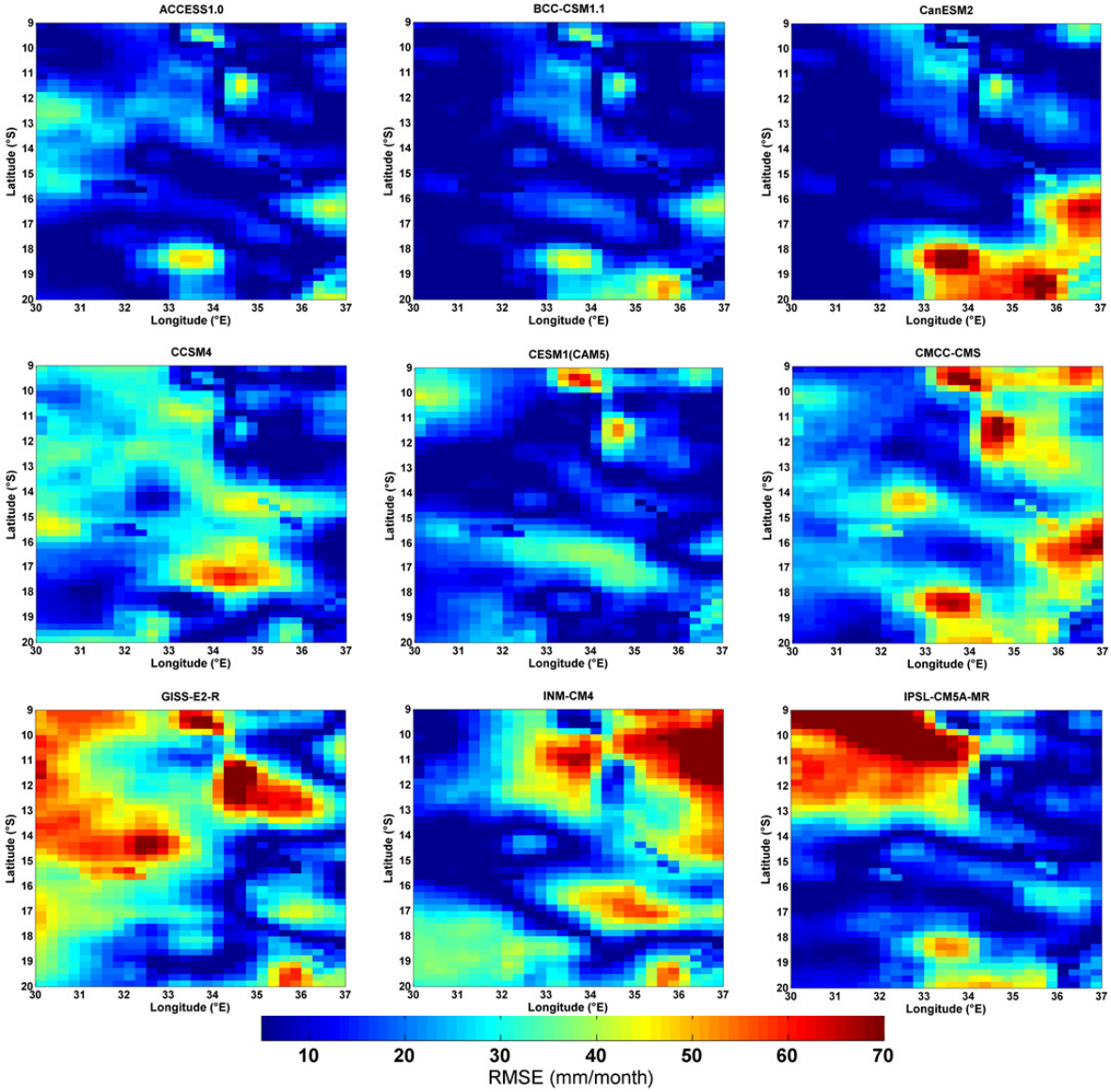

Figure 5.8: Spatial variability of RMSE of GCMs in relation TRMM 3B43-v7 precipitation standard deviation for the 1998-2005 period.

Comparisons of TRMM 3B43-v7 precipitation with GCMs outputs in over northwest [9-14.5°S, 30-33.5°E], northeast [9-14.5°S, 33.5-37°E], southwest [14.5-20°S, 30-33.5°E] and southeast [14.5-20°S, 33.5-37°E] subareas are presented in Figure 5.9. The annual variation of TRMM 3B43-v7 precipitation (in black) in the northwest region presents similar pattern to that of northeast and the southwest region present a similar annual variation to that of the southeast region. In the northwest and northeast region, there is a steeper decrease from January to February followed by a very little increase in March, which is followed by a relatively steeper decrease to May from where the mean monthly precipitation values remain close to zero until

October when a steeper increasing continues until December. Most of the CGMs reproduce most of the part of the annual pattern but do not reproduce the small increase from February to March. On the other hand, all the models overestimate or underestimate the values of TRMM 3B43-v7 precipitation such that none of them matches the TRMM 3B43-v7 precipitation in terms of absolute values. The ACCESS1.0 is the model which most overestimates the TRMM 3B43-v7 precipitation, with overestimation of about 150 and 100 mm/month during January and February in northwest and northeast regions respectively. The CanESM2 model is the model which most underestimates the TRMM 3B43-v7 precipitation, with underestimation of more than 100 mm/month during December to February in the northwest and northeast regions. The CESM1(CAM5), in turn, seems to be one of the models which deviate less to TRMM 3B43-v7 precipitation values in the northwest and northeast regions, especially during December-February, the period in which much over and underestimation are observed. In southwest and southeast regions, analogously to northwest and northeast regions, most of the models reproduce the annual variation of TRMM 3B43-v7 precipitation but with over or underestimation and some failure of precipitation variation between February and March. BCC-CSM1.1, CanESM2 and CCSM4 model showed an increase between February and March while TRMM 3B43-v7 showed a decreasing. For the southwest and southeast regions, the CMCC-CMS model is the model, which most overestimated the TRMM 3B43-v7 precipitation, with an overestimation of about 150 mm/month in January over the southwest region and about 50 mm/month in January and February over southeast region. Again for the southwest and southeast regions, CESM1(CAM5) model seems to be the models which less deviates from the TRMM 3B43-v7. Despite deviating less during December-January, the ACCESS1.0 model shows an underestimation of more than 100 mm/month in February and March over the southeast region. Based on the analysis of correlation, RMSE and the comparison of annual variation of the TRMM 3B43-v7 precipitation and GCMs, the CESM1(CAM5) model is selected as the one that can best describe the TRMM 3B43-v7 precipitation and thus, it will be used for the long-term analysis of influence of ENSO on precipitation over the lower Zambezi basin.

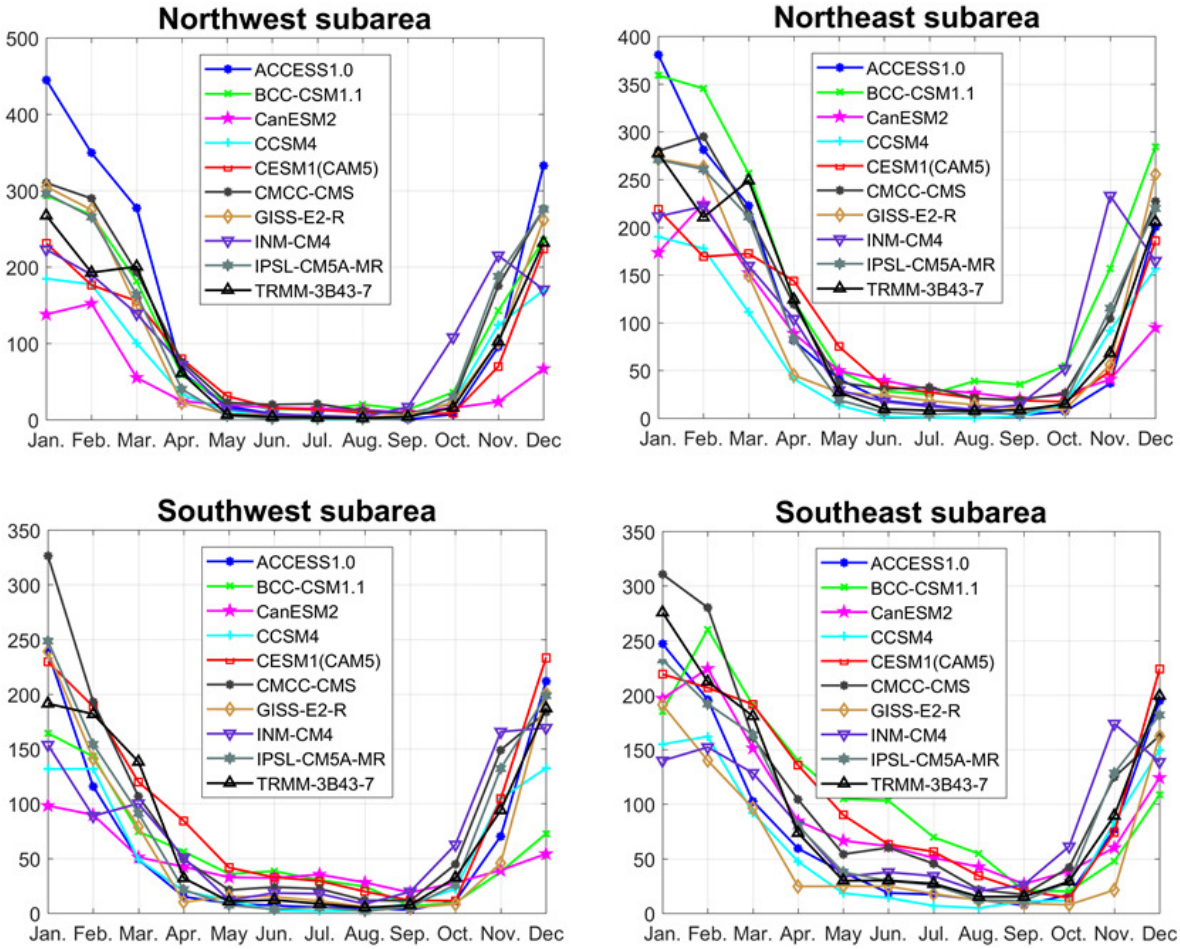

Figure 5.9: Overlaying of the climatology of annual variability of precipitation from TRMM 3B43-v7 and from GCMs output.

The times series of 20 years sliding correlation between 3.4 Niño index and CESM1(CAM5) model precipitation, overlapping of 20 years moving average of CESM1(CAM5) model precipitation and 3.4 Niño index, wavelet power spectrum of sliding correlation with its respective global spectrum are presented in Figures 5.10.1, 5.10.2, 5.10.3 and 5.10.4 for northwest, northeast, southwest and southeast regions respectively. In the north region there was a positive correlation between 3.4 Niño index and precipitation during the years 1900 and 1910, followed a phase quasi-null relation during years 1910 and 1925 when an inverse relation started to occur to become stronger during years 1930-1935. The years 1945-1960 were dominated by a relatively long period of inverse relation dominance and after that period, the negative correlation starts to become weaker, ending with a shift to a weak positive relation in years 1900. The long-term variation in correlation between Niño index and precipitation is compatible with the relation between the variation of 20 years moving average of Niño index and precipitation (upper right panel), which shows increasing precipitation and increasing Niño index during years 1990, increasing precipitation and decreasing Niño index in years 1930-1935, increasing precipitation and increasing Niño index in years 1990. The wavelet power spectrum, with power

increasing from blue to red, and the global spectrum (lower right panel) show that the main periodicity of oscillation of intercalation of strong inverse relation and weak or positive relation between Niño index and precipitation is about 256 months (~21 years) and this periodicity becomes weaker and insignificant from years 1970-1975. These findings suggest that the dominant inverse relationship between ENSO and precipitation in the northwest region of lower Zambezi basin is not constant in multi-decadal timescale.

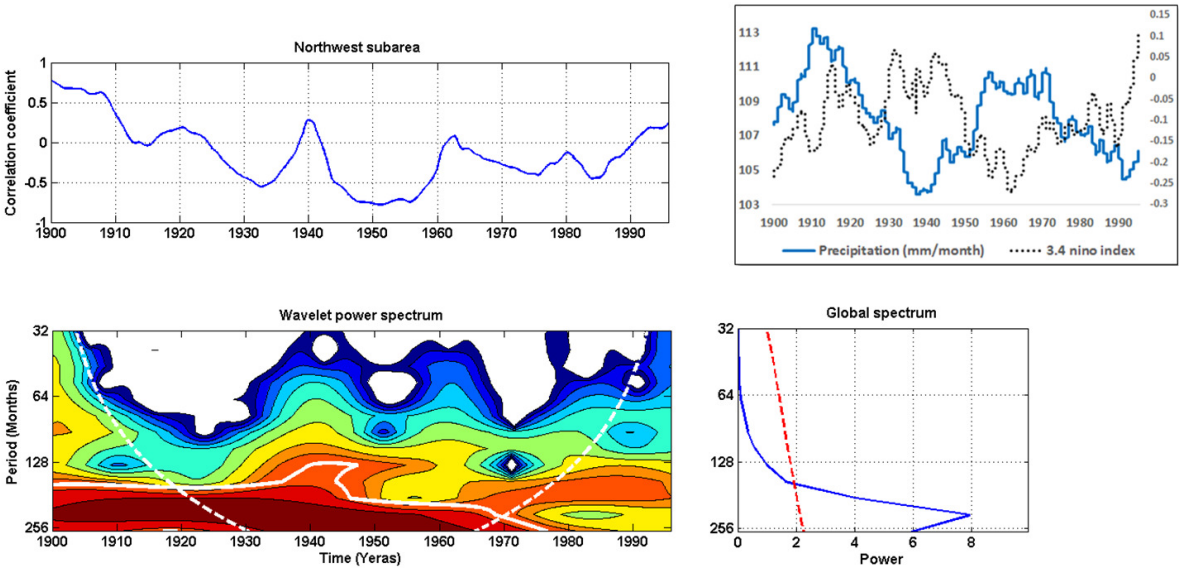

Figure 5.10.1: Times series of 20 years sliding correlation between 3.4 Niño index and CESM1(CAM5) model precipitation (upper left) for 1850-2005 period; overlapping of 20 years moving average of CESM1(CAM5) model precipitation and 3.4 Niño index for 1850-2005 period; wavelet power spectrum of sliding correlation between 3.4 Niño index and precipitation (lower left; the white line encloses the area with statistical significance greater than 95%), with its respective global spectrum (lower right, the blue line enclosing areas with statistical significance greater than 95%). This Figure corresponds to the northwest subarea.

The northeast region (Fig. 5.10.2) presents similar behavior to northwest region during years 1900-1960. In contrast to observation from the northwest region, during the years 1965-1970, there is a positive relation between Niño index and precipitation, with the correlation coefficient close to 0.5, which starts to become weaker, ending in strong positive relation with the correlation coefficient close to 0.7. In the northeast region, the dominance of positive correlation between Niño index and precipitation becomes more frequent than in the northwest region. This suggests that in this region there is an intercalation of phases of inverse ENSO-precipitation relation and positive ENSO-precipitation in inter-decadal time scale. Analogously to the northwest region, the signal of 250-256 months (~21 years) dominates the periodicity of correlation between Niño index and precipitation in the northeast region and becomes weaker after years 1970s.

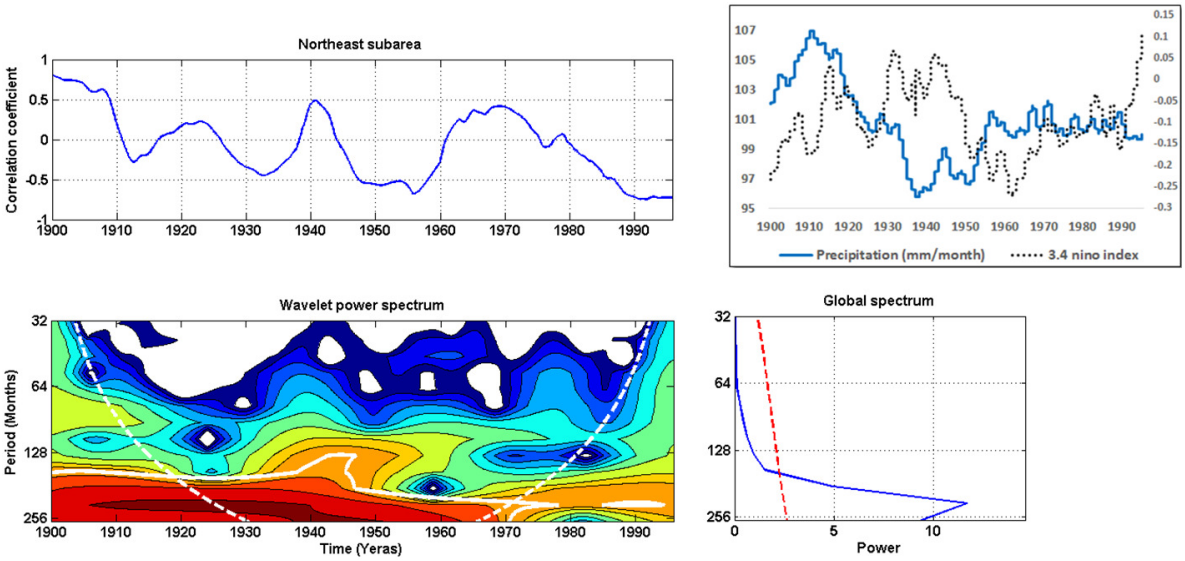

Figure 5.10.2: Times series of 20 years sliding correlation between 3.4 Niño index and CESM1(CAM5) model precipitation (upper left) for 1850-2005 period; overlapping of 20 years moving average of CESM1(CAM5) model precipitation and 3.4 Niño index for 1850-2005 period; wavelet power spectrum of sliding correlation between 3.4 Niño index and precipitation (lower left; the white line encloses the area with statistical significance greater than 95%), with its respective global spectrum (lower right, the blue line enclosing areas with statistical significance greater than 95%). This Figure corresponds to the northeast subarea.

In the southwest region (Fig. 5.10.3), the long-term variation of the relation between Niño index and precipitation is dominated by intercalation between phases of inverse relation and phases of quasi-null relation, which end from the years 1980s when the relationship shifts the positive until the years 1990s. The main phases of inverse relation dominance are years 1900-1920, 1945-1955, 1965-1975, all with absolute values of correlation coefficient greater than 0.5. From the years 1975, the inverse relation starts to show a continuous decreasing and becomes strong positive with a correlation coefficient greater than 0.5 in years 1985, keeping positive until the years 1990s. From the overlapping of 20 years moving average of precipitation and Niño index it is possible to note the tendency of increasing precipitation with increasing Niño index, suggesting that in years 1980-1990 the dominant inverse ENSO-precipitation relation was broken and the positive relation took place. The signal of 250-256 months (about 21 years) periodicity is also the most dominant in the southwest region and extends during the entire observation time.

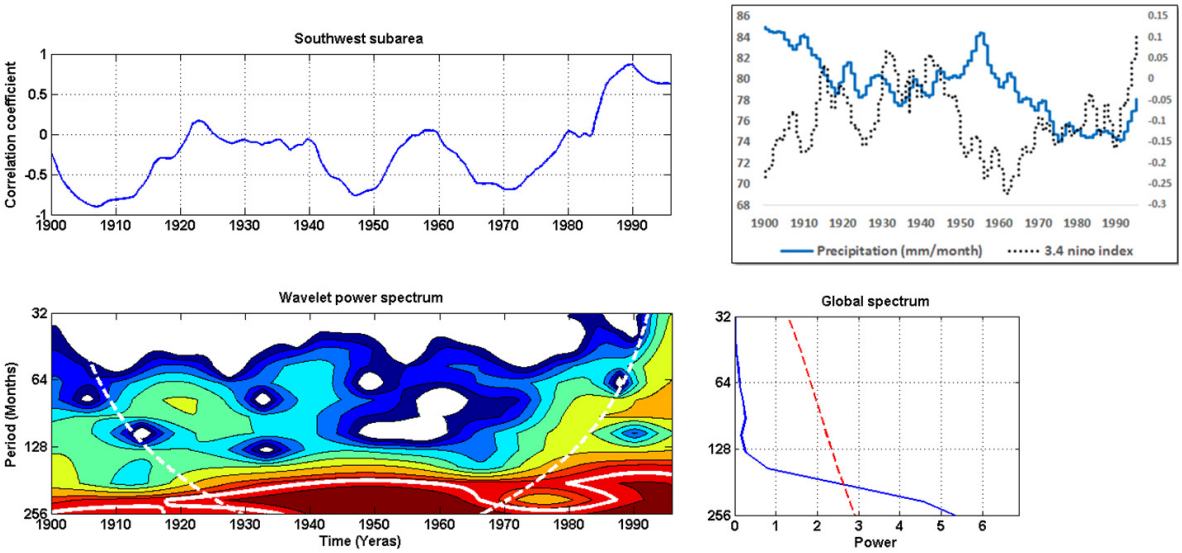

Figure 5.10.3: Times series of 20 years sliding correlation between 3.4 Niño index and CESM1(CAM5) model precipitation (upper left) for 1850-2005 period; overlapping of 20 years moving average of CESM1(CAM5) model precipitation and 3.4 Niño index for 1850-2005 period; wavelet power spectrum of sliding correlation between 3.4 Niño index and precipitation (lower left; the white line encloses the area with statistical significance greater than 95%), with its respective global spectrum (lower right, the blue line enclosing areas with statistical significance greater than 95%). This Figure corresponds to the southwest subarea.

In the southeast region (Fig. 5.10.4), analogously to the northwest, the long-term variation of correlation between Niño index and precipitation is characterized by alternating of phases of inverse relation with phases of null and positive relation. During years 1910-1920, there is a dominance of inverse relation between Niño index and precipitation, with correlation coefficient close to 0.7. A phase of weaker relation is observed between 1920 and 1940 when a very short phase of positive relation, with a correlation coefficient of about 0.5 is observed. The years 1945-1975 are characterized by another long phase of inverse relation, with correlation coefficient up to 0.5, which starts become weaker, ending in a weaker positive relation, with correlation coefficient below 0.5. The about 21 years periodicity of correlation coefficient time series is also present in the southeast region and is not significant after the years 1975.

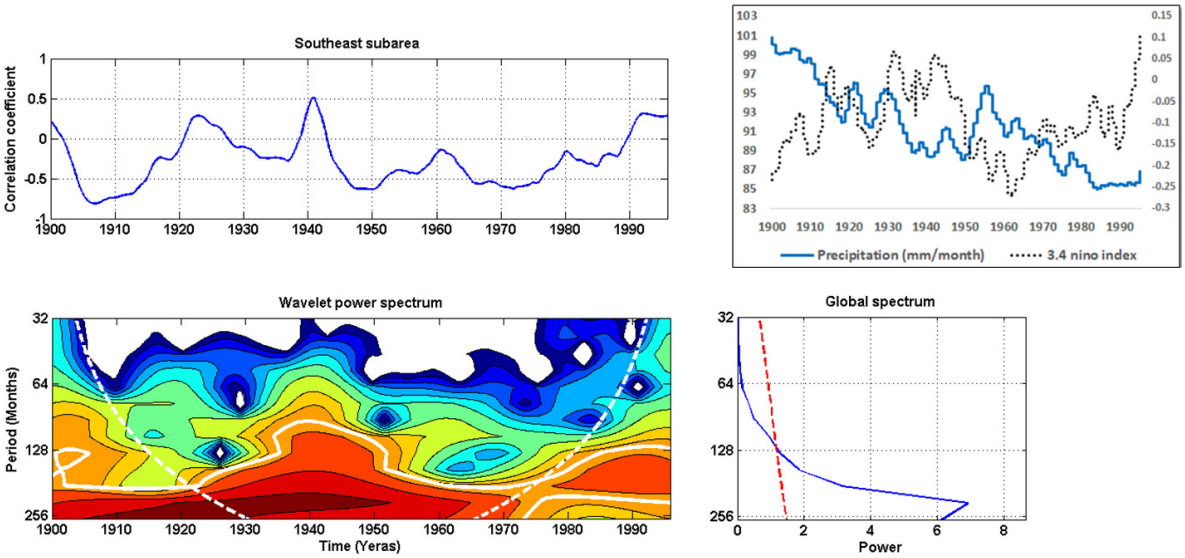

Figure 5.10.4: Times series of 20 years sliding correlation between 3.4 Niño index and CESM1(CAM5) model precipitation (upper left) for 1850-2005 period; overlapping of 20 years moving average of CESM1(CAM5) model precipitation and 3.4 Niño index for 1850-2005 period (upper right); wavelet power spectrum of sliding correlation between 3.4 Niño index and precipitation (lower left; the white line encloses the area with statistical significance greater that 95%), with its respective global spectrum (lower right, the blue line enclosing areas with statistical significance greater that 95%). This Figure corresponds to the southeast subarea.

For all four subareas of the lower Zambezi basin, the time series of 21 sliding correlation between Niño 3.4 index and precipitation shows a dominance of strong inverse ENSO-precipitation which is intercalated by intervals of weak or positive relationships. The breaking and weakening of the inverse ENSO-precipitation suggest the influence of different types of ENSO, with contrasting effects on precipitation variability. Yu and Kao (2007) found that there are two types of ENSO generated by two different mechanisms: an Eastern Pacific (EP-ENSO) whose generation mechanisms involves thermocline variation and Central tropical Pacific (CP-ENSO) whose generation mechanisms is not sensitive to thermocline variation. On the other hand, the decreasing in Monsoon precipitation caused by ENSO events characterized by warming Central Pacific is more severe than that caused by ENSO events characterized by Eastern Pacific warming (Kumar et al., 2006). The weakening of the 21 signal of the periodicity of ENSO-precipitation correlation, which began after the years 1970s, period suggested to be the period of climate shift in previous studies (Graham, 1994; Gaughan, et al., 2016), coincides with the weakening of the breaking of the inverse ENSO-Monsoon precipitation observed by Kumar et al., (1999). In addition, the inverse relationship between EP-ENSO type and south Asian Monsoon weakened significantly after years 1970, while the correlation between CP-ENSO type and Monsoon precipitation strengthened (Fan et al., 2017). The perturbation of ENSO-

precipitation relationship after years 1970 is attributed to the transition phase of Pacific Decadal Oscillation (Mantua and Hare, 2002), and anthropogenic global warming (Kumar et al., 1999).

5.4 Concluding Remarks

The TRMM 3B43-v7 precipitation in lower Zambezi basin showed two main seasons, one of higher precipitation extending between November and March and other of lower precipitation rates, extending between May and October. The spatial variability showed that the precipitation decreases from north to south.

The spatial variability of correlation between 3.4 Niño index and precipitation and the variation of precipitation anomalies during positive and negative 3.4 Niño index, and in years of ENSO events showed that ENSO influences most in the wet season of south of 15°S along the lower Zambezi in an inverse relationship such that the precipitation decreases with increasing ENSO intensity. However, the distribution of precipitation anomalies in years of moderate and strong ENSO events showed that in some years the ENSO effect is not reflected in the precipitation pattern, suggesting that besides ENSO there might be other factors influencing the inter-annual variability of precipitation in lower Zambezi.

The variability of the correlation coefficients, RMSE and the overlapping of the climatology of annual variation of TRMM 3B43-v7 precipitation against the GCMs outputs revealed that the GCMs reproduce the annual variation of TRMM 3B43-v7 precipitation in up to 90 %; however, all of the GCMs showed over or underestimate the TRMM 3B43-v7 precipitation.

The fact the values of lower correlation GCMs and TRMM 3B43-v7 precipitation is observed precisely in the south, where the influence of ENSO is more evident, with higher values of standard deviation, denoting higher inter-annual variability, suggest that the failure of GCMs in reproducing the precipitation in south region might be due to limitation in predicting the variations due to ENSO events.

Among the nine AR5 GCMs compared to find which would best replace the TRMM 3B43-v7, the CESM1(CAM5) model is the one which showed most coverage of high correlation with TRMM 3B43-v7 and low RMSE and thus was selected to be used for long-term analysis of ENSO-precipitation relation.

The analysis of long-term variation of the influence of ENSO on precipitation in lower Zambezi showed that the inverse ENSO-precipitation relation, denoted by the negative correlation between the Niño index and precipitation, is the most dominant and alternates with phases of weaker and positive relationship in a periodicity of about 21 years.

The existence of a relatively long periodicity (about 21 years) between the phases of inverse ENSO-precipitation relation and the phases of weaker or positive relation suggests that there might be a relatively low-frequency factor forcing these shifts. The 21 years periodicity disappeared after the years 1975, the period considered to be the period of climate shift, suggesting that the ENSO-precipitation relation over the lower Zambezi was also affected by the climate shift.

Chapter 6

Variability of satellite measured Chlorophyll in Sofala Bank and its relation to local and remote forcing parameters: El Niño/La Niña Effects

Abstract: This study investigates the variability of satellite measured chlorophyll concentration over Sofala Bank and its relation to Zambezi River discharge, wind speed, Sea Surface Temperature and El Niño Southern Oscillation (ENSO) for the 2003-2013 period through spatial linear regression analysis. For evaluation of annual variation along the shelf and offshore waters, the Sofala Bank was divided into two regions basing on bathymetry ranges, as follows: shelf region extending from the coast to 50 m depth and slope region extending from 200 m offshore. Climatology of monthly composites of chlorophyll concentrations indicates that there are two regimes of chlorophyll concentrations over Sofala Bank. The high regime, with concentrations varying between 3.5 and 4 mg m^{-3} in the plume cores occurs during high flow of Zambezi river flow between January and April; the low regime, with concentrations less than 3 mg m^{-3} in plume cores extends during May to December, the period of lower river flows in Sofala Bank. Along the slope, there are two pathways traversed by coastal chlorophyll-rich waters into deep offshore waters, which seem to be driven by the interaction of mesoscale features with the shelf. Spatial correlation between wind speed and chlorophyll concentrations indicate that despite not being the main forcing, the southerly and southeasterly wind which dominate the wind field in Sofala Bank might play an important role, pushing offshore chlorophyll-poor waters to coastal zones diluting, and thus decreasing the chlorophyll concentrations. Spatial correlation between 3.4 Niño index and chlorophyll concentration and the relation between anomaly of Zambezi River discharge and chlorophyll concentrations during years of El Niño/La Niña indicate that ENSO effects the Zambezi River discharge increasing it during ENSO cold events and decreasing it during ENSO warm events. As consequence of ENSO effect on Zambezi River discharge, the chlorophyll concentrations in regions under Zambezi River influence can decrease in more than 0.4 mg m^{-3} during El Niño event and increase in more 0.4 mg m^{-3} during La Niña events.

Keywords: Sofala Bank, remote sensing, Chlorophyll, Zambezi River discharge, wind speed, ENSO

6.1 Introduction

River discharge is the main mean of transport of continental material to the marine environment. Freshwater, nutrients, sediments, and pollutants brought to marine environment via river discharge play a major role on the physical, biological and ecological processes of shelves (Thomas and Weatherbee, 2006; Lihan, et al., (2011). Freshwater input in coastal waters influences nutrient fluxes and light availability, indispensable elements for primary production (Dagga, et al., 2004; Thomas and Weatherbee 2006). The enhanced concentration food in plume

areas due to input of nutrient from continent and the frontal zones between the plume and adjacent shelf waters provide growth and accumulation of higher marine trophic levels organisms (Dagga, et al., 2004). The dynamics of nutrients in shelf waters is controlled by a variety of factors such as the magnitude of river flow, local circulation and waves, and wind regime (Lihan, et al., 2011). One of the main indicators of productivity in the marine environment is phytoplankton, which accounts for more than 90% of fixation of inorganic carbon to organic matter (Valiela, 2015) and therefore supporting the marine food webs (Duarte and Cebrih, 1996). Phytoplankton also plays a major role on sequestration of carbon from the atmosphere to ocean deep waters through the process known as biological carbon dioxide pumping (Legendre and Fèvre, 1995). The chlorophyll concentration is widely used to access the trophic conditions and productivity of estuaries, coastal waters and open sea as it is in general proportional to phytoplankton biomass and is relatively easy the be measured (Steele, 1962; Platt, et al., 2008; Boyer, et al., 2009). Chlorophyll concentrations can be measured through satellite ocean color observations, which offer high spatial and temporal resolutions, ideal for monitoring the dynamics of coastal and open sea processes (Platt, et al., 2008). Chlorophyll concentrations in coastal and shelf waters can be regulated by river discharge, local wind speed and wind-induced coastal currents (Lihan, et al., 2011; Neto, et al., 2014; Shen, et al., 2018). In General, chlorophyll concentrations in offshore waters co-vary with Sea Surface Temperature and is often controlled by mesoscale circulation features (Venegas, et al., 2008; Chelton, et al. 2011). The interaction of mesoscale features with the shelf, as is the case of interaction of Mozambique Channel Eddies with shelf waters, can result in advection of chlorophyll-rich waters from coastal regions (Lutjeharms, 2006; José, et al., 2014). Many studies have shown that El-Niño Southern Oscillation (ENSO) induced changes in temperature and precipitation correlates with annual and seasonal discharges (Dettinger, et al., 2000; Ward, et al., 2010), suggesting that the effect of ENSO can be observed in coastal and shelf waters influenced by river discharge as is the case of Sofala Bank, central Mozambique shelf. Saldías, et al., (2016) and Dogliotti, et al., (2016), for example, found strong correlations between ENSO and turbidity plumes off central-southern Chile and Río de la Plata, respectively. The aim of this study is to evaluate the annual variation of chlorophyll in Sofala Bank and its relation to Zambezi River discharge, wind speed, and ENSO. The findings of this study can help to understand the mechanisms driving chlorophyll variability over Sofala Bank.

6.2 Study area

Figure 6.1 shows the map of Sofala Bank, located in the central shelf of Mozambique, between latitudes 17-21°S and between longitudes 34-49°E.

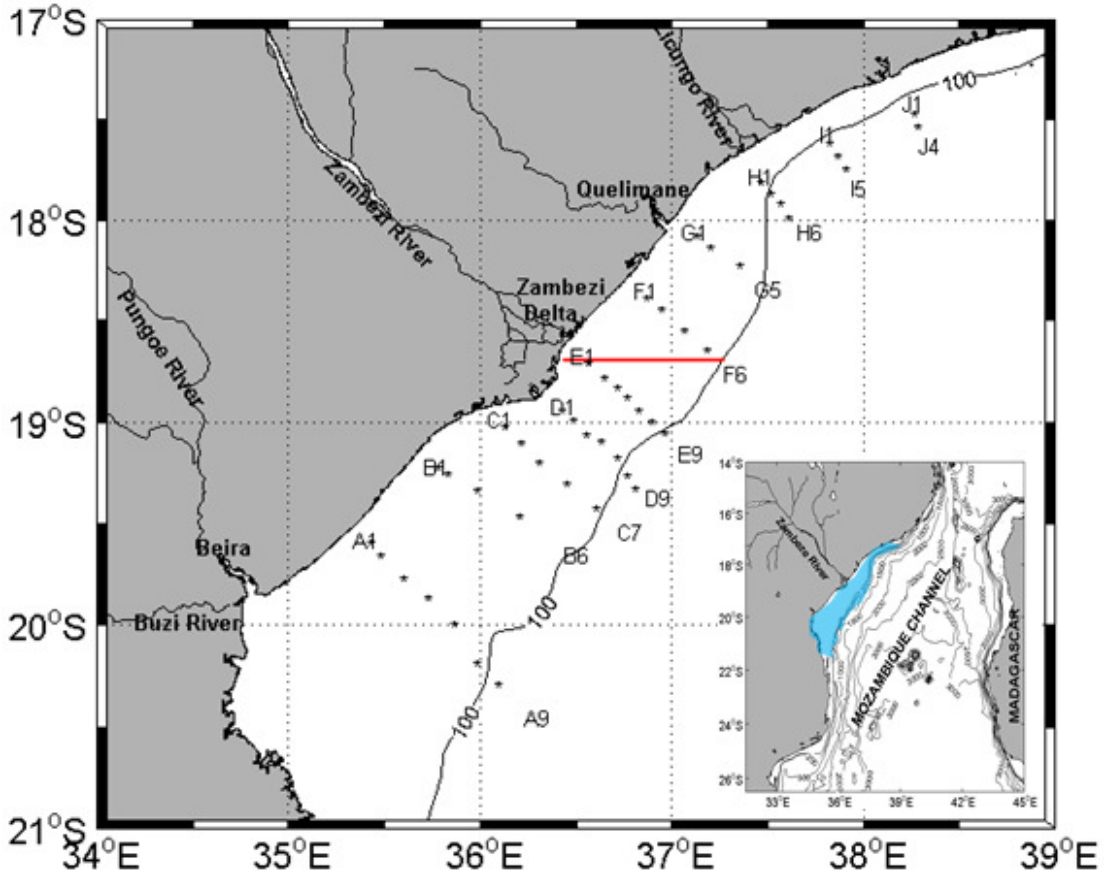

Figure 6.1: Map showing Sofala Bank including the sampling stations. The 100 m isobath is represented for bathymetry reference. The inner image locates regionally the Mozambique coast and the Mozambique Channel. The blue-shaded area in the inner image represents the position of Sofala Bank in the Mozambican shelf. The line in red represents the section analyzed for evaluation of the influence of ENSO on chlorophyll concentration near Zambezi River mouth

6.3 Data

Modis-Aqua Satellite chlorophyll and Sea Surface Temperature

Chlorophyll concentration (Chl-a) and 4µm Sea surface temperature (SST) images (Level 3 products) for the period between 2002 and 2013, calculated using NASA standard algorithm from MODIS-Aqua measurements are used. The data have a spatial resolution of 4 km and were downloaded in Giovanni platform (http://giovanni.gsfc.nasa.gov) on 15th August 2015.

Zambezi River discharge

Monthly mean of Zambezi river discharge River, collected at Tete station, about 440 km distant to the main Zambezi mouth in Sofala Bank was provided by the national directorate for water affairs of Mozambique.

Wind speed

NCEP/NCAR Reanalysis monthly zonal and meridional components of wind (Kalnay et al., 1996) at 10m above the surface, with 2.5° spatial resolution was downloaded in the website of NOAA Physical Sciences Division (https://www.esrl.noaa.gov/psd/data/gridded/data.ncep.reanalysis.derived.surface.html) on 7th September 2015.

Niño Index

The monthly Niño 3.4 index data (Rayner et al., 2003) was obtained from the Physical Sciences Division (PSD, https://www.esrl.noaa.gov/psd/gcos_wgsp/Timeseries/Nino34/). The Niño 3.4 region is the most commonly used region for classifying the intensity of El-Niño based on Sea Surface temperature anomalies in the central Pacific region.

6.4 Methods

Annual variability of satellite chlorophyll concentrations along the shelf and offshore Sofala Bank

To evaluate annual variability along the inner shelf, where the continental inputs are more important, and offshore waters, where the mesoscale circulation may be the main driver of the variability, monthly climatologies of chlorophyll concentrations were performed for two areas conceived according to bathymetry ranges. The first area extends from the coast up to 50 m and other extends from 200 m towards offshore. The inner shelf range was set to 50 m after observing from visual analysis of monthly composite maps of chlorophyll, that the influence of coastal waters including the Zambezi River plume does not exceed the 50 m isobath.

EOF decomposition

Empirical Orthogonal Function decomposition (EOF, Emery and Thomson, 2001) was performed to monthly composites time series of chlorophyll in order to infer spatial and temporal modes variability of chlorophyll in Sofala Bank.

Evaluation of the relationship between chlorophyll concentration and Zambezi River discharge, wind speed, and ENSO

The spatial relationship between chlorophyll concentrations and each of other parameters was performed through linear regression analysis, assuming strong and esthetically significant correlations as the denotation of a considerable relationship between the concentration of chlorophyll and a given parameter in the analysis. Based on the fact that the impacts of some marine processes can be observed with some delay time in relation to their occurrence and may extend for a longer time, the regression analysis was performed accounting for chlorophyll observed at the time of the observation of forcing parameter and for chlorophyll observed between one and three months after the observation of the given parameter (River discharge and ENSO index). Monthly longitudinal variation of chlorophyll concentrations in a line section starting from the coast offshore is plotted against monthly time series of the Niño3.4 index and monthly time series of Zambezi River discharge in order to have a detailed analysis of the relationship between ENSO, Zambezi River discharge and chlorophyll variability in Sofala Bank. Anomalies of Zambezi River discharge and chlorophyll concentrations were determined for wet (October-March) and dry (May-September) seasons corresponding to years of moderate and strong El Niño/La Niña years. This procedure was another attempt of evaluation of the influence of ENSO on Zambezi River discharge and its respective regions of influence during wet and dry seasons.

6.5 Results and discussion

Seasonal Variation of Zambezi River discharge

Figure 6.2 presents the seasonal variation of Zambezi River discharge measured at Tete hydrographic station located about 440 Km from the main Zambezi River mouth in Sofala Bank. There is possible to distinguish two flow regime: higher flow regime observed October-April with a peak of about 2600 $m^3 s^{-1}$ in February, and lower flows observed between May-September with minimum moth value of about 1700-1800 $m^3 s^{-1}$ in August-September. Higher standard deviation values are observed during high flow regime, varying between about 2900 and 4000 $m^3 s^{-1}$ between December and Mach, respectively.

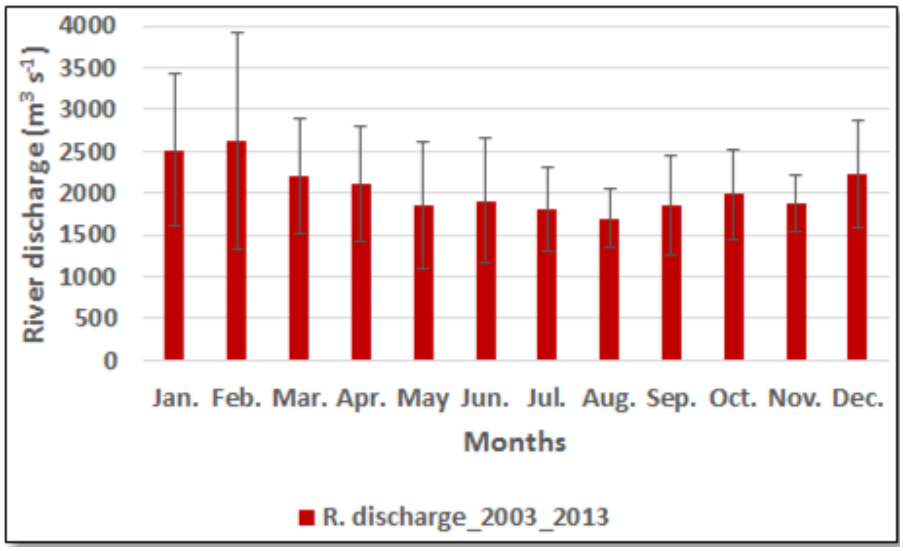

Figure 6.2: Monthly climatology of Zambezi river discharge measured at Tete station, about 440 Km to the main Zambezi mouth in Sofala Bank for 2003-2013 period.

Seasonal variability of chlorophyll concentration in inner Sofala Bank shelf

Monthly climatology of seasonal variation of chlorophyll concentrations over the inner shelf of Sofala Bank (up to 50 m depth) is shown in Figure 6.3. At the first sight, one can see that there are two plume cores of chlorophyll concentration; one in the south, in front of Pungue and Buzi mouths, and other in the center region, in front of Zambezi Delta mouths. In general, there are two regimes of chlorophyll concentration, which are more notable in center and north regions of Sofala Bank: (1) a high regime, with concentrations varying between 3.5 and 4 mg m^{-3} in plume cores, extending between January and April, in response to the high flow rates observed in this period, and (2) a low regime, with concentration not greater than 3 mg m^{-3} in center and north regions, occurring between May and December, and following the low flow rates of Zambezi River. The disparities between river discharge (Fig. 6.2) and chlorophyll concentration observed mainly in the center and north regions of Zambezi River, as for example, high river flow with low concentration in December and peak of river flow in February with peak of chlorophyll in March might be due delaying time between river flow and chlorophyll. The low concentration of chlorophyll observed in December might be due relatively low river flow observed in November while the peak in chlorophyll concentration observed in March might be due the peak of river flow observed in February. During high regime period mainly in March, the month of peak, the south and center chlorophyll plumes seem to merge and drift north, flowing the surface coastal current of Sofala Bank in agreement with Siddorn, et al., (2001). During the low regime, the concentrations of chlorophyll in the south region near Pungue and Buzi mouth are higher than in the center region near Zambezi River Delta, which indicates that the combination of Pungue and Buzi Rivers becomes more effective than Zambezi River in this period.

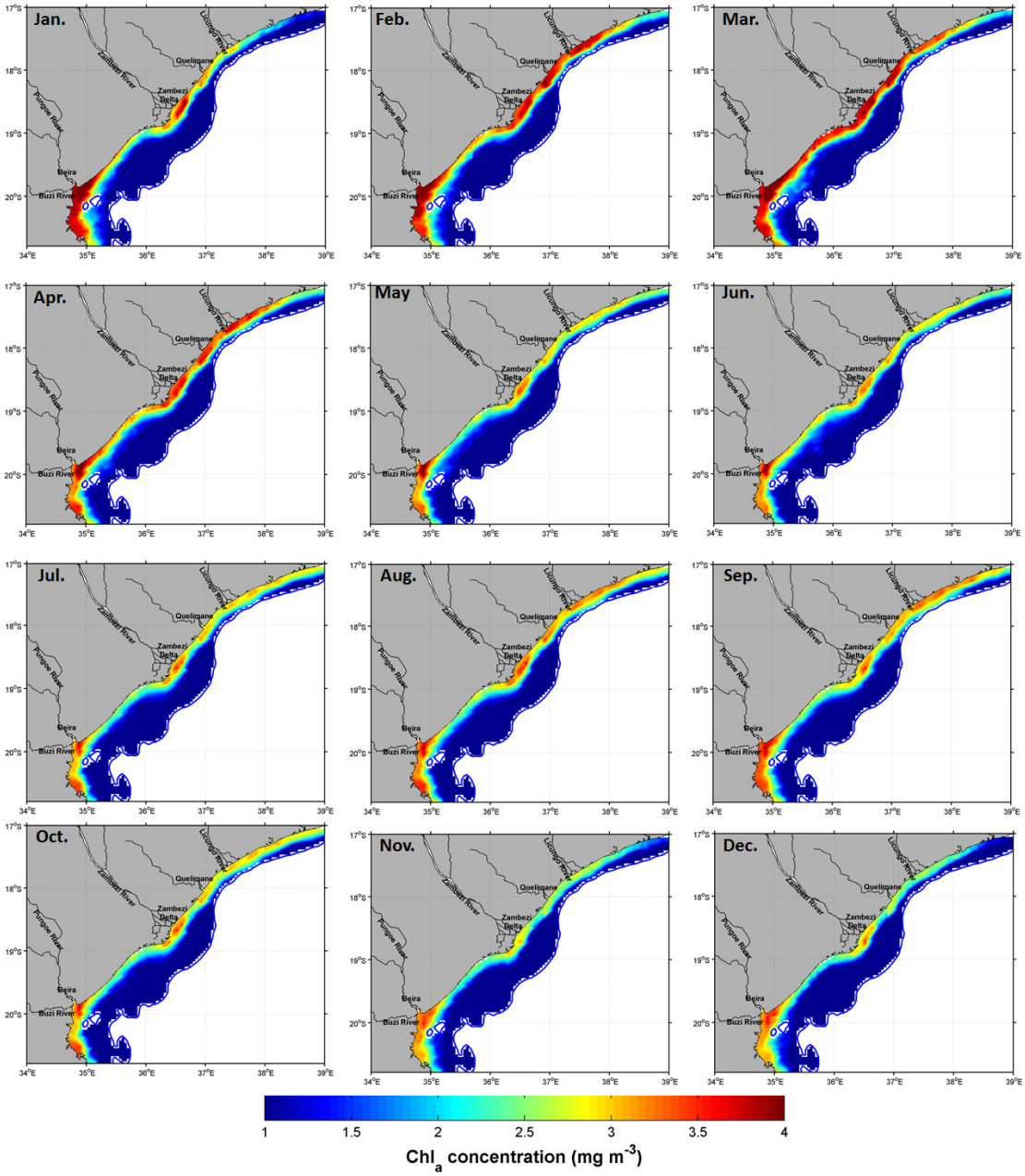

Figure 6.3: Monthly climatology of chlorophyll concentrations in the inner shelf (up to 50 m depth) of Sofala Bank during the 2003-2013 period.

Seasonal variability of chlorophyll concentration in the continental slope of Sofala Bank

The monthly climatologies of chlorophyll concentrations offshore Sofala Bank (from 200 m depth, Fig. 6.4) present a different pattern from that of inner shelf. In general, the chlorophyll concentration decreases from shallower waters (~200 m), with concentrations exceeding in 0.3 mg m^{-3} in the north and south regions towards offshore, where the concentrations are close to

zero. There are two features of higher concentrations, one is in the north region located between 17.5 and 18°S, off Quelimane City, occurring all year round, and other, less frequent along the year, located in the south region, along 20°S off Beira City. These two regions are probably the main pathways of the entrance of coastal waters to the Mozambique Channel as suggested in previous studies (Lutjeharms, 2006; Malauene, et al. 2014) which suggest that there is advection of nutrient-rich coastal waters to the Mozambique Channel through interaction of the anticyclonic eddies with the shelf. During July to September, the presence of chlorophyll-rich waters in north and south regions is more noticeable and they seem to penetrate more offshore The discrepancies between the period of occurrence of chlorophyll-rich waters and regime of high river flow reenforce that river discharge is not the main controller of these features. While the high regime of chlorophyll concentration within the shelf waters occurs between January and April accompanying the high regime in Zambezi River flow, the features of high chlorophyll concentration in north and south regions of continental slope are more pronounced during July to September. The occurrence of the more pronounced feature of high chlorophyll concentrations suggests that this period might be the period of greater intrusion of coastal waters into the Mozambique Channel, presumably due the interaction of the anticyclonic eddies with the shelf.

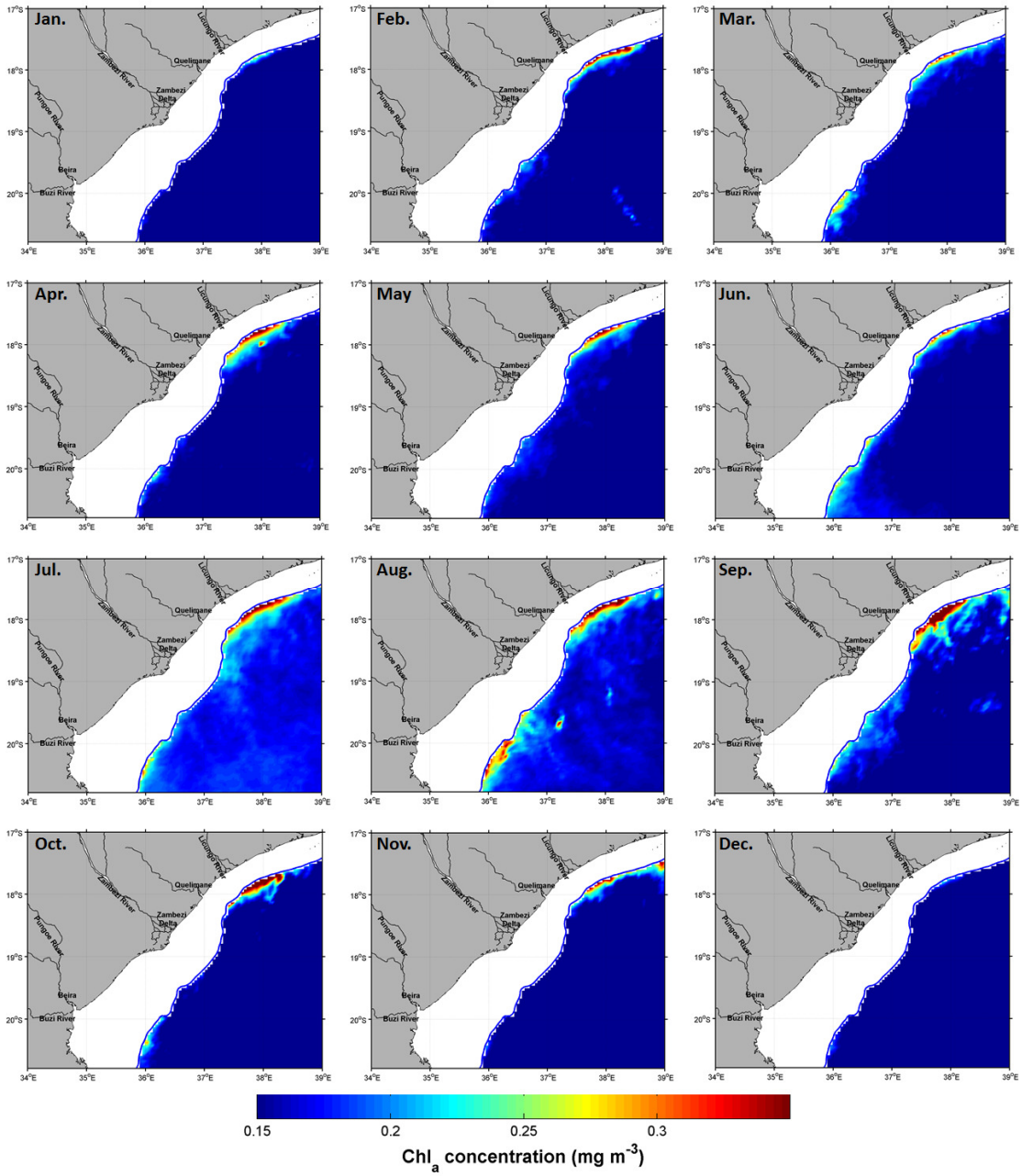

Figure 6.4: Monthly climatology of chlorophyll concentrations offshore (from 200 m depth offshore) of Sofala Bank during the 2003-2013 period.

EOF decomposition

The main four EOF modes of spatial and temporal patterns of chlorophyll variability in Sofala Bank are presented in Figure 6.5. These modes together explained about 60.8 % of the total with 36, 12, 8 and 4.8 % of variance explained by the first, second, third and fourth EOF modes respectively. The first and second modes (36 and 12%) explain seasonal patterns with higher

variability in regions near river mouths while the third and fourth modes (8 and 4.8 %) explain inter-annual patterns with higher variability near river mouths and offshore. Temporal amplitudes present strong negative anomalies in February 2008 for both seasonal and inter-annual patterns and strong positive amplitudes in March of 2003 and 2013 suggesting high concentration in offshore seasonal variability and nearshore inter-annual variability during those periods.

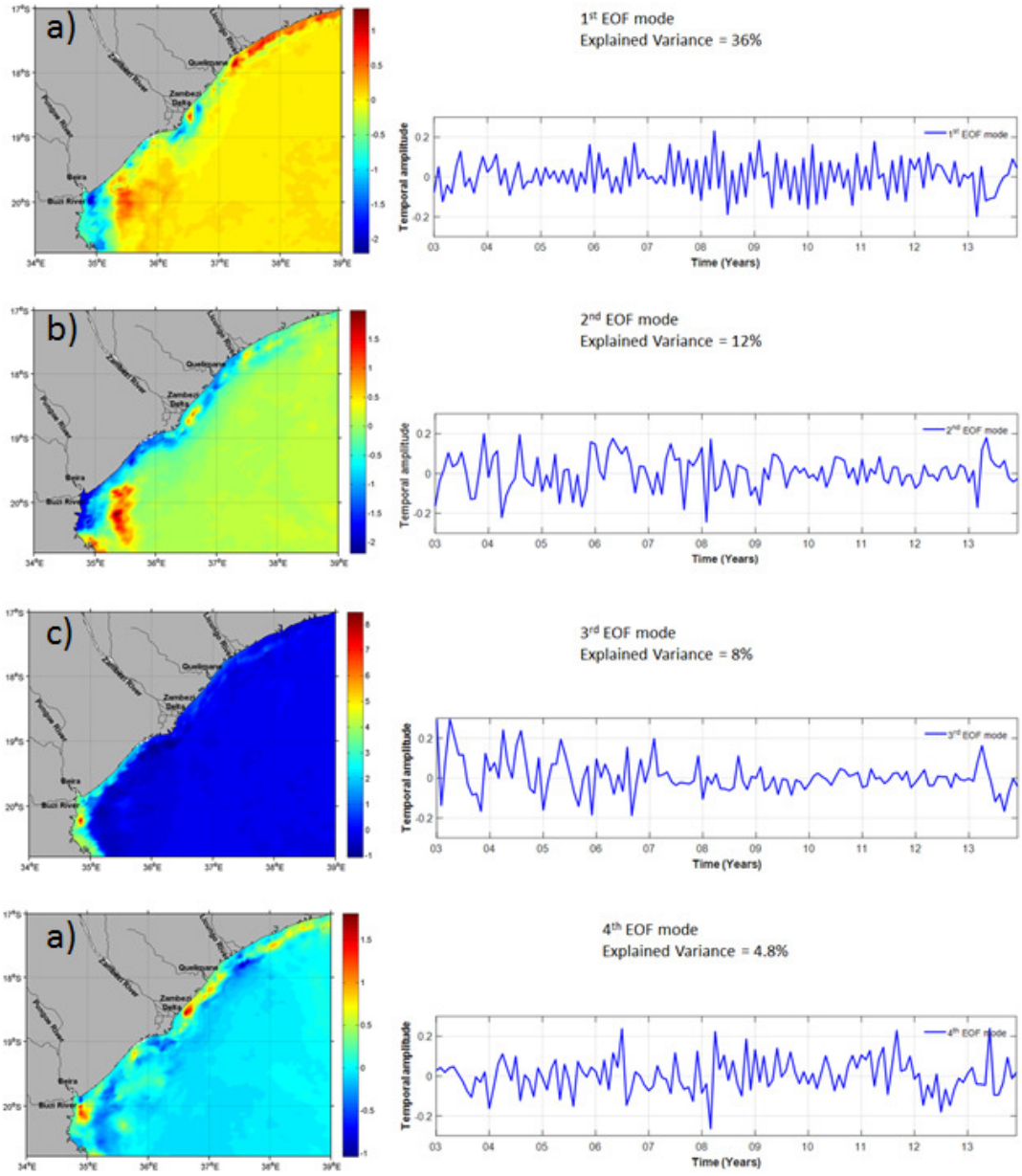

Figure 6.5: Spatial EOF modes (left) and respective temporal amplitudes (right) of chlorophyll concentrations in Sofala Bank: first (a), second (b), third (c) and fourth (d) modes.

Correlation with Zambezi River discharge

Spatial correlations between Zambezi River discharge and chlorophyll concentration along the inner shelf of Sofala Bank are mapped in Figure 6.6.1. The strongest correlations are found in front of the Zambezi Delta mouth and their value decrease from about 0.45 when river discharge and chlorophyll concentrations are correlated for the same time of observation (Lag=0) to about 0.37 when river discharge is correlated to chlorophyll concentration of three months after its occurrence (Lag = 3). Besides the spot of the region of Zambezi Delta, there is a second spot of strong positive correlation in the south region, a bit off the main mouths of Pungue and Buzi rivers during Lag=0. This pattern suggests that during Lag = 0 the Zambezi river influences most in the center region, in front of Zambezi Delta and in the south region where the location of the stronger positive correlation is a bit far from the coast. The weak, statically insignificant correlation near Pungue and Buzi river mouths suggests that their plumes push the Zambezi one offshore. The two spots of strong positive correlation between river discharge and chlorophyll concentrations seem to merge and drift more north as the legging time increases (from Lag=0 to Lag=3), indicating the main direction of Zambezi river plume, as observed in previous studies (Lutjeharms, 2006; Siddorn, et al., 2001) in Sofala Bank.

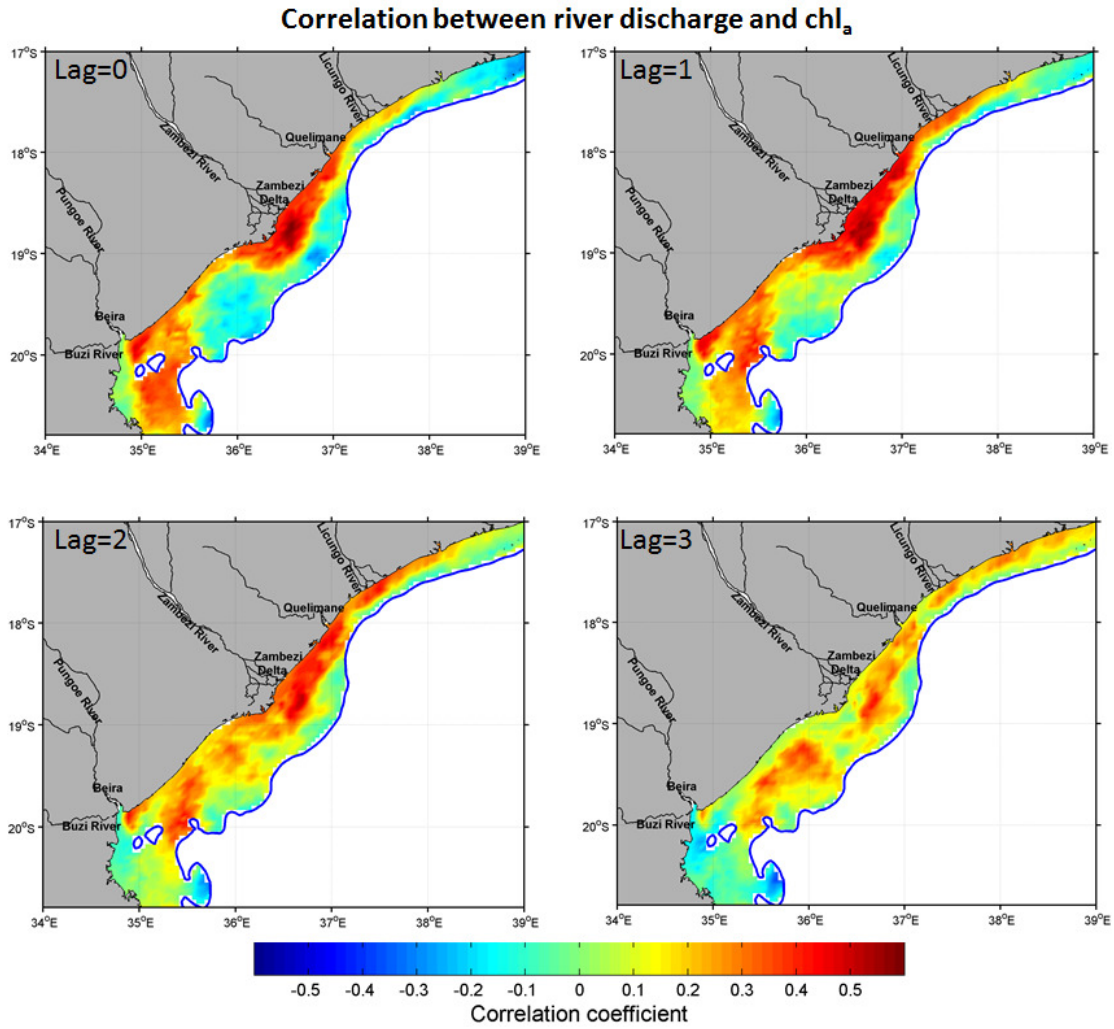

Figure 6.6.1: Spatial correlation between Zambezi River discharge and chlorophyll concentrations in Sofala Bank during the 2003-2013 period. Lag = α denotes the delay time in months considered between the time of observation of river discharge and chlorophyll concentrations. Lag=1 for example denotes the value of first element of river discharge time series was correlated to the second element of chlorophyll concentration, observed one month after of observation of river discharge.

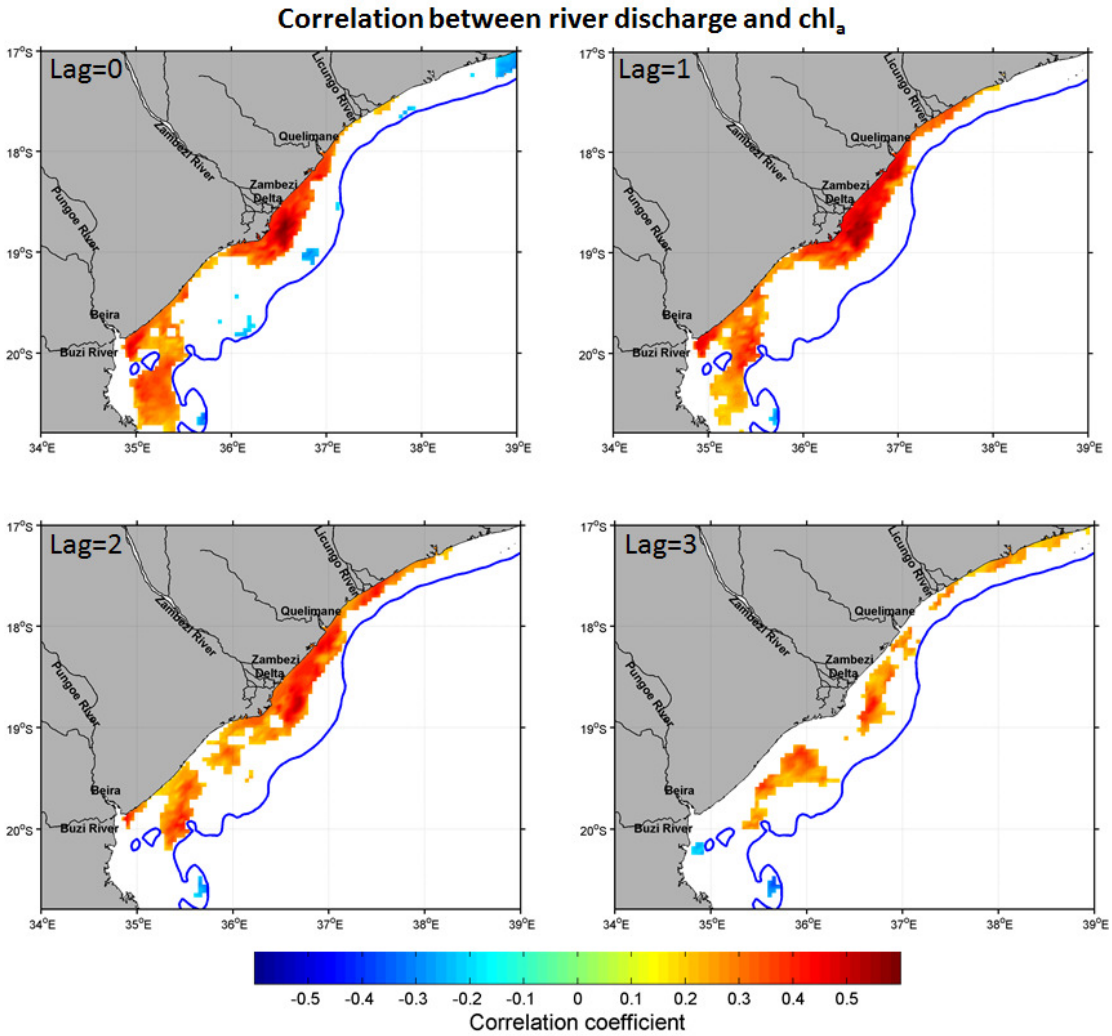

Figure 6.6.2: Same information presented in Figure 6.6.1 with the areas of statistical confidence less than 95% excluded.

Correlation with Wind speed

The spatial correlations between chlorophyll concentrations and alongshore component of wind speed over the continental shelf of Sofala Bank are shown in Figure 6.7. There are two patterns of correlation coefficients, one of strong negative correlation with the strongest value of R = -0.59, occurring over the whole shelf of south region and more onshore of central and north regions; other of strong positive correlation with the maximum value of R=0.57, occurring in the outer shelf of central and north regions of Sofala Bank. The regions of negative and positive strong correlations are separated by a transitional zone with weak and statically insignificant correlation coefficients (Fig. 6.7b). Counting that the most predominant winds in Sofala Bank are southerly and southeasterly, the negative correlation in the entire south shelf region and in the central and northern coastal regions may be justified by the flow of low chlorophyll open ocean

waters to the coast, favored by the transport Ekman. Brinca, et al., (1984), have reported inundation of south Sofala Bank coastal region by high salinity open sea waters in the south region of Sofala Bank. On the other hand, the northwards flowing coastal currents that dominate the circulation over the shelf of Sofala Bank can push nutrient-rich coastal waters to outer shelf, further north, favoring primary production, as observed in the outer shelf of the north region of the Sofala Bank.

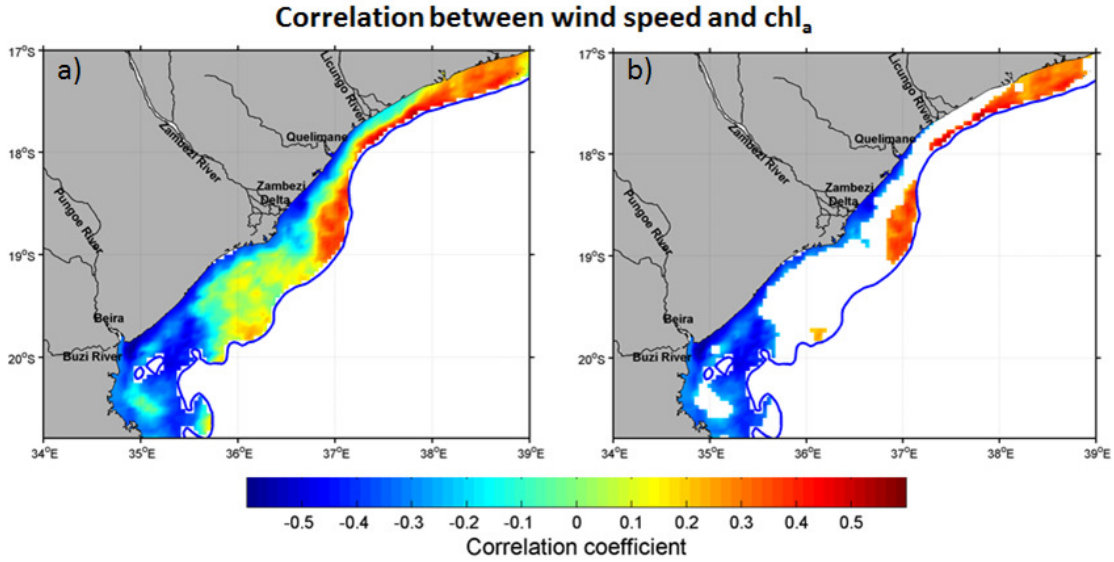

Figure 6.7: Correlation between alongshore component of wind speed and chlorophyll concentrations in Sofala Bank during the 2003-2013 period: a) for the entire shelf; b) same information presented in Figure 7a with the areas of statistical confidence less than 95% excluded.

Correlation with Sea Surface Temperature

Spatial correlations between Sea Surface Temperature (SST) and chlorophyll concentration are presented in Figure 6.8. Analogously to corrections between wind spend and chlorophyll, the correlations between SST and chlorophyll present two patterns, one of strong positive correlations with a maximum of R= 0.71, occurring along the shelf and other of strong negative correlations with maximum of module 0.68 occurring in outer shelf and offshore waters. Confronting the map of correlations between SST and chlorophyll concentrations to those of chlorophyll concentrations against Zambezi River discharge and winds, one can see that regions of positive correlations between river discharge and chlorophyll concentrations, denoting increasing of chlorophyll concentrations when increasing river discharge, are the ones where the chlorophyll concentrations correlate negatively with wind speed and positively with SST. Mentioned above make it possible to state that along the coastal waters of Sofala Bank where the variations in chlorophyll concentration are controlled by river discharge, the wind speed also plays a significant role through pushing offshore to those regions and thus decreasing the

chlorophyll concentrations. It is also possible to state that the high flow regime of river discharge coincides with the warmer season in the continent, and thus, chlorophyll concentrations along the regions of river influence increase with increasing of river discharge and SST.

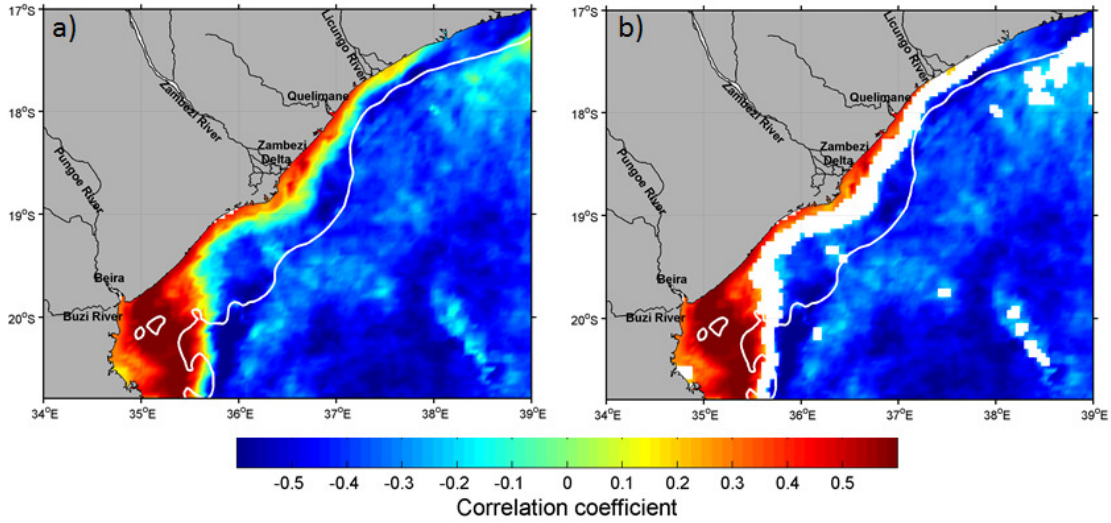

Figure 6.8: Correlation between Sea Surface Temperature and chlorophyll concentrations in Sofala Bank during the 2003-2013 period: a) for the entire shelf; b) same information presented in Figure 8a with the areas of statistical confidence less than 95% excluded.

The patens of spatial variability of correlation coefficients between SST and chlorophyll concentration can be related to the variation of stratification and mixing along the Sofala Bank. In Figure 6.9 the distribution of degree of stratification and mixing during August 2001 is presented in terms of the anomaly of potential energy (ϕ), which is defined as the amount of work required to bring about complete vertical mixing (Simpson, et al., 1990). The value ϕ is zero in a completely mixed water column and increases as the stratification increases. Lower ϕ values imply relatively mixed waters and higher values imply relatively stratified water column. In most of the sections (A, E, F, G, H, I, J) the first station (E1) near the coast and fourth station (E4) in outer shelf present higher values of ϕ and are separated by the second and third stations (E2 and E2) which present relatively low values of ϕ. This pattern of ϕ distribution along the section indicates that in these sections there are two zones of highly stratified waters columns separated by a relatively mixed zone. The stratification in inner shelf corresponds to areas where SST temperature correlates strong and positively to chlorophyll concentrations and is due to buoyancy input from the rivers. In outer shelf high stratification corresponds to the regions where the SST correlates strong and negatively to chlorophyll concentrations and is caused by the upwelling of open sea waters along the slope. The mixed zone corresponds to areas where the correlation coefficients between SST and chlorophyll concentrations are low and statically insignificant and is the transition zone between the haline stratification in the coastal region and

thermal stratification in the outer shelf. In sections B, C, and D, located more south (See Figure 6.1 for the location) the station 1 (E1) presents lower ϕ indicating that the water column is mixed. The mixing in these sections might be associated with the fact that they are located in shallower water columns filled up mostly by freshwater.

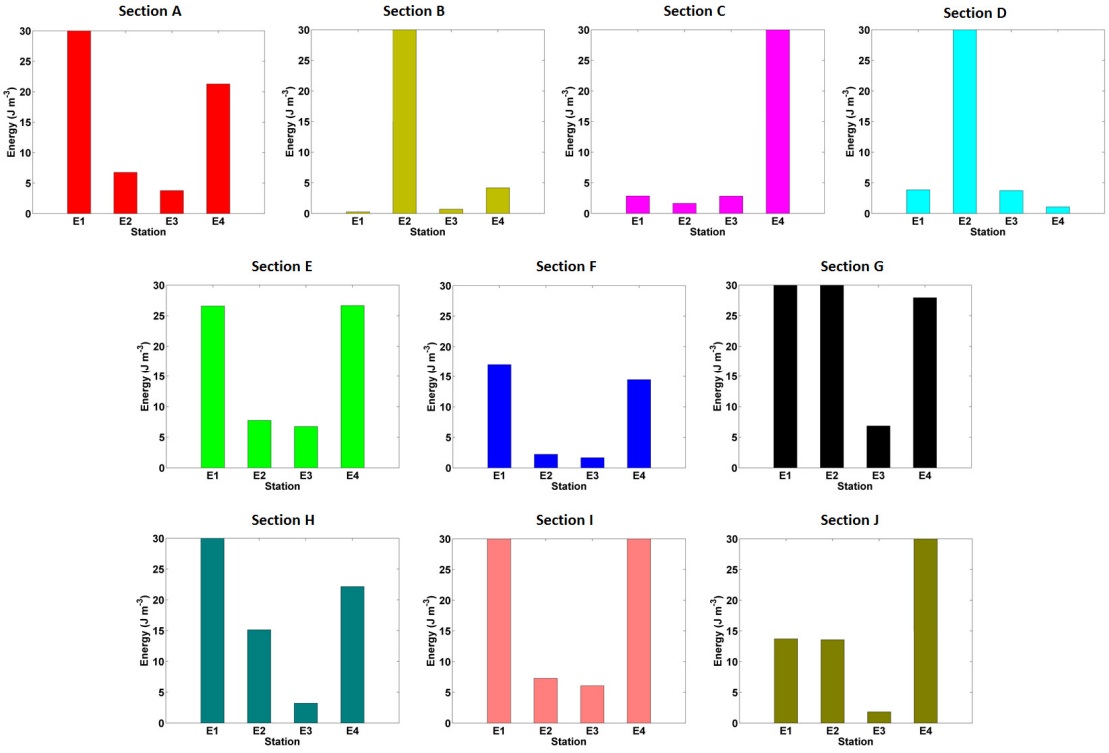

Figure 6.9: Variability of the anomaly of potential energy (ϕ) along Sofala Bank during August 2001. The positions of the sections along Sofala Bank are presented in Figure 6.1. For more details about data and procedures for the determination of ϕ in Sofala Bank, see Machaieie, (2012).

Maps of the distribution of the anomaly of potential energy (ϕ) along Sofala Bank and correlation coefficients between Sea Surface Temperature (SST) and chlorophyll concentrations in Sofala Bank are side by side in Figure 5.10 and relation between them are established. Region 1 corresponds to coastal regions of Soafal Bank under influence of river input presents mixture near the Zambezi delta mouths and stratification in north and south regions (Fig. 6.10a). The correlation between SST and chlorophyll concentrations is positive along region 1 (Fig. 6.10b). Region 2 corresponds to the middle shelf of Sofala Bank, and its water column present mixture (Fig 6.10a) and the correlation coefficients between SST and chlorophyll concentrations in this regions are weaker and statically insignificant (Fig. 6.10b). The region 3 corresponds to the outer shelf where the water columns present thermal stratification (Fig. 6.10a) and the correlation between SST and chlorophyll concentration is negative such that chlorophyll concentrations in this region increase with decreasing SST.

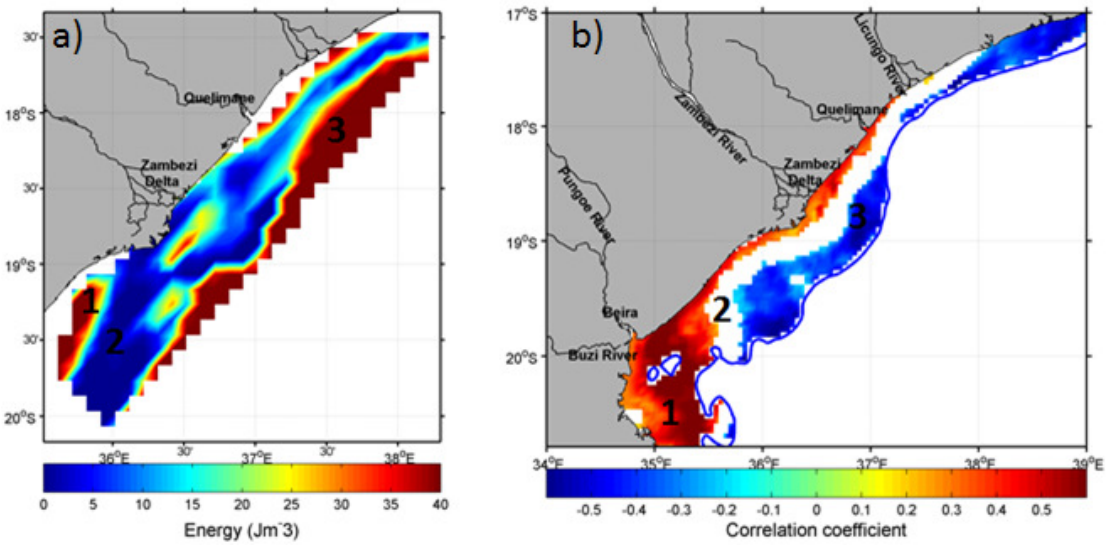

Figure 6.10: Distribution of anomaly of potential energy in Sofala Bank in August 2001 (a, adapted from Machaieie, (2012)). Spatial variability of correlation between Sea Surface Temperature and chlorophyll concentrations in Sofala Bank (b). Note that the maps have different spatial dimensions.

Correlations with ENSO

The spatial variability between 3.4 Niño index and chlorophyll concentrations are presented in Figure 6.11 for zero to three months time lag. The spatial variation of correlation coefficients is similar to that of river discharge against chlorophyll concentrations with two spots of strong correlations, one in the south region in front of the main mouth of Pungue and Buzi Rivers but a bit far from the coast and the other, more pronounced is located in central region close to main Zambezi Delta mouths. While the maximum values of positive correlation coefficients decrease from 0.27 in zero time lag to 0.24 in three months time lag, the module of negative correlation coefficients increasing from 0.48 in zero time lag to 0.58 in three months time lag. The similarity between the position of spots of positive correlations between Zambezi River discharge and spots of negative correlations between 3.4 Niño index and chlorophyll concentrations make it possible to state that ENSO influences the chlorophyll concentrations in Sofala Bank there influencing the Zambezi River discharge, which is the main forcing of chlorophyll variability along the inner Shelf. On the other hand, the increasing of correlation coefficients between 3.4 Niño index and chlorophyll concentrations with increasing lagging time suggest that the impact of ENSO affects Sofala Bank after a certain time after it is observed.

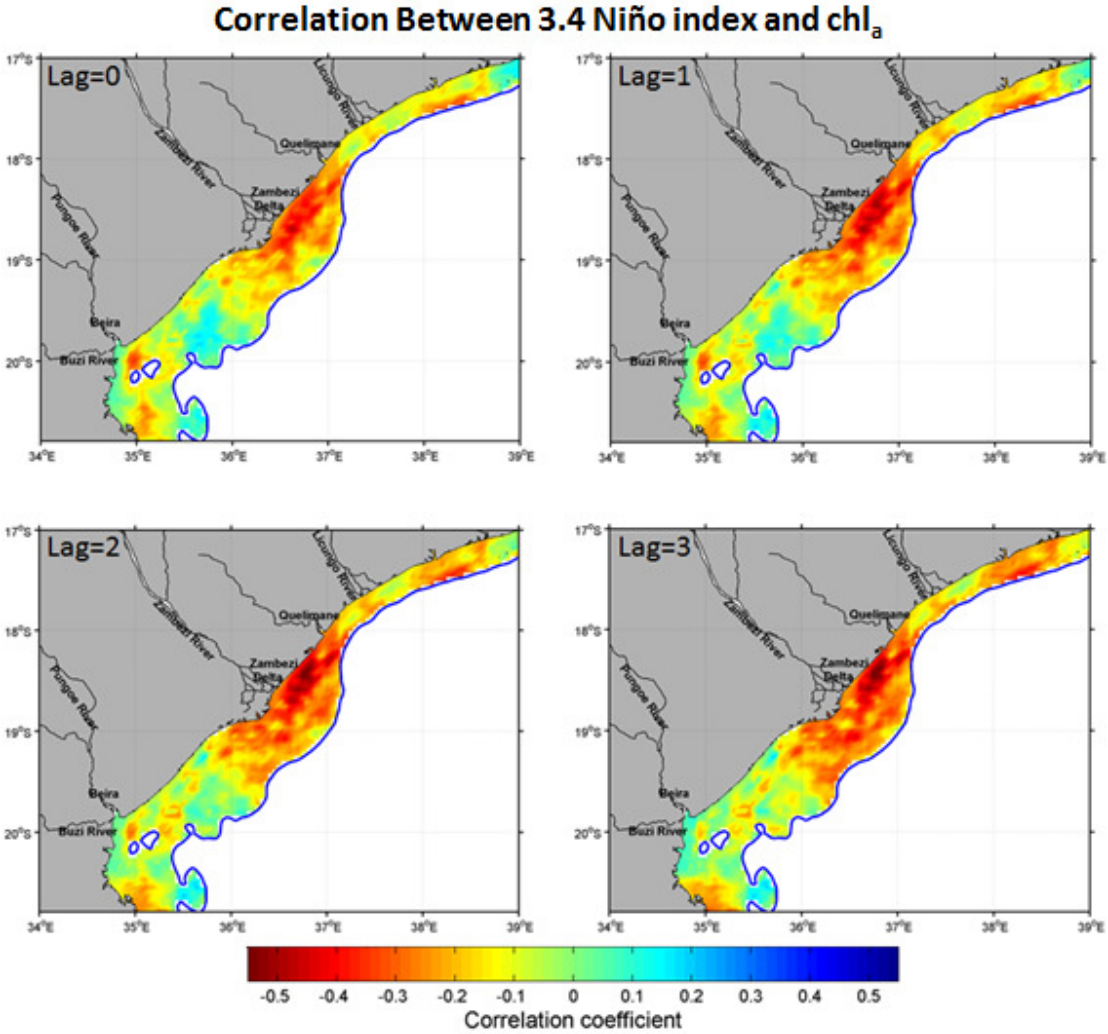

Figure 6.11.1: Spatial correlation between 3.4 Niño index and chlorophyll concentration in Sofala Bank for the 2003-2013 period. The maps of correlation coefficients are presented for zero, one, two and three months lagging time. Lag=3, for example, denotes that the value of the first element of 3.4 Niño index was correlated to the value of the third element of chlorophyll concentration.

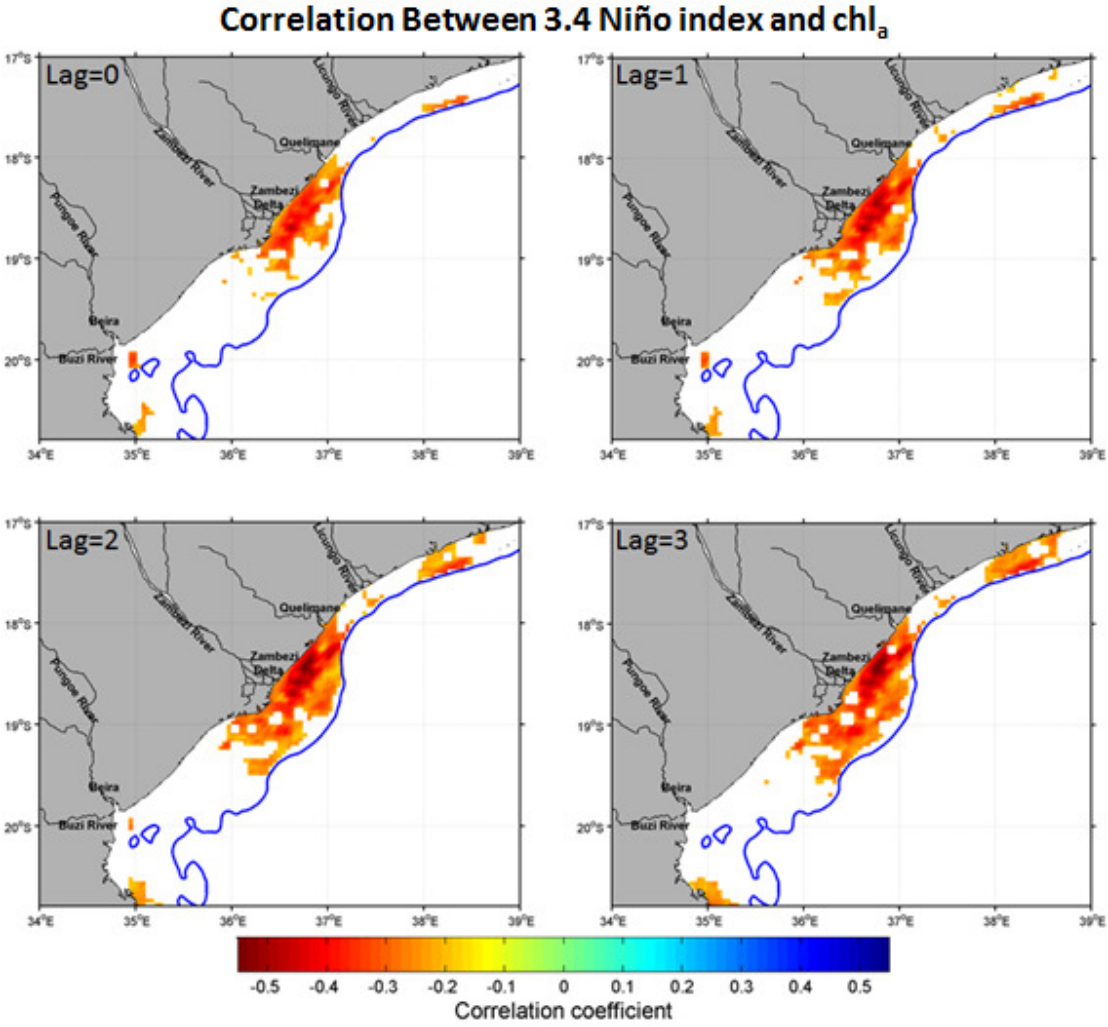

Figure 6.11.2: Same information presented in Figure 6.11.1 with the areas of statistical confidence less than 95% excluded.

Monthly scaled (maximum set to 1 and minimum set to 0) chlorophyll concentrations in the section near Zambezi Delta (see Fig. 6.1 for the location) and anomalies of Zambezi River discharge are plotted together with 3.4 Niño index in Figure 6.12. Pronounced peaks of chlorophyll concentrations are observed during the beginning of 2006, 2008, middle 2010 to the beginning of 2011, beginning of 2012, beginning and end of 2013, especially along the first Km of the section, near the Zambezi Delta mouths. Pronounced low concentrations are observed during the beginning and middle 2003 and 2005, middle 2009 to the begging of 2010. Most pronounced peaks and low chlorophyll concentration seem to be related to the Zambezi River discharge anomaly (middle panel) and in turn to 3.4 Niño index (right panel). Positive anomalies exceeding 500 m^3s^{-1} during the beginning of 2008, middle of 2010 and beginning of 2011, when there were registered peaks in chlorophyll concentrations, occurred during La Niña events of corresponding years. On the other hand, the more than 500 m^3s^{-1} negative anomalies of Zambezi

River discharge observed during 2003, 2004 and 2005, when the chlorophyll concentration where low, especially near the coast, occurred during El Niño events in corresponding years. During the middle 2009 and beginning of 2010, although the negative anomaly of Zambezi River discharge is relatively low, there is a pronounced low concentration chlorophyll, especially along the outer part of the section. These pronounced low chlorophyll concentrations coincided with moderate 2009-2010 El Niño event. These findings suggest again that the Zambezi River discharge, which is the main source of freshwater input and the primary driver of chlorophyll variability along the shelf of Sofala Bank, is affected by ENSO events, such that there is an increase of discharge during cold ENSO events and normal to low discharge during ENSO warmer events.

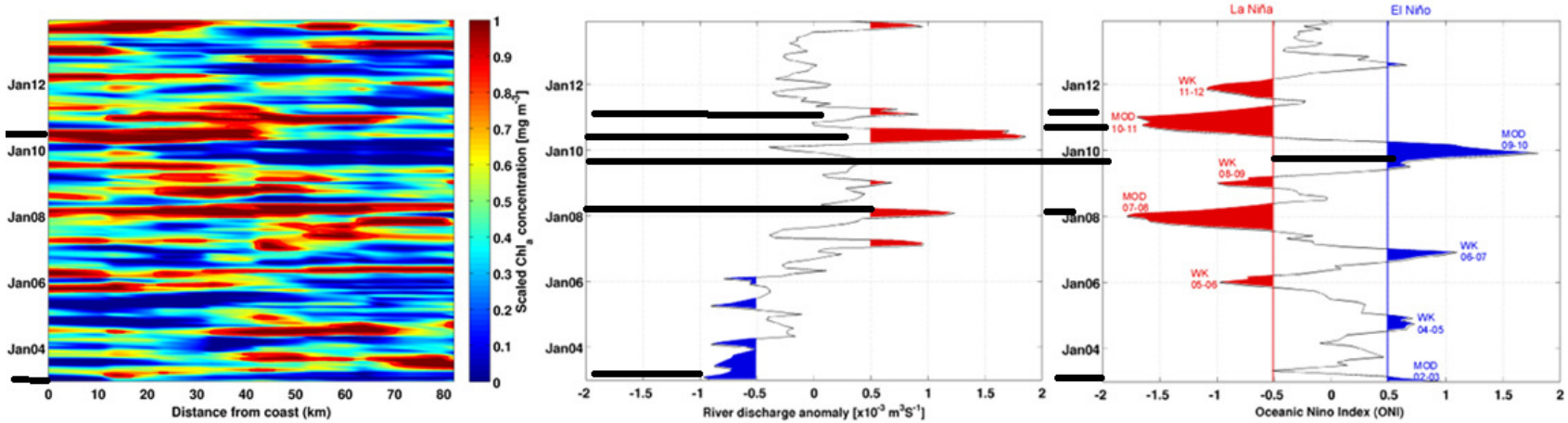

Figure 6.12: Space-time variability of chlorophyll along a section near Zambezi River Delta (left). Inter-annual anomaly of Zambezi River Discharge (center). Inter-annual variability of oceanic 3.4 Niño index (right). Weak (WK) and moderate (MOD) La Niña events (in red) are related to positive anomalies of river discharge and peaks in chlorophyll concentration. Weak (WK) and moderate (MOD) El Niño events (in blue) are related to the negative anomaly of river discharge and low chlorophyll concentrations. The best correspondences of high chlorophyll concentration-high river discharge-negative 3.4 Niño index (low chlorophyll concentration-low river discharge-positive 3.4 Niño index) are highlighted by the black lines.

.

Figure 6.13 shows the anomalies of the Zambezi River discharge during positive (above the threshold +0.5) and negative (below the threshold -0.5) 3.4 Niño index for the wet and dry seasons. The anomalies were calculated in relation to the climatological mean of the wet and dry seasons. For the wet season, the mean river discharge is about 100 m^3 s^{-1} below the climatological mean during positive 3.4 Niño index and about 300 m^3 s^{-1} above the climatological mean during negative 3.4 Niño index. For the dry season, the mean river discharge is about 50 m^3 s^{-1} above the climatological mean during positive 3.4 Niño index and about 150 m^3 s^{-1} above the climatological mean during the dry season. The anomalies of river discharge in both wet and dry seasons suggest that there is a decrease in river discharge during warm ENSO events and an increase during the cold events. The inverse relation between ENSO and river discharge revealed by the distribution of the anomalies of the Zambezi River discharge is in agreement with the findings of Ward, et al., (2010) who analyzed the sensitivity of river discharge to ENSO using Global Runoff database and observed that the runoff over Southern Africa is drier during El Niño and wetter during La Niña.

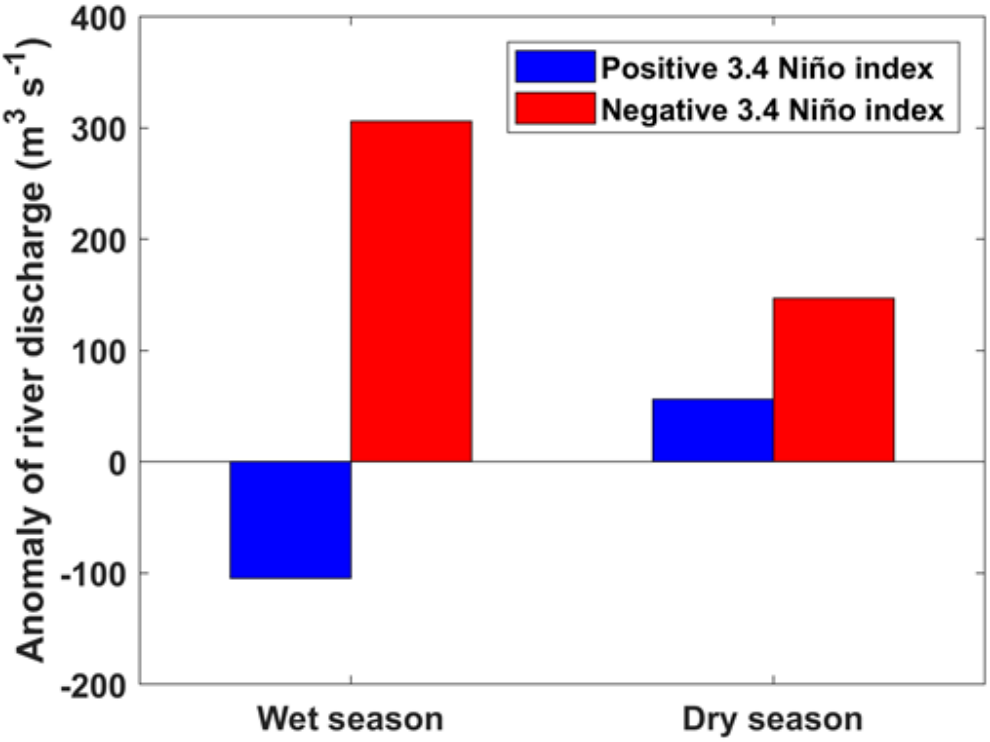

Figure 6.13: Anomaly of the Zambezi River discharge during positive and negative 3.4 Niño index of wet (October-March) and dry (May-September) seasons. The 3.4 index was taken as positive when it was above the threshold +0.5 and was taken as negative when it was below the threshold -0.5. For each of the seasons, the precipitation anomaly was determined by subtracting the climatological mean.

Spatial anomalies of chlorophyll concentrations over Sofala Bank during positive and negative 3.4 Niño index of wet and dry seasons are presented in Figures 6.14.1 and 6.14.2. The

distribution of the anomalies during positive 3.4 Niño index of the wet season corroborate with the corresponding river discharge anomalies, showing negative anomalies with values close to -0.2 mg m^{-3} along the coast of Sofala Bank, which denote a decrease in nutrient supply due to a decrease in river discharge. During negative 3.4 Niño index, there are positive anomalies of chlorophyll concentration over the central region of Sofala Bank with values close to 0.2 mg m^{-3}. The positive anomalies in the central Sofala Bank denote relatively higher nutrient supply in response to high discharge during the cold ENSO events. The negative anomalies observed in the south region of the Sofala Bank might be denoting the absence of influence of the Zambezi River discharge in the south and north regions and the possible absence of ENSO influence on the Pungue and Buzi discharges.

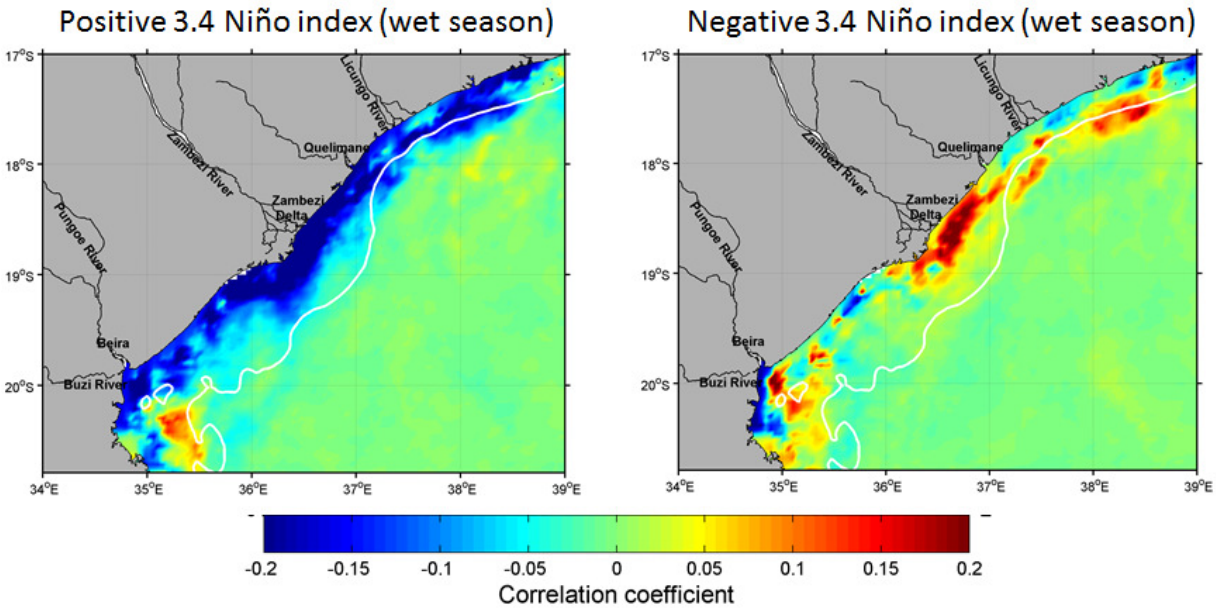

Figure 6.14.1: Anomaly of chlorophyll concentration over Sofala Bank during positive and negative 3.4 Niño index of the wet season (Oct.-Mar.). The 3.4 index was taken as positive when it was above the threshold +0.5 and was taken as negative when it was below the threshold -0.5. For each grid point, the chlorophyll anomaly was determined by subtracting the climatological mean.

In the dry season (Fig. 6.14.2), the distribution of the anomalies of chlorophyll concentration does not show a clear relation to the anomalies of the Zambezi River discharge as happens in the wet season. During positive 3.4 Niño index, there are negative anomalies of chlorophyll concentration near the coast of central Sofala Bank and a spot of positive located a little away from the coast. Similarly to the wet season, while the central region presents negative anomalies near the coast, the south region, in front of the mouths of Buzi and Pungue River and the north region near the Licungo River there present positive anomalies of chlorophyll concentration.

These findings suggest that while the Zambezi River, which crosses several countries before draining in Sofala
Bank has an inverse relation with ENSO, Buzi, Pungue, and Licungo Rivers whose discharge depend on local precipitation might have a different relationship with ENSO. During negative 3.4 Niño index of the wet season, the central region of Sofala Bank is characterized by positive anomalies of chlorophyll concentration with about 0.2 mg m^{-3}, in response to relatively high river discharge. Again, for the negative 3.4 index, the south and north regions present anomalies of opposite signal to those of the central region with values below -0.2 mg m^{-3}.

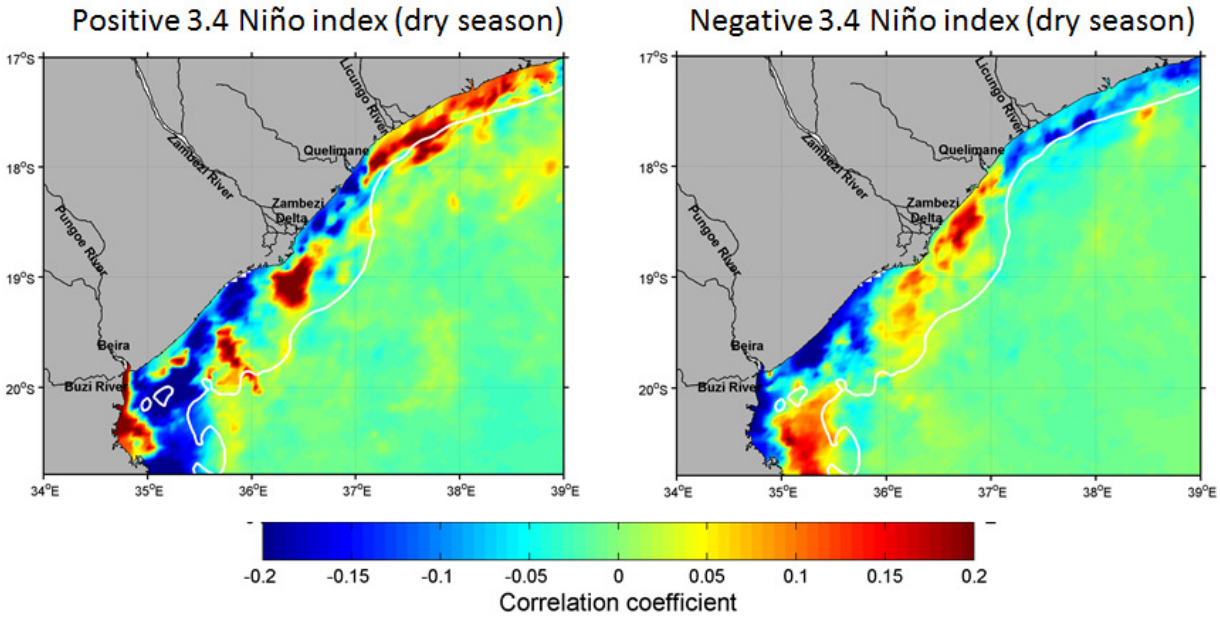

Figure 6.14.2: Anomaly of chlorophyll concentration over Sofala Bank during positive and negative 3.4 Niño index of the dry season (May-Sep.). The 3.4 index was taken as positive when it was above the threshold +0.5 and was taken as negative when it was below the threshold -0.5. For each grid point, the chlorophyll anomaly was determined by subtracting the climatological mean.

Figures 6.15a and 6.15b present the anomalies of Zambezi River discharge for wet (Oct.-March) and dry (May-Sep.) seasons during moderate El Niño/La Niña events of years 2002/03/ 2007/08, 2009/10 and 2010/11. For each season, the anomalies of river discharge correspond to the difference between annual mean and the mean of all four years together. During the wet season (Fig.6.15a), the values anomalies of river discharge are about -1000 $m^3 s^{-1}$ and less than 50 $m^3 s^{-1}$ during moderate El Niño events observed in 2002/03 and 2009/10, respectively. In years of moderate La Niña events, the anomalies of river discharge during the wet season are about 600 and 300 $m^3 s^{-1}$ in 2007/08 and 2010/11, respectively, and suggest that during this season there is a tendency of increasing river discharge in La Niña events and decreasing discharge in El Niño events. In contrast, during the dry season (Fig. 6.15b) there is no clear tendency of Zambezi river

discharge during El Niño/La Niña events. While a negative anomaly of about -1000 $m^3 s^{-1}$ is observed in 2002/03 El Niño event, about 1000 $m^3 s^{-1}$ positive anomaly is observed in 2009/10 El Niño event

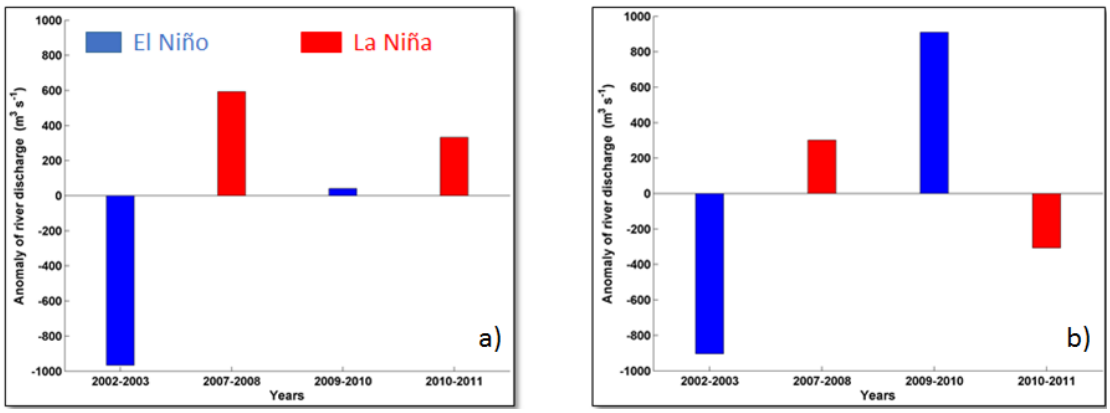

Figure 6.15: Anomaly of Zambezi River discharge during wet (a) and dry (b) seasons of moderate El Niño/ La Niña years.

Spatial anomalies of chlorophyll concentration during moderate El Niño/La Niña events of years 2002/03, 2007/08, 2009/10 and 2010/11 for wet (Oct.-Mar.) and dry (May-Sep.) seasons, determined through same procedure used for anomalies of river discharge presented in Figure 6.15, are presented in Figure 6.16.1 and 6.16.2. During the wet season, there is a clear relation between the anomalies of chlorophyll concentrations and anomalies of the Zambezi River discharge. The relation suggests that during El Niño events the river discharge is relatively lower and chlorophyll concentrations are relatively lower and during the La Niña events the river discharge is relatively higher and the chlorophyll concentrations are enhanced. Negative anomalies of chlorophyll concentrations exceed 0.4 mg m^{-3} along the central Sofala Bank in 2002/03 and along the central and north regions of Sofala Bank during 2009/10 El Niño events. During La Niña years, positive anomalies exceeding 0.4 mg m^{-3} were observed along the central and south region of Sofala Bank except near the Pungue and Buzi rivers in 2007/8 and along the central and north regions in 2010/11. Similarly to the positive and negative 3.4 Niño index presented in Figures 6.14a, it seems that the chlorophyll concentrations near the mouths of Pungue and Buzi Rivers, and Licungo Rivers do not show any relation to ENSO events.

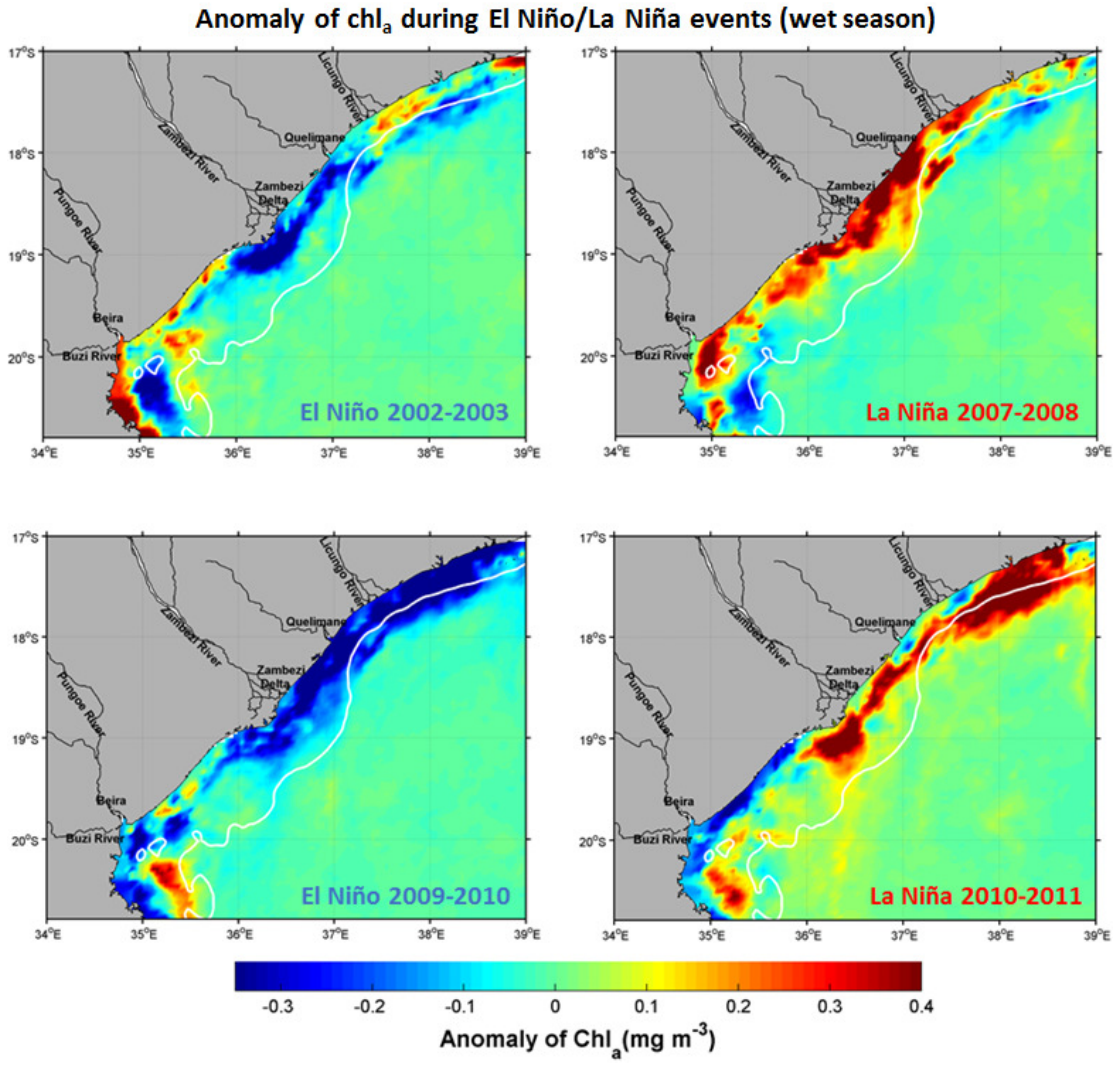

Figure 6.16.1: Anomaly of chlorophyll concentrations in Sofala Bank during the wet season (Oct-Mar.) of moderate El Niño/La Niña years.

During the dry season (Fig. 6.16.2), similarly to river discharge, there is no clear pattern of chlorophyll concentrations anomaly. In the central region of Sofala Bank, for example, the anomalies are negative during 2002/03 El Niño event and positive during 2009/10. In the north region near Licungo River mouth, the anomalies are negative during 2007/08 La Niña event and positive during 2010/11. The no relation between the variability of chlorophyll concentrations and ENSO events during the dry season suggest that the effect of ENSO in Sofala Bank during the dry season is small or inexistent.

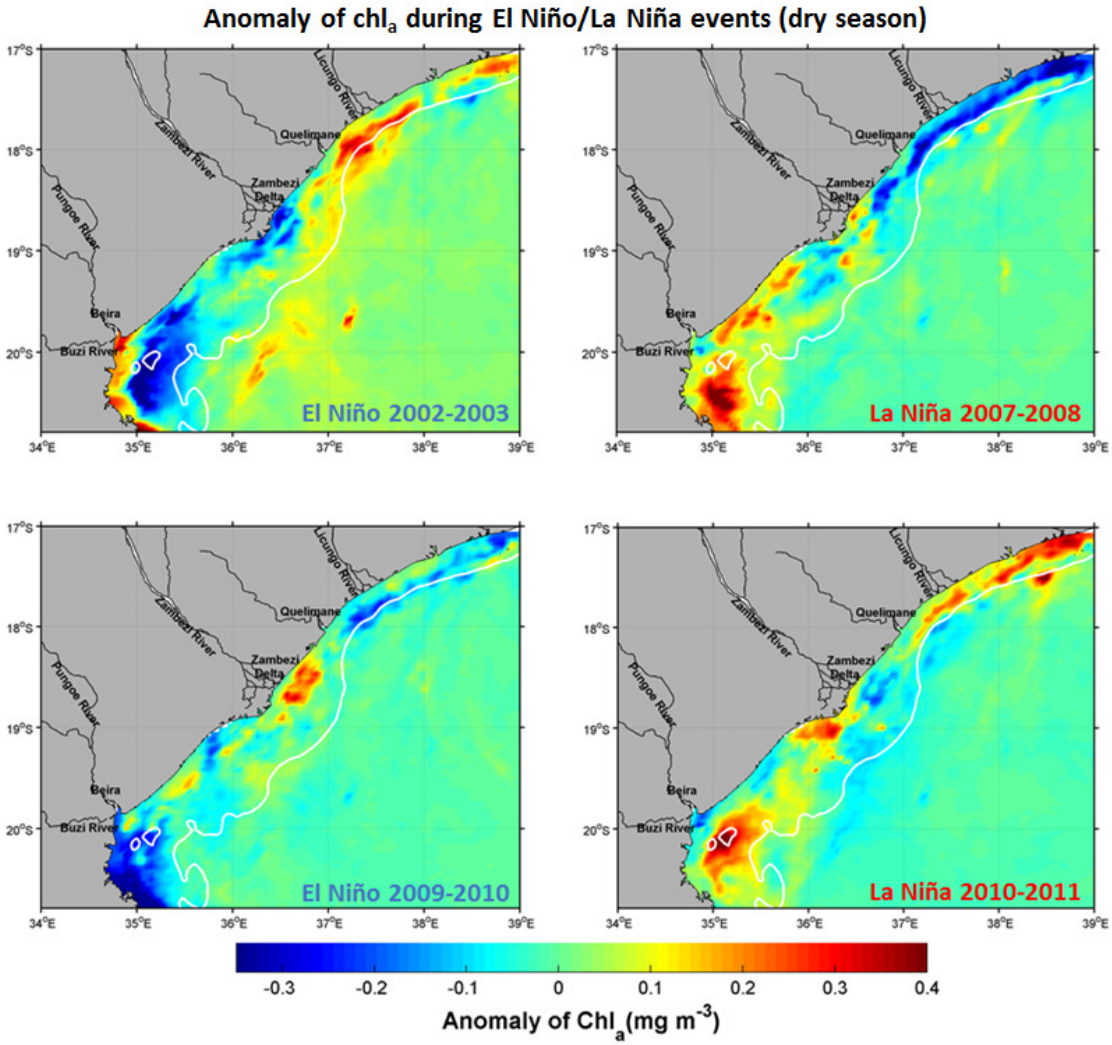

Figure 6.16.2: Anomaly of chlorophyll concentrations in Sofala Bank during dry season (May-Sep.) of moderate El Niño/La Niña years.

6.6 Conclusions

The satellite measured chlorophyll concentrations in the shelf of Sofala Bank present two main regimes: a high regime, with concentration varying between 3.5 and 4 mg m^{-3} in the plume cores, extending from January to April, and a low regime, with concentrations less than 3 mg m^{-3} in the plume cores, extending between May and December.

The Zambezi river discharge is the main controller of annual chlorophyll variability in Sofala Bank, especially in the central region near the main Zambezi delta mouths but the southerly and southeasterly winds, which dominate the wind field in Sofala Bank also play a role in pushing

low chlorophyll offshore waters to the coast decreasing chlorophyll concentrations in coastal waters.

Along the inner shelf, in regions under influence of freshwater input there is a positive correlation between Sea Surface Temperature and chlorophyll concentrations, which implies that high flow regime of river discharge coincides with warmer season in the continent, and thus, chlorophyll concentrations along the regions of river influence increase with increasing of river discharge and SST. In the outer shelf and slope, there is a negative correlation between Sea Surface Temperature and chlorophyll concentrations, indicating that increasing of chlorophyll concentrations is promoted by upwelling of subsurface waters.

There are two main pathways of intrusion of coastal chlorophyll-rich waters offshore, one in the north region, between 17.5 and 18°S, and other located in the south region of Sofala Bank, near 20°S. The disparity between the period of high regime chlorophyll concentrations within the shelf waters and period at which the pathways are more pronounced suggest that the interaction between mesoscale features with the shelf, previously pointed out in other studies, might be the main driver of the intrusion of coastal chlorophyll-rich waters offshore.

ENSO influences the Zambezi River discharge increasing the discharges during ENSO cold events and decreasing them during ENSO warm events. As consequence of ENSO effects on Zambezi River discharge, the regions of Sofala Bank where the Zambezi River presents more influence tend to present positive anomalies of chlorophyll concentrations during ENSO cold events and negative anomalies ENSO warm events, especially in wet season.

Chapter 7

Synthesis of the main conclusions

The main aim of this research was to evaluate the spatial and temporal variability of satellite estimated suspended sediment and chlorophyll and their relation to environmental variables. The main hypothesis of the thesis was that with the decrease in the Zambezi River discharge observed after the construction of the Cahora Bassa dam, the Zambezi River discharge might not be the actual main driver of the seasonal variation of suspended sediments in Sofala Bank.

The variability of suspended sediments was analyzed using three different approaches. The climatology of monthly-composites of nLw555 used as a proxy for the suspended sediments and the monthly climatology of the total suspended material, estimated from remote sensing reflectance, showed that the sediment plume is relatively narrow, with lower sediment concentrations from January to June and becomes wider, with higher sediment concentrations from July to December. From June to December, the south plume's core located near Pungue

and Buzi Rivers and the center plume's core in front of the Zambezi Delta merge and drift northwards. Both the plume dispersion and concentrations of suspended sediments co-vary with wind speed. The spatial correlations showed that the wind speed and waves correlate strong and positively with suspended sediments in most the part of Sofala Bank suggesting that the erosion and re-suspension by wind and waves are more important in controlling the seasonal variability of suspended sediment than the Zambezi River, except in the central region slightly away from the coast, where the Zambezi River discharge shows to be the main controller.

The satellite measured chlorophyll concentrations in the Sofala Bank present two main regimes: a high regime, with concentrations varying between 3.5 and 4 mg m^{-3} in the plume cores, extending from January to April, and a low regime, with concentrations less than 3 mg m^{-3} in the plume cores, extending from May to December.

The co-variation of Zambezi River discharge and chlorophyll concentrations and the strong positive correlation between them suggest that the Zambezi river discharge is the main controller of annual chlorophyll variability in Sofala Bank, especially in the central region near the main Zambezi delta mouth. However, the south and southerly and southeasterly winds, which dominate the wind field in Sofala Bank, seem to play a role in pushing low chlorophyll offshore waters to the coast, decreasing chlorophyll concentrations in coastal waters.

The river discharge increases during ENSO cold events and decreases during ENSO warm events. Therefore, in the Sofala Bank area under the influence of the river discharge, positive chlorophyll concentration anomalies occur during cold ENSO events and negative chlorophyll concentration anomalies are common during warm ENSO events, especially in the wet season.

The TRMM 3B43-v7 multi-satellite derived precipitation over the lower Zambezi basin showed relatively strong negative correlations to 3.4 Niño index and precipitation south of 15°S, where the main river channels drain to the Sofala Bank. The distribution of correlation coefficients between 3.4 index and precipitation, and the anomalies of precipitation during positive and negative 3.4 index over the south of 15°S reinforce the statement that the ENSO signal in the coastal waters over Sofala Bank is introduced by the Zambezi flow.

The present Zambezi River discharge does not have a significant seasonal variation, the supply of sediments through the erosion and re-suspension by the wind and waves along the coast becomes more important. However, the variation in chlorophyll concentrations along the coastal waters shows that the Zambezi River still controls the seasonal variation of water quality in Sofala Bank.

References

Altabet, Mark A., Mathew J. Higginson, and David W. Murray. "The effect of millennial-scale changes in Arabian Sea denitrification on atmospheric Co2." *Nature 415*, 2002: 159-162.

Alves, José M. B., et al. "Evaluation of the AR4CMIP3 and the AR5 CMIP5 Model and Projections for Precipitation in Northeast Brazil." *Frontiers in Earth Sciences*, 2016: doi: 10.3389/feart.2016.00044.

Anderson, David M., Jonathan T. Overpeck, and Anil K. Gupta. "Increase in the Asian Souwest Monsoon During the Past Four Centuries." *Science 297*, 2002: 596-599.

Baatz, Martin, and Arno Schape. "Mutiresolution Segmentation: an optimization approach for high quality mult-scale image segmentation." In *Angewandte Geographische Informationsverarbeitung*, by J. Strobl, T. Blaschke and G. Griesebner, 12-23. Heidelberg, Germany: Wichmann-Verlag, 2000.

Barnston, Anthony G., Muthuvel Chelliah, and Stanley B. Goldenberg. "Documentation of a Highly ENSO-Related SST Region in the Equatorial Pacific." *Atmosphere-Ocean; Vol. 35; No.3*, 1997: 367-383.

Binding, C. E. *The derivation of suspended sediment concentrations in the Irish Sea from in situ and remotely sensed ocean colour.* PhD Thesis, Wales: University of Wales Bangor, 2003.

Binding, C. E., D. G. Bowers, and E. G. Mitchelson-Jacob. "Estimating suspended sediment concentrations from ocean colour measurements in moderately turbid waters; the impact of variable particle scattering properties." *Remote Sensing of Environment; Vol. 94*, 2005: 373-383.

Bowers, D. G., and C. E. Binding. "The optical properties of mineral suspended particles: A review and synthesis." *Estuarine, Coastal and Shelf Science; Vol. 67*, 2006: 219-230.

Bowers, D. G., C. E. Binding, and K. M. Ellis. "Satellite remote sensing of the geographical distribution of suspended particle size in an energetic shelf sea." *Estuarine, Coastal and Shelf Science; Vol. 73* , 2007: 457-466.

Bowers, D. G., S. Gaffney, M. White, and P. Bowyer. "Turbidity in the southern Irish Sea." *Continental Shelf Research; Vol. 22*, 2002: 2115–2126.

Boyer, Joseph N., Christopher R. Kelble, Peter B. Ortner, and David T. Rudnick. "Phytoplankton bloom status: Chlorophyll a biomass as an indicator of water quality condition in the southern estuaries." *Ecological Indicators; Vol. 9* , 2009: 56-67.

Brinca, L., A. J. da Silva, L. Sousa, I. M. Sousa, and R. Saetre. *A survey of the fish resources at Sofala Bank-Mozambique, September 1982.* Unpublished , Maputo, Mozambique: Instituto de Investigação Pesqueira, 1983.

Brinca, L., et al. *A survey on the fish resources at Sofala bank, Mozambique, May-June 1983.* Repots on surveys with R/V "Dr. Fridtjof Nansen, Maputo and Bergen: Instituto de Investigação Pesqueira de Moçambique and Institute of Marine Research, 1984.

Chelton, Dudley B., Peter Gaube, Michael G. Schlax, Jeffrey J. Early, and Roger M. Samelson. "The Influence of Nonlinear Mesoscale Eddies on Near-Surface Oceanic Chlorophyll." *Science*, 2011: DOI: 10.1126/science.1208897.

Chenje, M. *State of the Environment Zambezi Basin 2000.* Communicating the Environment Programme (CEP), Maseru/Lusaka/Harare: SADC/IUCN/ZRA/SARDC, 2000.

Chevane, C. M., P. Penven, Nehama F. P. J, and C. J. C. Reason. "Modelling the tides and their impact on the vertical stratification over the Sofala Bank, Mozambique." *African Journal of marine Science*, 2016: 1-15.

Csillik, Ovidin. "Fast Segmentation and Classification of Very High Resolution Remote Sensing Data Using SIC Superpixel." *Remote Sensing*, 2017: 1-19.

Curran, P. J., and E. M. M. Novo. "The Relationship Between Suspended Sediment Concentration and Remotely Sensed Spectral Radiance: A Review." *Journal of Coastal Research; Vol. 4; No. 3*, 1988: 351-368.

Dagga, M., R. Bennerb, S. Lohrenzc, and D. Lawrence. "Transformation of dissolved and particulate materials on continental shelves influenced by large rivers: plume processes." *Continental Shelf Research; Vol. 24*, 2004: 833-858.

Davies, Bryan R., Richard D. Beilfuss, and Martin C. Thoms. "Cahora Bassa retrospective, 1974–1997: effects of flow regulation on the Lower Zambezi River." *Limnology in the developing world; Vol. 27*, 2000: 1-9.

Dettinger, Michael D., Daniel R. cayan, Gregory J. Mccabe, and José A. marengo. "Multiscale streamflow variability associated with El Niño/ Southern Oscillation." In *El Niño and the southern oscillation: multiscale variability and global and regional impacts*, by Henry F. Diaz and Vera Markgraf, 113-146. Cambridge, UK: Cambridge University Press, 2000.

Dogliotti, A. I., K. Ruddick, and R. Guerrero. "Seasonal and inter-annual turbidity variability in the Río de la Plata from 15 years of MODIS: El Niño dilution effect." *Estuarine, Coastal and Shelf Science; Vol. 182*, 2016: 27-39.

Dorji, Passang, and Peter Fearns. "A Quantitative Comparison of Total Suspended Sediment Algorithms: A Case Study of the Last Decade for MODIS and Landsat-Based Sensors." *Remote Sensing; Vol. 8; No. 810; doi:10.3390/rs8100810*, 2016: 1-32.

Doxaran, D., J. -M. Froidefond, and P. Castaing. "A refectance band ratio used to estimate suspended matter concentrations in sediment-dominated coastal waters." *International Journal of Remote Sensing; Vol. 23; No: 23*, 2002: 5079-5085.

Doxaran, David, Jean_Marie Froidefond, Samantha Lavender, and Patrice Casting. "Spectral signature of highly turbidd waters: Application with SPOT data to quantify suspended particulate matter concentrations." *Remote Sensing of Environment 81*, 2002: 149-161.

Doxaran, David, Jean-Marie Froidefond, and Patrice Castaing. "Remote-sensing refletance of turbid sediment-dominated waters. Reduction of sediment type variations and changing illumination conditions effects by use of refletance rations." *Applied Optics*, 2003: 2623-2634.

D'sa, E. J., and R. L. Miller. "Bio-optical Properties of Coastal waters." In *Remote Sensing and Digital Image Processing, Series: Remote Sensing of Coastal Aquatic Environments; Vol 7*, by R. L. Miller, C. E. Del Castillo and B. A. McKee, 129-155. Enschede: Springer, 2005.

Duarte, Carlos A., and Just Cebrih. "The fate of marine autotrophic production." *Limnology and Oceanography; Vol. 41. No. 8*, 1996 : 1758-1766.

Emery, William J., and Richard E. Thomson. *Data Analysis Methods in Physical Oceanography.* Amsterdam, Netherlands: Elsevier Science, 2001.

Fan, Fangxing, Xiao Dong, Xianghui Fang, Feng Xue, Fei Zheng, and Jiang Zhu. "Revisiting the relationship between the South Asian summer monsoon drought and ElNiño warming pattern." *Atmospheric Science Letters; Vol. 18*, 2017: 175-182.

Fernandez-Nóvoa, D., M. Gomez-Gesteira, R. Mendes, M. deCastro, N. Vaz, and J. M. Dias. "Influence of main forcing affecting the Tagus turbid plume under high river discharges using MODIS imagery." *PLoS ONE; Vol. 12; No. 10*, 2017: 1-27.

Gammelsrod, T. "Improving shrimp production by Zambezi River regulation." *Ambio; Vol 21; No 2*, 1992: 145-147.

Gammelsrod, Tor. "Effect of Zambezi River management on the prawn fishery of the Sofala." In *Water Management and*, by Michael C. Acreaman and G. E. Hollis, 119-124. Gland, Switzerland: IUCN, 1996.

Gaughan, Andrea E., Caroline G. Staub, Andrew Hoell, Ariel Weavera, and Peter R. Waylenb. "Inter-and Intra-annual precipitation variability and associated relationships to ENSO and

the IOD in southern Africa." *International Journal of Climatology; Vol. 36*, 2016: 1643–1656.

Giannini, Alessandra, Michela Biasutti, Isaac M. Held, and Adam H. Sobel. "A Global Perspective of on African Climate." *Climatic Change vol. 90*, 2008: 359-383.

Graham, N. E. "Decadal-Scale Climate Variability in the Tropical and North Pacific during the 1970s and 1980s - Observations and Model Results." *Climate Dynamics; Vol. 10*, 1994:

Halo, I., B. Backeberg, P. Penven, I. Ansorge, C. Reason, and J. E. Ullgren. "Eddy properties in theMozambique Channel: Acomparison betweenobservation and two numerical ocean circulation models." *Deep-Sea Research II; Vol.100*, 2014: 38-53.

Heinrich, Hartmuz. "Origin and Consequance of Cycle Ice Rifting in the Northesat Atlantic Ocean during past 130,000 Years." *Quarternary Research 29*, 1988: 142-152.

Heinz, P., and C. Hemleben. "Foraminifera response ti the Northeast Monsoon in the wester and southern Arabian Sea." *Marine Micro-paleoontology 58*, 2006: 103-113.

Hoguane, Antonio Mubango. "Perfil Diagnósticoda Zona Costeira de Moçambique." *Journal of Integrated Coastal Management;7*, 2007: 69-89.

Holben, B. N., and Y. E. Shimabukuro. "Linear mixing model applied to coarse spatial resolution data from multispectral satellite sensors." *Internation Journal of Remote Sensing; Vol 14*, 1993: 2231-2240.

Huffman, George j., et al. "The TRMM Multisatellite Precipitation Analysis (TMPA): Quasi-Global, Multiyear, Combined-Sensor Precipitation Estimates at Fine Scales." *Journal of Hydrometeorology; Vol. 8*, 2007: 38-55.

Hughes, D. A. "Comparison of satellite rainfall data with observations from gauging station networks ." *Journal of Hydrology; Vol. 327*, 2006: 399–410.

Hulme, Mike, Ruth Doherty, Todd Ngara, Mark New, and David Lister. "African Climate Change: 1900-2100." *Climate Research; Vol.17;*, 2001: 145-168.

IPCC. *Climate Change 2007: The Physical Science Basis. Contribution of Working Group I to the Fourth Assessment Report of the Intergovernmental Panel on Climate Change.* Cambridge, UK: Cambridge University Press, 2013.

Ittekkot, Venugopalan, Christoph Humborg, and Petra Schafer. "Hydrology Alterations and marine Biochemistry: A silicate issue?" *BioScience; Vol.5 0; No. 9*, 2000: 776-782.

Jansen, John R. *Sensoriamento Remoto do Ambiente: Uma prespectiva em Recursos Terrestres.* São José dos Campos: Parêntese, 2011.

José, Y. S., O. Aumont, E. Machu, P. Penven, C. L. Moloney, and O. Maury. "Influence of mesoscale eddies on biological production in the Mozambique Channel: Several contrasted examples from a coupled ocean-biogeochemistry model." *Deep-Sea Research II; Vol. 100*, 2014: 79–93.

Jury, Mark. "Statistical models for seasonal forecasts of southern Africa summer rainfall." *CPC Experimental Long-lead Forecast Bulletin; Vol. 6; no. 4*, December 1997: Online at: www.cpc.noaa.gov/products/predictions/experimental/.

Kalnay, E., et al. "The NCEP/NCAR 40-year Reanalysis Project." *Bolletin of American Meteorological Society; Vol. 77; No. 3*, 1996: 437-471.

Kampel, Milton, and Evlyn M. L. M. Novo. "O Sensorimaento Remoto da Cor da Água." In *Oceanografia por satélites*, by Ronald Buss de Souza, 179-196. São paulo: Oficina de Textos, 2005.

Kane, R. "Some characteristics and precipitation effects of the El Niño of 1997-1998." *Journal of Atmospheric and Solar-Terrestrial Physics; Vol. 61*, 1999: 1325-1346.

Kirk, John T. O. *Light and Photosynthesis in Aquatic Ecosystems. Third Ediation.* Cambridge: Cambridge University Press, 2011.

Krishnamurthy, V., and James L. Kinter. "The Indian Monsoon and its relation to Global Climate Variability." In *Global Climate*, by Xavier Rodo, 1-84. Spring-Verlag, 2002.

Kumar, K. Krisha, Balaji Rajagopalan, and Mark A. cane. "On the Weakening Relationship Between the Indian Monsoon end ENSO." *Science*, 1999: 2156-2159.

Lahet, Florence, and Dariusz Stramski. "MODIS imagery of turbid plumes in San Diego coastal waters during rainstorm events." *Remote Sensing of Environment; Vol. 114*, 2010: 332–344.

Legendre, Luis, and Jacques Le Fèvre. "Microbial food webs and the export of biogenic carbon in oceans." *Aquatic Microbial Ecology; Vol. 9* , 1995: 69-77.

Liechti, T. Cohen, J. P. Matos, J. L. Boillat, and A. J. Schleiss. "Comparison and evaluation of satellite derived precipitation products for hydrological modeling of the Zambezi River Basin." *Hydrology and Earth System Sciences; Vol. 16*, 2012: 489–500.

Lihan, T., M. A. Mustapha, S. A. Rahim, S. Saitoh, and K. Lida. "Influence of River Plume on Variability of Chlorophyll a Concentration using Satellite Images." *Journal of Applied Sciences; Vol. 11; No. 3*, 2011: 484-493.

Lihan, Tukimat, Sei_Ichi Saitoh, Takahiro Lida, Toro Hirawake, and Kohji Iida. "Satellite-measured temoporal and spatial variability of the Tokachi River plume." *Estuarine, Coastal and Shelf Science 78*, 2008: 237-249.

Lutjeharms, Johann R. E. "The Coastal Ocean of The South-Eastern Africa." In *The Sea; Vol. 14B*, by A. R. Robinson and K. H. Brink, 783-834. Harvard University Press: Cambridge, 2006.

Machaieie, Hélder A. *Water masses, circulation and fronts in Sofala Bank.* Dissertação de mestrado, Quelimane: Escola Superior de Ciências marinhas e Costeiras, 2012.

Malauene, B. S., F. A. Shillington, M. J. Roberts, and C. L. Moloney. "Cool, elevated chlorophyll-a waters off northern Mozambique." *Deep-Sea Research II; Vol. 100*, 2014: 68–78.

Mantua, Nathan J., and Steven R. Hare. "The Pacific Decadal Oscillation." *Journal of Oceanography*, 2002: 35-44.

Mason, S. J. "El nino, climate change, and Southern Africa Climate." *Invironmetrics; Vol. 12; No. 4;*, 2001: 327-345.

Maueua, Clousa, Obadias Cossa, Gildo Mulhovo, and Magno Pereira. *Vulnerabilidade Climática nas Zonas Costeiras. Caso de estudo: Delta do Zambezi.* Relatório de Trabalho, Maputo, Mozambique: Istituto Nacional de Hidrografia e Navegação-INAHINA, 2007.

Meneses, Paulo Roberto. "Princípios de Sensoriamento Remoto." In *Introdução ao Processamento de Imagens de Sensoriamento Remoto*, by Paulo Roberto Meneses and Tati de Almeida, 1-33. Brasilia: Unb, 2012.

Meters, Leal A. K., and Jonathan Warrick. "Measuring flood outpts from 110 coastal watersheds in California with field measurements and SeaWifs." *Geology; vol: 29: No: 7*, 2001: 659-662.

Miller, Richard L., and Brent A. Mckee. "Using MODIS Terra 250 m imagery to map concentratios of total suspended matter in coastal water." *Remote sensing of Environment 93*, 2004: 259-266.

Mobley, C. D. "Radiative Transfer in the Ocean." *Sequoia Scientific*, 2001: 2321-2330.

Mooley, D. A., and B. Parthasarathy. "Indian Summer Monsoon and the East Equatoria Pacific Sea Surface Temperature." *Atmosthere-Ocean 22*, 1984: 23-35.

Moore, Andy E., Fenton P. D. Cotterill, Mike P. L. Main, and Hugh B. Williams. "The Zambezi River." In *Large Rivers: Geomorphology and Management*, by Avijit Gupta, 311-332. West Sussex, England: John Wiley & Sons, Ltd, 2007.

Moreira, Maurício Alves. *Fundamentos de Sensoriamento Remoto e Metodologias de Aplicação; Terceira Edição.* Viçosa: UFV, 2007.

Morel, A., and B. Gentil. "Diffuse reflatance of oceanic waters. III Implications of bidirectionality for remote -sensing problem." *Applied Optcs 35:4*, 1996: 850-862.

Morel, A., and L. Prieur. "Analysis of variations in ocean color." *limnology and oceanography 22*, 1977: 709-722.

Nehama, Fialho P. J. *Modelling the Zambezi River Plume using the Regional Oceanic* . PhD Thesis, Cape Town: University of Cape Town, 2012.

Nehama, Fialho P. J., Muhamade Ali Lemos, and Helder Arlindo Machaieie. "Water masses characteristics in a shallow bank highly influenced by river discharges: the Sofala Bank in Mozambique." *Journal of Integrated Coastal Zone Management ; Vol.15; No. 4*, 2015: 523-532.

Nehring, D. Ne, et al. "Results of oceanological studies in the Mozambique Channel in February – March 1980." *Beitr. Meereskd; Vol. 56*, 1987: 51-63.

Neto, José L. Rosa, Carlos Ruberto Fragoso Jr, Ana C. M. Malhado, and Richard J. Ladle. "Spatio-temporal Variability of Chlorophyll-A in the Coastal Zone of Northeastern Brazil." *Estuaries and Coasts*, 2014: DOI 10.1007/s12237-014-9809-2.

Nezlin, Nikolay P., and Paul DiGiacomo. "Satellite ocean color observation of storm runoff plumes along the San Pedro Shelf (Southern California) during 1997-2003." *Continental Shelf Research; 25*, 2005: 1692-1711.

Nezlin, P. Nicolay, and Paul M. DiGiacomo. "Stormwater runoff plums observed by SeaWifs radiometer in Southern California Bight." *Remote Sensing of Environment 98*, 2005: 494-510.

Nicholson, Sharon E. "The nature of rainfall variability over Africa on time scales of decades to millenia." *Global and Planetary Change; Vol.*, 2000: 137–158.

Novo, E. M., and Y. E. Shimabukuro. "Spectral mixing analysis of inland tropical waters." *International Journal of Remote Sensing; Vol 15 (6)*, 1994: 1351-1356.

Novo, Evlyn M. L. de Moraes. *Sensoriamento Remoto - Princípios e Aplicações. Quarta Ediação.* São Paulo: Edgard Blucher Ltda, 2010.

O'Donnell, James. "The formation and fate of a River plume: A Numerical model." *Jounal of Physical Oceanography; Vol. 20*, 1990: 551-569.

Overpeck, Jonathan, David Anderson, Susan Trumbore, and Warren Prell. "The South Indian Monsoon over the last 18000 years." *Climate Dynamics 12*, 1996: 213-225.

Padman, Laurie. *Tidal Model Driver (TMD) manual.* Washington, USA: Earth & Space Research, 2005.

Piola, Alberto, Silvia I. Romero, and Uriel Zajaczkovski. "Space-time variability of the Planta plume inferred from ocean color." *Continental shelf Research v. 28*, 2008: 1556-1567.

Platt, Trevor, Nicolas Hoepffner, Venetia Stuart, and Christopher Brown. *Why Ocean Colour? The Societal Benefits of Ocean Colour Technology.* Reports and Monographs of the International Ocean-Colour Coordinating Group-IOCCG Report Number 7, Dartmouth, Canada: The International Ocean-Colour Coordinating Group (IOCCG), 2008.

Preisendorfer, R. W. *Application of radiative transfer theory to light measurements in the sea.* Union Geod. Geophys. Inst. Monogr, 1961.

Quartly, G. D., and M. A. Srokosz. "Eddies in the southern Mozambique Channel." *Deep-Sea Research II; Vol. 51* , 2004: 69–83.

Rashid, H., B. P. Flower, and R. Z. Quinn. "A ~25 ka Indian monsoon variability record from the Andaman Sea." *Quaternary Science Reviews 26*, 2007: 2586-2597.

Rayner, N. A., et al. "Global analyses of sea surface temperature, sea ice, and night marine air temperature since the late nineteenth century." *JOURNAL OF GEOPHYSICAL RESEARCH; VOL. 108; No. D14, 4407;* , 2003: doi:10.1029/2002JD002670.

Rayner, N. A., et al. "Global analyses of sea surface temperature, sea ice, and night marine air temperature since the late nineteenth century." *JOURNAL OF GEOPHYSICAL RESEARCH; VOL. 108; NO. D14, 4407*, 2003: doi:10.1029/2002JD002670.

Ritchie, Jerry C., Frank R. Schiebe, and J. Roger McHenry. "Remote sensing of Suspended Sediments in Surface waters." *Photogrammetric Engineering & Remote Sensing; Vol. 42; No: 12*, 1976: 1539-1545.

Ronco, Paolo, Giacomo Fasolato, Michael Nones, and Giampaolo Di Silvio. "Morphological effects of damming on lower Zambezi River." *Geomorphology; Vol. 115*, 2010: 43–55.

Rudorff, C. M., E. M. Novo, and L. S. Galvão. "Spectral Mixture Analysis of EO-1 Hyperion Imagery focused on the Spatial-Temporal Variability of the Amazon Floodplain Multicomponental Waters." *XIII Simposio Brasileiro de Sensoriamento Remote*, April 21st-26th, 2007: 6519-6526.

Rudorff, N. M., M. Kampel, and C. E. Rezende. "Spectral mapping of Paraíba do Sul River plume (Brazil) using multitemporal Landsat Images." *Journal of Applied Remote Sensing; Vol 5*, 2011; : 19p.

Ruijter, Wilhelmus P. M. de, Herman Ridderinkhof, Johann R. E. Lutjeharms, Mathijs W. Schouten, and Cornelis Veth. "Observations of the flow in the Mozambique Channel." *Geophysical Research Letters; Vol. 29; No. 10*, 2002: doi: 10.1029/2001GL013714.

Ryan, Paddy A. "Environmental effects od sediments on New Zealand Streams: a review." *New Zealand Journal of Marine and Freshwater Research; Vol. 25*, 1991: 207-221.

Saetre, R. "Surface currents in the Mozambique Channel." *Deep-Sea Research; Vol. 32; No.12*, 1985: 1457-1467.

Saldías, Gonzalo S., John L. Largier, Renato Mendes, Iván Pérez-Santos, and Cristian A. Vargas. "Satellite-measured interannual variability of turbid river plumes off central-southern Chile: Spatial patterns and the influence of climate variability." *Progress in Oceanography; Vol. 146*, 2016: 212-222.

Schemainda, Rudolf, and Eberhard Hagen. "On steady state intermediate vertical currents induced by the Mozambique current." *Océanogr. trop.; Vol. 18; No. 1* , 1983: 81-88.

Schoutena, Mathijs W., Wilhelmus P. M. de Ruijtera, Peter Jan van Leeuwena, and Herman Ridderinkhof. "Eddies and variabilityin the Mozambique Channel." *Deep-Sea Research II; Vol. 50*, 2003: 1987–2003.

Schulz, Hartmut, Ulrich von Rad, and Helmut Erlenkeuser. "Correlation Between Arabian Sea and Greenland climate oscilation of the past 110,000 years." *Nature 393*, 1998: 54-57.

Seatre, R., and R. de Paula e Silva. *The marine fish resources of Mozambique.* Reports on surveys with the R/V Dr Fridtjof Nansen, Maputo; Bergen: Serviço de Investigações Pesqueiras; Institute of Marine Research, 1979.

Shankar, D., P. N. Vinayachandran, and A. S. Unnikrishnan. "The monsoon currents in the north Indian Ocean." *Progress in Oceanography 52*, 2002: 63-120.

Shen, Chunyan, Yunrong Yan, Hui Zhao, Jiayi Pan, and Adam T. Devlin. "Influence of monsoonal winds on chlorophyll-α distribution in the Beibu Gulf." *PLoS ONE; Vol. 13; No. 1*, 2018: e0191051.

Shi, Wei, and Menghua Wang. "Characterization of Global Ocean Turbidity from Moderate Imaging Spectroradiameter Ocean Color observations." *Journal of Geophysical research; vol 115; c11022*, 2010: doi:10.1029/2010JC006160.

Siddorn, J. R., D. G. Bowers, and A. M. Hoguane. "Detecting the Zambezi River Plume using Observed Optical Properties." *Marine Pollution Bulletin; Vol. 42; No: 10*, 2001: 942-950.

Silva, A. J. da. "Hydrology and fish distribution at Sofala Bank (Mozambique)." *Revista de Investigação Pesqueira; Vol.12* (Revista de Investigção Pesqueira; No.12; 5-36), 1984: 5-36.

Silva, A. Jorge da. "Report on the oceanographic investigations carried out at the Sofala Bank by the Soviet trawler ”Sevastopolsky Rybak” in September-December 1982." *Revista de Investigação Pesqueira - Instituto de Investihgação Pesqueira de Moçambique; Vol. 10;* , 1984: 5-35.

Simpson, J. H., J. Brown, J. Matthews, and G. Allen. "Tidal Straining, Density Currents, and Stirring in the Control of Estuarine Stratification." *Estuaries; Vol. 13; No. 2*, 1990: 125-132.

Sirocko, F., D. Garbe-Schonberg, A. Mcintyre, and B. Molfino. "Teleconnections Between the Subtropical Monsoon and high-Latitude Climates During the Last Deglaciation." *Science 272*, 1996: 526-529.

Smith, David G., and Robert James Davies-Colley. "If visual water clarity is the issue, they wahy not measure it?" *Advisor committe of water informatio, National Monitoring Conference*, May 21-23, 2002: 1-10.

Steele, J. H. "Environmental Control of Photosyntheis in the Sea." *Limnology and Oceanography*, 1962: 137_150.

Steen, Jan-Erik, and A. M. Hoguane. *Oceanographic results on expedition carried out by R/ V Dr. Frodjof Nansen in Mozambique waters during April - May 1990.* Maputo, Mozambique: Instituto de Investigação Pesqueira, 1990.

Su, Fengge, Yang Hong, and Dennis P. Lettenmaier. "Evaluation of TRMM Multisatellite Precipitation Analysis (TMPA) and Its Utility in Hydrologic Prediction in the La Plata Basin." *Journal of Hydrometeorology; Vol. 9*, 2007: 622-639.

Syvitski, James P. M., Charles J. Vorosmarty, Albert J. Kettner, and Pamela Green. "Impact of Humans on the Flux of Terrestrial Sediment to the Global Coastal Ocean." *Science. Vol. 308*, 2005: 376-380.

Talley, Lynne D., George L. Pickard, William J. Emery, and James H. Swift. *Descriptive Physical Oceanography: An Introduction.* London, UK: Academic Press, 2011.

Tew-Kai, E., and F. Marsac. "Influence ofmesoscale eddies on spatial structuring of top predators'communities in the Mozambique Channel." *Progress in Oceanography; Vol. 86*, 2010: 214-223.

Tew-Kai, Emilie, and Francis Marsac. "Patterns of variability of sea surface chlorophyll in the Mozambique Channel: A quantitative approach." *Journal of Marine Systems*, 2008: doi: 10.1016/j.jmarsys.2008.11.007.

Thieming, Vera, Rodrogo Rojas, and Mauricio Zambrano-Bigiarini. "Validation of Satellite-Based Precipitation Products over Sparsely Gauged African River Basins." *Journal of Hydrometeorology; Vol. 13*, 2012: 1760-1783.

Thomas, Andrew C., and Ryan A. Weatherbee. "Satellite-measured temporal variability of the Columbia River Pluma." *Remote Sensing of Environment 100*, 2006: 167-178.

Tolman, Hendrik L. *User manual and system documentation of WAVEWATCH III version 3.14.* MMAB Technical Note 276, Camp Springs, MD 20746: NOAA/NWS/NCEP, 2009.

Tomczak, Matthias, and J. Stuart Godfrey. *Regional Oceanography: An Introduction.* London: Butler & Tanner Ltd, 2001.

Toole, A. Diedre, and A. David Siegel. "Modes and Mechanisms of Ocean Color variability in Santa Barbara Channel." *Jornal of Geophysical Research. vol 106. No c11*, 2001: 26985-27000.

Torrence, C., and G. P. Compo. " A Practical Guide toWavelet Analysis." *Bulletin of the American Meteorological Society; Vol. 79*, 1998: 61-78.

Trimble. *eCognition Developer User Guide.* Munich, German: Trimble German GmbH, 2013.

Valiela, Ivan. *Marine Ecological Processes; 3rd Edition.* Massachusetts, USA: Springer, 2015.

Venegas, Roberto M., et al. "Satellite-derived variability in chlorophyll, wind stress, sea surface height, and temperature in the northern California Current System." *Journal of Geophysical Research; Vol. 113; C03015*, 2008: doi:10.1029/2007JC004481.

Wang, Bin, In-Sik Kang, and June-Yi Lee. "Ensemble Simulations of Asian–Australian Monsoon Variability by 11 AGCMs." *American Meteorology Society; Vol. 17*, 2004: 803-818.

Ward, M., K. Maskell, C. K. Folland, D. P. Rowell, and R. Washington. *A tropic-wide oscillation of boreal summer rainfall and patterns of sea-surface temperature.* Climate Research Technical Note CRTN48, Bracknell, UK: Hadley Center, Meteorological Office, 1994.

Warrick, J. A., L. A. K. Mertes, L. Washbum, and D. A. Siegel. "Dispersal forcing of southern California river plumes, based on field and remote sensing observations." *Geo-Mar Letters; Vol 24*, 2004: 46-52.

Warrick, Jonathan A. "Dispersal of Fine Sediment in Nearshore Coastal Waters." *Journal of Coastal Research; Vol. 29; No. 3*, 2013: 579-596.

Wright, L. D. "Sediment transport and deposition at river mouths: A synthesis." *Geological Society of America Bulletin; Vol. 88; No. 70614*, 1977: 857-868.

Wright, L. D., and C. A. Nittrouer. "Dispersal of river sediments in coastal seas: Six contrasting cases." *Estuaries; Vol. 18; No. 3*, 1995: 494-508.

Xie, Pingping, and Phillip A. Arkin. "Global Precipitation: A 17-Year Monthly Analysis Based on Gauge Observations, Satellite Estimates, and Numerical Model Output." *Bolletin of the American Meteorological Society; Vol. 78; No. 11*, 1997: 2539-2558.

Yankovisky, Alexander E., and David C. Chapman. "A Simple Theory for the Fate of Buoyant Coastal Discharges." *Journal of Physical Oceanography; Vol. 27*, 1997: 1386-1401.

Yoo, Chulsang, and Eunsaem Cho. "Comparison of GCM Precipitation Predictions with Their RMSEs and Pattern Correlation Coefficients." *Water; Vol. 10; No. 28*, 2018: doi:10.3390/w10010028.

Yu, Jin-Yi, and Hsun-Ying Kao. "Decadal changes of ENSO persistence barrier in SST and ocean heat content indices: 1958–2001." *Journal of Geophysical Research; Vol. 112*, 2007: doi:10.1029/2006JD007654.

Zhang, H., R. W. Reynolds, and J. J. Bates. "Blended and gridded high resolution global sea surface wind speed and climatology from multiple satellites: 1987-present." *14th Conference on Satellite Meteorology and Oceanography*, January-February 29-02, 2006: P2.23.

Zhang, Qiang, Jianfeng Li, Vijay P. Singh, Chong-Yu Xu, and Jingyun Deng. "Influence of ENSO on precipitation in the East River basin, south China." *Journal of Geophysical Research: Atmospheres; Vol. 118*, 2013: doi:10.1002/jgrd.50279.

Zoffoli, Maria Laura, Milton Kampel, and Leila Maria Garcia Fonseca. "Caracterização da pluma do rio Doce (ES) utilizando dados TM-Landsat 5." *Anais XV Simpósio Brasileiro de Sensoriamento Remoto-SBSR*, Maio 5, 2011: 5025-5031.